


5-2013

INVESTIGATING THE ROLES OF THE p63 ISOFORMS IN THE MICRORNA BIOGENESIS PATHWAY

Deepavali Chakravarti

Follow this and additional works at: https://digitalcommons.library.tmc.edu/utgsbs_dissertations

 Part of the [Biology Commons](#), [Cancer Biology Commons](#), [Cell Biology Commons](#), and the [Other Cell and Developmental Biology Commons](#)

Recommended Citation

Chakravarti, Deepavali, "INVESTIGATING THE ROLES OF THE p63 ISOFORMS IN THE MICRORNA BIOGENESIS PATHWAY" (2013). *The University of Texas MD Anderson Cancer Center UTHealth Graduate School of Biomedical Sciences Dissertations and Theses (Open Access)*. 370.
https://digitalcommons.library.tmc.edu/utgsbs_dissertations/370

This Dissertation (PhD) is brought to you for free and open access by the The University of Texas MD Anderson Cancer Center UTHealth Graduate School of Biomedical Sciences at DigitalCommons@TMC. It has been accepted for inclusion in The University of Texas MD Anderson Cancer Center UTHealth Graduate School of Biomedical Sciences Dissertations and Theses (Open Access) by an authorized administrator of DigitalCommons@TMC. For more information, please contact digitalcommons@library.tmc.edu.

**INVESTIGATING THE ROLES OF THE *p63* ISOFORMS IN THE MICRORNA
BIOGENESIS PATHWAY**

by

Deepavali Chakravarti, M.S.

APPROVED:

Elsa Flores, Ph.D
Supervisory Professor

Dihua Yu, MD, Ph.D

Jeffrey Rosen, Ph.D

Pierre McCrea, Ph.D

Guillermina Lozano, Ph.D

APPROVED:

Dean, The University of Texas
Graduate School of Biomedical Sciences at Houston

**INVESTIGATING THE ROLES OF THE *p63* ISOFORMS IN THE MICRORNA
BIOGENESIS PATHWAY**

**A
DISSERTATION**

Presented to the Faculty of
The University of Texas
Health Science Centre at Houston
Graduate School of Biomedical Sciences
and
The University of Texas
M. D. Anderson Cancer Center
Graduate School of Biomedical Sciences
In Partial Fulfillment

Of the Requirements

For the Degree of

DOCTOR OF PHILOSOPHY

By
Deepavali Chakravarti, M.S.
May, 2013

Dedication

I dedicate this dissertation to my whole family for their unconditional love and continuous support, especially to my husband Akash Agarwal.

Acknowledgements

This work would not have been possible without the support of several people throughout my journey in graduate school.

I would like to thank Dr. Elsa Flores, who has been a wonderful mentor. She has taught me how to do and think science, but above all how to keep an open mind and be optimistic. I have learnt that it is important to see the bigger picture while working on the details. She has also shown tremendous patience in day to day dealings with me. It has been a great pleasure to have known her and worked with her. It would not have been possible to achieve my goals without her.

I was also very lucky to have Dr. Jeffrey Rosen, Dr. Dihua Yu, Dr. Guillermina Lozano, and Dr. Pierre McCrea on my committee. All of them have always been constructive in their suggestions and have always encouraged me. It has been a pleasure to collaborate with Dr. Rosen's lab for the short of period of time.

I would also like to thank all the past and present colleagues in the Flores lab. I would like to thank Dr. Xiaohua Su, especially for her guidance and the leisure scientific discussions that we have had. I would also like to thank Dr. Marco Napoli for our candid scientific discussions and healthy debates. I would also like to thank Dr. Ramon Flores Gonzalez and Avinash Venkatanarayana and Marlese Pisegna for their suggestions, Dr. Minsoon Cho who helped me in the beginning of my entry into the lab, Lingzhi Liu and Youngjin Gi for their help with the mouse work.

I would like to thank some of the rotation students and summer students like Marco Leung and Serge Korijian. It has been a lot of fun working with them. I would also like to thank some of the members from other labs, Sumaiyah Rehman (Yu lab, MDAnderson), Dr. Abhinav Jain (Barton lab, MDAnderson), Dr. Li Fang (Zwaka lab, Baylor), Jenny Deng (Behringer lab, MDAnderson) and Jennifer Alana.

Finally I would like to thank my husband Akash Agarwal. The credit for this thesis goes to him in a lot of ways along with my parents Ratnabali and Dipak Chakrabarti who always believed in me and to my in-laws Jyoti and Ashok Agarwal for their love and support through this endeavor.

Abstract

Investigating the roles of the *p63* isoforms in the microRNA biogenesis pathway:

Implications in tumorigenesis and pluripotency

Publication No. _____

Deepavali Chakravarti, M.S.

Supervisory Professor: Elsa Flores, Ph.D.

MicroRNAs play roles in various biological processes like development, tumorigenesis, metastasis and pluripotency. My thesis work has demonstrated roles for *p63*, a *p53* family member, in the upstream regulation of microRNA biogenesis. The *p63* gene has a complex gene structure and has multiple isoforms. The *TAp63* isoforms contain an acidic transcription activation domain. The $\Delta Np63$ isoforms, lack the TA domain, but have a proline rich region critical for gene transactivation. To understand the functions of these isoforms, the Flores lab generated *TAp63* and $\Delta Np63$ conditional knock out mice. Using these mice and tissues and cells from these mice we have found that *TAp63* transcriptionally regulates *Dicer* while $\Delta Np63$ transcriptionally regulates *DGCR8*. *TAp63*^{-/-} mice are highly tumor prone. These mice develop metastatic mammary adenocarcinomas, squamous cell carcinomas, and lung adenocarcinomas to distant sites including the liver, lungs, and brain. I found that *TAp63* suppresses metastasis by transcriptionally activating *Dicer*. *TAp63* and *Dicer* levels were very low or lost in high grade human tumors like mammary adenocarcinomas, squamous cell carcinomas, and lung adenocarcinomas. Expression of *Dicer* in these tumor cell lines reduced their invasiveness. Using $\Delta Np63$ ^{-/-} mice, I found that $\Delta Np63$ transcriptionally activates *DGCR8*, resulting in a miRNA profile that is critical to reprogram cells to pluripotency. Analysis of epidermal cells derived from $\Delta Np63$ ^{-/-} mice revealed that these cells expressed markers of pluripotency, including Sox2, Oct 4 and Nanog; however, genome-wide analysis revealed a novel profile of genes that are common between $\Delta Np63$ ^{-/-} epidermal cells and embryonic stem cells. I also found that mouse cells depleted of $\Delta Np63$ form chimeric mice and teratomas in SCID mice, demonstrating that $\Delta Np63$ deficient cells are pluripotent. Further, I found that restoration of *DGCR8* in $\Delta Np63$ ^{-/-} epidermal cells reduces their

pluripotency and induces terminal differentiation. I also demonstrated that iMS (induced multipotent stem) cells could be generated using human keratinocytes by knockdown of $\Delta Np63$ or *DGCR8*. Taken together, my work has placed *p63* and its isoforms at a critical node in controlling miRNA biogenesis.

Table of Contents

Dedication	iii
Acknowledgements	iv
Abstract	v
Table of Contents	vii
List of Illustrations	xiv
List of Tables.....	xvii
List of Appendices	xviii
 1. Chapter 1: Introduction.....	 1
1.1. The <i>p53</i> family	2
1.2. Phylogeny of <i>p63/p73</i>	3
1.3. <i>p63</i> gene structure.....	4
1.4. Germline heterozygous <i>p63</i> mutations in humans	6
1.5. Role of <i>p63</i> in Human Tumorigenesis.....	6
1.6. The <i>p63</i> knock-out mouse models and contradictory phenotypes	7
1.7. Role of <i>p63</i> in stem cell biology.....	10
1.7.1. The Epidermis	10
1.7.2. <i>p63</i> and stem cell	11
1.8. Stem cells.....	14
1.8.1. Induced pluripotent stem cells.....	15
1.8.2. Application of iPS cells and associated problems	17

1.8.3. Role of <i>p53</i> in iPS cell.....	18
1.9. Role of the p63 isoforms in tumorigenesis –lessons learnt from mouse models	19
1.10. MicroRNAs	21
1.10.1. MicroRNA Gene Transcription.....	21
1.10.2. MicroRNA biogenesis pathway	23
1.10.3. Mode of action of microRNAs	23
1.10.4. Role of <i>p53</i> in the regulation of microRNA biogenesis	24
1.10.5. DGCR8 knock-out mouse phenotype and its role in pluripotency.....	24
1.10.6. <i>Dicer</i> knock-out mouse phenotype.....	25
1.10.7. Conditional knock-out mouse model for <i>Dicer</i> /DGCR8 specifically in the skin demonstrate a similar phenotype	25
1.10.8. Role of microRNA in iPS cell generation	26
1.10.9. Role of microRNAs in tumorigenesis and metastasis	26
1.10.10. Expression of <i>Dicer</i> in cancers.....	28
2.Chapter 2: Materials and Methods.....	29
2.1. Genotyping of <i>TAp63</i> and <i>ΔNp63</i> conditional knock-out mice	31
2.2. Generation of <i>ΔNp63</i> Conditional Knockout Mice	31
2.3. Quantitative Real time RT-PCR	32
2.4. Generation of mice and tumor analysis	32
2.5. Histology and immunostaining of E18.5 embryos	33
2.6. Keratinocyte cells – proliferation assay	34
2.7. Migration and invasion assay	34
2.8. Mouse and human tumor cell lines.....	34
2.9. Immunocytochemistry	35
2.10. Immunofluorescence and immunohistochemistry of tumors	35

2.11. Human HNSCCs and lung adenocarcinomas.....	36
2.12. Quantitative Real time PCR	36
2.13. Cytogenetics	36
2.14. Northern blot analysis.....	37
2.15. miRNA TaqMan assays.....	37
2.16. MicroRNA overexpression.....	37
2.17. ChIP assay	38
2.18. Lentiviral infection	39
2.19. Adenovirus-Cre infection	40
2.20. Cloning of dgcr8-luciferase reporter genes	40
2.21. Dual luciferase reporter assay	40
2.22. Western Blot	41
2.23. Normal Human Epidermal Keratinocytes (NHEK) culture and infection	41
2.24. Cell Culture	42
2.25. Immunofluorescence – Cell culture.....	42
2.26. Small RNA Sequencing and Analysis.....	43
2.27. RNA Sequencing and Analysis	44
2.28. Multi-species analysis of smRNA-Seq and RNA-Seq data	44
2.29. Generation of an inducible DGCR8 lentiviral vector.....	45
2.30. Southern Blot Analysis of mouse $\Delta Np63^{-/-}$ epidermal cells and iPS ^{Yam} cells.....	45
2.31. Calculation of Timing and Efficiency of Reprogramming.....	45
2.32. Teratoma Formation Assay	46
2.33. Generation and analysis of chimeric mice.....	47
2.34. Raft culture	47

3. Chapter 3: TAp63 suppresses metastasis through coordinate regulation of <i>Dicer</i> and miRNAs	48
3.1. Introduction	49
3.2. Results	51
3.2.1. <i>TAp63</i> mutant mice develop highly metastatic tumors	51
3.2.2. Histological analysis of the tumors from <i>TAp63</i> ^{-/-} and <i>TAp63</i> ^{+/-} mice demonstrate a diverse profile	53
3.2.3. <i>TAp63</i> is a haploinsufficient tumor suppressor	55
3.2.4. <i>TAp63/p53</i> double mutant mice have a tumor profile that is distinct from the <i>p53</i> mutant mice	57
3.2.5. <i>TAp63</i> does not undergo LOH in the <i>TAp63/p53</i> double mutant mice tumors	60
3.2.6. Loss of <i>TAp63</i> is tumor protective in some tissues	63
3.2.7. Carcinomas are the more malignant of the tumor types in the <i>TAp63</i> mutant and <i>TAp63/p53</i> double mutant mice.....	65
3.2.8. Genomic instability empowers the carcinomas to overcome senescence and metastasize in the absence of <i>TAp63</i>	67
3.2.9. The <i>TAp63</i> ^{-/-} cells and tumor cell lines are more invasive	69
3.2.10. <i>Dicer</i> mutant mice exhibit similarities to the <i>TAp63</i> mutant mice.....	71
3.2.11. <i>Dicer</i> mRNA level is low in <i>TAp63</i> mutant human and murine cells, tumors and cell lines.....	71
3.2.12. Low levels of <i>Dicer</i> expression in human metastatic tumors correlate with <i>TAp63</i> expression levels.....	74
3.2.13. <i>TAp63</i> transcriptionally regulates the <i>Dicer</i> promoter	76
3.2.14. Loss of <i>Dicer</i> expression in MEFs causes increased invasion	79
3.2.15. <i>TAp63</i> regulates metastasis through the regulation of <i>Dicer</i> in cells and cell lines	81

3.2.16. Loss of <i>TAp63</i> and <i>Dicer</i> expression increases the metastatic potential of the non-metastatic cells.....	83
3.2.17. <i>TAp63</i> ^{-/-} MEFs express low levels of mature microRNAs	85
3.2.18. Modulation of <i>TAp63</i> effects the expression of mature microRNA.....	87
3.2.19. <i>TAp63</i> ^{-/-} cells and tumors express low level of miR-130b compared to <i>p53</i> ^{-/-} cells	89
3.2.20. Expression level of mature miR-130b correlates with <i>TAp63</i> and <i>Dicer</i> expression in human cancers	91
3.2.21. <i>TAp63</i> transcriptionally regulates the activation of miR-130b promoter site	92
3.2.22. <i>TAp63</i> regulates metastasis by the regulation of <i>miR-130b</i>	95
3.2.23. Loss of <i>miR-130b</i> causes increase in invasion	97
3.2.24. <i>Dicer</i> and miR-130b coordinately regulate invasion and migration	99
3.3. Discussion.....	102
4. Chapter 4: Induced multipotency in adult keratinocytes through down regulation of $\Delta Np63$ or <i>DGCR8</i>	103
4.1. Introduction	104
4.2. Results	107
4.2.1. Generation of a $\Delta Np63$ conditional knock-out mouse model.....	107
4.2.2. Phenotype of the $\Delta Np63$ mutant mice	110
4.2.3. $\Delta Np63$ ^{-/-} mouse epidermis displays defects in terminal differentiation.....	112
4.2.4. Loss of $\Delta Np63$ results in hyperproliferation of the epidermis.....	116
4.2.5. $\Delta Np63$ deficient epidermal cells can self-renew	118
4.2.6. $\Delta Np63$ deficient epidermal cells express high levels of factors associated with induced pluripotency	120
4.2.7. <i>DGCR8</i> expression is low in $\Delta Np63$ mutant cells and $\Delta Np63$ ^{-/-} epidermis.....	122

4.2.8. <i>ΔNp63</i> transcriptionally activates the DGCR8 promoter	125
4.2.9. <i>ΔNp63</i> represses Oct-4, Sox-2 and Nanog through transcriptional regulation of DGCR8	128
4.2.10. <i>ΔNp63</i> ^{-/-} epidermal cells, iPS cells and mouse ES cells have a similar microRNA and mRNA signature	130
4.2.11. <i>ΔNp63</i> deficient epidermal cells are pluripotent and can differentiate into multiple cell fates in vivo.....	142
4.2.12. Generation of chimeric mouse embryos from <i>ΔNp63</i> ^{-/-} epidermal cells.....	145
4.2.13. Normal human epidermal keratinocytes can be induced to pluripotency by knockdown of <i>ΔNp63</i>	149
4.2.14. NHEK-Sh <i>ΔNp63</i> /shDGCR8 cells can form teratomas	153
4.2.15. Deregulated microRNA processing in the NHEK-sh <i>ΔNp63</i> /shDGCR8 cells demonstrated by Northern blot analysis	161
4.3. Discussion.....	163
5. Chapter 5: Induced multipotent (iMS) NHEK-sh <i>ΔNp63</i> /DGCR8 cells can be induced to differentiate into epidermal tissue.....	167
5.1. Introduction	168
5.2. Results	169
5.2.1. NHEK-sh <i>ΔNp63</i> /shDGCR8 can be induced to differentiate to ectodermal lineage	169
5.2.2. Loss of pluripotency marker expression in NHEK-sh <i>ΔNp63</i> /shDGCR8 cells under differentiating conditions.....	171
5.2.3. Defects in terminal differentiation of the NHEK-sh <i>ΔNp63</i> /shDGCR8 cells as demonstrated in raft culture assay	174
5.3. Discussion.....	176

6. Chapter 6: Role of $\Delta Np63$ in tumor suppression and oncogenesis is context dependent	177
6.1. Introduction	178
6.2. Results	179
6.2.1. $\Delta Np63$ heterozygous mice develop tumors of the epithelial origin	179
6.2.2. Loss of $\Delta Np63$ is tumor protective in the thymus <i>in vivo</i>	182
6.2.3. Loss of $\Delta Np63$ leads to increased apoptosis and reduced proliferation <i>in vivo</i>	184
6.2.4. Loss of $\Delta Np63$ induces apoptosis, senescence and cell cycle arrest <i>in vitro</i>	186
6.2.5. $\Delta Np63$ undergoes proteasomal degradation on γ -radiation	189
6.2.6. $\Delta Np63$ transcriptionally represses the <i>TAp63</i> promoter	191
6.2.7. $\Delta Np63^{+/-}; p53^{-/-}$ mice die of multiple metastatic tumors	193
6.2.8. $\Delta Np63^{+/-}; p53^{+/-}$ mice develop varied metastatic carcinomas	195
6.2.9. $\Delta Np63^{-/-}$ MEFs and keratinocytes have high migration and invasion potential	197
6.3. Discussion	200
7. Chapter 7. Conclusion and Future Direction	202
7. Conclusion and Future Directions	203
7.1. <i>p63</i> , microRNAs and cancer	206
7.2. <i>p63</i> and EMT	207
7.3. <i>p63</i> , stem cell maintenance, differentiation and stratification	207
7.4. Role of <i>p63/p73</i> in iPS cell generation	208
7.5. <i>p63</i> and cancer stem cells	209
7.6. $\Delta Np63$ and tumor suppression	210
8. Bibliography	351
9. Vita	372

List of Illustrations:

Chapter 1

Figure 1: <i>p63</i> gene structure and similarity to <i>p53</i> gene	5
Figure 2: Role of <i>p63</i> in stem cell maintenance in the dermis and epidermis.....	13
Figure 3: Canonical microRNA biogenesis pathway	22

Chapter 3

Figure 4: <i>TAp63</i> ^{-/-} mice develop metastatic tumors	52
Figure 5: Tumor spectrum of <i>TAp63</i> mutant mice	54
Figure 6: <i>TAp63</i> is a haploinsufficient tumor suppressor.....	56
Figure 7: <i>TAp63/p53</i> double mutant mice have a distinct tumor profile from the <i>p53</i> mutant mice	59
Figure 8: <i>TAp63</i> does not undergo LOH in <i>TAp63/p53</i> double mutant tumors	61
Figure 9: Loss of <i>TAp63</i> is tumor protective in some tissues.....	64
Figure 10: Tumors lacking <i>TAp63</i> exhibit senescence.....	66
Figure 11: Loss of <i>TAp63</i> leads to high levels of genomic instability in tumors	68
Figure 12: <i>TAp63</i> ^{-/-} primary cells and cell lines are highly invasive	70
Figure 13: <i>Dicer</i> levels are low in <i>TAp63</i> mutant tumors	73
Figure 14: Low levels of <i>Dicer</i> expression in human metastatic tumors correlate with <i>TAp63</i> expression levels.....	75
Figure 15: <i>TAp63</i> transcriptionally regulates <i>Dicer</i> by directly binding to its promoter	78
Figure 16: Loss of <i>Dicer</i> expression in MEFs causes increased invasion	80
Figure 17: <i>TAp63</i> regulates metastasis through the regulation of <i>Dicer</i> in cells and cell lines.	82
Figure 18: Loss of <i>TAp63</i> and <i>Dicer</i> expression increases the metastatic potential of the non-metastatic cells.....	84
Figure 19: <i>TAp63</i> ^{-/-} MEFs express low levels of mature microRNAs	86

Figure 20: Modulation of TAp63 effects the expression of mature microRNA	89
Figure 21: <i>TAp63</i> ^{-/-} cells and tumors express low level of miR-130b compared to <i>p53</i> ^{-/-} cells.....	90
Figure 22: <i>TAp63</i> transcriptionally regulates the activation of miR-130b promoter site.....	94
Figure 23: Modulating <i>TAp63</i> levels correlate with the level of miR-130b.....	96
Figure 24: Loss of miR-130b causes an increase in invasion	98
Figure 25: <i>Dicer</i> and miR-130b coordinately regulate invasion and migration.....	101

Chapter 4

Figure 26: Generation of a conditional <i>ΔNp63</i> knock-out mouse model	109
Figure 27: Phenotype of the <i>ΔNp63</i> mutant mice.....	111
Figure 28: <i>ΔNp63</i> mutant mice exhibit epidermal abnormalities and defects in terminal differentiation	115
Figure 29: Loss of <i>ΔNp63</i> results in hyperproliferation of the epidermis	117
Figure 30: <i>ΔNp63</i> deficient epidermal cells can self-renew	119
Figure 31: <i>ΔNp63</i> deficient epidermal cells express high levels of factors associated with induced pluripotency	121
Figure 32: DGCR8 expression is low in <i>ΔNp63</i> mutant cells and <i>ΔNp63</i> ^{-/-} epidermis	124
Figure 33: <i>ΔNp63</i> transcriptionally activates the DGCR8 promoter.....	127
Figure 34: <i>ΔNp63</i> represses Oct-4, Sox-2 and Nanog through transcriptional regulation of DGCR8	129
Figure 35: Pearson's Correlation Analysis from miRNA-Seq	132
Figure 36: Heat map showing supervised hierarchical clustering from mouse miRNA seq...	134
Figure 37: Unsupervised and supervised clustering for mRNA-seq mouse.....	135
Figure 38: <i>ΔNp63</i> deficient epidermal cells are pluripotent.....	140
Figure 39: <i>ΔNp63</i> deficient cells can form embryoid bodies	141
Figure 40: <i>ΔNp63</i> deficient epidermal cells can form teratomas	144

Figure 41: Generation of chimeric mouse embryos from $\Delta Np63^{-/-}$ epidermal cells.....	146
Figure 42: Analysis of $\Delta Np63^{-/-}$ chimeras	147
Figure 43: Reprogramming of NHEK cells by down regulation of $\Delta Np63$ or DGCR8.....	150
Figure 44: Characterization of NHEK-sh $\Delta Np63$ /DGCR8 cells	152
Figure 45: NHEK-sh $\Delta Np63$ /shDGCR8 cells can form teratomas.....	154
Figure 46: MicroRNA-seq data analysis in mouse and humans	157
Figure 47: mRNA-seq data analysis in mouse and humans	159
Figure 48: Unsupervised mRNA seq clustering comparing human and mouse cell line.	160
Figure 49: Northern blot analysis in the NHEK-sh $\Delta Np63$ /shDGCR8 cells.....	162
Chapter 5	
Figure 50: Cytokeratin 5 expression in NHEK-sh $\Delta Np63$ / shDGCR8.....	170
Figure 51: Differentiation of NHEK-shDNp63 towards ectodermal lineage.....	172
Figure 52: Differentiation of NHEK-shDGCR8 towards ectodermal lineage	173
Figure 53: Raft culture assay to differentiate NHEK-shDNp63/shDGCR8 cells to full thickness epidermis	175
Chapter 6	
Figure 54: Loss of $\Delta Np63$ leads to a shortened life-span	181
Figure 55: Loss of $\Delta Np63$ is tumor protective in the thymic lymphomas.....	183
Figure 56: Loss of $\Delta Np63$ leads to increased apoptosis and reduced proliferation in vivo	185
Figure 57: Loss of $\Delta Np63$ leads to increased apoptosis and senescence in vitro	187
Figure 58: Loss of $\Delta Np63$ leads to upregulation of the $TAp63$ protein.....	189
Figure 59: $\Delta Np63$ suppresses $TAp63$ transcription by binding to its promoter	191
Figure 60: $\Delta Np63^{+/-};p53^{-/-}$ mice die of multiple metastatic tumors.....	193
Figure 61: $\Delta Np63^{+/-};p53^{+/-}$ mice develop varied metastatic carcinomas.....	195

List of Tables:

Table 1: Tumor landscape of the <i>TAp63/p53</i> mutant mice	62
Table 2: <i>TAp63</i> and <i>Dicer</i> expression in human tumors	75
Table 3: <i>p63/p53</i> response element on <i>Dicer</i> promoter	77
Table 4: <i>TAp63</i> , <i>Dicer</i> and miR-130b expression in human tumors	91
Table 5: <i>p63/p53</i> response elements.....	93
Table 6: miRNA-mRNA functional pair analysis	135
Table 7: Embryos generated from iPS cells.....	148
Table 8: Tumor spectrum of $\Delta Np63^{+/-};p53^{-/-}$	181
Table 9: <i>p53/p63</i> response element on the <i>TAp63</i> promoter.....	192
Table 10: Tumor spectrum of $\Delta Np63^{+/-};p53^{-/-}$ mice	194

List of Appendices:

Appendix 1: mouse miRNA Pearson's correlation analysis.....	210
Appendix 2: mouse-miRNA heat map.....	211
Appendix 3: mouse up-regulated miRNAs and gene targets from mRNA-seq.....	217
Appendix 4: mouse down-regulated miRNA and their gene targets from mRNA-seq.....	232
Appendix 5: mouse and human miRNA Pearson's correlation analysis.....	283
Appendix 6: mouse-human miRNA Principal component analysis plot.....	284
Appendix 7: mouse-human miRNA signature.....	285
Appendix 8: mouse and human mRNA Pearson's correlation analysis.....	286
Appendix 9: mouse-human mRNA Principal component analysis plot	287
Appendix 10: mouse-differentially expressed miRNA in null vs. ips cells.....	288
Appendix 11: mouse mRNA heat map.....	300
Appendix 12: mouse-human mRNA heat map.....	319

1. Chapter 1: Introduction

1.1. The *p53* family

In 1979 the *p53* protein was identified by several laboratories simultaneously (1, 2). It was identified as a protein being bound to the SV40 large T antigen (2, 3). In 1984 the cDNA was cloned (4-7). For the longest time it was thought to be an oncogene due to its overexpression in mutated and tumorigenic cells(8, 9). In the late 1980's researchers started to realize that the *p53* cDNA that was cloned had mutations in several site. This was followed by the realization that the experiments performed with this mutated *p53* protein cDNA was the reason why the cells transfected with the *p53* protein ended up becoming transformed (10, 11). Thus began the search for the wild-type protein. In 1989 Dr. Arnie Levine's lab cloned the *wild-type p53* and showed that it could suppress transformation (12, 13). By the late 1980's it was identified not as an oncogene but as a tumor suppressor (12, 13). More than 50% of human tumors exhibit loss or mutation of the *p53* protein(14). Since then researchers had been looking for other *p53* family members in the hope that this could lead to discovery of more tumor suppressors, which are potentially not mutated in tumors. The *p53 knock-out* mouse exhibits early tumorigenesis as expected, but seemed to have less developmental defects, suggesting the role of *p53* to be mainly limited to tumorigenesis (15). Although, recently there has been an exponential increase in literature on *p53*'s role in development and stem cell maintenance (Ref), the functions of *p53* are diverse and the most intriguing feature is its role in tumor suppression. Soon researchers started to realize that apoptosis and senescence was triggered even in the absence of *p53* (16-18). Therefore the identification of *p63* and *p73* was very exciting in the field of cancer biology and tumor suppression. Researchers thought these like *p53* could contribute to tumor suppression.

Unlike *p53* these proteins are not frequently mutated in tumors and therefore theoretically could compensate for *p53* loss. Interestingly this was soon found to be not completely true. Both proteins have structural similarities to *p53* in their gene structure. Like *p53* the full length protein has a transactivation domain, a DNA binding domain and an oligomerization domain. Additionally it has a sterile alpha motif domain (SAM) at its C-terminus.

1.2. Phylogeny of *p63/p73*

Although the *p63/73* proteins were identified first in mice, modified forms of these proteins are present in lower organisms (19-21). In fact an ancestor of *p53* has been found in single cell flagellates and in metazoans (20). This ancestral gene resembles *p63/73* more than *p53*. All these members have a SAM domain like *p63/73* (19, 22). The main function of this gene is the protection of the female germ-line in many organisms. This function of *p63/73* has also been conserved in mice as has been demonstrated by the construction of knock-out mouse models. With the evolution of bony fishes, there was a duplication of this ancestral gene and *p63* and *p73* genes evolved as separate genes with their own identities. From bony fishes to amphibians, reptiles and mammals, there is more selection pressure leading to another duplication (23). This time the protein product was expressed in somatic cells and it came to be known as *p53*. In lower organisms like the sea anemone (the gene is called *nvp63*) (24) and fruit-flies (called *dmp53*) (22, 25), the main function of the *p63/73* gene seems to be in guarding the female gamete from DNA damage and induction of apoptosis in case of severe damage in these lower organisms (26). In *C.elegans* this hybrid gene (*CEP-1*) not only protects the germline but also regulates glucose activity and longevity (25). Finally in higher organisms like bony fishes for example zebrafish, amphibians, reptile, birds and mammals this group of hybrid genes gave rise to three distinct family members, *p53*, *p63* and *p73* (23). Each member in the family has individual functions but also overlapping functions. *p53*, *p63* and *p73* ensures germline fidelity. *p63* plays a major role in development in mice. *p73* plays roles in development of the immune system, the neuronal system and also fertility in mice. These members together can induce apoptosis, cell death and have tumors suppressive roles. They are also important in the maintenance of the genomic integrity (27, 28).

1.3. *p63* gene structure

The *p63* gene has 15 exons. This protein was cloned in 1998 for the first time (29-31). In humans it is located at 3q27-29 and in mouse at chromosome 16 between anonymous DNA markers D16Mit1 and D16Mit3 (30). The full-length protein has three main domains, the transactivation domain, the DNA binding domain and the oligomerization domain. Additionally it has a sterile alpha motif domain (SAM domain)(**Figure 1**) (30). The transactivation domain renders the proteins their transcriptional activity, the DNA binding domain helps them to bind to the DNA and the oligomerization domain is important for their interaction within the family members. They can form homo oligomers or hetero oligomers (32). The *p63* proteins belong to the *p53* family of proteins and resembles *p53* protein in most of its domains. It has high resemblance to *p53* in its transactivation domain (25%) DNA binding domain (68%) and the oligomerization domain (35%) (30). The protein has two main isoforms. The full-length protein is called *TAp63*. It retains the N-terminal acidic transactivation (TA) domain (30) and is thought to be transcriptionally the most active form. The N-terminally truncated isoform is known as the $\Delta Np63$ isoform. It lacks the N-terminal domain but can still transactivate targets by a 33 amino acid proline rich N-terminal domain (30, 31). The promoter of *TAp63* is located at exon 1 while the promoter of $\Delta Np63$ is located at an intronic site in a cryptic promoter denoted exon 3'. These proteins have various other spliced isoforms at the C-terminus like α , β and γ . Together there are 6 different *p63* isoforms (**Figure 1**).

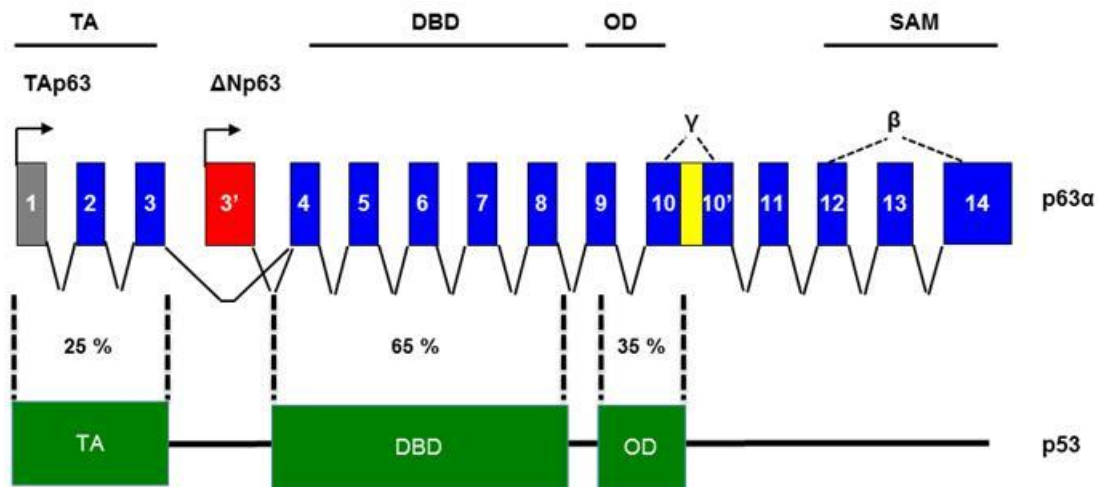


Figure 1: *p63* gene structure and similarity to *p53* gene

p63 gene has four domains, transactivation domain (TA), DNA binding domain(DBD), oligomerization domain(OD) and sterile alpha motif domain(SAM) (present only in the α isoforms). *TAp63* contains all the domains including the transactivation domain (Exon1-3). *ΔNp63* lacks the TA domain, but has an internal promoter within exon 3'. C-terminal spliced variants for both isoforms are marked α, β, γ . Exon1 is non-coding. Domains of the *p53* gene is depicted in green and percent identity is denoted.

Modified and reproduced with permission from the copyright clearance center, p63 steps into the limelight: crucial roles in the suppression of tumorigenesis and metastasis, Nat Rev Cancer. 2013 Feb;13(2):136-43. doi: 10.1038/nrc3446.

1.4. Germline heterozygous *p63* mutations in humans

p63 has been shown to be extremely important in development in organisms. *p63* mutations in humans are heterozygous. In humans, point mutation of this protein causes severe epidermal abnormalities and is associated with various syndromes like cleft lip and palate, limb malformations, ectodermal dysplasia and mammary gland hypoplasia. The different syndromes related to *p63* mutations, that have been described are EEC (ectrodactyly, ectodermal dysplasia and clefting) (33), AEC (ankyloblepharon, ectodermal dysplasia and clefting) (34, 35), LMS (limb-mammary syndrome) (36), ADULT (acro-dermato-ungual-lacrimo-tooth) (37, 38), SHFM (split hand/foot malformation)(39-41), Rapp-Hodgkin's syndrome (42) and Hay-Wells syndrome (43). Many of these mutations in humans phenotypically resemble the *p63* knock-out mouse, albeit with much less severity. Most of these malformations are the cause of mutations in the DNA-binding domain or the SAM domain of *p63*. SAM domains are thought to be important for protein-protein interaction. The functions of the *p63* SAM domain has not been well studied yet. One point mutation has been found in patients with the EEC syndrome. This reduces the transcriptional potential of *p63* due to reduction in DNA binding ability. LMS diseases are characterized by frame-shift mutations in exon 13 and exon14. This leads to a truncated protein, which does not have the TID domain and parts of the SAM domain in the α form of the protein. The β and γ isoforms are unaffected by this truncation. In AEC predominant mutation is in the SAM domain causing loss of protein-protein interaction. In ADULT patients the main isoform affected is the $\Delta Np63$, although there are mutations present in the DNA binding domain as well. Taken together these mutations seemed to be similar to the mutations in *p53*, in which most of the hot-spot mutations are in the DNA binding transactivation domain. (Reviewed in (44))

1.5. Role of *p63* in Human Tumorigenesis

Prior to work from our lab, the role of *p63* in tumorigenesis was not well understood. There is literature which indicates that *p63* is an oncogene (45, 46). In many human tumors *p63* expression has been shown to be increased (47-51). In human head and neck squamous cell carcinomas (45), nasopharyngeal carcinomas (47), urinary tract (52), mammary

adenocarcinomas (53), lung (50) ovarian tumors (54) and prostate tumors (55) *p63* is overexpressed. Interestingly in many metastatic tumors *p63* has been shown to be lost (53, 56, 57). The antibody used in many of these studies does not distinguish between $\Delta Np63$ and *TAp63*. Therefore these studies are difficult to interpret. In some studies, $\Delta Np63$ has been shown to be lost in invasive tumors of the bladder (82% of the invasive bladder carcinomas) (58),(59). In many CML patients *p63* have been shown to have point mutations specifically the the patients who progressed to blast crisis (12%) (60). In some tumors *p63* locus was shown to be amplified (61, 62). Significant progress in sequencing has identified mutations in the *p63* locus from tumor samples. Recently a paper from TCGA demonstrated amplification of the *p63* locus and amplification of specifically $\Delta Np63$ mRNA in lung squamous cell carcinomas (63). Another study showed that atleast 8% of the head and neck squamous cell carcinoma samples carried mutations or amplifications in the *p63* gene (64). *TAp63* has specifically been shown to be lost in metastatic lung and mammary adenocarcinomas (100% of the samples tested from grade IV tumor samples) (59, 65). There is a reduced expression of *TAp63* in high grade head and neck squamous cell carcinomas (65). In all of these studies *p63* have been implicated as an oncogene at times and tumor suppressor at other times.

1.6. The *p63* knock-out mouse models and contradictory phenotypes

Two different groups generated the *p63*^{-/-} mice in 1999. Both these groups demonstrated that the total *p63*^{-/-} mice exhibit developmental defects (30, 66). They had craniofacial abnormalities, cleft palate, limb development defects and defects in the formation of all the different epithelial structures like mammary glands, lacrymal glands and salivary glands. They lack eyelids and tooth primordial (29, 66). The mice in the McKeon lab were generated by replacing exon 6,7,8 and the flanking introns with a neomycin resistant cassette, thereby deleting the DNA binding domain of the protein. Upon detailed analysis Frank McKeon's groups at Harvard found that the embryos at E18.5 days expressed patches of rudimentary epidermis. These cells expressed early basal layer marker like keratin5 and differentiation marker like loricrin (30). Later on they performed clonogenicity assays with the epidermal cells from the thymus of these animals and detected loss of proliferation in these cells (30, 67).

They thus concluded that *p63* is required for the proliferative potential of basal layer of skin and also of the transient amplifying cells (67).

The other mouse model generated in Alan Bradley's lab had a similar phenotype, but upon analysis of the epidermis did not show expression of any of the later differentiation markers. These mice were generated by mutating the *p63* gene using the embryonic cell technology. By this technology they developed two target vectors pTV6H(90) and pTV12E(60). These target the *p63* gene at two different points creating a transcript truncated at exon 6 (Brdm1) which would produce a protein lacking the DNA binding domain and the other vector would generate a recombinant allele that truncates the *p63* mRNA at exon 10 (Brdm2). This transcript would give rise to a protein with intact DNA binding domain, but without the highly conserved 3' region of the *p63* protein (66). In these mice they detected very faint expression of keratin 14 in the single layered epidermis of the newborn mice. They attributed this phenotype to the role of *p63* in the regulation of commitment to stratification. Recently this model has been characterized to be a hypomorph and not a complete null (68-70). Thus the two mice demonstrate contrasting phenotypes muddling the interpretation for the role of *p63* in stem cell maintenance or stem cell differentiation. This led to the path of the development of the isoform specific knock-out mouse models, which could specifically dissect the role for *TAp63* and *ΔNp63*.

1.6.1. *TAp63* knock-out mouse models

One of the major reasons for this difficulty in interpretation of *p63*'s role in human cancer is the existence of multiple isoforms of *p63*. It became evident that in order to truly understand the role of *p63*, isoform specific knock-out mouse models would have to be generated. This was done first in the lab of Dr. Frank McKeon in 2006 (71). This mouse is a total knock-out for *TAp63*. Exon 2 and exon 3 were deleted by insertion of a neomycin cassette. This mouse did not present any phenotypic abnormality (71). *TAp63* expression is very high in the ovary and the oocyte nuclei of the wild-type mice but not in the testis. Therefore to delineate the function of *TAp63* in the female germ line, the mice were irradiated with various doses of radiation at p5. At lower dosage (0.1Gy) no apoptosis was observed in

the in the oocytes. But at higher dosage like 0.45Gy and 4.5 Gy all the oocytes in the primordial follicles died due to apoptosis both in the wild-type and *p53*^{-/-} mice. The *TAp63*^{-/-} mice were resistant to such loss of oocytes, suggesting that *TAp63* and not *p53* is the main mediator of apoptosis in the female germ cells (71).

The other *TAp63*^{-/-} mouse was made by the lab of Dr. Elsa Flores in 2009. This mouse has a deletion in exon 2. These mice have several phenotypic abnormalities. They develop a premature ageing phenotype (72). They exhibit alopecia and kyphosis as early as 6 months of age. Defects in hair regeneration are observed in young mice at 1 month of age. They show reduced hair follicle density. Also these mice have defects in wound healing (72). On further analysis these mice demonstrate a defect in stem cell regulation. The proliferation of stem cells in the dermal papilla and dermal sheath are under the regulation of *TAp63*. These cells are called SKPs (skin precursor cells). The loss of *TAp63* therefore causes them to hyperproliferate initially and then to undergo senescence. This explains the premature ageing in these mice and the defects in wound healing (72).

1.6.2. *ΔNp63* knock-out mouse models

ΔNp63 has been shown to be the predominant *p63* isoform that is expressed in the basal layer of the skin and other tissue epithelium (73). Unlike *TAp63*, the expression of which is hardly detectable in tissue under stress-free conditions, this isoform is expressed at all times. Therefore the hypothesis was that *ΔNp63* is the main player among the two isoforms and most of the phenotypic abnormalities of the total *p63* knock-out mice can be attributed to the loss of this isoform. Recently a *ΔNp63* knock-out mouse model has also been published (74). This model was developed in the lab of Dr. Satrajit Sinha. They substituted exon-3' with a GFP cassette (*ΔNp63*^{gfp/gfp}), which carries the promoter for *ΔNp63* specifically. Thus these mice lose the *ΔNp63* expression while retaining the *TAp63* expression. Phenotypically these mice are similar to the *p63*^{-/-} animals. They develop truncated forelimbs and do not develop hind limbs. They have craniofacial abnormalities, palate formation and defects in epithelial tissue formation. These mice die a few hours after birth. They show defects in stratified epidermis formation (74). Interestingly a more detailed analysis revealed patched of epidermis like

structure covering the embryos at E14.5dpc and E18.5 dpc. Analysis of the epidermis from the E18.5 embryos showed expression of K8 a marker of simple epithelium and K5 a marker of the basal layer of epidermis. These patches expressed keratin 1 and keratin 10, markers of the spinous layer. They also observed expression of other terminal differentiation markers in these patches, like loricrin, involucrin and filaggrin. Surprisingly when they co-stained from keratin 5 and keratin 1 or keratin 10, they observed double positive cells. They thus concluded that these mice exhibit improper accelerated terminal differentiation in the epidermis (74). They also checked for expression of integrins $\alpha 6$, $\alpha 5$ and collagen IV. The expression of all the proteins important in regulating cell adhesion and maintaining cell-cell junction, was low in these mice. To explain the differentiation pattern of the epidermis in these animals, they analyzed the Notch pathway and determined that *ΔNp63* regulates the Notch pathway and that the accelerated differentiation seen in the patches of epidermis in these animals is a result of the activation of the Notch pathway through over expression of Notch 2 and Notch 3(74).

1.7. Role of *p63* in stem cell biology

1.7.1. The Epidermis

The skin is the outermost barrier of the body. This layer protects the organism from loss of water, pathogens and the environmental stresses (75-77). The skin is divided into two major layers; the dermis and the epidermis. The epidermis constitutes of the bottom basal layer, the spinous layer, the granular layer and the cornified layer. The basal layer can be identified by the expression of keratin 5 and keratin 14. The basal layer contains some of the epithelial stem cells. This layer gives rise to all the other layers of the epidermis. The outer layer from the basal layer is the spinous layer. This layer expresses keratin 1/keratin10. The basal layer and the spinous layer together form the Malpighian layer. These two layers give rise to the granular layer. As the name suggests the granular layer is comprised of keratin granules. The granular layer can be identified by its expression of filaggrin. This layer does not divide at all. This layer gives rise to the more differentiated cornified layer. The outermost layer is known as the cornified layer. This layer expresses loricrin or involucrin. All the outermost three layers are generated from the basal layer, which continuously cycles and is

mitotically active. All the layers of the epidermis are well-defined segregate from each other (76, 78).

1.7.2. *p63* and stem cell

p63 is one of the major proteins expressed in the basal layer of skin. The $\Delta Np63$ isoform is predominantly expressed in the basal layer, while *TAp63* is expressed in the dermal sheath and the dermal papillae and also in the hair follicles (72, 79). The McKeon lab investigated the role of *p63* in stem cell maintenance with the help of their total *p63* knock-out mouse. The *p63*^{-/-} mouse developed in their lab has a hypoplastic thymus (67). They analyzed the epithelial cells from the thymus at different embryonic stages and compared their proliferative capacity to that of the wild type. They show that the epidermal cells from the thymus are defective in proliferation. When passaged, they lose the capacity to form holoclones and mainly form paraclones and meroclones signifying the loss of the stem cell population. In comparison epidermal cells from the wild-type thymus forms an increased number of holoclones (67). They immunostained the single layered epidermis from the embryos and as mentioned earlier found that these express both markers of late differentiation like loricrin and involucrin, but not keratin 5, basal cell marker. They therefore concluded the loss of *p63* leads to a defect in stem cell renewal. In wild-type epidermis the stem cells undergo asymmetric division to give rise to transiently amplifying (TA) cells and a multipotent stem cell. These transiently amplifying cells have limited stemness and behave like progenitors. These divide and form the more differentiated cells and more transiently amplifying cells, thus maintaining a sufficient number of TA cells and differentiated cells. In the *p63*^{-/-} embryos, all the stem cells undergo symmetric division giving rise to only transiently amplifying cells, which divide and form the more differentiated cells. In this way they exhaust their proliferation capacity and eventually senesce. The basal cells in the epidermis according to their hypothesis behaves like these TA cells which are absent in the *p63*^{-/-} embryos giving rise to the more differentiated cells (67).

The *TAp63*^{-/-} mice develop a full thickness epidermis. They are born and the median age of survival is 12 months (65, 72). Recently it was shown that *TAp63* is expressed in the

hair follicle stem cell niche in the dermal sheathe and the dermal papillae where skin derived precursor cells reside (72) (**Figure 2**). The loss of *TAp63* causes hyperproliferation in the precursor stem cells and eventually leads to senescence. This causes premature ageing in the *TAp63*^{-/-} mice. Thirty three percent of these mice develop blisters and skin ulcerations by 1 month of age. By 10 months of age eighty six percent of the mice develop kyphosis and alopecia compared to ten percent of the wild-type mice. They also exhibit wound-healing defects due to the loss of proliferation potential of the SKPs (72).

ΔNp63 is the major isoform expressed in the basal layer (**Figure 2**), where it is thought regulate self-renewal capacity of the adult skin stem cells or induce differentiation (30, 79). The role of *ΔNp63* in stem cell regulation is yet to be delineated. The current understanding is that *ΔNp63* regulates differentiation of the skin stem cells and loss of *ΔNp63* causes a loss in a differentiated epidermis, craniofacial and other epithelial defects which induces post-natal death in the *ΔNp63* knock-out mice due dehydration, desiccation and maternal neglect (74).

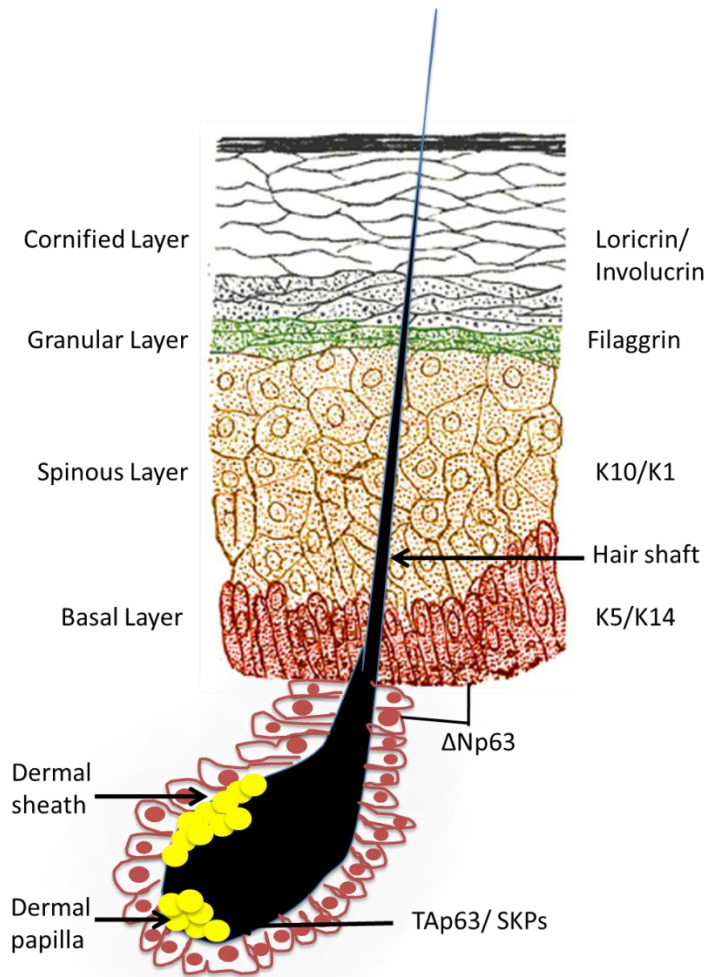


Figure 2: Role of *p63* in stem cell maintenance in the dermis and epidermis

Shown is the structure of the epidermis with basal layer keratin 5/14 (K5/K14), spinous layer expressing keratin10/1 (K10/K1), granular layer expressing filaggrin and cornified layer expressing loricrin and involucrin. The Sox-2 positive hair follicle dermal cells (SKPs) are marked in yellow in the dermal sheath and the dermal papilla. *TAp63* is expressed in these cells. *ΔNp63* is expressed in the basal layer cells. These cells are proliferative and give rise to the top differentiated layers of the epidermis as indicated.

Modified and adapted from [http://en.wikipedia.org/wiki/Epidermis_\(skin\)](http://en.wikipedia.org/wiki/Epidermis_(skin)).

1.8. Stem cells

Stem cells are capable of giving rise to a whole organism. These cells can give rise to all kinds of tissues of the body, skin, heart, lungs, muscle, bone, blood, sperm, egg and others. Stem cells can be derived from the inner cell mass of the blastocyst known as embryonic stem cells. The other types of stem cells are called adult stem cells. These are present in most of the adult tissues including the bone marrow, skin, brain and muscle. Stem cells can participate in wound healing and repair. They divide asymmetrically giving rise to an undifferentiated stem cell and a more differentiated daughter cell. These daughter cells then give rise to the more differentiated cells forming various tissues. This is how a constant pool of stem cells are maintained in the body for times of tissue damage. The stem cells derived from the blastocysts are known as pluripotent cells as each of these cells can give rise to cells of three tissue lineages ectoderm, endoderm and mesoderm. Whereas the adult stem cells may be multipotent (give rise to multiple tissue of one lineage like hematopoietic stem cells), oligopotent (can give rise to only a few cell types of a lineage like myeloid or lymphoid precursors) or unipotent (can differentiate into cells of a specific tissue type, but with limited self-renewal capacity, like transiently amplifying cells of the epidermis) (80).

One of the important characteristic features of stem cells is their property of self-renewal. The two main proteins shown to be crucial in maintenance of this property are *Oct-4* (81) and *Nanog* (82). *Oct-4* (encoded by *Pou5f1*) is expressed at the four cell stage of the embryo and the pluripotent cells (83, 84). It is expressed at high levels in ES cells and its expression is important for the maintenance of self-renewal of these cells (85). *Oct-4* is a transcription factor and regulates expression of downstream targets like *Nanog*, *Utf1*, *Rex1*, *Sox-2*, *Fbx15* and of itself as well (86-89). *Nanog* is another transcription factor important for the regulation of self-renewal and pluripotency (82). Like *Oct-4* it can (88) also regulate the expression of *Rex-1* a self-renewal associated protein (89). It can also regulate the expression of *Oct-4*. *Oct-4*, *Sox-2* and *Nanog* have been shown to be the most important proteins in the maintenance of self-renewal and pluripotency.

Apart from embryonic and adult stem cells, recently a lot of progress has been made in the field of reprogramming differentiated cells into pluripotent stem cells. These are called induced pluripotent cells or iPS cells.

1.8.1. Induced pluripotent stem cells

Recently Dr. John B Gurdon and Dr. Shinya Yamanaka was awarded the Nobel Prize in Physiology or Medicine in 2012 for the discovery of induced pluripotent stem cells (iPS cells). As the name suggests this is a method by which adult cells can be induced to become stem like cells. In 1962 Dr. Gurdon performed an experiment where he took nuclei from the differentiated intestinal cells of tadpoles and transplanted them into the anucleate egg cells of a donor *Xenopus laevis*. Many of these eggs then gave rise to functional feeding tadpoles. Thus he concluded that the nucleus of differentiated cells have all the information in them to differentiate into other types of differentiated cells (90). Since then many scientist have demonstrated that cells can be reprogrammed by nuclear transplantation or cells and nuclear fusion (91). But the proteins inducing these changes remained a mystery until in 2006 Dr. Shinya Yamanaka published a ground breaking paper where they found four specific factors required to reprogram adult differentiated cells (mouse fibroblasts) into undifferentiated stem cells (pluripotent cells), which can then be differentiated into various lineages and even into a complete organism. These four factors are *Oct-4*, *Sox-2*, *Klf-4* and *c-Myc* (92). These pluripotent cells when injected into the blastocysts of a pseudopregnant mouse could give rise to chimeras. They also demonstrated that these cells could contribute to the formation of chimeras. They further published a second paper in 2007 where they demonstrated this was possible with primary human cells as well. Human dermal fibroblasts (HDF), neonatal fibroblasts (BJ cells) and human fibroblast-like synoviocytes (HFLS) can be reprogrammed with the same four factors and induced to pluripotency (93). In the same year another group in the lab of James A. Thomson reported a similar phenomenon. They screened through initial 14 factors and found that over expression of *Oct4*, *Sox2*, *Nanog* and *Lin28* could reprogram human haematopoietic CD45⁺ cells to induced pluripotent stem cells (94). They also performed similar reprogramming assays with the primary human fibroblasts IMR90 (fetal fibroblasts) and postnatal fibroblasts (CRL-2097). Both of these group demonstrated that the iPS cells

generated by these methods were similar to human ES cells in their genetic profile. They express the stem cell markers, *Oct-4*, *Sox-2*, *Nanog*, *Rex-1*, *Lin28*, *Klf-4* and other genes similar to human ES cells. They also expressed stage specific embryonic antigen-3 (SSEA-3) and 4 (SSEA-4) and Tra-1-60 and Tra-1-81, markers of human ES cells (93, 94). They had similar methylation pattern on promoters of certain genes (93, 94). They exhibited active telomerase enzyme and high rate of proliferation similar to human ES cells. They also differentiated into three germ layers when a teratoma assay was performed with these cells (93, 94). Since then there has been an exponential increase in the knowledge base of factors which could make differentiated cells pluripotent.

Since then iPS cells have been made from various cells types like pancreatic β cells, stomach and liver cells, neural stem cells, melanocytes, mature B cells, adipocytes and keratinocytes (95-99). This demonstrates the intrinsic capability of differentiated cells to revert back to a stem like state that can then be induced to differentiate into various other lineages.

Many other researchers have published the use of other downstream targets of these transcription factors in an attempt to delineate the pathway of reprogramming, as this process seems to be largely stochastic. Also the main problem with the use of *c-Myc* and *Klf-4* is that, these are known oncogenes and thus their use in vivo is of major concern. A few such downstream target genes, which have been successful in reprogramming cells in combination are *UTF1*, *Esrrb*, *Sall4* and *Dppa2* (94). The overexpression of these genes have also been shown to be good predictors of reprogrammed cells. These factors can replace *Klf-4* and *c-Myc*. Also the use of retroviral vectors (Yamanaka's group) or lentiviral vectors (James Thomson's group) are not suitable delivery methods as they have been shown to be oncogenic. Thus other groups have tried to design viral free vectors like plasmids {Chou, #542} or mini-circle DNAs (100), non-integrative episomal vectors (101) and excisable viral vectors. The use of transient overexpression plasmids has also been reported. The other ways of avoiding viral vectors are introducing the mRNA for the reprogramming factors or the purified proteins themselves (102). This was successfully done, but resulted in even lower efficiencies. Also there was a problem in selecting the right host for the protein production and the isolation process, as this requires strong chemicals, which could contaminate the proteins and cause toxicity during reprogramming. Transfection of cells with mRNA is a better method, but

entails a lot of time and effort. The cells have to be transduced with mRNA for 17 days. Also the mRNAs may cause strong immune responses in human cells (103).

The method of iPS cells generation from differentiated cells has also been reported to be very inefficient (.001%). In an attempt to overcome such inefficiencies the use of histone modifying enzymes, 5-azacytidine (AZA) and three HDAC inhibitors including suberoylanilide hydroxamic acid, trichostatin A, valproic acid (VPA) (104-106). Most of these are small molecule inhibitors that prevent the DNA from being methylated keeping it in a more open state like that found in ES cells. This has increased the reprogramming efficiency to 1%. In order to increase efficiencies secondary iPS cells have also been made from iPS cells derived differentiated cells. This improves the efficiency of reprogramming from .01% to about 5% {Maherali, 2008 #641}.

1.8.2. Application of iPS cells and associated problems

When James Thomson first isolated human ES cells in 1998, researchers thought this could be another 'magic bullet'. Human ES cells were thought to be able to differentiate into multiple cell types. Therefore multiple incurable diseases like degenerative diseases of the nervous system and muscle could be cured. Although this proved to be true, but there are multiple problems associated with this strategy. First is the challenge to obtain enough adult stem cells from patients. Since adult stem cells are very few in numbers and are very hard to obtain the next choice is to obtain stem cells from normal human embryos. Second is immune rejection of tissues generated from these cells as they are not matched to the recipient's tissue or cell type. Thus in 2006 with the derivation of successful iPS cells from mouse fibroblasts ushered a new era of hope in stem cell therapy. This meant that differentiated cells could be isolated from patients induced to become iPS cells and differentiated into the required tissue type in vitro or vivo. These could then be transplanted back to the patients without risk of immune rejection. Unfortunately the iPS cells that have been derived until now have been shown to be different in the genetic and epigenetic make up from the normally occurring ES cells. Therefore further research is necessary to derive iPS cells which would mimic the ES cells better. In spite of this, iPS cells are being investigated for their potential to differentiate.

Various cell types have been obtained from these iPS cells like neuronal cells, hematopoietic cells, pancreatic β cells capable of secreting insulin, cardiomyocytes, epidermal cells and many others (107-110).

Although there are concerns with transplantation of the differentiated tissues from iPS cells, this has paved way for better disease modeling in vitro. Human primary cell lines are mortal and are hard to culture. Also the immortalized human cell lines have their own mutations and are not suitable to be studied for disease specific cell culture models. Therefore patient specific iPS cells are now being generated to study the effects of various mutations in specific tissue type obtained from these iPS cells. These cell lines may be maintained for indefinite periods of time with only disease specific mutation and minimum other alterations. Examples of the iPS cells made from patient specific tissues are familial dysautonomia, long QT syndrome (111), Parkinson's disease (112), Huntington's disease (113), Down's syndrome (114), Fanconi anemia (115), Sickle-cell anemia (116), beta-thalassemia (117), Type I diabetes (118), SCID or leaky SCID (119), cystic fibrosis (120), retinitis pigmentosa and many others. Some of these diseases do not have appropriate mouse models and many of the existing mouse models do not recapitulate the human disease symptoms. Therefore now with the help of disease specific iPS cells and the tissue derived from them, these diseases can be better studied.

The other important aspect of iPS cell generated tissue is that they can be used for drug testing. This will allow for screening of drugs in these cells. Many drugs exhibit cardiotoxicity. Cardiomyocytes can be derived from iPS cells and screened for such toxic effects.

1.8.3. Role of *p53* in iPS cell

Several proteins have been shown to have an inhibitory effect on reprogramming of adult cells. As murine fibroblasts are passaged they lose their ability to be reprogrammed. On the other hand if *p53* is silenced, then cells which show lack of reprogramming can be reprogrammed (121, 122). Telomerase deficient cells usually cannot be reprogrammed, but silencing of *p53* allows these cells to be reprogrammed. Immortalized cell lines are more amenable to reprogramming than primary cells and with higher efficiencies (about 1%) (121,

123, 124). This provided researchers with a clue that senescence may be the roadblock to reprogramming. Many factors affecting cellular senescence like p16^{Ink4a}, p19^{Arf}, p21, JmjD3 and p53, have been shown to suppress reprogramming (121, 125-127). There is an increase in p53 levels with overexpression of the Yamanaka factors in the cells. This leads to the increase in expression of p53 target genes and p53 mediated growth arrest and apoptosis. Therefore induction of p53 expression is critical in inhibiting the reprogramming process through its mediator p21.

Interestingly cells have been shown to be partially reprogrammed by transient downregulation of p53. These cells are called Gene suppression plastic cells (GSPCs). Researchers observed that when p53 is downregulated with the help of lentiviral shRNA in fibroblasts from Oct4-GFP mice, these cells expressed GFP suggesting expression of Oct4. They also downregulated p53 in normal human keratinocytes and found that these cells phenotypically looked like human ES or iPS cells. They expressed alkaline phosphatase and could be passaged for more than five times and still retained AP staining. These cells could also form neuronal cells when cultured in neuron specific media. When injected into SCID mice these cells gave rise to partially differentiated teratomas showing structures of ectodermal origin. Thus scientists concluded that these cells could not be reprogrammed to a state more undifferentiated than the primitive ectoderm. These cells could also form neurons *in vitro* and *ex vivo* when transplanted into brain slices from mice. They gave rise to nestin positive cells (128).

1.9. Role of the p63 isoforms in tumorigenesis –lessons learnt from mouse models

Eighty percent of all tumors are epithelial in origin. p63 is one of the predominant proteins expressed in the epithelial tissues specifically in the basal layer (73). Therefore its role in tumor suppression and epithelial tissue homeostasis is not surprising. Although it took researchers several years to realize that apart from playing a big part in development, p63 is also involved in the suppression of tumorigenesis. In 2002 Flores et. al. showed that cells and tissues lacking p63 could not induce apoptosis efficiently. There was a defect in the transactivation of some of the target genes like *PERP*, *BAX* and *NOXA*. This was found to be

due to the inability of *p53* to bind to these target genes in the absence of *p63* (129). In 2005, Flores et al. further investigate the tumor suppressive role of *p63* by crossing the *p63* heterozygous mice to the *p53*^{+/-} (130). These mice had a shorter lifespan in comparison to the *p53*^{+/-} mice. Median survival was 7 months for the double mutants in comparison to 10 months in the *p53*^{+/-} mice. Ten percent of the *p63*^{+/-} mice develop squamous cell carcinomas and 20% of the mice developed histiocytic carcinomas by 12 months. The mutant mice for *p63* and *p53* showed a high rate of transitional carcinomas (20%) and mammary adenocarcinoma (10%). Tumors from *p63*^{+/-} mice displayed loss of heterozygosity, a hallmark of tumor suppressors. Interestingly 50% of the *p63*^{+/-}; *p53*^{+/-} mice developed metastatic diseases like squamous cell carcinomas that metastasized to the lung and the heart and also osteosarcomas and rhabdomyosarcomas metastatic to liver and the lung. Seven out of eight of the osteosarcomas were found to be metastatic in the *p63*^{+/-}; *p53*^{+/-} mice compared to only 1 out of 8 in the *p53*^{+/-} mice (130). These mice also developed myelogenous leukemia. These results suggest that *p63* plays a tumor suppressive role in various epithelial tissues (130). Since then several papers have been published on the function of the *p63* isoforms and their role in tumor suppression (65, 131). *TAp63* has been shown to be the main isoform capable of inducing apoptosis and cell cycle arrest in a similar manner to *p53*. The *TAp63* γ and *TAp63* β isoforms are structurally the closest to *p53*. They are also induced after stress and behave like *p53* in many aspects. *TAp63* can transactivate apoptotic, cell cycle arrest and senescence targets like *BAX*, *PUMA*, *NOXA*, *PERP*, *p21*, (129, 132). Recently mutant *p53* was shown to bind to *p63* and sequester it from binding to SMAD proteins and inhibit its suppression on metastasis (133). $\Delta Np63$ on the other hand have been shown to be oncogenic (45, 46). It's over expression in human cancer implicated it as an oncogene, although the data from human tumors is plagued with misinterpretations due to lack of specific antibodies towards these two isoforms. In tissue culture studies $\Delta Np63$ has also been found to behave as an oncogene. $\Delta Np63$ has also been shown to behave as a dominant negative regulator of *p53* and *TAp63*. $\Delta Np63$ also behaves as an oncogene by its dominant negative interaction with *p53* and *TAp63*. The $\Delta Np63$ protein has been shown to bind to these proteins and inhibit them from binding to their target promoters. An alternative model also suggests $\Delta Np63$ binding to the target thereby inhibiting *p53* and *TAp63* from binding to it. Either way it inhibits the transactivation of

apoptotic and senescence targets in this manner. Therefore, in humans, its over expression may be enough to sequester *p53* and *TAp63* causing loss of apoptosis (77). Interestingly $\Delta Np63$ have been shown to be able to transactivate genes involved in DNA repair mechanism suggesting that it too may have tumor suppressive ability (134). $\Delta Np63$ has also been shown to be able to induce p21 and GADD45 (89).

1.10. MicroRNAs

1.10.1. MicroRNA Gene Transcription

MicroRNAs were first discovered in 1993 in the laboratory of Dr. Victor Ambros as small non-coding RNAs important in the regulation of molting in *C.elegans* (135). Since then they have been shown to regulate almost all biological processes. This was the first demonstration that what was thought to be ‘junk’ DNA in eukaryotes was in reality a very important component of cellular RNA make-up. MicroRNAs are a group of small 17-22 nucleotide RNAs which regulate gene expression post-transcriptionally (136). Their role has been most studied in the repression of protein expression in context of both development and diseases. MicroRNAs are often transcribed from their own transcriptome which are mainly present in the intergenic regions (137). Recently they also have been shown to be present in protein coding region of the DNA or the non-coding intronic areas of the genome. They are transcribed by both Polymerase II and Polymerase III enzymes (137, 138). Many of the microRNAs are present in close proximity to one another forming a polycistronic RNA unit. These usually give rise to a polycistronic primary transcript (139). The intergenic microRNAs have their own promoter from where they are transcribed. On the other hand the intronic microRNAs may be under the control of the promoter site of their host mRNA.

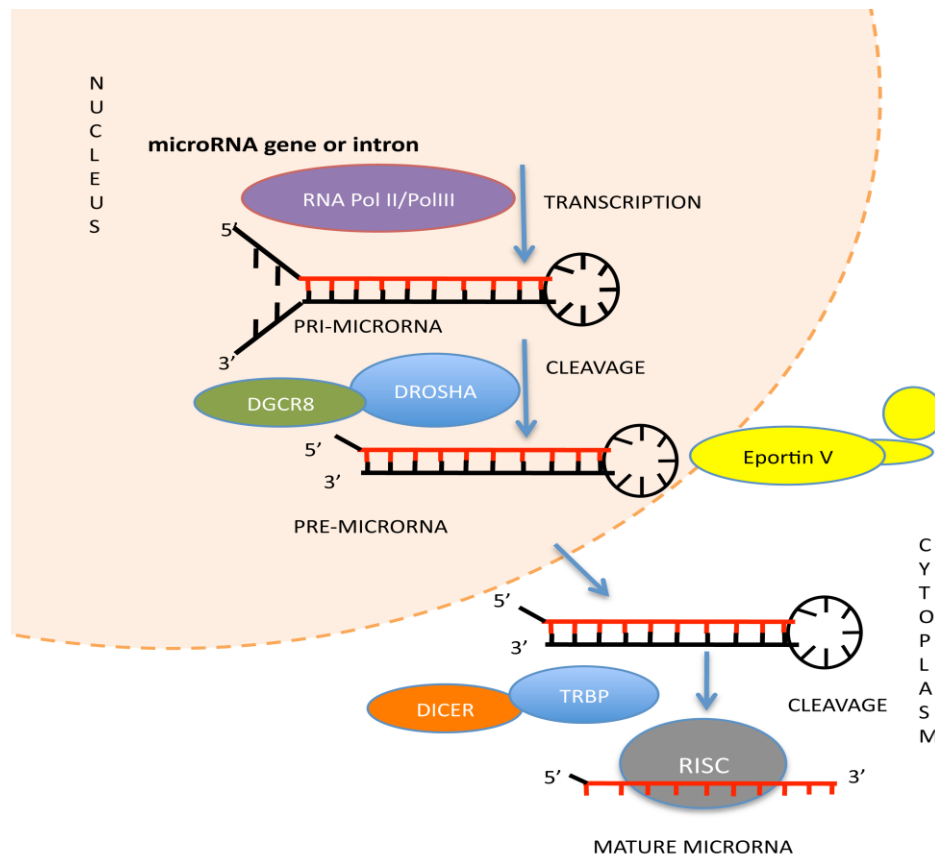


Figure 3: Canonical microRNA biogenesis pathway

The microRNAs are transcribed by RNA polymerase II/III. They form hairpin loop structures which are 2-3Kb in length. They are called primary microRNAs (PRI-MICRORNA). They get cleaved by DGCR8/DROSHA complex in the nucleus to form the precursor microRNAs (PRE-MICRORNA) 70-90 nucleotide in length. They are then transported to the cytoplasm by Exportin V, where are they cleaved by the *Dicer* complex to form the single stranded mature microRNA (MATURE MICRORNA). They are then loaded onto the RISC complex and guided to their target mRNAs (140).

Modified and reproduced with permission from the copyright clearance center, Many roads to maturity: microRNA biogenesis pathways and their regulation, Nat Cell Biol. 2009 Mar;11(3):228-34. doi: 10.1038/ncb0309-228

1.10.2. MicroRNA biogenesis pathway

MicroRNAs are transcribed as primary microRNA or pri-miR in the nucleus by polymerase II and polymerase III (137) (137, 138, 141). These usually have 7-methylguanosine cap and a poly-A tail. These transcripts are several kilobases long and carry a hairpin loop structure (142). This primary transcript is then cleaved by the microprocessor complex in the nucleus made up of Drosha and the DiGeorge's syndrome critical region gene 8 (DGCR8) (142, 143). The Drosha protein is a 160KDa protein, has two tandem Rnase III domain and a double stranded RNA binding domain (dsRBD)(142). The DGCR8 protein is 120KDa. This protein has tandem double stranded RNA binding domain. These domains have been shown to be critical in binding to the primary microRNAs and also in recognizing the primary miR transcripts. The Drosha nuclease cannot cleave the primary transcript in the absence of DGCR8. The precursor miR or pre-miR is a 70-90 nucleotide double stranded RNA molecule that has hairpin-loop structure. It also has a 2-nt 3' overhang (142, 143). This pre-miR gets exported from the nucleus to the cytoplasm by the nuclear transporter exportin V enzyme (144). In the cytoplasm the hairpin loop structure is removed the nuclease called *Dicer* (Rnase III nuclease protein) in coordination with its other partners, HIV-1 transactivation response (TAR) RNA-binding protein (TRBP), PACT and argonaute protein family (Ago1/2) (145, 146). *Dicer* recognizes the 3' overhang in the precursor miR. This produces a miR-miR* duplex with 3' overhangs on both ends. Once the hairpin loop is cleaved by *Dicer* only one strand (guide strand) is loaded onto the AGO protein to form the RISC complex (mi-RISC) (145, 146). Although recent literature has also shown that both the guide strand and passenger strand (miR*) may both be loaded onto to the RISC complex and mediate gene-silencing. These microRNAs are called mature miRs. They are 17-19 nucleotides in length.

1.10.3. Mode of action of microRNAs

These small RNAs bind primarily to the 3'UTR of mRNAs and regulate their silencing in several ways (145). Although recently it has been shown that they can also bind to the 5' end of mRNAs and regulate their expression level (147). The 2-8 nucleotide sequence in the

microRNA are known as the 'seed' sequence. This sequence determines which mRNA will be targeted by which microRNAs based on the complementarity between the 'seed' region and the 3'UTR of the mRNA (148). In animal cells the downregulation of mRNAs by microRNAs is achieved by mRNA deadenylation and degradation, translational arrest or sometimes by mRNA cleavage (149). In most cases the complementarity between the mRNA and microRNA is imperfect leading to a hindrance in translation, but not degradation (150). Usually the mismatches are in the middle of the duplex complex (151).

1.10.4. Role of *p53* in the regulation of microRNA biogenesis

Recently *p53* has been shown to play a role in the regulation of the microRNA biogenesis pathway. First in 2007 Lin He et al found that *p53* can regulate the promoter of the miR-34 family of microRNAs (152). In the same year David Corney et al found that *p53* regulates proliferation and adhesion in *p53*-dependant cell growth by the regulation of miR-34b and miR-34c. This regulation was later shown by many to be important in inhibition of tumorigenesis, metastasis and the induction of apoptosis. Later in 2009 *p53* was found to interact with the p68 helicase protein (153). This protein forms a complex with the Drosha/DGCR8 complex in the nucleus and has been shown to be important in the proper processing of the pri-miRs to the pre-miRs (154). *p53* has since been shown to be very important in the regulation of several other microRNAs by directly binding to their promoters (miR-15a/b, miR-106a, miR-23a, miR-17-5p, miR-25, miR-103), or by regulating them indirectly through their processing in the nucleus from pri-miRs to pre-miRs (miR-103, miR-107, miR-145, miR-182, miR-203) (155, 156).

1.10.5. DGCR8 knock-out mouse phenotype and its role in pluripotency

The DGCR-8 knock-out mouse was created by targeting exon-3 of the DGCR8 gene. This exon next to the exon-4 which codes for the WW domain is required for the proper processing by microRNAs. Deletion of this exon causes a frame-shift and creation several premature stop codons. The ES cells generated by this method were slow growing and drastically defective in differentiation. They retained the expression of some of the

pluripotency related proteins like Oct-4, Sox-2, Nanog and Rex-1 inspite of treatment with retinoic acid. When injected into nude mice, they formed very undifferentiated teratomas with some glandular structures. The ES cells were profiled for microRNA expression. There was a global reduction in precursor and mature microRNAs in these cells (157). This indicated that loss of DGCR8 leads to a defect in proper differentiation although not a complete loss of differentiation.

1.10.6. *Dicer* knock-out mouse phenotype

Dicer1 knock-out mice were created by targeting exon-21 in the *Dicer* gene. This gave rise to ES cells, which lacked *Dicer*. But when injected into blastocysts of pseudopregnant mice no *Dicer* null mice were obtained. On further investigation it was found that the *Dicer* mutant embryos die at E7.5. These embryos showed a decrease in the expression of Oct-4 suggesting premature differentiation of the blastocysts in these mice leading to trophoblast differentiation in these embryos driving lethality (158).

1.10.7. Conditional knock-out mouse model for *Dicer*/DGCR8 specifically in the skin demonstrate a similar phenotype

The *Dicer* and DGCR8 conditional knock-mice (cko) were crossed with mice carrying the K14-Cre ER transgene. The resultant mice had depleted *Dicer* and DGCR8 in their epithelium. Both types of mice were born. But they die at p5 mainly due to dehydration. Their skin showed defects in morphogenesis although all the epidermal layers (basal, spinous, granular and stratum corneum) are present. The pups had very thin skin and evaginated hair follicles. Interestingly the microRNA make-up of the *Dicer* cko skin and the DGCR8 cko skin were distinct. Most of the abundantly present skin microRNAs were not expressed in the skin from both these animals, whereas there were some microRNAs like miR-320 and miR-484 which were present only in the DGCR8 knock-out animals, but not in the *Dicer* knock-out animals. Also miR-21 showed a very high expression in both the cko mice (159).

1.10.8. Role of microRNA in iPS cell generation

MicroRNAs have been reported to drive or assist in reprogramming. Most of these microRNAs have been selected in the basis of their high expression in human ES or mouse ES cells. The miR-302/miR-367 has been shown to be a potent microRNA combination in induction of pluripotency. These microRNAs when overexpressed in mouse and human fibroblast along with treatment of these cells with valproic acid (Hdac2 inhibitor) induces pluripotency (160). These cells express all markers of stem cells and can form chimeras. Another group of microRNA hsa-miR-370 cluster which is homologous to the mouse miR-290 cluster has been shown to be able to induce pluripotency with only three factors (Oct4, Sox2, Klf4) in mouse cells. Many microRNAs have been shown to be downregulated by c-Myc, like miR-21 and miR-29a (161). This event occurs early in reprogramming. These microRNAs are called embryonic stem cell cycle specific microRNAs (ESCC). Certain microRNA have been shown to directly inhibit *p53* or p21. miR-138 repress *p53* expression in mouse cells. MicroRNA clusters 17-92, 106b-25, 106a-363 and 302-367 shares similar seed sequences with ESCC. Therefore these microRNAs are also instrumental in the regulation of cell cycle. As mentioned before down regulation of *p53* and p21 is an important event in the reprogramming process and increases efficiency of reprogramming. MicroRNA like miR-130b, miR-301b and miR-721 targets the transcription factor Meox2. This affects MET and may affect senescence. Most of these microRNAs work in co-ordination with the Yamanaka factors. Except miR-302, miR-367, miR-369 and miR-200. Overexpression of miR-302 and miR-367 by a lentiviral system was shown to induce pluripotency in both human and mouse cells (160). Also another group showed that cells could be reprogrammed by the transient transfection of miR-200c, miR-302 cluster and miR-369 (162).

1.10.9. Role of microRNAs in tumorigenesis and metastasis

Since their first implication in CLL patients, microRNAs have been shown to be intimately involved in tumorigenesis and metastasis. In 2002 Dr. George Calin demonstrated for the first time demonstrated that miR-15 and miR-16-1 locus is at the break point of the

BCR/ABL. In 60% of the chronic lymphocytic leukemia (CLL) patients there was a loss of miR-15 and miR-16-1 (163). MicroRNAs have been shown to be important in tumor suppression and also suppression of metastasis (153). Recently they have been shown to be important in oncogenesis as well. miR-34 family have been shown to be a target of *p53* and has been important in inducing tumorigenesis and apoptosis (152). The main targets of this family are Bcl-2, Cyclin D2, Cyclin E1, c-Myc, MET, E2F3, N-Myc, Sirt-1 and other targets (164, 165). All these proteins are important in the regulation apoptosis, cell cycle, senescence and invasion and migration. Therefore miR-34 inhibits all of these processes, which promote tumorigenesis and metastasis. In many tumor type miR-34a, miR-34b/c expression is reduced or lost mainly by CpG island methylation of its promoter (166). miR-17-miR-92 cluster reduces the tumorigenic levels of E2F1 in lymphomas. There is a global downregulation of microRNAs in several tumors. The let-7 family of microRNAs repress KRAS, NRAS and high mobility group A2 and MYC in lung cancers. miR-15a-miR-16-1 cluster downregulates BCL-2 and cyclinD1 in chronic lymphocytic leukemias, mantle cell lymphomas and prostate cancer. miR-126, miR-335 and miR-206 were found to be downregulated in metastatic breast cancer (167). Their restoration of these microRNAs in breast cancer cells decreased the number of metastases. Their suppression of SOX-4 mediates their ability to reduce metastasis (168). miR-335 have also been shown to reduce expression of tenascin, which is a predominant protein in the microenvironment of many solid tumors (168). Loss of miR-126 has been shown to increase proliferation but not metastasis in breast cancer, whereas in lung cancer it acts by suppressing motility (168). Mir-200 family has been shown to be a major repressor of EMT. They inhibit the main inducers of metastasis Zeb-1, and Zeb-2, by repressing E-cadherin (169, 170). miR-205 represses prostate cancer by the downregulation of protein kinase C. miR-203 has also been to suppress specifically bone metastasis by suppressing Zeb-2, surviving, bmi and bone specific metastatic factor Runx2. miR-146 has been shown to play tumor suppressive roles in breast cancer (inhibits EGFR), prostate cancer and (targets Rock 1) and glioblastoma (targets Notch1). Many of these microRNAs have been downregulated in tumors by the hypermethylation of their promoter or the promoter of the genes locus where they reside.

MicroRNAs also play roles in the induction of tumors. miR-155 has been shown to be overexpressed in several solid tumors and leukaemias and lymphomas . miR-21 in

overexpressed in several tumor types, like pancreatic, gastric, head and neck, breast, lung, lymphomas and glioblastomas. miR-21 regulates PTEN, SERPINB5, TIMP3 and other targets. PTEN is a tumor suppressor and down regulation of PTEN causes increased tumorigenesis (171). miR-26 has been shown to be both tumor suppressive and oncogenic in lymphomas, hepatocellular carcinomas and thyroid carcinoma (172). Overexpression of miR-9 and miR-10 has been implicated in breast cancers (173). miR-9 targets E-cadherin directly inducing an EMT response thereby increasing the invasiveness of tumors. miR-9 has also been shown to be secreted by cancer cells to recruit endothelial cells and increase angiogenesis through the JAK-STAT pathway (174). It has been shown that miR-10b can inhibit HOXD10 thereby inducing the expression of RHOC (173). This leads to an increased invasion in breast cancers.

1.10.10. Expression of *Dicer* in cancers

MicroRNAs have been shown to be downregulated in various types of cancers. Infact recently the global loss of microRNAs is emerging as a hallmark of cancer. Various mechanisms of loss of microRNAs have been described. One of the common one being CpG methylation of the microRNA promoter or the gene promoter where the microRNA is located (253). Apart from this other mechanisms like mutations in the proteins responsible for the processing of microRNAs are also thought to be major contributors to this loss. The proteins like TARBP2, XPO5 (ExportinV) and *DICER1* have been shown to be mutated in various types of cancers (124). Truncating mutations in TARBP2 also causes impaired processing of microRNAs by *Dicer*. This type of abnormality has been shown to be present in the hereditary and sporadic carcinomas with microsatellite instability (MSI). In case of *DICER1*, heterozygous germline truncating mutation of *DICER1* has been shown in pleuropulmonary blastoma-inherited cancer syndrome and hypomorphic somatic mutations have been found to be present in non-epithelial ovarian tumors. Interestingly heterozygous deletion of *Dicer* is further deleterious than the homozygous deletion. This was also demonstrated by Kumar et al in a mouse model for lung cancer. They showed that when *Dicer*^{fl/fl} and *Dicer*^{fl/+} mice were crossed to Kras^{G12D} mice (lung cancer model), the resulting mice treated intranasally with adenoviral -Cre, develop aggressive lung tumors. Curiously the *Dicer*^{fl/+};Kras^{G12D} mice have a

more aggressive tumor phenotype and a reduced survival curve than the *Dicer*^{fl/fl};Kras^{G12D}. This suggests that *Dicer* is a haplo-insufficient tumor suppressor (145).

The *p63* field is filled with contradictory data on the role of *p63* in development, stem cell biology and tumorigenesis. The primary reason for this is the lack of isoform specific-knockout mouse models. There has been a lot of work on the isoforms *in vitro*, which has further led to more contradictory findings on these isoforms. The generation of the isoform specific knock-out mouse models allows us to study the different mode of action of the *p63* isoforms. Although they originate from the same gene, their functions are distinct from one another. Therefore my thesis work focuses on dissecting the roles of these isoforms *in vivo* in stem cell biology, tumorigenesis and metastasis. The common theme of my work focuses on the role of *p63* in regulation of the microRNA biogenesis pathway. For the first time I show that *p63* can regulate the microRNA biogenesis pathway thereby regulating various biological processes.

2. Chapter 2: Materials and Methods

2.1. Genotyping of *TAp63* and $\Delta Np63$ conditional knock-out mice

Genomic DNA was analyzed by PCR amplification to detect the wild-type, *TAp63^{flox}*, and *TAp63^{KO}* alleles using the following primers and annealing temperatures: 1) for wild-type: wt-F, 5' - ACTGGTGAGCTTGTAGAATCGG - 3' and wt-R, 5' - ACTGAGCATATAGGCCTAGCAC, annealing temp: 60°C, 2) for *TAp63^{flox}*: fl-F, 5' - CCACATAGCCATATCTGCC - 3' and fl-R, 5' - TCGCCATAACTTCGTATAGC - 3', annealing temp: 60°C, and 3) for *TAp63^{KO}*: fl-F and wt-R, annealing temp: 60°C. Primers used to genotype for the CRE gene are as follows: Cre-F, 5' - TGGGCGGCATGGTGCAAGTT - 3' and Cre-R, 5' - CGGTGCTAACCAGCGTTTTTC - 3', annealing temp: 60° C. The PCR products were electrophoresed on a 1.2% agarose gel. Genomic DNA from tail biopsies was also genotyped by Southern blot analysis by digesting genomic DNA with AflIII.

Genomic DNA from tail biopsies was genotyped by Southern blot analysis by digesting genomic DNA with BglII or by PCR using the following primers and annealing temperatures: 1) for wild-type: wt-F, 5'- ACAGTCCTCTGCTTTCAGC-3' and wt-R (fl-R), 5'- CACACAGCA CTGGCCTTGC -3', annealing temp: 62°C, 2) for $\Delta Np63^{\text{flox}}$: fl-F, 5' – TTAGGTGGA TCCCTAGGAAGAG - 3' and fl-R (wt-R), 5' – CACACAGCACTGGCCTTGC - 3', annealing temp: 62°C, and 3) for $\Delta Np63^{\text{KO}}$: ko-F, 5'– TACAGCTCCTGGAGGATC CCATGC-3' and wt-R, annealing temp: 62°C. Primers used to genotype for the CRE gene are as follows: Cre-F, 5' –TGGGCGGCATGGTGCAAGTT - 3' and Cre-R, 5' – CGGTGCTAACCAGCGTTTTTC - 3', annealing temp: 60° C. The PCR products were electrophoresed on a 1% agarose gel.

2.2. Generation of $\Delta Np63$ Conditional Knockout Mice

The cre-loxP strategy was used to generate the $\Delta Np63$ conditional knockout allele (*$\Delta Np63^{\text{fl}}$*). Genomic *p63* DNA from intron 3 to intron 3' was amplified from BAC clone DNA (BAC RP23-186N8, Children's Hospital Oakland Research Institute). LoxP sites flanking exon

3' of *p63* and neomycin (*neo*) gene flanked by *frt* sites inserted in intron 3' were cloned into pL253.(175) Mouse embryonic stem cells (ESCs) were analyzed by Southern blot analysis for proper targeting of the $\Delta Np63$ allele. Chimeras resulting from ESC clones injected into C57BL/6 blastocysts were mated with C57BL/6 albino females and genotyped as described below. Mice with germ line transmission of the targeted allele (conditional, flox neo allele, fn) were crossed to the FLPeR mice to delete the neo cassette (176). Resulting progeny were intercrossed with Zp3-Cre (C57BL/6) (177)transgenic mice. $\Delta Np63^{fl/+}$; Zp3-Cre females were mated with C57BL/6 males to generate $\Delta Np63^{+/-}$ mice. The $\Delta Np63^{+/-}$ mice were intercrossed to generate $\Delta Np63^{-/-}$ mice. All procedures were approved by the IACUC at U.T. M.D. Anderson Cancer Center.

2.3. Quantitative Real time RT-PCR

RNA was isolated from keratinocytes or MEFs using the RNeasy kit (Qiagen) followed by quantitative real time PCR for *TAp63* and $\Delta Np63$ using the StepOnePlus real-time PCR system (Applied Biosystems) and iScript™ One-Step RT-PCR Kit with SYBR Green (Bio-Rad) following the manufacturer's protocol. The following primers were used: 1) for $\Delta Np63$: forward, 5'-CAAAACCCTGGAAGCAGAAA-3' and reverse, 5'-GAGGAGCCGTTCTGAATCTG-3' and 2) for *TAp63*: forward 5'-GTGTATGAACCTTCCGAAAA-3' and reverse, 5'- GAGGAGCCGTTCTGAATCTG-3'. GAPDH was used as internal control: forward 5'- TCACCACCATGGAGAAGGC-3' and reverse 5'-GCTAAGCAGTTGGTGGTGCA-3'.

2.4. Generation of mice and tumor analysis

TAp63 mutant mice were intercrossed with *p53* mutant mice to generate compound mutant *TAp63/p53* mice on an enriched C57BL/6 background ((C57BL/6 95%) and (129/SvJ 55%)). $\Delta Np63$ mutant mice were crossed to *p53* mutant mice to generate $\Delta Np63/p53$ compound mutant mice on an enriched C57BL/6 background. For analysis of tumor formation and metastatic disease, 30 mice of each genotype were aged for 2.5 years. Moribund mice

were killed, following the approved guidelines of the IACUC at the University of Texas M. D. Anderson Cancer Center and analyzed histologically by haematoxylin/eosin (H&E) staining as described previously⁸. Tumor-free survival of mice was plotted with PRISM5 software (GraphPad).

2.5. Histology and immunostaining of E18.5 embryos

Pregnant females at day 18.5 of gestation were injected three times at 1 hour intervals with BrdU (100 mg / gram of total body weight). Embryos were extracted 1 hour later and fixed in 10% formalin at room temperature for 18 hours. Fixed embryos were embedded in paraffin, sectioned, and stained with hematoxylin and eosin (H&E) for microscopic analysis. For immunofluorescence (IF), paraffin-embedded sections were dewaxed in xylene and rehydrated using decreasing concentrations of ethanol. Sections were subjected to antigen unmasking in citrate buffer unmasking solution (Vector Laboratory) followed by incubation with blocking solution, and 18 hour incubation at 4°C with the following primary antibodies: K5 (1:1000) (Abcam), K14 (1:500) (LifeSpan BioSciences), K10 (1:1000) (Covance), K1 (1:500) (gift from Dennis Roop), K18 (1:200) (Sigma), and filaggrin (1:1000) (Abcam). Visualization was performed using an anti-rabbit secondary antibody conjugated to Texas-red (1:5000) (Jackson ImmunoResearch Laboratories), an anti-guinea pig secondary antibody conjugated to FITC (1:1000, Jackson ImmunoResearch Laboratories), or an anti-chicken secondary antibody conjugated to Alexa 488 (1:1000) (Molecular Probes) followed by counterstaining with DAPI (Vector Laboratory). Incorporation of BrdU was analyzed using the BrdU detection kit II (Roche). For BrdU analysis by IF, an anti-rabbit secondary antibody conjugated to Texas Red was used with the BrdU detection kit II (Roche). For immunohistochemistry (IHC), paraffin-embedded sections were prepared as described above and incubated with K8 primary antibody (1:80) (University of Iowa) or DGCR8 primary antibody (1:100)(Abcam). Visualization was performed using the Vectastain Elite ABC and DAB Peroxidase Substrate Kits (Vector Laboratory).

2.6. Keratinocyte cells – proliferation assay

1×10^3 $\Delta Np63^{fl/fl}$ and $\Delta Np63^{D/D}$ epidermal cells were plated on mitomycin c (Roche)-treated J2 3T3 feeder cells in F media as described (67, 72, 178, 179). Colonies cultured for 7 days were trypsinized, counted, and plated at limiting dilution 10 cells, 100 cells, and 1000 cells per 6 cm dish. At each passage, dishes were fixed in 10% formalin for 30 min and stained with 2% rhodamine B (Sigma). Some dishes were treated with 10 mM BrdU, fixed in 70% ethanol for 30 minutes, denatured with 0.01N NaOH, and double immunostained with anti-cytokeratin 5 (Abcam) (1:1000) and BrdU-FITC conjugated antibody (GeneTex, Inc.). To detect and visualize cytokeratin 5 staining, Texas Red-conjugated goat anti-rabbit secondary antibodies were used (Jackson ImmunoResearch) (1:500).

2.7. Migration and invasion assay

MEFs, keratinocytes or mouse and human tumor cell lines were resuspended in 500 μ l of DMEM with 10% FBS and penicillin/streptomycin (5×10^4 cells) and added to the top of each chamber containing BD BioCoat cell culture inserts (354578; BD Biosciences) or Matrigel Invasion Chamber (354480; BD Biosciences). Non-invasive cells were removed from the upper chamber. Cells remaining on the membrane were fixed, stained with Diff-Quik (DadeBehring, Inc.), and counted with a Zeiss AxioObserver A1 inverted microscope.

2.8. Mouse and human tumor cell lines

Tumors were excised from *p53* and *TAp63* mutant mice and from $\Delta Np63$ mutant mice at the time of necropsy. Half of the tumor was fixed in 10% formalin and analyzed histologically by H&E staining. The other half of the tumor was minced and treated for 20 min with 0.25% trypsin EDTA solution at 37°C. Cells were suspended in DMEM medium containing 10% fetal bovine serum (FBS) and 13 penicillin/streptomycin. Human primary and metastatic squamous cell carcinomas (cell lines 10A, 10B, 17A, 17B, 22A and 22B) were cultured similarly.

2.9. Immunocytochemistry

Cells were fixed on chamber slides for 30 min at room temperature (25°C) with 4% paraformaldehyde in PBS and incubated in blocking buffer (8% FBS, 0.3% Triton X-100 in PBS) for 30 min at room temperature as described previously. Samples were incubated overnight in anti- γ H2AX (dilution 1:100; Upstate Biotechnology, Inc.) at 4°C under humidified conditions, followed by incubation for 1 h with secondary antibodies (goat anti-mouse Texas Red, dilution 1:500; Jackson ImmunoResearch Laboratories) at room temperature. 4',6-Diamidino-2-phenylindole (DAPI; Pierce Biotechnology) was used as a nuclear counterstain. Photomicrographs were taken with a Zeiss AxioObserver A1 inverted fluorescence microscope.

2.10. Immunofluorescence and immunohistochemistry of tumors

Paraffin-embedded sections of tumors were prepared as described previously⁸. Tissue microarrays containing primary and metastatic HNSCCa (HN242), lung adenocarcinomas and squamous cell carcinomas (LC1005) and mammary adenocarcinomas (BR480) were obtained from US Biomax. For detection of *Dicer*, PCNA and cleaved caspase 3 sections were incubated overnight with anti-*Dicer* (dilution 1:100; Abcam), anti-PCNA (dilution 1:200, Cell Signaling) and anti-cleaved caspase-3 (dilution 1:200, Cell Signaling) at 4°C in a humidified chamber followed by incubation for 1 h with goat anti-mouse-fluorescein isothiocyanate (dilution 1:500; Jackson ImmunoResearch Laboratories) at room temperature for immunofluorescence or using the Vectastain universal ABC Kit (Vector Labs), followed by the DAB kit (Vector Labs) for immunohistochemistry. For detection of *Tap63*, sections were incubated with anti-*Tap63* (dilution 1:100; gift from C.Prives) followed by detection for immunohistochemistry as described above. For detection of γ H2AX in frozen tumor sections, tumours were fixed in 4% paraformaldehyde, frozen in OCT medium (Tissue Tek) and detected by incubation in anti- γ H2AX (dilution 1:100; Upstate Biotechnology, Inc.) followed by incubation for 1 h with goat anti-mouse Texas Red (dilution 1:500; Jackson ImmunoResearch Laboratories) at room temperature. DAPI (Pierce Biotechnology) was used

as a nuclear counterstain for immunofluorescence or haematoxylin (Vector) for immunohistochemistry. Photomicrographs were taken with a Zeiss Axioplan2 imaging fluorescence microscope.

2.11. Human HNSCCs and lung adenocarcinomas

Total RNA was isolated from 25 human HNSCCs and 19 lung adenocarcinomas of various grades (well differentiated (grade I), moderately differentiated (grade II) and poorly differentiated and invasive (grade III)) for qRT-PCR using primers for *TAp63*, *Dicer* and miR-130b as described below. SA-b-gal staining. SA-b-gal staining was performed on frozen sections of tumors as described previously.

2.12. Quantitative Real time PCR

Total RNA was isolated from mouse MEFs, human squamous cell carcinomas and cell lines, or mouse tumors and tumour cell lines by using TRIzol LS Reagent (Invitrogen). qRT-PCR was performed with a StepOnePlus real-time PCR system (Applied Biosystems), a SuperScript First-Strand Synthesis System (Invitrogen) and PowerSYBRGreen PCR Master Mix (Applied Biosystems) in accordance with the manufacturers' protocols. The following primers were used: human *TAp63*(132), human $\Delta Np63$ (132, 180) and murine or human *Dicer*. Murine or human glyceraldehyde-3-phosphate dehydrogenase was used as an internal control. Average cycle threshold (Ct) values were calculated from triplicate reactions of three biological replicates.

2.13. Cytogenetics

Tumor cells at 70% confluence were treated for 3 h with 0.02 mg/ml colcemid and prepared as described previously¹⁹. Images were captured and processed with MetaMorph Premier (Molecular Devices) using a Nikon Eclipse E400 microscope.

2.14. Northern blot analysis

Total RNA was fractionated on a denaturing 15% polyacrylamide gel containing 8M urea, and transferred to Hybond-N1 membrane (Amersham Biosciences) by a semi-dry gel transfer method. Membranes were hybridized with end-labelled [³²P]ATP miRCURY LNA detection probes (Exiqon) in ULTRA hyb-Oligo Hybridization Buffer (Ambion) at 37°C. Membranes were washed twice for 5 min in 23SSC, 0.1% SDS at 37 °C followed by a prolonged wash for 15 min at 25 uC, and then exposed to X-ray film overnight.

2.15. miRNA TaqMan assays

Applied Biosystems TaqMan miRNA assays were used to detect and quantify mature miRNAs using looped-primer real-time PCR. Total RNA samples were prepared from tumor cell lines and MEFs with TRIzol LS Reagent (Invitrogen). Total RNA (1 mg) was used to synthesize complementary DNA with the Two-Step TaqMan MicroRNA Assay kit (Applied Biosystems) in accordance with the protocol. qRT-PCR was performed with the Step One Real Time PCR System, TaqMan PCR master mix, and TaqMan primers for the specific miRNAs (Applied Biosystems). Each sample was run in triplicate. Ct values for miRNAs were calculated and normalized to Ct values for RNU6B.

2.16. MicroRNA overexpression

MicroRNA mimics were bought from Qiagen (miScript). NHEK-sh*INp63* and NHEK-shDGCR8 cells were transfected with either control or microRNA mimics for let-7, miR-141 and miR-203 (20um) in 6-well dish. Media was changed next day and cells were allowed to grow for the next 4 days in keratinocyte specific media. At 2 days and 4 days cells were collected lysed and microRNA Taqman assay was performed and western blot analysis was performed.

2.17. ChIP assay

ChIP was performed with nuclear extracts from wild-type and *p63*^{2/2};ArfG/G keratinocytes as described previously. qRT-PCR was performed with the following primer sequences specific for *p63*-binding sites: murine *Dicer*, 21433, 5'-AGGCTGGCCTTGATCTGTGA-3' (forward) and 21333, 5'-CACATCCTCGGCTGTCTTTCA-3' (reverse); mmu-miR-34a, 1367, 5'-TAGCCAAACAGCCACCATCTT-3' (forward) and 1457, 5'-CCCCAGCCCTCCACAAG-3' (reverse); and mmu-miR-130b, 2850, 5'-CACGTGAGTAACTGGTCTGGGATA-3' (forward) and 2763, 5'-TCCTAACAGATTCTCCTGCCTAGAA-3' (reverse). Primer sequences for non-specific binding sites were as follows: murine *Dicer* promoter, 22560, 5'-CGAACCCAGAGAGTCCACAAG-3' (forward) and 22499, 5'-CCCATCCCCGACACTTAC-3' (reverse); mmu-miR-34a promoter, 1732, 5'-AAGCGGGTTTCAAGTGCATCTCAG-3' (forward) and 1796, 5'-TCAGGCTACTAAACCAGTTGCCCT-3' (reverse); and mmu-miR-130b promoter, 21431, 5'-AAATGTCCCATCCTGGAGGAGCAA-3' (forward) and 21323, 5'-TCACCAAATTAGCGAGGGCTCTGA-39 (reverse). Primers for the *p53*-binding site for miR-34a were used as described previously²³.

Wild type keratinocytes and *ΔNp63*^{-/-} epidermal cells were grown to near confluence on J2-3T3m feeder cells in F media as described previously (72, 179). Feeder cells were removed with 0.02% EDTA 24 hours prior to collecting keratinocytes for chromatin extraction. Cellular proteins were crosslinked to DNA using 1% formaldehyde and chromatin was prepared as described earlier (72, 129, 179). *p63* ChIP analysis was performed using a pan-*p63* antibody (4A4, Abcam) as described previously. Each ChIP was performed in triplicate using keratinocytes from three embryos of each genotype. Q-RT-PCR was performed by using primers specific for the indicated regions of the DGCR8 promoter: Site1 (-3393) - forward 5'-AGTCACCTTGGTGCC TCTCATAG-3' and (-3348) -reverse 5'-AAACAGGTGGCAAGGCTTCTT-3', Site2 (-1459) - forward 5'-CATTTTTTTCTGTGGATCTTTTGGT-3' and (-1397) - reverse 5'-CACAGGGCAGGCAGATCAG-3', and nonspecific site (-3893) - forward 5'-

CAAATCAAAATCTGCATCCATAGG -3' and (-3833) - reverse 5'-GCCCTCCTGCCTGTAAACCT-3'.

Wild-type MEFs and *ΔNp63*^{-/-} MEFs were grown in 10% FBS, DMEM. Cellular protein was cross-linked. ChIP was performed using antibody for total *p63*. qRT-PCR was performed with primers directed towards the *TAp63* promoter region: forward 5'-GCTATAAATGTTTCCATGTGATGGATTGC-3' and reverse 5'-TGCAGACTTAGCTATGGTCTCTTG-3'.

2.18. Lentiviral infection

Lentivirus-based vectors (2 mg) containing shRNAs (SBI System Biosciences) for mmu-miR-34a, mmu-miR-126, mmu-miR-130b or scramble sequence (as control) and tagged with green fluorescent protein (GFP) or pDESTmyc*DICER28* were transfected into 293T cells along with 2 mg of each vector required for lentivirus packaging (pCMV-VSVG, pRSV-REV or pMDLg/pRRE) using Fugene HD (Roche) in accordance with the manufacturer's protocol. After transfection of 293T cells, supernatants containing the lentivirus were collected, filtered and added to target MEF or tumour cells for 24 h in the presence of 8 mg/ml 21 Polybrene. At 24 h after infection, puromycin was added to the media at 3 mg/ml 21 for 7 days. Infection efficiency of the cells was calculated by dividing the number of GFP-expressing cells by the total number of cells, with the use of a Zeiss AxioObserver A1 inverted fluorescence microscope. The infection efficiency was calculated to be 100% in all experiments. Infected cells were analysed by TaqMan assay to determine the level of miRNA silencing. These cells were further analysed by migration and invasion assays. All experiments were performed in triplicate. Retroviral infection (pSuper mouse *Dicer1*). Wild-type and *TAp63*^{2/2} MEFs (10⁶) were infected with pSupermouse *Dicer1* (Addgene) as described previously (181).

2.19. Adenovirus-Cre infection

TAp63^{fl/fl} MEFs (10^6) were plated on 10-cm dishes and infected with 53103 Ad-Cre-GFP (Vector Development Laboratory) particles per cell. Infection efficiency was calculated on the basis of expression of GFP and found to be 98%. To verify recombination, qRT-PCR was performed for *TAp63* mRNA.

2.20. Cloning of dgcr8-luciferase reporter genes

To generate the dgcr8 S luciferase construct, DNA was amplified from wild type mouse genomic DNA (C57BL/6) using primers containing the *p63* binding site shown by ChIP and 5' XhoI and 3' BglII cloning restriction enzyme sites: 1. forward - DGCR8- Luc F: XhoI 5'-CCGCTCGAGGCTTCTAGTTGTCTATTCC-3' and 2. reverse - DGCR8- Luc R: BglII 5'-GGA AGATCTGCTCACCAGATAGCTTGGA -3'. PCR amplicons were digested with XhoI and BglII and ligated into pGL3 basic luciferase reporter vector (Promega). The QuickChange® Multi Site-Directed Mutagenesis kit was used to generate dgcr8 Sm using the dgcr8 S luciferase construct as a template and the following primers: 1. 5'-ATGCCTGTCTAAAGTCACTTTTGTGCCTCTCATAGGCCTG-3', 2. 5'-GCATGTATCTCCTAAGAAGCTTTTCCACCTGTTTACAACACCAG-3', and 3. 5'-TGGTGCCTCTCATAGGCCTGTTTTTATCTCCTAAGAAGCCTTGC-3'.

2.21. Dual luciferase reporter assay

Luciferase assays were performed with *p532/2;p632/2* MEFs as described previously. Briefly, *p53^{-/-};p63^{-/-}* MEFs (129) were plated on 6-well plates (3.5×10^5 cells per well). Twelve hours after plating, the MEFs were transiently transfected using Fugene HD (Roche) with 1 µg of dgcr8 S or dgcr8 Sm, 0.5 µg of Renilla luciferase plasmid (transfection control), and 0.5 µg plasmids encoding the *p63* isoforms [*TAp63α*, *TAp63β*, *TAp63γ*, *ΔNp63α*, *ΔNp63β*, or *ΔNp63γ* or 0.5 µg of empty vector (pcDNA3)]. After 24 hr, cells were harvested and luciferase activity was measured using the Dual-Luciferase Reporter Assay system (Promega)

and a Veritas microplate luminometer (Turner BioSystems). Each experiment was performed in triplicate. To generate the luciferase reporter genes pGL3-*Dicer*, pGL3-miR-130b and pGL3-miR-34a, the DNA fragment containing the *p63*-binding site identified by ChIP was amplified from C57BL/6 genomic DNA by PCR with the following primers containing 5' NheI and 3' BglII cloning restriction enzyme sites: *DICER1*, 5'-GCTAGCATGTGCCAGG GCTTTGGCATGTA-3' (forward) and 5'-AGATCTTCCTGGAAGTTGCTCTGTACACCA-3' (reverse); mmu-miR-34a, 5'-GCTAGCTGGAGTGTGAGCACTTCTGGCTAA-3' (forward) and 5'-AGATCTTGGACATTCAGGTGAGGGTCTTGT-3' (reverse); and mmu-miR-130b, 5'-GCTAGCATGGTTAAAGATGGAGCCGAGGGA-3' (forward) and 5'-AGATCTTCTCCTGCCTAGAAGAGCAGAACT-3' (reverse).

2.22. Western Blot

Total lysates were generated from wild-type and *TAp63*^{-/-} MEFs infected with vector or *Dicer* overexpression plasmid. Western blot was performed on a 7.5% SDS PAGE gel

Total cell lysates were generated from mouse ES, mouse iPS^{Yam}, keratinocytes or skin from E18.5 day embryos. 50 µg of protein were electrophoresed on a 10% SDS PAGE and transferred to PVDF membrane as described previously (72, 179). Blots were probed with anti-*ANp63* (1:1000) (BioLegend), K5 (1:1000) (Abcam), K10 (1:1000) (Covance), filaggrin (1:1000) (Abcam), DGCR8 (1:200) (Abcam), Oct4 (1:1000) (Santa Cruz), Sox2 (1:500) (Santa Cruz), Nanog (1:1000)(Abcam), or *p53* (1:1000)(Vector Labs) at 4°C for 18 hours followed by incubation for one hour at room temperature with the appropriate secondary antibodies conjugated to horseradish peroxidase (1:5000)(Jackson Lab). Actin (Sigma 1:5000) was used as a loading control. Detection was performed using the ECL Plus Kit (Amersham) following the manufacturer's protocol and x-ray autoradiography.

2.23. Normal Human Epidermal Keratinocytes (NHEK) culture and infection

NHEKs (Lonza) were cultured in serum free media containing supplements according to the manufacture's protocol (Lonza). NHEKs were infected with pGIPZ lentiviral vectors

with shRNAs for human *p63* and *DGCR8* (Open Biosystems). Cells were selected for 48 hours with puromycin (2 μ g/ml). Selected cells were subsequently used for the generation of embryoid bodies.

2.24. Cell Culture

Wild type, $\Delta Np63^{-/-}$, $\Delta Np63^{fl/fl}$ keratinocytes were isolated from E18.5 day embryos as described previously (72, 179). Cells were plated on J2-3T3m feeder cells and cultured in F media (Sigma) supplemented with 0.4 mg/ml hydrocortisone, 24 ng/ml adenine, 8.4 ng/ml cholera toxin, 5 mg/ml insulin, 13 ng/ml 3,3,5-triiodo-L-thyronine, and 10 ng/ml EGF as described earlier (72, 178, 179). Mouse ES cells or iPS^{Yam} (S3) cells (gift from Dr. Austin Cooney, Baylor College of Medicine) (182) were cultured on mitomycin treated feeder cells in the presence of ES cell media containing Knockout™ D-MEM(Invitrogen), 20% ESC screened FBS (Hyclone), 200mM L-glutamine (Gibco), 100ug/ml penicillin/streptomycin (Gibco), 0.1mM β -mercaptoethanol(Sigma) and 10ng/ml recombinant mouse Leukemia inhibitory Factor (LIF, Gibco). Human iPS^{Yam} cells (a gift from Dr. Brian Davis, MD Anderson Cancer Center) were maintained on hESC qualified Matrigel (BD Biosciences) following manufacturer's protocol in mTeSR1(Stemcell Technologies) media.

2.25. Immunofluorescence – Cell culture

Mouse iPS^{Yam}, mouse ES, and $\Delta Np63^{-/-}$ epidermal cells were cultured in 24 well dishes on feeder cells. These cells were fixed in 4% paraformaldehyde for 30 minutes and incubated with the following antibodies: SSEA-1(1:200 Developmental Studies Hybridoma Bank), Oct4 (1:100 Santa Cruz), Nanog (1:100 Abcam) for 18 hours at 4°C. Visualization was performed using an anti-mouse secondary antibody conjugated to Texas-red (1:5000) (Jackson ImmunoResearch Laboratories), or an anti-rabbit secondary antibody conjugated to FITC (1:1000, Jackson ImmunoResearch Laboratories) for one hour, followed by counterstaining with DAPI (Vector Laboratory). Human iPS cells were fixed in 4% paraformaldehyde for 30 minutes at room temperature and incubated with SEEA-4 (1:200 Developmental Studies

Hybridoma Bank), Tra-1-60 (1:200 Millipore), Oct4 (1:100 Santa Cruz), Sox2 (1:100 Santa Cruz), Nanog (1:100 Abcam) for 18 hours at 4°C. Secondary antibodies were used as mentioned above and DAPI was used for visualization. Cells were rinsed in PBS and photomicrographs were taken with a Zeiss AxioObserver A1 inverted fluorescence microscope.

2.26. Small RNA Sequencing and Analysis

For small RNA library construction, RNA samples were prepared using the DGE-Small RNA Sample Prep Kit (Illumina, San Diego, CA) as described previously (183, 184). A total of two Solexa-ready small RNA templates were analyzed on an Illumina GA-IIx Genome Analyzer at University of Houston. Cluster generation was performed and clusters were sequenced. Initial sequence process and analysis was followed as described previously (183, 184). Small RNA-Seq sequencing data was uploaded and processed using the Genboree Small RNA Toolset (<http://genboree.org>). The Illumina adapter was trimmed, and reads with length between 11 and 30, a copy number of at least 4, and finishing in monomers with length less than 10, were selected for further processing, similar to the processing described previously (183, 184). The reads were mapped to the mouse genome and build UCSC mm9 (NCBI 37) using Pash 3.0 (185). Reads mapping up to 100 locations were selected for further analysis. The miRNA definitions from miRBase (186-189) were used to construct a known miRNA profile for each sample; the abundance of the known miRNAs were normalized as a fraction of the usable reads. For each species, a combined profile of all samples was computed; miRNA abundance was mean-centered and z-score transformed for each miRNA individually. Principal component analysis was performed using the implementation within the R statistical analysis system. Hierarchical clustering of samples was performed by first computing the symmetrical sample distance matrix using the Pearson correlation between microRNA profiles as a metric. Supervised sample analysis was performed using the t-test statistics, and heatmaps were generated using the heatmap.2 package in R.

2.27. RNA Sequencing and Analysis

Approximately 5 µg of polyA⁺ RNA was used to construct RNA-Seq libraries using the standard Illumina protocol. Mouse and human mRNA sequencing yielded 30-40million read pairs for each sample. The mouse mRNA-Seq reads were mapped using TopHat (190) onto the mouse genome and build UCSC mm9 (NCBI 37) and the RefSeq mouse genes. The human mRNA-Seq reads were mapped using TopHat onto the human genome and build UCSC hg19 (NCBI 37) and the RefSeq human genes. Gene expression and gene expression differences were computed using Cufflinks (190). For each species, a combined profile of all samples was computed; miRNA abundance was mean-centered and z-score transformed for each miRNA individually. Principal component analysis was executed using the implementation within the R statistical analysis system. Hierarchical clustering of samples was executed by first computing the symmetrical sample distance matrix using the Pearson correlation between mRNA profiles as a metric, supervised sample analysis was performed using the t-test statistics, and heatmaps were generated using the heatmap.2 package in R. For gene signatures, we further explored gene enrichment using DAVID and the GSEA implementation at the Molecular Signature Database (MSigD) (191).

2.28. Multi-species analysis of smRNA-Seq and RNA-Seq data

To integrate the smRNA-seq datasets between mouse and human, first we selected the conserved microRNAs between mouse and human; next, we combined the z-score transformed miRNA abundance obtained from the human and the mouse cell types. For integrated mRNA-seq analysis, the z-score transformed mRNA abundance datasets for mouse and human were combined by selecting only the conserved miRNAs. For each resulting dataset, principal component analysis and hierarchical clustering using the Pearson correlation coefficient metric were carried out using the implementations available within the R statistical analysis system.

2.29. Generation of an inducible DGCR8 lentiviral vector

A tetracycline inducible *DGCR8* lentiviral vector was generated by cloning a PCR amplified product from pFLAG/HA-DGCR8 (192). Primers used to amplify the DGCR8 cDNA were as follows: FOR –GGATCCCATGGAGACAGATGAGAGC, REV –GAATTCGGTGCACAGGGGCTCAC. The resulting PCR product was cloned into the EcoRI sites in the pLVX-Tight-Puro vector (Clontech).

2.30. Southern Blot Analysis of mouse $\Delta Np63^{-/-}$ epidermal cells and iPS^{Yam} cells

Genomic DNA was extracted from mouse iPS cells generated using the Yamanaka factors (miPS^{Yam}) and $\Delta Np63^{-/-}$ epidermal cells, digested with EcoRI, and separated on a 0.7% agarose gel. Hybridization was performed as described previously (72) using a probe for Klf4 amplified from miPS^{Yam} DNA using forward primer 5'-GCAGCCACCTGGCGAGTCTGA-3' and reverse primer 5'-GAGCCCTCCACCTGTGTTGCT-3'.

2.31. Calculation of Timing and Efficiency of Reprogramming

1×10^5 normal human epidermal keratinocytes (NHEK) were plated on 6 cm dishes coated with 0.1% gelatin and infected for 48 hours with the following lentiviruses: shTRP63-pGIPz (Open BioSystems), shDGCR8-pGIPz (Open BioSystems), or OKSIM (Addgene) (182). On day 3, ES cell media was added to the cells. The cells were fixed with 4% paraformaldehyde on day 6, 8, and 14 to determine the timing of reprogramming by immunofluorescence staining with Oct-4 (Santa Cruz; 1:100), Tra-1-60 (Millipore; 1:200) or Nanog (1:100; Abcam) antibodies. DAPI (Vector Laboratory) was used as counterstain. To determine percentage of reprogramming efficiency the cells were fixed at days 8 and 14 and visualized by immunofluorescence using the antibodies listed above. Photomicrographs were taken with a Zeiss AxioObserver A1 inverted fluorescence microscope at 10x magnification. Percent efficiency was calculated by counting Tra-1-60 positive colonies, dividing by 1×10^5 cells, and multiplying by 100.

2.32. Teratoma Formation Assay

$\Delta Np63^{-/-}$ epidermal cells were infected with the tet-inducible *DGCR8* vector and the pTet-On Advanced vector (Clontech) as described previously (193). Severe combined immunodeficiency disease (SCID) mice were injected subcutaneously in the dorsal flank with a wild-type mouse ES cells or $\Delta Np63^{-/-}$ epidermal cells transduced with the tet-inducible *DGCR8* vector as described previously (92). Mice were administered 2 mg/mL doxycycline in the drinking water to induce expression of DGCR8, 3 weeks post injection after palpable tumors had formed. Another group of mice were administered water without doxycycline as controls for the same amount of time. Tumors were harvested 6 weeks after injection and fixed in 10% formalin. Paraffin embedded cross-sections were analyzed by hematoxylin and eosin staining and IHC using antibody for DGCR8 (1:250)(Abcam). Visualization was performed using the Vectastain Elite ABC and DAB Peroxidase Substrate Kits (Vector Laboratory). For immunofluorescence (IF), paraffin-embedded sections were rehydrated in xylene and decreasing concentrations of ethanol. Sections were subjected to antigen unmasking in citrate buffer unmasking solution (Vector Laboratory) followed by incubation with blocking solution, and 18 hour incubation at 4°C with the following primary antibodies: Nestin (1:50 Millipore), AFP (1:100 Santa Cruz), Brachyury (1:50 Santa Cruz). Visualization was performed using an anti-mouse secondary antibody conjugated to Texas-red (1:5000) (Jackson ImmunoResearch Laboratories), an anti-rabbit secondary antibody conjugated to FITC (1:1000, Jackson ImmunoResearch Laboratories) or an anti-goat secondary antibody conjugated to Texas-red (1:1000, R&D Systems) for one hour, followed by counterstaining and mounting in Vectashield with DAPI (Vector Laboratory). Teratomas from normal human epidermal keratinocytes (NHEK) transduced with sh $\Delta Np63$ cells were performed by Applied StemCell, Inc. NHEK-sh $\Delta Np63$ and NHEK-sh*DGCR8* cells were grown on feeders in ES cells media. 1×10^6 cells were injected into the testes or the kidney capsule of SCID mice. Tumors were then fixed in 10% formalin, embedded in paraffin, cross-sectioned, and analyzed by H&E. Immunofluorescence was performed on paraffin embedded sections following rehydration and antigen retrieval (Vector Laboratories) as mentioned earlier. The slides were blocked for an hour in blocking solution (Vector Laboratories) and incubated for 18 hours at 4°C with the following primary antibodies: AFP (1:100, Santa Cruz), brachyury (1:50, Santa

Cruz), K5, (1:200, Abcam), E-cadherin, (1:100, Abcam). Visualization was performed using anti-mouse Texas red or FITC (1:1000, Vector Laboratories), anti-rabbit Texas red or FITC (1:5000, Vector Laboratories) and anti-goat Texas red antibody (1:1000, R&D Systems). Counterstaining and mounting was performed using Vectashield with DAPI (Vector Laboratory).

2.33. Generation and analysis of chimeric mice

$\Delta Np63^{-/-}$ cells (12-18 cells) expressing pLenti-GFP (Vector Development Laboratory, Baylor College of Medicine) or iPS^{Yam} (S3) cells (12-18 cells) expressing eGFP (194) were injected into albino B6 blastocysts and implanted in CD-1 pseudopregnant mice. Embryos at E18.5 were analyzed for GFP expression using a Zeiss SteREO Lumar, V12 microscope, with fluorescent and bright field capability. Non-chimeric E18.5 day embryos were used as negative controls. The embryos were fixed in 10% formalin, embedded in paraffin, and immunofluorescence was performed on cross-sections using an anti-GFP antibody.

2.34. Raft culture

Human immortalized keratinocytes (BC-1-Ep/SL) were grown as described previously. Skin raft culture was performed as described previously (195). Collagen was mixed with human fibroblasts was layered onto an insert of a well. The collagen was allowed to solidify. Keratinocytes were plated onto this collagen plug and cultured in a submerged culture for 3-4 days. The insert is lifted and placed on a support grid with media in the bottom chamber for 14 days. The raft is then fixed in 10% formalin and stained (195).

3. Chapter 3: TAp63 suppresses metastasis through coordinate regulation of *Dicer* and miRNAs

3.1. Introduction

MicroRNAs have been shown to be very important in the regulation of metastasis. Several microRNAs like *miR-126*, *miR-10b*, *miR-34a*, *miR200* –family play critical role in the regulation of mammary, lung, prostate, ovarian, colorectal and other types of cancer metastasis and in EMT (initiation of metastasis)(196-204). In many cancers the expression of these microRNAs are lost(205-207). Recently *p53* was found to transcriptionally regulate *miR-34a* (164, 165). Also *p53* has been shown to regulate the microRNA biogenesis pathway by binding to p68 and p72 thereby affecting pre-miR biogenesis(154, 208). Drosha is a critical component in the cleavage of the primary microRNAs in the nucleus along with DGCR8 that processes them into precursor microRNAs (141, 209). p68 and p72 have been shown to be associated with Drosha/DGCR8 microprocessor complex in the nucleus (210). The loss of these proteins cause a downregulation in the processing of pri-miR to pre-miR by thirty five percent.

p63 being a *p53* family member has been shown to be important in development, senescence and tumorigenesis (65, 74, 79). There are conflicting data on whether it is a tumor suppressor or an oncogene primarily due to the presence of the two isoforms of *p63*, which play significantly different roles. *TAp63* has been shown to be important in the regulation of the stem cell compartment and *ΔNp63* has been shown to be important in development (72, 74, 211). In the context of tumorigenesis their roles have not yet been clearly delineated. Most of the *in vitro* cell culture based assays indicate *TAp63* to be a tumor suppressor (211) and *ΔNp63* to be an oncogene (212). *p63* protein has also been shown to be highly expressed in various types of human tumors (50). However the roles of these isoforms have never been tested *in vivo*. The construction of the total *p63* knock-out only added more confusion to the field. This mouse lacks both the isoforms of *p63* and has severe developmental defects (29). Owing to the lack of epithelium formation these mice die postnatally a few hours after birth from dehydration and desiccation.

Thus it became imperative to generate mouse models, which lack these individual isoforms of *p63*. Because these two isoforms of *p63* have their own promoters and transcription start sites, it was possible to generate the *TAp63* knock-out mouse model which

retained the expression of the $\Delta Np63$ isoforms (65). The *TAp63* knock-out mice showed skin defects. It demonstrates skin erosions, blisters, ulcerations and wound healing defect, all indications of a premature ageing phenotype (72). These mice are highly tumor prone and develop metastatic carcinomas. In this chapter we investigate the role of *TAp63* in tumorigenesis and metastasis. We show that *TAp63* regulates microRNA expression by the transcriptional regulation of *Dicer*. *TAp63* also regulates *miR-130b* by transcriptional activation of their promoter sites. We show both these regulations to be important in mouse carcinomas and human lung adenocarcinoma, mammary adenocarcinoma and head and neck squamous cells carcinoma metastasis. In humans high grade tumors lose *TAp63/Dicer/miR-130b*. We also show that introducing *TAp63*, *Dicer* and *miR-130b* in murine and human metastatic cells and tumor cell lines reduces the metastatic potential of these cells and cell lines.

3.2. Results

3.2.1. *TAp63* mutant mice develop highly metastatic tumors

To delineate the role of *TAp63* in tumorigenesis and to determine whether it behaves like a tumor suppressor or an oncogene, a cohort of mice was generated with 30 mice for *TAp63*^{-/-}, 30 for *TAp63*^{+/-} and 30 for wild-type and aged them for 2.5 years analyzing them for spontaneous tumors. Both these cohorts developed highly metastatic tumors and had a reduced life span when compared to the wild-type cohort (**Figure 4A**). The *TAp63*^{-/-} mice died at a median age of 23 months and the *TAp63*^{+/-} mice died at a median age of 17 months (**Figure 4A**). These mice developed highly metastatic sarcomas and carcinomas to the lung, liver, bone and even to the brain, a rare occurrence in tumor mouse models. Shown is an example of a *TAp63*^{-/-} mouse with a highly metastatic mammary adenocarcinoma (**Figure 4B**) which metastasized to the lung (**Figure 4C**), liver (**Figure 4D**) and brain (**Figure 4E**). Interestingly 10% of the *TAp63*^{-/-} mice develop mammary adenocarcinomas, which metastasize to the brain.

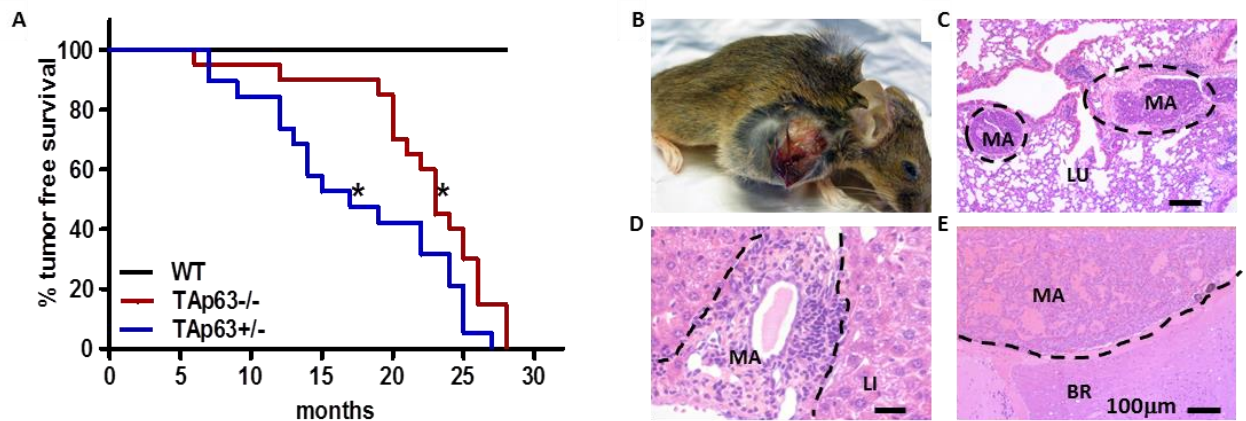


Figure 4: *TAp63*^{-/-} mice develop metastatic tumors

A) Tumor free survival curves of wild-type (WT), *TAp63*^{+/-} and *TAp63*^{-/-} mice; n= 30 and p≤0.05. **B)** Mammary adenocarcinoma in a *TAp63*^{-/-} mouse. **C)** Metastatic mammary adenocarcinoma to the lung (LU), **(D)** liver (LI) and **(E)** brain (BR). Bar in panel E denotes 100μm.

Reproduced with permission from the copyright clearance center, TAp63 suppresses metastasis through coordinate regulation of Dicer and miRNAs, Nature. 2010 Oct 21;467(7318):986-90. doi: 10.1038/nature09459.

3.2.2. Histological analysis of the tumors from *TAp63*^{-/-} and *TAp63*^{+/-} mice demonstrate a diverse profile

Since *p63* has been shown to be important in the maintenance of the integrity of the epithelium (72), it was not surprising to find that the *TAp63*^{-/-} and the *TAp63*^{+/-} mice developed a high percentage of carcinomas (animals analyzed, n=30 from each cohort). They also developed sarcomas and lymphomas. 46% of the *TAp63*^{-/-} mice developed various types of carcinomas of the lung, mammary gland, liver and transitional cell (**Figure 5**). 26% of the mice developed sarcomas of various types including osteosarcoma, histiocytic sarcoma and rhabdomyosarcoma (**Figure 5 and Table 1**). A very small percentage (5%) developed lymphoma. Similar percentage of the *TAp63*^{+/-} mice developed similar types of carcinomas and sarcomas. A greater number of mice (10%) developed lymphomas. Paradoxically a higher number of the *TAp63*^{-/-} mice lived tumor free (about 24%) compared with the *TAp63*^{+/-} mice (15%) (**Figure 5 and Table 1**).

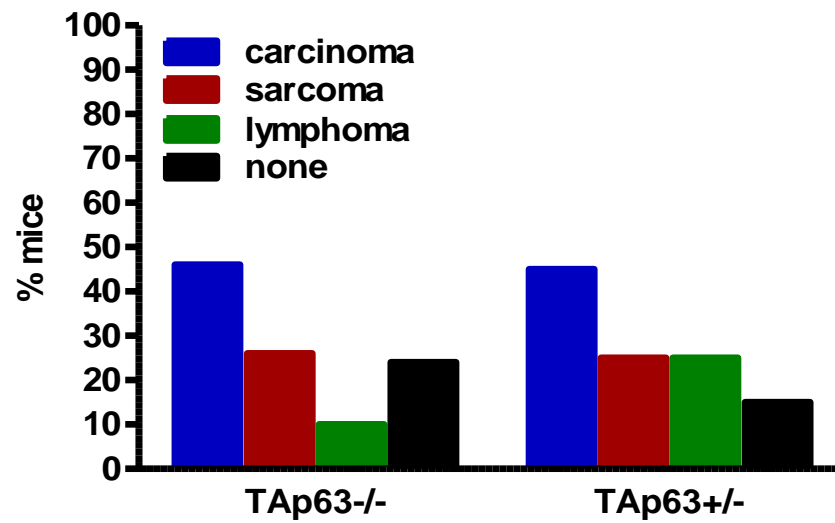


Figure 5: Tumor spectrum of *TAp63* mutant mice

Percentage of carcinomas (blue), sarcomas (red) and lymphomas (green) in the *TAp63*^{-/-} and the *TAp63*^{+/-} mice. Black bar denotes percentage of mice without tumors; n=30.

Reproduced with permission from the copyright clearance center, TAp63 suppresses metastasis through coordinate regulation of Dicer and miRNAs, Nature. 2010 Oct 21;467(7318):986-90. doi: 10.1038/nature09459.

3.2.3. *TAp63* is a haploinsufficient tumor suppressor

Interestingly we found that the *TAp63*^{+/-} mice had a higher incidence of metastatic tumors. Both the *TAp63*^{-/-} and *TAp63*^{+/-} developed equal percentage of metastatic carcinomas (73% and 80% respectively) but a higher percentage of the sarcomas metastasized in *TAp63*^{+/-} mice (100%) compared to the *TAp63*^{-/-} (60%) (**Figure 6A**). Additionally the proportion of mice with multiple tumors was greater in the *TAp63*^{-/-} cohort (50%) compared to the *TAp63*^{+/-} cohort (12%) (**Figure 6B**). In agreement to their tumor make-up the *TAp63*^{+/-} mice also had a shorter life span suggesting that *TAp63* acts as a haploinsufficient tumor suppressor. We analyzed the sarcomas (n=10) and carcinomas (n=10) from these mice and found that they did not present loss of heterozygosity for *TAp63* and retained the wild-type allele (**Figure 6C**). These data taken together suggests that *TAp63* is a haploinsufficient tumor suppressor gene and heterozygous loss of *TAp63* is more deleterious than complete loss of this gene.

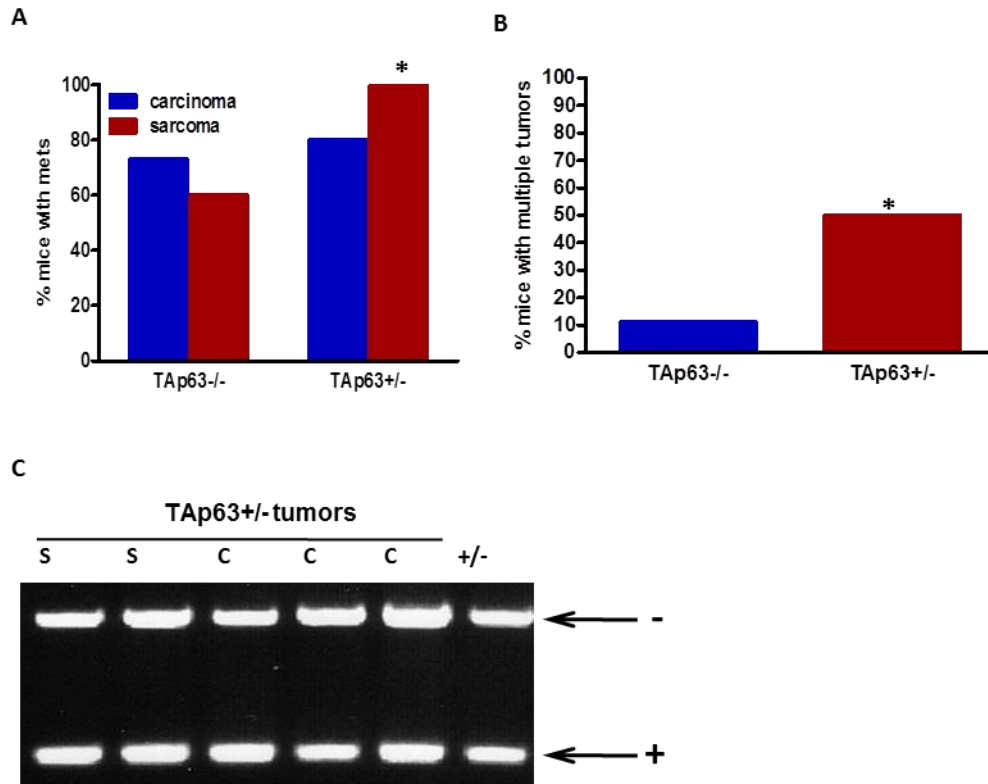


Figure 6: *TAp63* is a haploinsufficient tumor suppressor

A) Percentage of mice with metastatic sarcomas and carcinomas of the indicated genotypes; n=30. **B)** Percentage of mice with multiple malignancies. **C)** Loss of heterozygosity in sarcomas (S) and carcinomas (C) from the mice of the indicated genotypes; n=10. Asterisk indicates statistical significance, p value ≤ 0.05 .

Reproduced with permission from the copyright clearance center, TAp63 suppresses metastasis through coordinate regulation of Dicer and miRNAs, Nature. 2010 Oct 21;467(7318):986-90. doi: 10.1038/nature09459.

3.2.4. *TAp63/p53* double mutant mice have a tumor profile that is distinct from the *p53* mutant mice

The *p53*^{-/-} and *p53*^{+/-} mice were shown to develop non-metastatic tumors. In human tumors both *p53* and *p63* has been shown to be mutated many a times (130). Also mutant *p53* can act in a dominant negative manner over *p63* by binding to and inactivating *p63* (213). To understand the co-operation between *p53* and *p63* in tumors we generated six cohorts of mice, 30 each: *TAp63*^{-/-};*p53*^{+/-}, *TAp63*^{+/-};*p53*^{+/-}, *TAp63*^{-/-};*p53*^{-/-} and *TAp63*^{+/-};*p53*^{-/-}. Cohorts of *p53*^{+/-} and *p53*^{-/-} mice were also generated as controls. These mice were aged for 2.5 years and analyzed for spontaneous tumors (**Table1**). The *TAp63/p53* compound mutant mice developed high numbers of metastatic tumors in contrast to the *p53* mutant (*p53*^{+/-} and *p53*^{-/-}) mice which did not display any metastases (**Figure 7A-F and Table 1**). While 80% of the *p53*^{+/-} mice developed sarcomas and 20% of these mice developed lymphoma, only 55% of *TAp63*^{-/-};*p53*^{+/-} mice developed sarcomas and 11% developed thymic lymphoma (**Figure 7G**). However 60% of the *TAp63*^{-/-};*p53*^{+/-} mice developed carcinomas, including lung adenocarcinoma (15%) and mammary adenocarcinomas (10%), squamous cell carcinomas (SCC) (15%), and transitional carcinoma (10%) (**Figure 7G**). Although the *TAp63*^{+/-};*p53*^{+/-} mice has a similar tumor spectrum to the *TAp63*^{-/-};*p53*^{+/-} mice, the sarcomas from these mice were significantly more invasive and metastatic (88%) than those in the *TAp63*^{-/-};*p53*^{+/-} cohort (14%). In contrast, the carcinomas in the *TAp63*^{-/-};*p53*^{+/-} cohort were more metastatic (44%) than those in the *TAp63*^{+/-};*p53*^{+/-} cohort (29%) (**Figure 7H**).

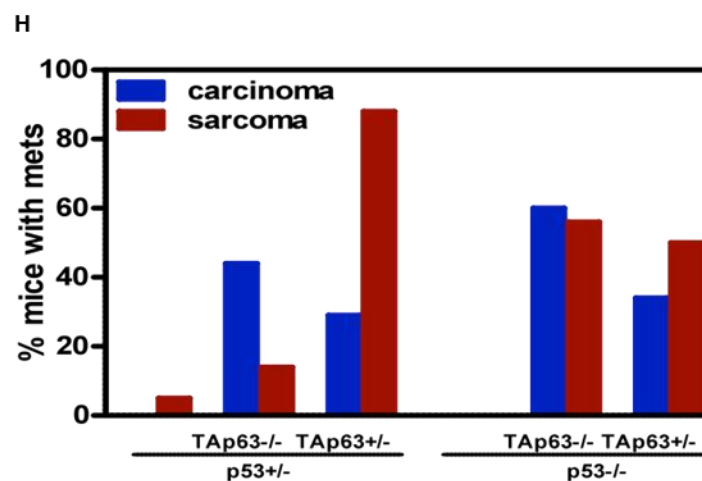
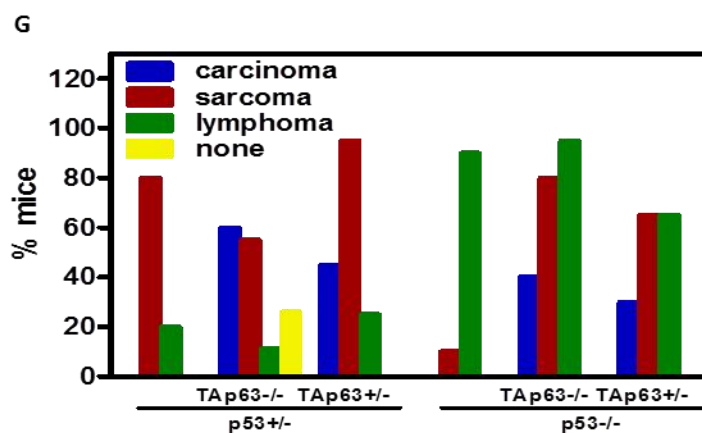
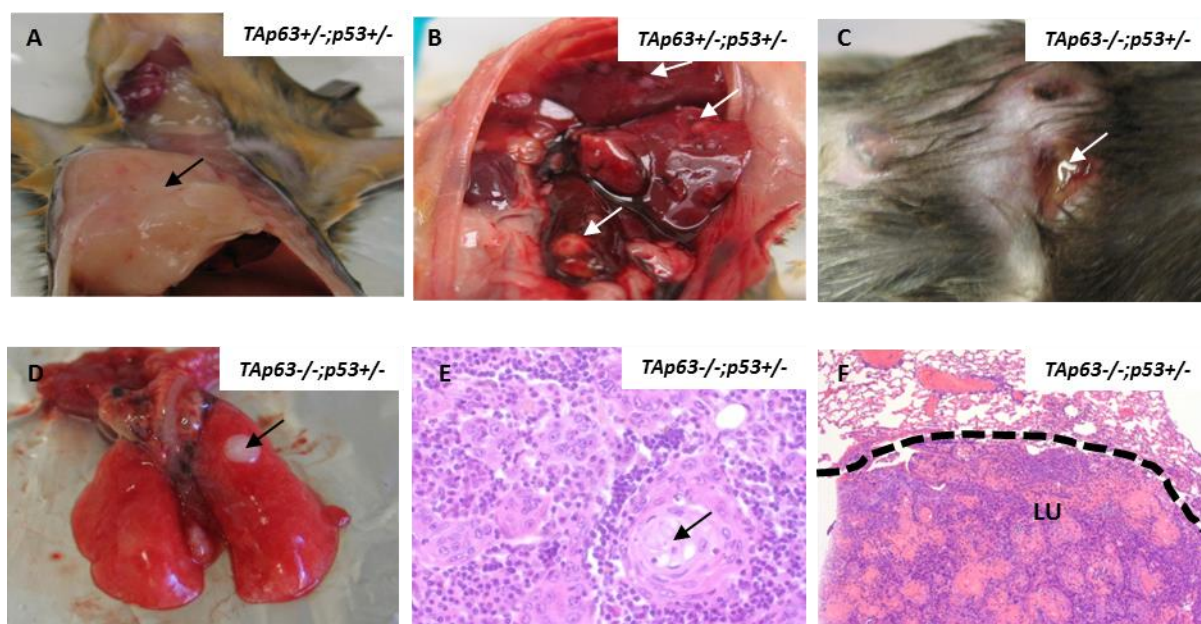


Figure 7: *TAp63/p53* double mutant mice have a distinct tumor profile from the *p53* mutant mice

A & B) Metastatic rhabdomyosarcoma **C)** Metastatic squamous cell carcinoma of the skin (SCC) metastasized to the lung, (LU) **(D & F)** and lymph nodes **(E)** of a *TAp63*^{-/-};*p53*^{+/-} mouse. **G)** Percentage of mice of the indicated genotypes with carcinomas (blue), sarcomas (red), lymphomas (green). Yellow bar indicates percentage of mice without tumors; n=30. **H)** Percentage of mice of the indicated genotypes with multiple metastatic carcinomas (blue) and sarcomas (red); n=30. Asterisks indicate significance, pvalue ≤0.05.

Reproduced with permission from the copyright clearance center, TAp63 suppresses metastasis through coordinate regulation of Dicer and miRNAs, Nature. 2010 Oct 21;467(7318):986-90. doi: 10.1038/nature09459.

3.2.5. *TAp63* does not undergo LOH in the *TAp63/p53* double mutant mice tumors

We examined the *TAp63/p53* double mutant sarcomas and carcinomas for the loss of heterozygosity in *TAp63* and *p53* in order to determine whether they lose their wild-type allele. We examined sarcomas (n=10) and carcinomas (n=10) from the *TAp63*^{+/−};*p53*^{+/−} mice and found that they retain the wild-type allele of *TAp63* (**Figure 8A**). We also examined the same tumors and *TAp63*^{−/−};*p53*^{+/−} tumors for the loss of the *p53* wild-type allele. We found that 1 out of 10 sarcomas exhibit loss of the *p53* wild-type allele in the *TAp63*^{+/−};*p53*^{+/−} tumors. A somewhat higher percentage of tumors from the *TAp63*^{−/−};*p53*^{+/−} sarcomas (1 out of 8) and carcinomas (1 out of 8) lost the *p53* wild-type allele. This indicates that there is an increase in selection pressure to lose the *p53* allele in the complete absence of *TAp63* (**Figure 8B**).

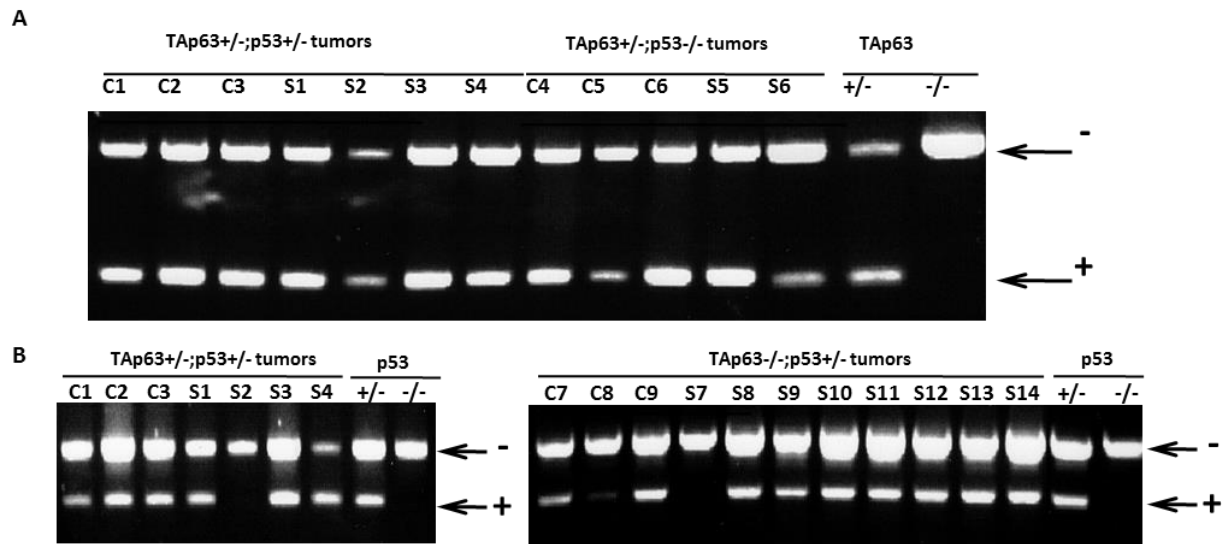


Figure 8: *TAp63* does not undergo LOH in *TAp63/p53* double mutant tumors

A) PCR analysis for the loss of *TAp63* from the tumors of the indicated genotype (n=10). **B)** PCR analysis for LOH of *p53* in these tumors (n=10).

Reproduced with permission from the copyright clearance center, TAp63 suppresses metastasis through coordinate regulation of Dicer and miRNAs, Nature. 2010 Oct 21;467(7318):986-90. doi: 10.1038/nature09459.

Table 1: Tumor landscape of the *TAp63/p53* mutant mice

Tumor	WT	<i>TAp63</i> ^{-/-}	<i>TAp63</i> ^{+/-}	<i>p53</i> ^{+/-}	<i>TAp63</i> ^{+/-} ; <i>p53</i> ^{+/-}	<i>TAp63</i> ^{-/-} ; <i>p53</i> ^{+/-}	<i>p53</i> ^{-/-}	<i>TAp63</i> ^{+/-} ; <i>p53</i> ^{-/-}	<i>TAp63</i> ^{-/-} ; <i>p53</i> ^{-/-}
osteosarcoma	0%	10%	10%	25%	55%	45%	0%	5%	10%
histiocytic sarcoma	0%	4%	5%	20%	20%	0%	5%	5%	10%
angiosarcoma	0%	8%	5%	10%	10%	0%	5%	35%	25%
rhabdomyosarcoma	0%	4%	5%	25%	10%	10%	0%	20%	35%
lymphoma	5%	10%	10%	20%	25%	20%	90%	65%	95%
lung adenocarcinoma	0%	22%	25%	0%	10%	15%	0%	0%	5%
lung adenoma	0%	4%	0%	0%	10%	0%	0%	0%	0%
mammary adenocarcinoma	0%	8%	10%	0%	5%	10%	0%	15%	5%
mammary hyperplasia	0%	0%	0%	0%	0%	0%	0%	0%	5%
hepatocellular carcinoma	0%	12%	0%	0%	0%	0%	0%	0%	0%
squamous cell carcinoma	0%	2%	10%	0%	20%	15%	0%	15%	10%
transitional cell carcinoma	0%	2%	0%	0%	10%	10%	0%	0%	0%
intestinal adenocarcinoma	0%	0%	0%	0%	0%	0%	0%	0%	5%
intestinal adenoma	0%	0%	0%	0%	0%	5%	0%	10%	10%
thyroid carcinoma	0%	0%	0%	0%	0%	10%	0%	0%	0%
salivary adenocarcinoma	0%	0%	0%	0%	0%	0%	0%	0%	10%
carcinoma (unknown primary)	0%	0%	0%	0%	0%	0%	0%	0%	5%
CML	0%	0%	0%	0%	0%	0%	0%	5%	0%
skin papillomas	0%	8%	0%	0%	5%	10%	0%	0%	15%
none	95%	24%	15%	0%	0%	25%	0%	0%	0%

Percentage of mice within each cohort with the indicated tumor. N= 30 mice per genotype

Reproduced with permission from the copyright clearance center, TAp63 suppresses metastasis through coordinate regulation of Dicer and miRNAs, Nature. 2010 Oct 21;467(7318):986-90. doi: 10.1038/nature09459.

3.2.6. Loss of *TAp63* is tumor protective in some tissues

We found that the *TAp63*^{-/-} mice age early in life. Ageing has been shown to be tumor protective in certain tissues. Age-related senescence has been shown to have tissue-specific tumor suppressive potential. We wanted to investigate this phenomenon in the *TAp63/p53* double mutant mice. Multiple *TAp63*^{-/-}; *p53*^{+/-} mice developed carcinomas and sarcomas simultaneously in various tissues. The osteosarcomas from a number of *TAp63*^{-/-}; *p53*^{+/-} mice were non-metastatic (**Figure 9A**). On the contrary the carcinomas from the same *TAp63*^{-/-}; *p53*^{+/-} and *TAp63*^{+/-}; *p53*^{+/-} mice were highly metastatic (**Figure 9B-D**).

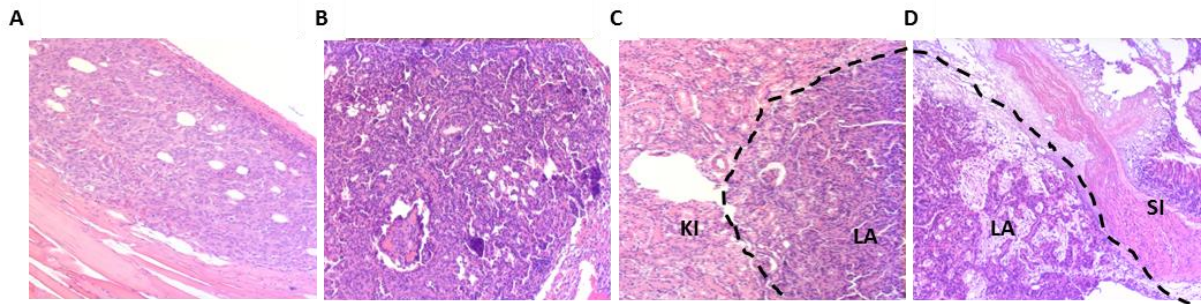


Figure 9: Loss of *TAp63* is tumor protective in some tissues

A) Non-metastatic osteosarcoma from *TAp63*^{-/-}; *p53*^{+/-} mouse. **B)** Metastatic lung adenocarcinoma (LA) from a *TAp63*^{-/-}; *p53*^{+/-} mouse that has metastasized to the kidney (KI) **(C)** and small intestine (SI) **(D)**.

Reproduced with permission from the copyright clearance center, TAp63 suppresses metastasis through coordinate regulation of Dicer and miRNAs, Nature. 2010 Oct 21;467(7318):986-90. doi: 10.1038/nature09459.

3.2.7. Carcinomas are the more malignant of the tumor types in the *TAp63* mutant and *TAp63/p53* double mutant mice

To test whether the arrest in metastasis of the osteosarcomas was due to the expression of senescence markers in these tumors, we wanted to test the expression of SA- β -galactosidase in these tumors and also perform real time PCR for some known senescence markers like *PML*, *p16^{Ink4a}* and *p19^{Arf}*. Interestingly the osteosarcomas and rhabdomyosarcoma from the *TAp63^{-/-};p53^{+/-}* mice were found to be highly senescent but not the same tumor types from the *TAp63^{+/-};p53^{+/-}* (**Figure 10A-C**). All the carcinomas from the *TAp63^{-/-};p53^{+/-}* and *TAp63^{+/-};p53^{+/-}* mice were found to be negative for the validated senescence markers (**Figure 10D**). This suggests that the loss *TAp63* has variable effect on the tumor phenotype in different tissues. These findings were also in accordance with the aggressiveness and metastatic capacity of these tumors.

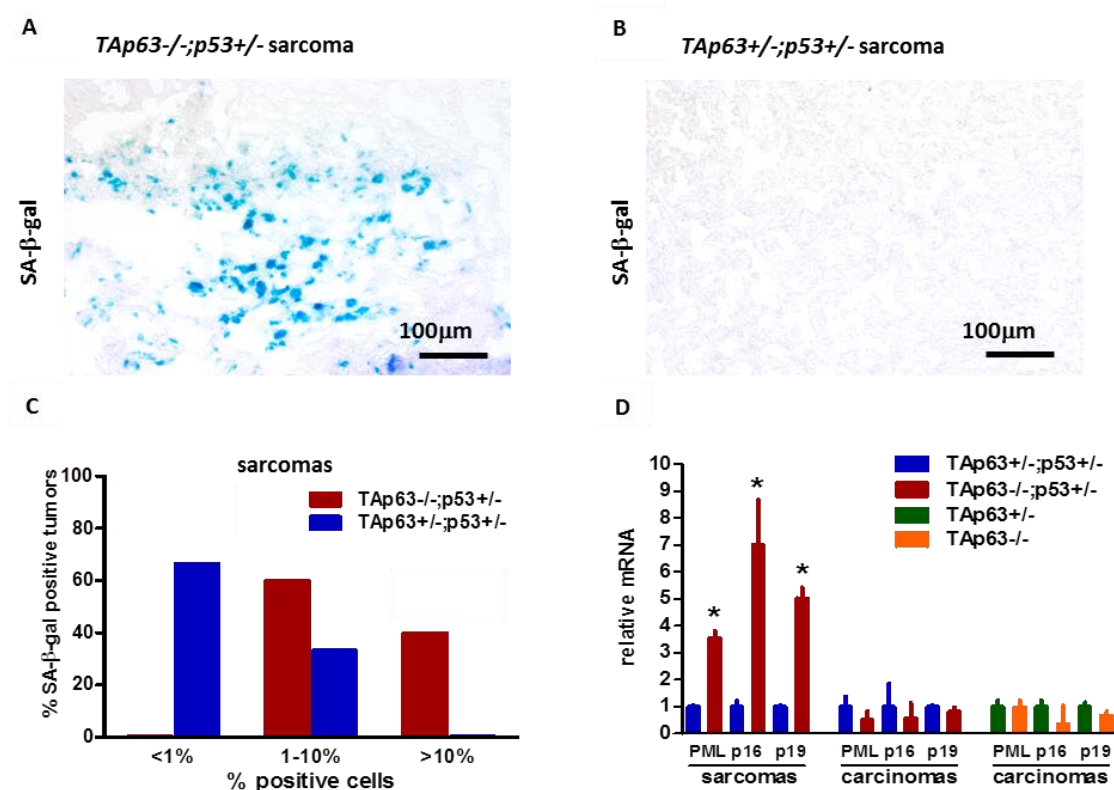


Figure 10: Tumors lacking *TAp63* exhibit senescence

A & B) SA-β-gal staining of sarcomas of the indicated genotypes. **C)** Quantitation of the SA-β-gal positive sarcomas from the indicated genotypes expressed in percentage; n=6. **D)** Quantitative real-time PCR for *PML*, *p16*^{*Ink4a*} and *p19*^{*Arf*} in the indicated tumors (n=6) of each genotype.

Reproduced with permission from the copyright clearance center, TAp63 suppresses metastasis through coordinate regulation of Dicer and miRNAs, Nature. 2010 Oct 21;467(7318):986-90. doi: 10.1038/nature09459.

3.2.8. Genomic instability empowers the carcinomas to overcome senescence and metastasize in the absence of *TAp63*

Genomic instability from the *TAp63*^{-/-} mouse tissues have been demonstrated to be high (72). In order to determine whether the tumors from the *TAp63*^{-/-}; *p53*^{+/-} mice displayed a similar level of genomic instability, and whether this correlated with their metastatic potential, γ -H2AX (**Figure 11D-F**) staining and metaphase spreads (**Figure 11A-C**) were performed on tumors from these mice. The *TAp63*^{-/-} carcinomas were indeed found to express high levels of γ -H2AX, chromosomal aberrations and polyploidy (**Figure 11A-C**). This suggests that tumors lacking *TAp63* specifically of epithelial origin, acquire additional changes in order to overcome the senescence pathway and promote metastasis. In sarcomas decreased levels of *TAp63* can induce senescence and make these tumors non-metastatic.

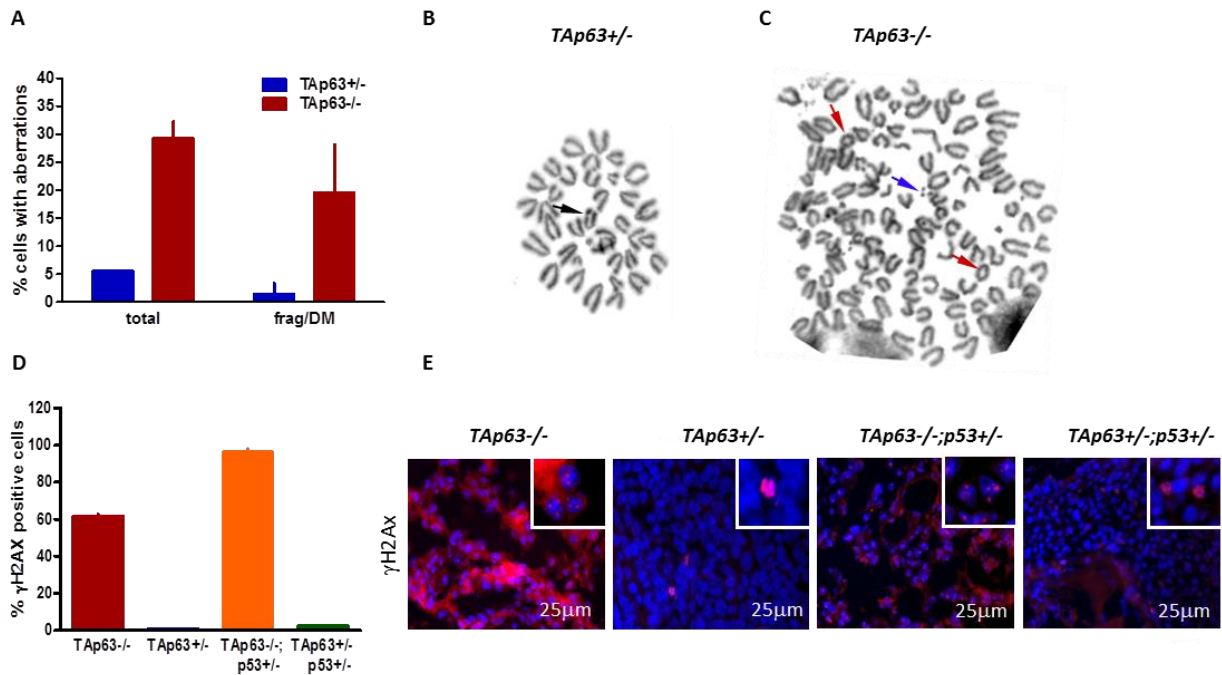


Figure 11: Loss of *TAp63* leads to high levels of genomic instability in tumors

A) Percentage of $TAp63^{-/-}$ and $TAp63^{+/-}$ tumors with chromosomal aberrations determined by metaphase spread; $n=6$ of each genotype. Frag/DM, fragmented, double –minute chromosome. **B & C)** Representative images of metaphase spreads of the indicated genotypes. Colored arrows indicate aberration; ring (red) , double-minute (blue). **D)** Percentage of γ -H2AX positive cells from carcinomas of the indicated genotypes. **E)** Representative image of lung adenocarcinomas stained for γ -H2AX from the mice of the indicated genotypes. 200X magnification; insets shown are 400X magnification.

Reproduced with permission from the copyright clearance center, TAp63 suppresses metastasis through coordinate regulation of Dicer and miRNAs, Nature. 2010 Oct 21;467(7318):986-90. doi: 10.1038/nature09459.

3.2.9. The *TAp63*^{-/-} cells and tumor cell lines are more invasive

Since the *TAp63* mutant tumors in mice exhibited such aggressiveness, we wanted to investigate the loss of *TAp63* in inducing metastasis in tumors, MEFs and other cell lines. We found that the mouse embryonic fibroblasts derived from the *TAp63*^{-/-} mice showed 1.8 fold increased invasion in a Boyden chamber assay (**Figure 12A**). In order to determine whether this was true for human tumors, we went on to probe the migratory and invasive capacity of the tumor cell lines generated from the primary head and neck squamous cell carcinomas (10A, 17A, 22A) and the matched metastases (10B, 17B, 22B) from the same patient (214). Interestingly the *TAp63* mRNA levels were found to be low in all the metastatic cell lines when compared to the cell line generated from the primary tumors (**Figure 12B**). In Boyden chamber assay the cell lines with low levels of *TAp63* were more invasive compared to the cell lines which retained *TAp63* (**Figure 12C**). The cell lines 22A and 22B had low levels of *TAp63* and demonstrated comparably high levels of invasion (**Figure 12C**). This suggests that *TAp63* is an important regulator of invasion in vitro and metastasis in vivo.

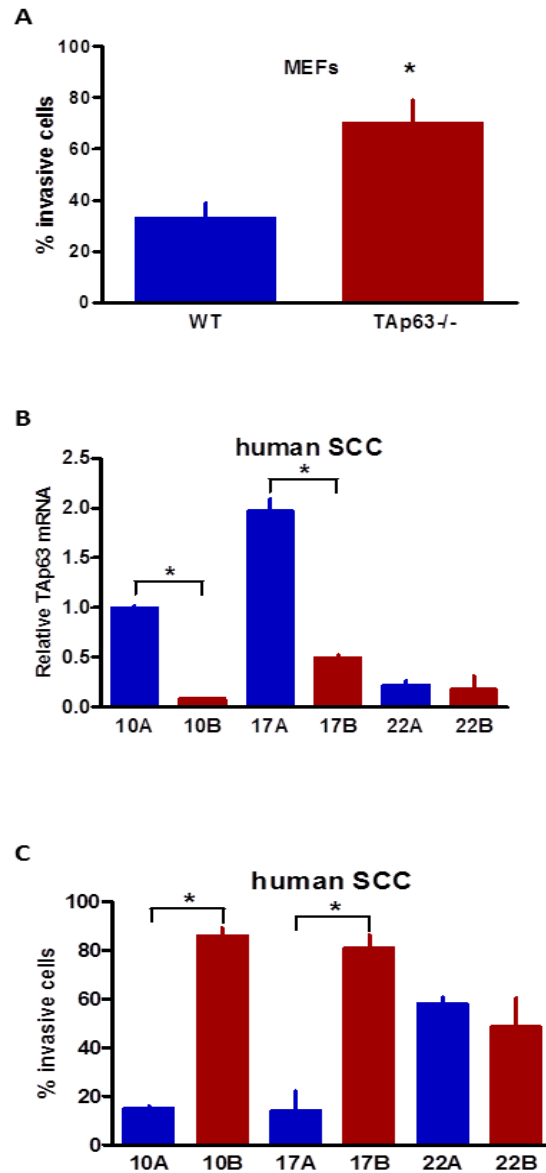


Figure 12: *TAp63*^{-/-} primary cells and cell lines are highly invasive

A) Percentage of invasive wild-type (n=3) and *TAp63*^{-/-} (n=3) MEFs subjected to Boyden chamber assay. **B)** Real-time PCR of *TAp63* mRNA levels in the human head and neck squamous cells carcinoma cell lines (n=5) of the indicated types. **C)** Percentage of invasive cells of the indicated head and neck squamous cell carcinoma cell lines in Boyden chamber assay. Asterisk indicate significance, p≤0.05.

Reproduced with permission from the copyright clearance center, TAp63 suppresses metastasis through coordinate regulation of Dicer and miRNAs, Nature. 2010 Oct 21;467(7318):986-90. doi: 10.1038/nature09459.

3.2.10. *Dicer* mutant mice exhibit similarities to the *TAp63* mutant mice

In many human cancers there is a heterozygous deletion of *Dicer* (180). In most tumors only a single allele of *Dicer* is lost (180). Our recent findings that *TAp63*^{+/-} tumors are more aggressive than those from *TAp63*^{-/-} mice are reminiscent of the recently reported phenotype of *Dicer* conditional knock-out (*Dicer*^{fl/+}) mice intercrossed to the *Kras*^{LSL-G12D} lung cancer model. *Dicer*^{fl/+}; *Kras*^{LSL-G12D} mice displayed a more aggressive tumor phenotype and shortened lifespan as compared to the *Dicer*^{fl/fl}; *Kras*^{LSL-G12D} mice following treatment with Adenovirus-Cre, indicating that *Dicer* is a haploinsufficient tumor suppressor (180, 215), similar to what we observed for *TAp63*^{-/-} mice on an enriched C57/B6 background, where we have observed that 35% of *TAp63*^{-/-} embryos die between E6.5 and E8.5dpc.

3.2.11. *Dicer* mRNA level is low in *TAp63* mutant human and murine cells, tumors and cell lines

Given the similarities between *TAp63* mutant mice and *Dicer* mutant mice, we wanted to investigate whether the *TAp63* mutant tumors have lower expression of *Dicer*. *Dicer* levels were significantly low in the *TAp63* and *TAp63/p53* mutant murine tumors compared to *TAp63*^{+/-} and *p53*^{-/-} tumors (**Figure 13A**). *Dicer* mRNA level was analyzed in the cell lines derived from osteosarcomas, lung and mammary adenocarcinomas deficient for *TAp63* (n=6 of each cell line) (**Figure 13A**). We also immunostained carcinomas from *TAp63*^{+/-} and *TAp63*^{-/-} mice (n=10 for each genotype) and found that highly metastatic tumors lose expression of *Dicer* (**Figure 13D-I**). To determine whether *Dicer* was specifically low in the absence of *TAp63*, we analyzed primary cells (MEFs) deficient for *TAp63* and compared mRNA expression level of *Dicer* to wild-type MEFs. We found *Dicer* levels were significantly low in the *TAp63*^{-/-} MEFs (about 50folds) suggesting loss of *TAp63* leads to a loss of *Dicer* mRNA levels (**Figure 13B**). We also tested *Dicer* levels in the human HNSCC cell lines with predetermined *TAp63* levels and found that *Dicer* was lost in the more metastatic cell lines (10B, 17B) compared to their primary tumor cell line (10A, 17B) (**Figure 13C**). The cell lines with low levels of *TAp63* (22A and 22B) also had low levels of *Dicer* (**Figure 13C**). These data indicate that *Dicer* levels are low in metastatic human lesions of HNSCC comparable to the loss of *TAp63* in

these metastatic tumors. This also suggests a critical role of *TAp63* in the regulation of *Dicer* levels. Interestingly *Dicer* levels have been shown to be low in various human cancers.

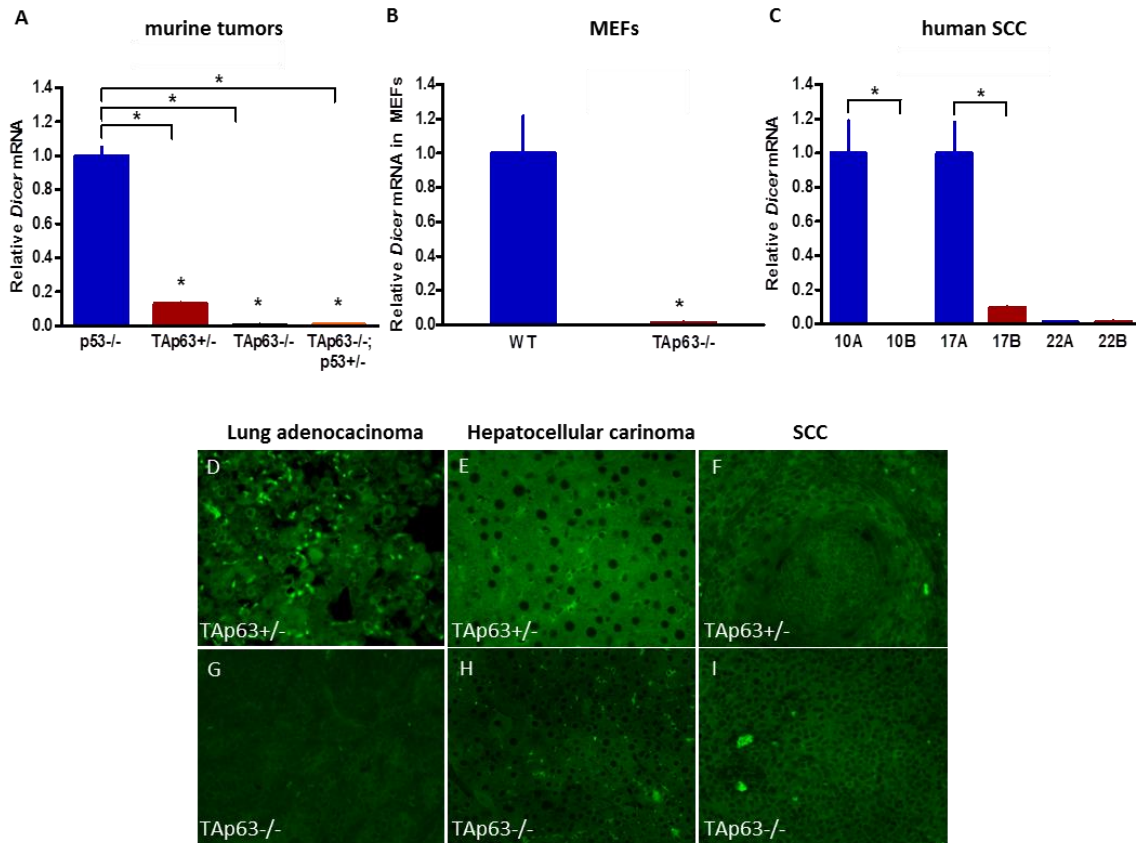


Figure 13: *Dicer* levels are low in *TAp63* mutant tumors

A) Quantitative real-time PCR analysis of *Dicer* mRNA levels in murine tumors of the indicated genotypes; n=3. **B)** Quantitative real-time PCR analysis of *Dicer* mRNA levels in primary MEFs of the indicated genotypes; n=3. **C)** Quantitative real-time PCR analysis of *Dicer* mRNA levels in human primary and matched metastatic tumor cell lines of the indicated types; n=5. **D-I)** *Dicer* immunofluorescence staining of lung adenocarcinomas, hepatocellular carcinomas and squamous cell carcinomas of the indicated genotypes. 200X magnification. Asterisk indicate significance. $p \leq 0.05$.

Reproduced with permission from the copyright clearance center, TAp63 suppresses metastasis through coordinate regulation of Dicer and miRNAs, Nature. 2010 Oct 21;467(7318):986-90. doi: 10.1038/nature09459.

3.2.12. Low levels of *Dicer* expression in human metastatic tumors correlate with *TAp63* expression levels

TAp63 level and *Dicer* level was determined in human tumors of various grades with the help of immunohistochemistry for *Dicer* and *TAp63*. We found that the more the advanced metastatic tumors had a greater loss of *TAp63* and in turn *Dicer* (**Figure 14A-D and Table 2**). This was true for all the tumor types tested including head and neck squamous cell carcinoma (n=46), mammary adenocarcinoma (n=43) and lung adenocarcinomas (n=92). The higher grades of tumors, which were more metastatic, lost *TAp63* expression and *Dicer* expression.

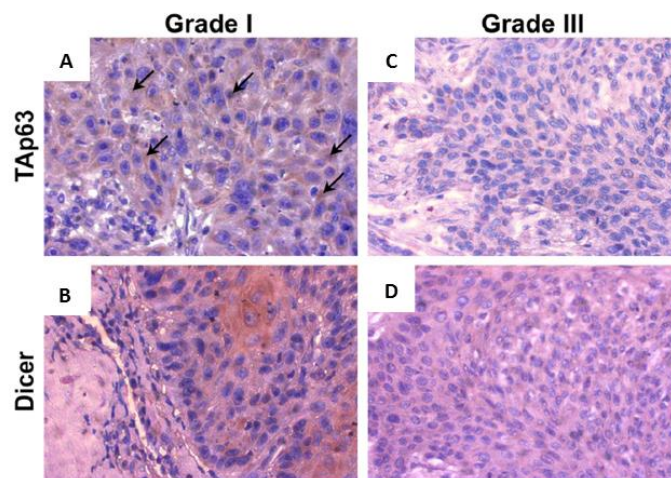


Table 2: *TAp63* and *Dicer* expression in human tumors

Tumor Type	HNSCC (n=19)			Mammary Ad (n=43)			Lung Ad & SCC (n=73)		
Tumor Grade	I (n=6)	II (n=10)	III-IV (n=3)	I (n=10)	II (n=12)	III-IV (n=21)	I (n=7)	II (n=31)	III-IV (n=35)
<i>TAp63</i> / <i>Dicer</i> -ve	0%	30%	100%	80%	83%	100%	14%	55%	74%

Figure 14: Low levels of *Dicer* expression in human metastatic tumors correlate with *TAp63* expression levels

A & B) *TAp63* and *Dicer* immunostaining of human HNSCC (Grade I) and **C & D)** (Grade III) tumors. Arrows indicate positive cells for *TAp63*. Magnification 200x.

Reproduced with permission from the copyright clearance center, TAp63 suppresses metastasis through coordinate regulation of Dicer and miRNAs, Nature. 2010 Oct 21;467(7318):986-90. doi: 10.1038/nature09459.

3.2.13. *TAp63* transcriptionally regulates the *Dicer* promoter

These data together suggests *TAp63*'s role in the transcriptional regulation of *Dicer*. Since *TAp63* is a transcription factor and shares its consensus site homology with *p53* we first scrutinized the *Dicer* promoter for *TAp63* binding site and found a binding site (*p63BS*) 1446 nucleotides upstream of the *Dicer* transcriptional start site (**Table 3**). We found several binding sites in accordance with the consensus binding sequence. We performed a chromatin immunoprecipitation assay using an antibody towards *p63* using lysates from wild-type and *p63*^{-/-}; *Arf*^{G/G} keratinocytes. We found that *p63* bound to the *Dicer* promoter (**Figure 15A**). We used a non-specific sequence located 2560 nucleotides upstream of the start site where no *p63* binding was detected (**Figure 15A**). We further verified whether *TAp63* transactivated the *Dicer-luciferase* reporter gene promoter with a luciferase assay. We constructed a luciferase reporter gene containing the *p63* binding site on the *Dicer* promoter. We found that all isoforms of *TAp63* α , β and γ could transcriptionally activate the *Dicer* promoter (**Figure 15C**). On the contrary *p53* could not bind to and activate the *Dicer* promoter. This indicates that *p63* and not *p53* is a specific transcriptional activator of the *Dicer* (**Figure 15B**).

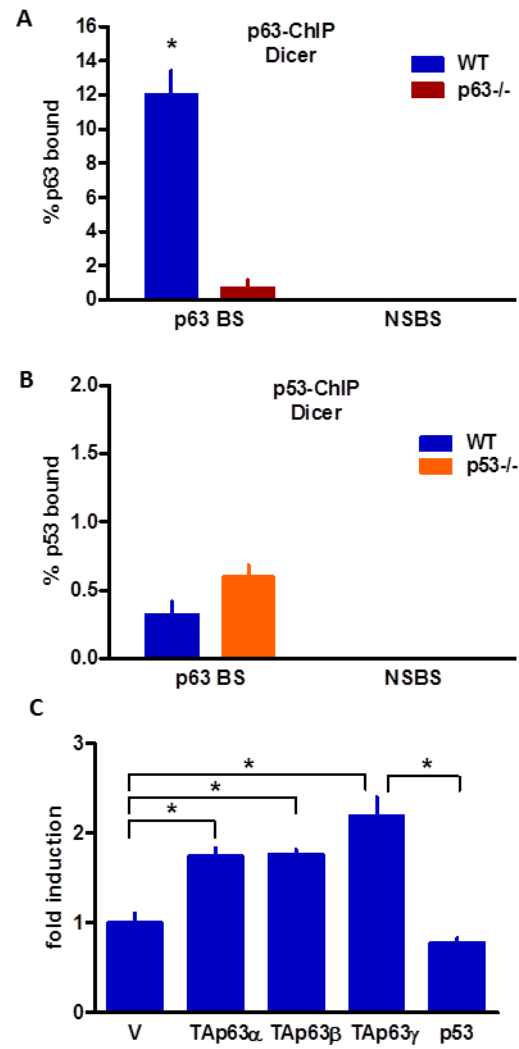


Table 3: *p63/p53* response element on *Dicer* promoter

Element	Location	Sequence	MM / spacer
DICER	-1446 to -1418	tggCATGtag ctcaggct gccCTTGatc	6 / 8

Figure 15: TAp63 transcriptionally regulates *Dicer* by directly binding to its promoter

A) Quantitative real-time PCR of ChIP assay using keratinocytes from wild-type and *p63*^{-/-};ArfG/G cells. *P63* binding site is indicated by *p63BS* and non-specific binding site by NSBS on the *Dicer* promoter, n=3. **B)** Quantitative real-time PCR of ChIP assay using keratinocytes from wild-type and 53^{-/-} cells at the *p63* binding site. **C)** Luciferase assay for the *Dicer*, n=5, V, pcDNA3 vector. **D)** Table demonstrating the *p63* binding site on the *Dicer* promoter. Asterisk indicates significance. $p \leq 0.05$.

Reproduced with permission from the copyright clearance center, TAp63 suppresses metastasis through coordinate regulation of Dicer and miRNAs, Nature. 2010 Oct 21;467(7318):986-90. doi: 10.1038/nature09459.

3.2.14. Loss of *Dicer* expression in MEFs causes increased invasion

To understand the contribution of *Dicer* in the invasiveness of the *TAp63*^{-/-} cells we re-expressed *Dicer* with an overexpression plasmid (pDESTmyc*DICER*) (216) in the *TAp63*^{-/-} MEFs (**Figure 16A**). To test any changes in their invasiveness, these cells were then assayed for invasion by a Boyden chamber assay. These cells demonstrated a significant decrease in their invasive potential compared to their *TAp63*^{-/-} control without *Dicer* expression (**Figure 15B**). Conversely when wild-type cells are treated with a short-hairpin for *Dicer* (pSuper-*Dicer1*) (181) (**Figure 16A**) they show increased invasion in a Boyden chamber assay compared to the wild-type control. This indicates that *Dicer* affects the invasive capacity of cells similar to *TAp63* (**Figure 16C**).

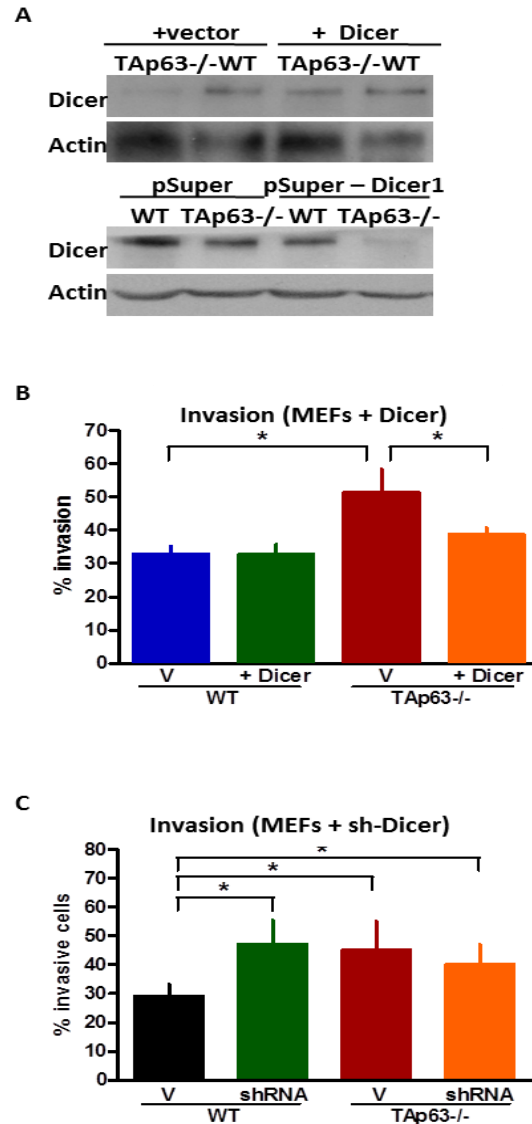


Figure 16: Loss of *Dicer* expression in MEFs causes increased invasion

A) Western blot analysis of MEFs overexpressing *Dicer* and ablation of *Dicer* infected with the indicated vectors. **B)** Percent invasion of MEFs overexpressing *Dicer* and MEFs treated with shRNA for *Dicer* **(C)** Asterisk indicate significance. $p \leq 0.05$.

Reproduced with permission from the copyright clearance center, TAp63 suppresses metastasis through coordinate regulation of Dicer and miRNAs, Nature. 2010 Oct 21;467(7318):986-90. doi: 10.1038/nature09459.

3.2.15. *TAp63* regulates metastasis through the regulation of *Dicer* in cells and cell lines

To determine whether *TAp63* regulates metastasis through the transcriptional regulation of *Dicer*, we re-expressed *TAp63* γ in the *TAp63* deficient MEFs (**Figure 17A**) and the more metastatic HNSCC cell lines (10B and 17B) (**Figure 17D**). The *TAp63* γ isoform was re-expressed in these cells and cell lines and subjected to invasion assay by a Boyden chamber. These cells became less invasive and comparable to wild-type cells (**Figure 17C & 17F**). When we measured *Dicer* levels in these cells and cell lines, we found that *Dicer* expression was as high as the wild-type MEFs on expression of *TAp63* γ (**Figure 17B & 17E**).

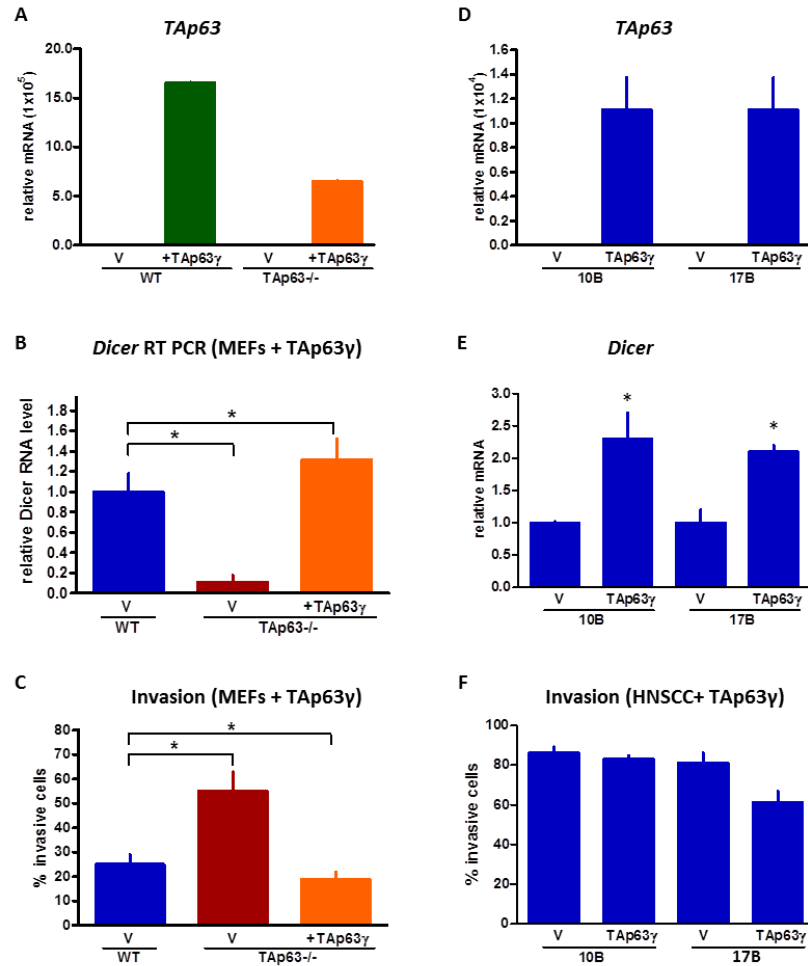


Figure 17: *TAp63* regulates metastasis through the regulation of *Dicer* in cells and cell lines

A) Quantitative real-time PCR for *TAp63* in MEFs of the indicated genotype with vector control (V) or *TAp63 γ* . **B)** Quantitative real-time PCR for *Dicer* in MEFs of the indicated genotype with vector (V) or *TAp63 γ* . **C)** Percentage of invasive MEFs treated with vector control or overexpressing *TAp63 γ* ; n=3. **D)** Quantitative real-time PCR for *TAp63 γ* and **E)** *Dicer*, after overexpression of control vector (V) or *TAp63 γ* in the HNSCC cell lines of the indicated genotypes. **F)** Percentage of invasion of the cells infected with vector (V) or *TAp63 γ* . Error bars indicate s.e.m. Asterisks indicate statistical significance, p \leq 0.

Reproduced with permission from the copyright clearance center, TAp63 suppresses metastasis through coordinate regulation of Dicer and miRNAs, Nature. 2010 Oct 21;467(7318):986-90. doi: 10.1038/nature09459.

3.2.16. Loss of *TAp63* and *Dicer* expression increases the metastatic potential of the non-metastatic cells

To understand whether downregulation of *TAp63* with a short hairpin RNA could ablate the expression of *Dicer* as seen in the mouse and human tumors, we treated the *wild-type* MEFs (*TAp63^{fl/fl}*) with either adenovirus-GFP as control or adenovirus-Cre and acutely ablated *TAp63* (*TAp63^{Δ/Δ}*) (**Figure 18A**). In these cells *Dicer* was concomitantly down regulated and resulted in increased invasion when subjected to Boyden chamber assay. This indicates that modulation of *TAp63* in turn affects *Dicer* levels and invasion (**Figure 18B-C**). Therefore loss of *TAp63* is an important factor in the invasiveness of primary cells, tumor cell line and tumors. Taken these data into consideration, *TAp63* is important in the regulation of *Dicer* in the suppression of metastasis.

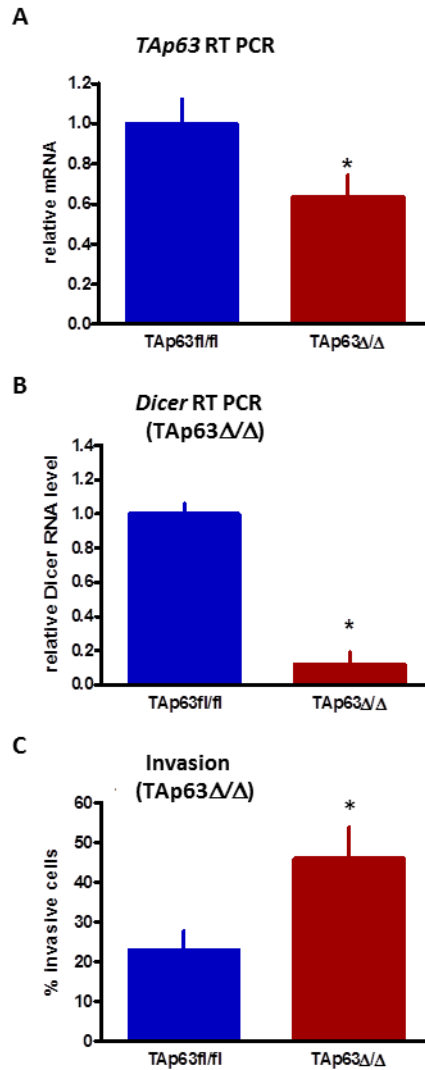


Figure 18: Loss of *TAp63* and *Dicer* expression increases the metastatic potential of the non-metastatic cells

A) Quantitative real time PCR analysis for *TAp63* in MEFs infected with adenovirus-GFP (*TAp63^{fl/fl}*) and adenovirus-Cre (*TAp63^{Δ/Δ}*). **B)** Quantitative real time PCR analysis for *Dicer* in MEFs infected with adenovirus-GFP (*TAp63^{fl/fl}*) and adenovirus-Cre (*TAp63^{Δ/Δ}*). **C)** Invasion assay of MEFs infected with Adenovirus-GFP or Adenovirus-Cre; n=3. Error bars indicate s.e.m. Asterisks indicate statistical significance, $p \leq 0.05$.

Reproduced with permission from the copyright clearance center, TAp63 suppresses metastasis through coordinate regulation of Dicer and miRNAs, Nature. 2010 Oct 21;467(7318):986-90. doi: 10.1038/nature09459.

3.2.17. *TAp63*^{-/-} MEFs express low levels of mature microRNAs

Since *Dicer* is one of the key enzymes in the cleavage of precursor microRNAs to mature microRNAs, we investigated whether all the mature microRNA species in the *TAp63*^{-/-} MEFs were expressed at low levels. Interestingly we found several microRNAs, miR-10b, miR-34a, miR-130b, miR-200b and miR-200c, that were expressed at significantly low levels in these cells by Northern blot analysis (**Figure 19**). All of these microRNAs have been shown to play roles in lung and mammary adenocarcinoma metastasis. In most of these tumors these microRNAs were downregulated (152, 196, 204, 217).

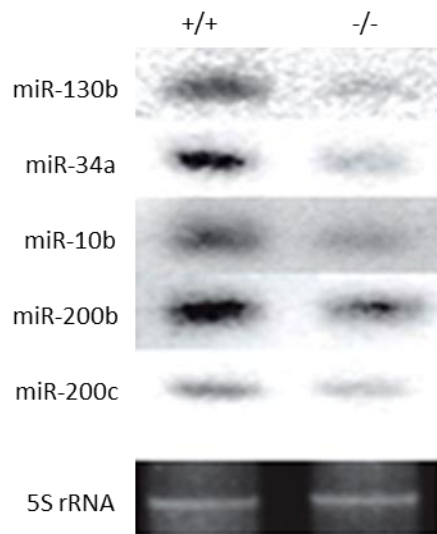


Figure 19: *TAp63*^{-/-} MEFs express low levels of mature microRNAs

Northern blot analysis in wild-type (^{+/+}) and *TAp63*^{-/-} (^{-/-}) MEFs for the indicated mature microRNAs. 5S rRNA is used as a loading control.

Reproduced with permission from the copyright clearance center, TAp63 suppresses metastasis through coordinate regulation of Dicer and miRNAs, Nature. 2010 Oct 21;467(7318):986-90. doi: 10.1038/nature09459.

3.2.18. Modulation of *TAp63* effects the expression of mature microRNA

To determine whether modulating the levels of *TAp63* could affect the expression of mature microRNA, we expressed *TAp63* γ in the *TAp63*^{-/-} MEFs and acutely ablated *TAp63* in the *TAp63*^{fl/fl} MEFs with the help of adenovirus-Cre infection (*TAp63* ^{Δ/Δ}). Northern blot was performed for miR-10b and miR-130b with probes against mature microRNAs. This probe detects the precursor microRNA species as well. As expected we observed a loss of mature miR-10b in the *TAp63*^{-/-} and the *TAp63* ^{Δ/Δ} MEFs, but no effects on the precursor levels of this microRNA (**Figure 20A**). Surprisingly we found a loss of miR-130b precursor expression in the *TAp63*^{-/-} and the *TAp63* ^{Δ/Δ} MEFs suggesting that *TAp63* possibly regulates its transcription at the primary microRNA stage and therefore loss of *TAp63* causes a loss in the precursor microRNA expression (**Figure 20B**). Re-expression of *TAp63* γ isoform in the *TAp63*^{-/-} MEFs rescued the loss of expression of mature and precursor microRNAs suggesting that *TAp63* not only regulates the expression of mature microRNAs through the regulation of *Dicer* but may indeed regulate microRNA transcription.

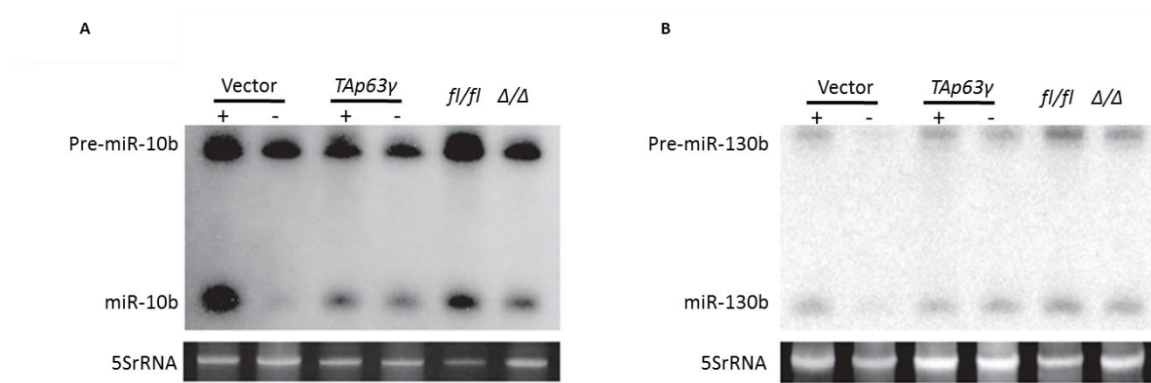


Figure 20: Modulation of TAp63 effects the expression of mature microRNA

A) Northern blot analysis of miR-10b or **(B)** miR-130b using MEFs expressing vector (V) or TAp63γ, TAp63^{fl/fl} (^{fl/fl}) and TAp63^{Δ/Δ} (^{Δ/Δ}). 5SrRNA is used as loading control.

Reproduced with permission from the copyright clearance center, TAp63 suppresses metastasis through coordinate regulation of Dicer and miRNAs, Nature. 2010 Oct 21;467(7318):986-90. doi: 10.1038/nature09459.

3.2.19. *TAp63*^{-/-} cells and tumors express low level of miR-130b compared to *p53*^{-/-} cells

We performed a Taqman reverse transcriptase assay to determine the expression levels of *miR-130b* and *miR-34a* in *wild-type*, *TAp63*^{-/-} and *p53*^{-/-} MEFs (**Figure 21A**), murine tumors (**Figure 21B**) and HNSCC (**Figure 21C**). Interestingly we found that *miR-130b* was expressed at lower levels in the *TAp63* mutated cells and tumors in comparison to the *p53*^{-/-} cells and murine tumors (**Figure 21A-B**). *miR-130b* was found to be expressed at lower levels in the metastatic HNSCC (10B and 17B), which express low levels of *TAp63* as shown earlier, compared to their primary matched tumors (10A and 17A) (**Figure 21C**). Since *p53* has been shown to be a transcriptional regulator of *miR-34a*, we hypothesized that *TAp63* could be the transcriptional regulator of *miR-130b* and *miR-34a*.

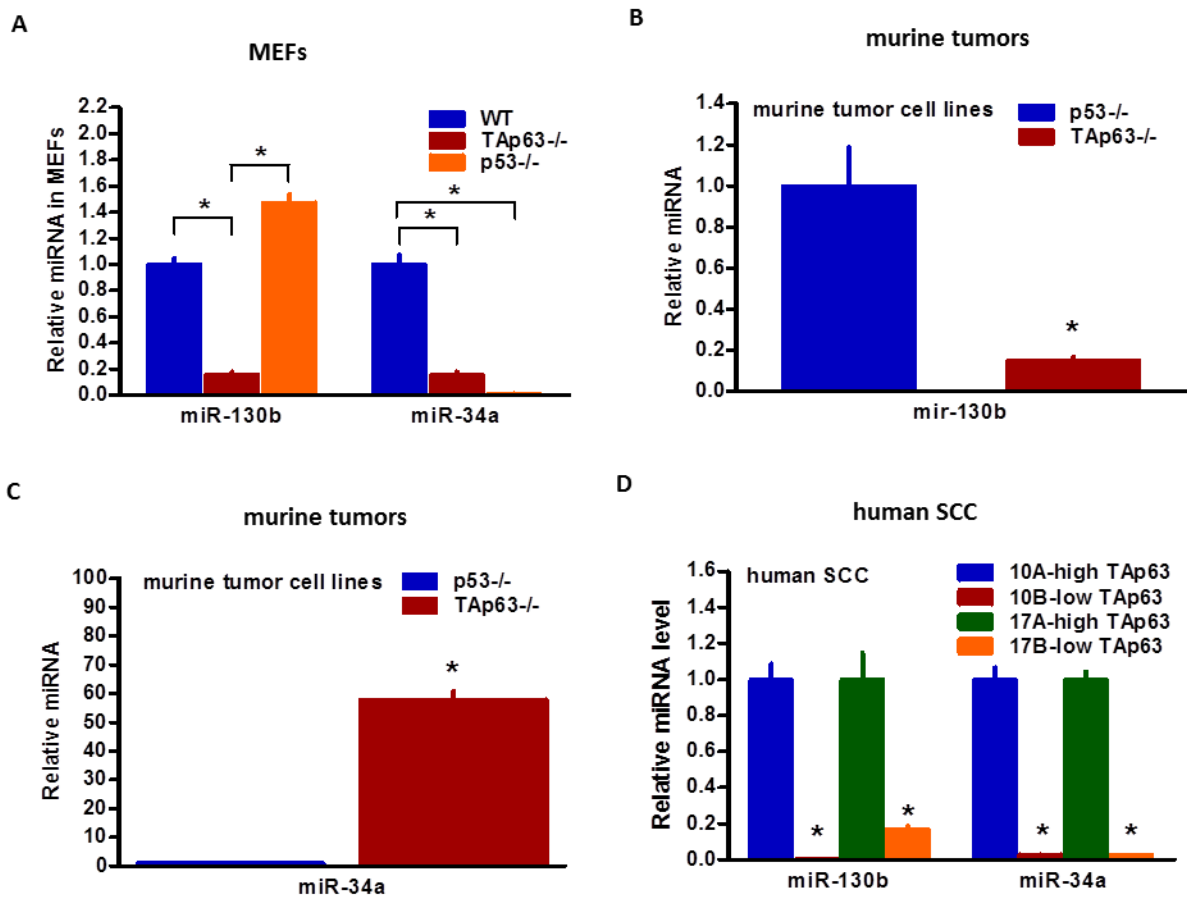


Figure 21: *TAp63*^{-/-} cells and tumors express low level of miR-130b compared to *p53*^{-/-} cells

A-C) Quantitative reverse transcriptase Taqman assay for miR-130b and miR-34a in *TAp63*^{-/-}, *p53*^{-/-} and *wild-type* MEFs (**A**), murine tumors and cell lines (**B**) and (**C**). **D)** Quantitative reverse transcriptase Taqman assay for miR-130b and miR-34a of the indicated human tumor cell lines as specified earlier; n=5. Error bars indicate s.e.m. Asterisk indicate statistical significance, $p \leq 0.05$.

Reproduced with permission from the copyright clearance center, TAp63 suppresses metastasis through coordinate regulation of Dicer and miRNAs, Nature. 2010 Oct 21;467(7318):986-90. doi: 10.1038/nature09459.

3.2.20. Expression level of mature miR-130b correlates with *TAp63* and *Dicer* expression in human cancers

We wanted to determine whether *TAp63* is an effector of miR-130b. We analyzed the levels of mature miR-130b in the panel of primary and metastatic head and neck squamous cell carcinomas and lung adenocarcinomas. The level of miR-130b correspond with the level of expression of *TAp63* and *Dicer* in these tumors. The more metastatic tumors (Grade II and Grade III) have a loss in *TAp63*, *Dicer* and miR-130b expression (**Table 4**).

Table 4: *TAp63*, *Dicer* and miR-130b expression in human tumors

Tumor Type	HNSCC (n=25)			Lung Ad (n=19)		
Tumor Grade	I (n=12)	II (n=5)	III (n=8)	I (n=11)	II (n=5)	III (n=3)
<i>TAp63/Dicer</i> LOW	83%	100%	100%	82%	80%	100%
<i>TAp63/miR-130b</i> LOW	42%	60%	38%	9%	60%	67%
<i>TAp63/Dicer/miR-130b</i> LOW	42%	60%	38%	9%	60%	67%

Percentage of head and neck squamous cell carcinomas HNSCC), and lung adenocarcinomas (Lung Ad) of various grades :I denotes well-differentiated, II denotes moderately differentiated and III denotes poorly differentiated.

Reproduced with permission from the copyright clearance center, TAp63 suppresses metastasis through coordinate regulation of Dicer and miRNAs, Nature. 2010 Oct 21;467(7318):986-90. doi: 10.1038/nature09459.

3.2.21. *TAp63* transcriptionally regulates the activation of miR-130b promoter site

To further elucidate the role of *TAp63* in the transcriptional regulation of *miR-130b* and *miR-34a*, we searched the upstream region of *miR-130b* for a *p53/p63* consensus binding site. Putative *p63* binding sites were identified by analyzing 1000 nucleotides upstream of each microRNA and 500 base pairs downstream of the transcriptional start site (**Table 5**). We performed chromatin immunoprecipitation for these sites and found a specific site for *p63* binding at 786 nucleotides upstream of the miR-130b transcription start site (**Figure 22A**). We also found a binding site of *p63* on the *miR-34a* promoter besides the published *p53* binding site at 432 bases downstream of the transcription start site (**Figure 22B**). We also performed ChIP analysis for *p63* binding at the published *p53* binding site, but found that although *p53* binds to this site, *p63* does not (**Figure 22D**). Interestingly we found that *p53* did not bind to the miR-130b binding site (**Figure 22C**). To determine whether *p63* can transactivate the *miR-130b* and *miR-34a* promoters, we cloned these sites into a luciferase reporter vector and performed a luciferase assay. We found that while all the isoforms of *TAp63* indeed transactivate the *miR-130b* promoter site, they do not transactivate the *miR-34a* promoter binding site (**Figure 22E-F**).

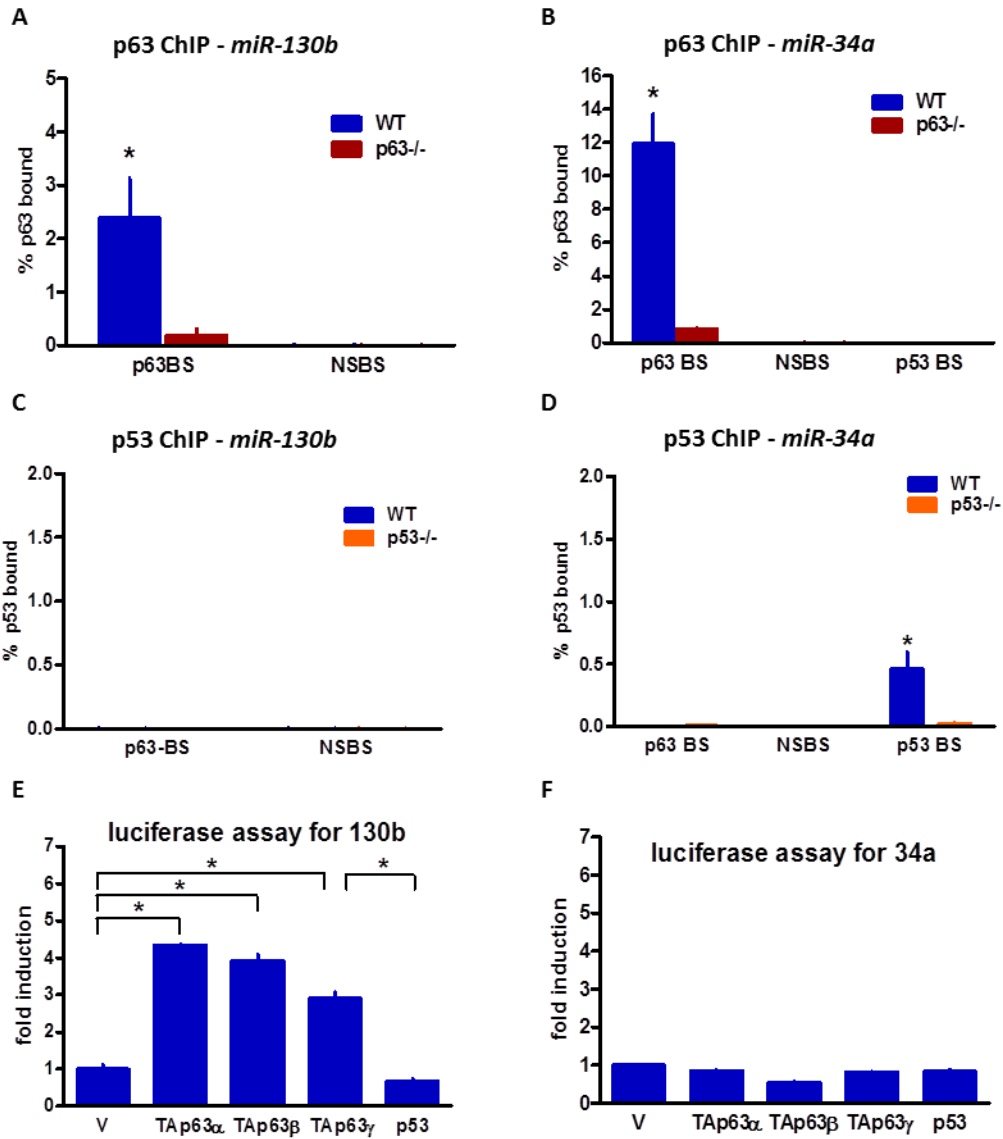


Table 5: p63/p53 response elements

Element	Location	Sequence	MM/Spacer
miR-34a	+432 to+461	gggCTTGctg gctgtttaca cttCTTGtgg	6 / 10
miR-130b	-786 to -763	gccCTAGttc tgct cttCTAGgca	7 / 14

Figure 22: TAp63 transcriptionally regulates the activation of miR-130b promoter site

A & B) Chromatin immunoprecipitation assay for *p63* binding (*p63BS*) at the miR-130b and miR-34a promoter sites using *p63* antibody. Quantitative real time PCR was performed to quantify the binding potential. **C & D)** Chromatin immunoprecipitation assay for *p53* binding (*p53BS*) at the miR-130b and miR-34a promoter sites using *p53* antibody. Quantitative real time PCR was performed to quantify the binding potential. Published *p53* binding site at miR-34a promoter site was used as positive control. Non-specific binding site (NSBS) was used as negative control. **E & F)** Luciferase assay for miR-130b and miR-34a promoter binding site with MEFs transfected with the indicated vectors, (n=3). Error bars indicate s.e.m. Asterisk indicate statistical significance, $p \leq 0.05$.

Reproduced with permission from the copyright clearance center, TAp63 suppresses metastasis through coordinate regulation of Dicer and miRNAs, Nature. 2010 Oct 21;467(7318):986-90. doi: 10.1038/nature09459.

3.2.22. *TAp63* regulates metastasis by the regulation of *miR-130b*

To further address whether *TAp63* could regulate metastasis by the regulation of miR-130b, we overexpressed and downregulated *TAp63* in the *TAp63*^{-/-} MEFs and *TAp63*^{fl/fl} MEFs as specified earlier. *miR-130b* levels were infact dependant on the *TAp63* status and increased upon *TAp63* upregulation in the *TAp63*^{-/-} MEFs (**Figure 23A**), while ablated in the *TAp63*^{Δ/Δ} MEFs (**Figure 23B**). This clearly indicates that *miR-130b* is a direct target of *TAp63*.

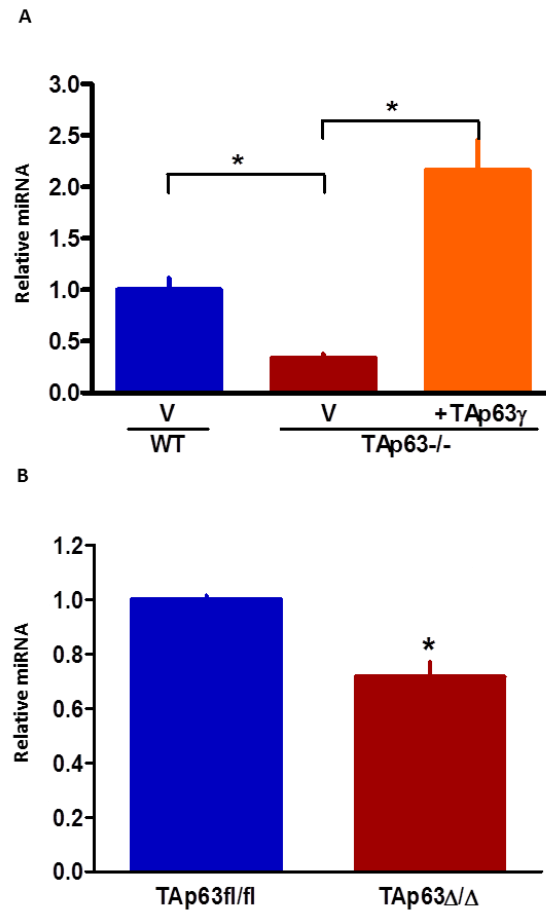


Figure 23: Modulating *TAp63* levels correlate with the level of miR-130b

A) Quantitative real time Taqman PCR assay determining miR-130b levels in MEFs of indicated genotypes transfected with either vector (v) or *TAp63 γ* overexpression plasmid **B)** Quantitative real time Taqman PCR assay determining miR-130b levels in MEFs infected with Adenoviral-GFP (*TAp63^{fl/fl}*) or Adenoviral-Cre (*TAp63^{Δ/Δ}*). Experiments done in triplicate. Error bars indicate s.e.m. Asterisk indicated statistical significance, $p \leq 0.05$.

Reproduced with permission from the copyright clearance center, TAp63 suppresses metastasis through coordinate regulation of Dicer and miRNAs, Nature. 2010 Oct 21;467(7318):986-90. doi: 10.1038/nature09459.

3.2.23. Loss of *miR-130b* causes increase in invasion

Further to test whether this regulation was relevant to the metastatic phenotype seen in the tumors, we assessed the ability of the wild-type and *TAp63*^{-/-} MEFs to migrate and invade after downregulation of *miR-130b*. With the help of a lentiviral shRNA, we downregulated the expression of *miR-130b* in wild-type cells and tested their invasion and migration by Boyden chamber assay. Taqman quantitative real-time PCR was performed to quantify the levels of *miR-130b*. *miR-130b* level was 50% lower in these cells compared to the wild-type (**Figure 24A**) . When assayed for migration and invasion in the Boyden chamber assay, these cells about 1.5 fold increase in their invasiveness compared to the wild-type vector only control cells (**Figure 24B**). This suggests loss of *miR-130b* alone can increase invasion of cells

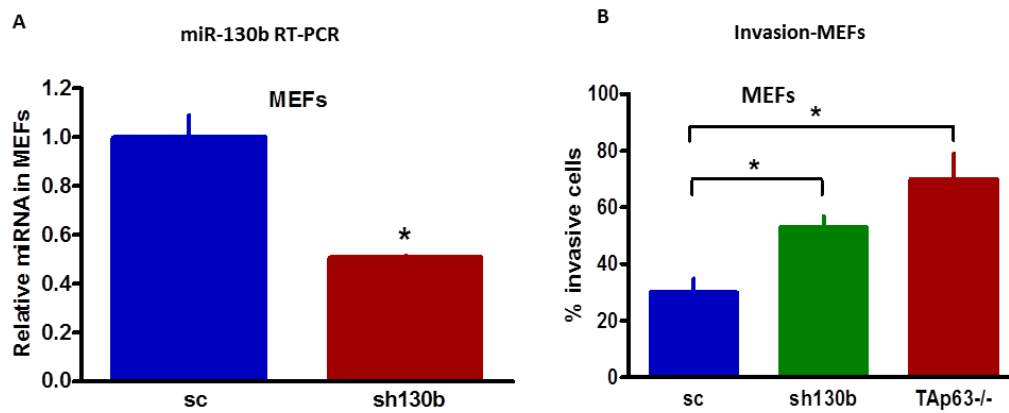


Figure 24: Loss of miR-130b causes an increase in invasion

A) MEFs treated with lentiviral scramble control (sc) or lentiviral shRNA for *miR-130b* (sh130b). **B)** Invasion assay with wild-type cells treated with scramble, *miR-130b* shRNA treated MEFs and *TAp63*^{-/-} MEFs. Experiments done in triplicate. Error bars indicate s.e.m. Asterisk indicated statistical significance, $p \leq 0.05$.

Reproduced with permission from the copyright clearance center, TAp63 suppresses metastasis through coordinate regulation of Dicer and miRNAs, Nature. 2010 Oct 21;467(7318):986-90. doi: 10.1038/nature09459.

3.2.24. *Dicer* and miR-130b coordinately regulate invasion and migration

To further analyze if there was a co-operation between *Dicer* and miR-130b in the induction of the invasive phenotype of cells and whether expressing both miR-130b and *Dicer* in *TAp63*^{-/-} cells could reduce their invasion potential to wild-type levels, we modulated the levels of miR-130b and *Dicer* alone or in combination in *TAp63*^{-/-} MEFs (**Figure 25A-B**). These cells were assayed for invasion migration with the Boyden chamber as before. We found that overexpression of miR-130b in these did not have an effect on their invasion potential possibly due to the low levels of *Dicer* present in these cells and therefore a lack of proper miRNA processing (**Figure 25C**). So we overexpressed both *Dicer* and miR-130b in these cells and assayed for their invasion potential. We found that when expressed in combination (*Dicer* and miR-130b) the level of invasion is even lower than when *Dicer* is expressed alone similar to wild-type levels (**Figure 25C**). This indicates a co-ordination between *Dicer* and miR-130b in the suppression of metastasis. Also *TAp63* plays an important role in the suppression of metastasis by the co-ordinate regulation of *Dicer* and miR-130b.

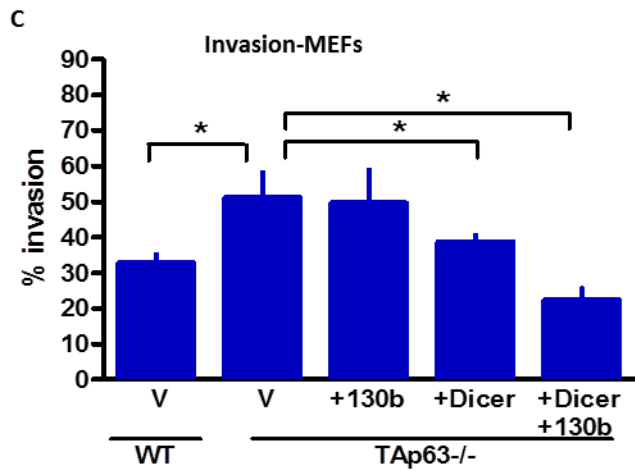
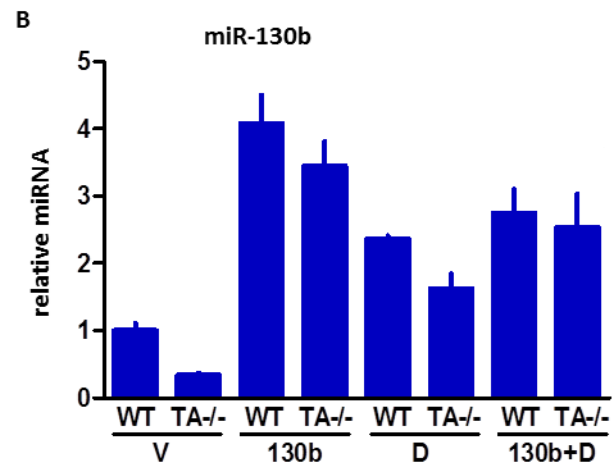
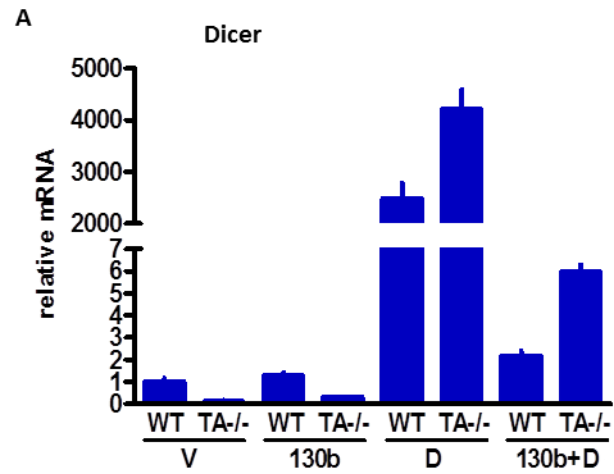


Figure 25: *Dicer* and miR-130b coordinately regulate invasion and migration

A & B) Quantitative real time PCR for *Dicer* and miR-130b in MEFs of the indicated genotypes expressing vector only (V), miR-130b (130b), *Dicer* (D) and miR-130b and *Dicer* together (130b+D). **C)** Invasion Assay with MEFs of the indicated genotypes expressing vector only (V), miR-130b, *Dicer* or both together. Experiments done in triplicate. Error bars indicate s.e.m. Asterisk indicated statistical significance, $p \leq 0.05$.

Reproduced with permission from the copyright clearance center, TAp63 suppresses metastasis through coordinate regulation of Dicer and miRNAs, Nature. 2010 Oct 21;467(7318):986-90. doi: 10.1038/nature09459.

3.3. Discussion

We have shown that *TAp63* can regulate metastasis by the transcriptional regulation of individual microRNA (*miR-130b*) and *Dicer* and that this regulation is important in the suppression of metastasis in many tissues. The regulation of *Dicer* by *TAp63* has global biological implications. MicroRNAs are involved in regulation of an array of different processes like cancer, differentiation (218-222), stem cell biology (223, 224), DNA damage response (225, 226), apoptosis (227, 228), senescence (229), regulation of other microRNAs (230), and also in diseases like diabetes (230), inflammatory diseases (231, 232) and many others. *Dicer* has been implicated in the processing of other small RNAs like siRNAs (233), Alu RNA and 7SL RNAs (*Dicer*-Dependent Biogenesis of Small RNAs Derived from 7SL RNA). *Dicer* has also been shown to play a role in the regulation of apoptosis in *Caenorhabditis elegans*. This seems to be an independent mechanism of *Dicer* that does not involve processing of microRNA. *Dicer* is processed by the caspase CED-3 in the worms giving rise to a C-terminal fragment with deoxyribonuclease activity. It can then digest the DNA and promote apoptosis (234). In primates since the *Dicer* protein function is conserved to a certain extent, this could potentially be a possible mechanism promoting apoptosis (234). Therefore *TAp63* may play a role in all of these processes. *TAp63* is a stress response protein similar to *p53* in certain aspects of its mode of action. This would also suggest that there may be differences in *Dicer* regulation by *TAp63* in an unstressed situation compared to a stressed scenario. This interaction will also need to be evaluated. Finally the feedback loop between *Dicer*, microRNAs and *TAp63* will be an interesting aspect of this interaction as microRNAs have been also been shown in turn to regulate *Dicer* like let-7 (234) and *p63* like miR-203 (234-236). Taken these together it will be intriguing to find the interplay between these proteins and the microRNAs and ultimately their effects on the various biological processes.

**4. Chapter 4: Induced multipotency in adult keratinocytes through down regulation
of $\Delta Np63$ or *DGCR8***

4.1. Introduction

The factors required to reprogram adult somatic cells to induced pluripotent stem (iPS) cells is an area of intense research. The introduction of defined factors, such as *Oct4*, *Sox2*, *Klf4*, and *c-myc*, gives rise to the efficient reprogramming of fibroblasts to iPS cells (92). Cells deficient for *p53* also show enhanced ability for reprogramming with the addition of *Oct4* and *Sox2* only (127, 237-240). Unfortunately, overexpression of oncogenes or down regulation of tumor suppressor genes while leading to the generation of cells that are pluripotent, can also lead to the production of tumorigenic cells (238). Consequently, an alternative method for creating iPS cells or cells with stem-like properties from somatic cells is desirable. Here, we show that one such method is through the down regulation of the *p53* family member, *ΔNp63*, or through downregulation of its transcriptional target, *DGCR8*, in adult keratinocytes.

Both miRNAs and the *p53* family member, *p63*, have been implicated in processes that control stem cell proliferation and cell fate determination (30, 66, 67, 72, 241). As demonstrated using genetically engineered mice, *p63* is critical for the development and maintenance of stratified epithelial tissues (30, 66). Mice lacking *p63* cannot form skin, have craniofacial and skeletal defects and die within hours after birth. These defects are partially due to the functions of *p63* as a transcriptional regulator of genes involved in multiple processes in skin development including epithelial stem cell proliferation, differentiation, and adhesion (67, 75, 242-244). While it is clear that *p63* plays a crucial role in epidermal morphogenesis, its roles as an essential gene in stem cell proliferation and/or differentiation are still not well understood. The controversial roles of *p63* in epidermal development are due, at least in part, to the complexity of the gene and existence of multiple isoforms (245). There are two major isoforms, those with a transactivation domain (*TAp63*) that structurally resemble *p53* and those lacking this domain (*ΔNp63*); however, *ΔNp63* also transcriptionally regulates unique target genes shown to be involved in limb and epidermal morphogenesis (75, 246).

To determine the roles of these isoforms in skin development and maintenance, we and others have constructed isoform specific conditional knock out alleles of *p63*. Using the *TAp63*

conditional knock out mouse, we generated *TAp63*^{-/-} mice and found that they age prematurely, develop blisters, and display wound-healing defects, which result from hyperproliferation of dermal stem cells resulting in premature senescence and depletion of these cells that are necessary for wound repair (72). While we found that *TAp63* plays a critical role in maintaining adult stem cells, it is dispensable for epidermal morphogenesis. This data along with work from other labs indicates that *ΔNp63* is the critical isoform in the development of epithelial tissues (67, 72, 75, 247).

To further study the role of *ΔNp63* in skin development, we generated *ΔNp63* conditional knock out mice (*ΔNp63*^{fl/fl}), allowing for deletion of *ΔNp63* and retention of the *TAp63* isoforms in any tissue of interest. We then generated *ΔNp63* knock out mice by intercrossing the *ΔNp63* conditional knock out mice to germline specific cre transgenic mice (*Zp3cre*). Surprisingly, in contrast to the skin of *p63*^{-/-} mice, the *ΔNp63*^{-/-} mice developed a hyperproliferative, disorganized epidermis that expressed some markers of terminal differentiation similar to the phenotype observed in another mouse model deficient for *ΔNp63* (*ΔNp63*^{gfp/gfp}) (247) or with *in vivo* siRNA knock down of *ΔNp63α* (75). The *ΔNp63*^{gfp/gfp} mice are born with a fragile epidermis that has accelerated differentiation in some areas of the epidermis and expression of K8 and K18 in other areas (247). The mice expressing an siRNA to knock down *ΔNp63α* exhibited skin that is hyperproliferative and cells within the basal layer fail to exit the cell cycle (75). These observations are similar to the phenotypes observed in our allele of the *ΔNp63*^{-/-} mice, which have areas of terminal differentiation in the epidermis, expression of K8 and K18, and hyperproliferative skin.

We however have gone a step further and characterized the hyperproliferative skin of the *ΔNp63*^{-/-} mice. Epidermal cells derived from the epidermis of *ΔNp63*^{-/-} mice had the ability to hyperproliferate and phenotypically resembled embryonic and induced pluripotent stem cells. Indeed, using a genome wide analysis, we found that epidermal cells deficient for *ΔNp63* express *Oct4*, *Sox2*, *Nanog*, and other genes associated with pluripotency, suggesting that *ΔNp63* is critical for silencing of these factors to induce terminal differentiation. The *DGCR8*^{-/-} embryonic stem cells (ESCs) were found previously to display a hyperproliferative defect by failure of silencing pluripotency genes (157), and the phenotype of the epidermis of *ΔNp63*^{-/-} mice is similar to the *DGCR8* and *Dicer* conditional knockout mice with *DGCR8* and

Dicer ablated in the skin (159, 194, 248). Additionally, we previously identified *TAp63* as a transcriptional activator of *Dicer* and hypothesized that $\Delta Np63$ may similarly regulate enzymes required for microRNA biogenesis. Indeed, we found that $\Delta Np63$ transcriptionally activates *DGCR8* and in turn regulates a unique miRNA signature critical for reprogramming. Murine $\Delta Np63$ deficient epidermal cells had the capacity to hyperproliferate at late passages, expressed a miRNA signature that is similar to that of mouse embryonic and iPS cells, and could be differentiated into multiple cell fates *in vitro* and *in vivo*. Additionally, $\Delta Np63$ deficient epidermal cells can be forced into a keratinocyte cell fate by re-expression of *DGCR8*. We recapitulated this stem cell phenotype in normal human epidermal keratinocytes (NHEKs) by deletion of $\Delta Np63$ or *DGCR8*. Our data indicate that down regulation of $\Delta Np63$ or *DGCR8* in cells derived from the epidermis are reprogrammed into stem cells that can be differentiated into multiple cell types.

4.2. Results

4.2.1. Generation of a *ΔNp63* conditional knock-out mouse model

To delineate the role of *ΔNp63* in vivo we generated a *ΔNp63* conditional knock-out mouse model using the Cre-loxP system. This allows for tissue specific deletion of the *ΔNp63* isoform when crossed to a transgenic tissue specific *Cre* mouse and retention of the *TAp63* isoform. LoxP sites were inserted flanking exon 3' (**Figure 26A**). This exon contains the transcriptional start site of the *ΔNp63* protein. Southern blotting analysis was performed to confirm proper targeting (**Figure 26B**).

To understand the role that *ΔNp63* plays in skin development, we crossed the *ΔNp63* conditional knock-out mice to FLPeR transgenic mouse to exclude the neomycin cassette ref. These mice were then crossed to the female germline-specific cre transgenic mice (Zp3-Cre) to generate the *ΔNp63*^{+/-} mice. These mice were intercrossed to obtain the *ΔNp63*^{-/-} mice. We found that these mice are born in proper Mendelian ratios, but die a few hours after birth. Genotyping PCR determined the genotypes of the mice (**Figure 26C**). Quantitative real-time PCR was performed on RNA derived from E9.5 embryos and from the skin of E18.5dpc embryos (**Figure 26D**). We further verified the absence of *ΔNp63* RNA and protein from embryo and the skin of the embryos while retaining wild-type levels of *TAp63* mRNA (**Figure 26 E-F**).

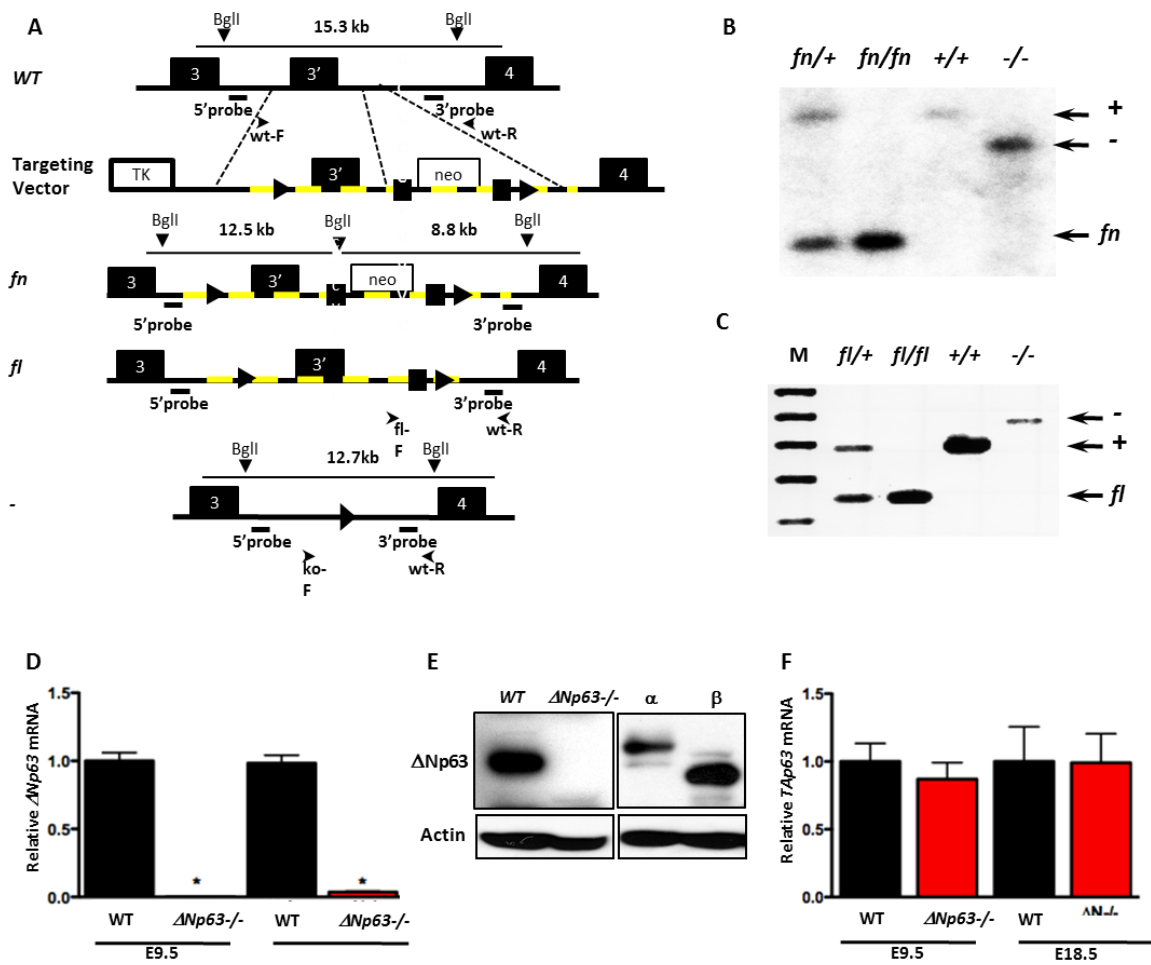


Figure 26: Generation of a conditional *ΔNp63* knock-out mouse model

A) The *ΔNp63* targeting vector was generated by inserting loxP sites (triangles) flanking exon 3' and a neomycin cassette (neo) flanked by frt sites (squares). Location of primers used for genotyping is indicated by arrows. The targeted region of the allele is depicted by a dashed yellow line. Flox neo (fn) mice were crossed to the FLPeR mice expressing the flp recombinase to delete the neo cassette in vivo and to generate the flox (fl) allele. The knock out (KO) allele is shown after cre recombination. **B)** Southern analysis of genomic DNA from: *ΔNp63^{fn/+}*, *ΔNp63^{fn/fn}*, *ΔNp63^{+/+}* and *ΔNp63^{-/-}* mice. **C)** PCR analysis of genomic DNA from: *ΔNp63^{fl/+}*, *ΔNp63^{fl/fl}*, *ΔNp63^{+/+}* and *ΔNp63^{-/-}* mice. **D)** Quantitative (q) RT PCR analysis of *ΔNp63* mRNA from E9.5 and E18.5 wild-type and *ΔNp63^{-/-}* embryos. Asterisks indicate statistical significance, (p<0.001). **E)** Western blot analysis for *ΔNp63* using epidermal cells derived from wild-type and *ΔNp63^{-/-}* embryos (E18.5) (left panel) and *p53^{-/-};p63^{-/-}* MEFs expressing *ΔNp63α* and *ΔNp63β* cDNAs. Actin was used as a loading control. **F)** qRT-PCR analysis of *TAp63* mRNA from E9.5 and E18.5 wild-type and *ΔNp63^{-/-}* embryos. qRT-PCR values are normalized to GAPDH.

4.2.2. Phenotype of the $\Delta Np63$ mutant mice

The $\Delta Np63^{-/-}$ mice had phenotypic resemblance to the $p63^{-/-}$ mice and the $\Delta Np63^{gfp/gfp}$ mice. The mice lacked limbs and had cleft lip and palate (**Figure. 27D**). These mice develop a rudimentary fragile epidermis, which lacks proper adhesion to the dermis (**Figure 27C**). Therefore during birth this epidermal layer easily detaches. The death of the $\Delta Np63^{-/-}$ mice is mainly due to dehydration and desiccation from the loss of an intact epidermal layer. Microscopic analysis of the epidermis from E18.5dpc embryos by hematoxylin and eosin staining demonstrated partial stratification of the epidermis with clusters of basal epidermal cells that were apparent in patches over 20%-30% of the embryo (**Figure 27C**). On the contrary the wild-type embryos have a perfectly stratified epithelium (**Figure 27A**) and the total $p63^{-/-}$ embryos are completely denuded (**Figure 27D**). Interestingly the $\Delta Np63^{+/-}$ embryos seemed to have excessive epidermal folding (**Figure 27B**). On analysis of the skin from the $\Delta Np63^{+/-}$ embryos displayed an expanded basal epidermal layer.

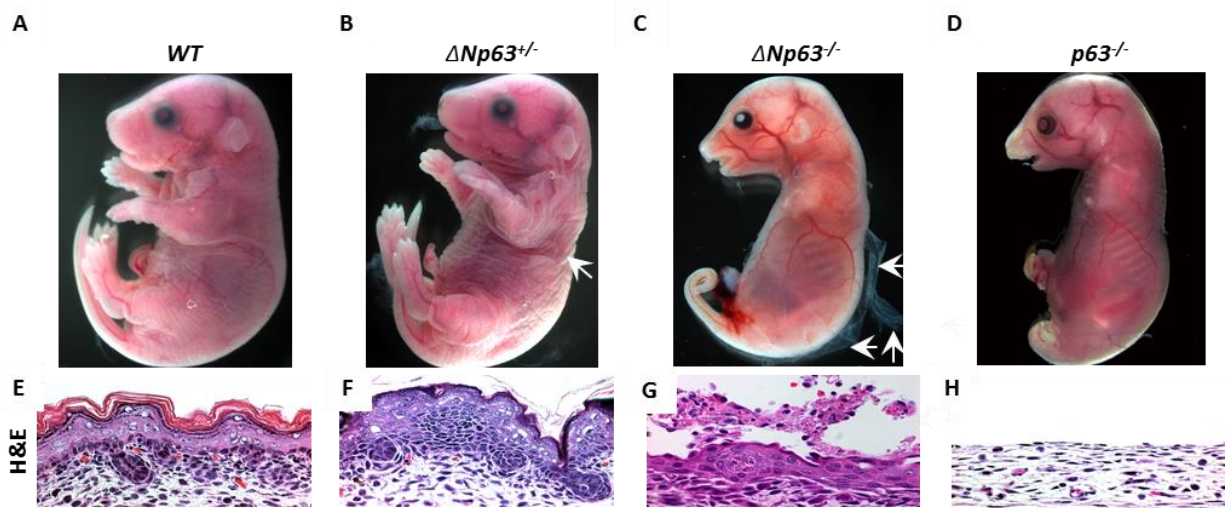


Figure 27: Phenotype of the $\Delta Np63$ mutant mice

Embryos at day E18.5 of the following genotypes: **(A)** wild-type, **(B)** $\Delta Np63^{+/-}$, **(C)** $\Delta Np63^{-/-}$ and **(D)** $p63^{-/-}$. Arrows in panel (B) indicate extra folds of skin and in panel (C) indicate non-adherent skin. **E-H** Hematoxylin and eosin (H&E) stained cross sections of the skin of E18.5 embryos of the indicated genotypes.

4.2.3. $\Delta Np63^{-/-}$ mouse epidermis displays defects in terminal differentiation

Since the $\Delta Np63^{+/-}$ and $\Delta Np63^{-/-}$ embryos had expanded disorganized epidermis, we hypothesized that loss of $\Delta Np63$ could lead to a loss of proper differentiation in the epidermal layer from these mice. In an attempt to characterize the differentiation potential of the epidermal cells, we immunostained the epidermis from the $\Delta Np63^{+/-}$ and $\Delta Np63^{-/-}$ embryos and compared them to the epidermis from wild-type and $p63^{-/-}$ embryos (**Figure 28A-B'**). We performed immunofluorescence staining with markers for epidermal differentiation assessing the expression of keratin 5(K5) and keratin 14(K14) for the basal layer, keratin 10(K10) and keratin 1(K1) for the spinous layer and filaggrin (Fila) in the granular layer (**Figure 28A-T**). All marker of terminal differentiation was expressed in the wild-type embryos (**Figure 28A,E,I,M**) while all these marker expression was absent in the $p63^{-/-}$ embryos (**Figure 28D,H,L,P**), which does not possess any epidermis. Curiously both $\Delta Np63^{-/-}$ and $\Delta Np63^{+/-}$ epidermis expressed all the markers for terminal differentiation (**Figure 28B,F,J,N & 28C,G,K,O**). In the $\Delta Np63^{+/-}$ mice, there was an expansion in the expression of these markers almost giving an impression that the layers were several cell layers thick and merged into the next more differentiated layer (**Figure 28B,F,J,N**). There was inappropriate expression of these markers in the epidermis from the $\Delta Np63^{-/-}$ embryos as well (**Figure 28C,G,K,O**). K5 and K14 markers expression was found in multiple layers of the epidermis in contrast to the wild-type embryos where the expression of these markers were restricted to the basal layer (**Figure 28A,E**). The $\Delta Np63^{-/-}$ embryos also expressed K10 and Filaggrin in several patches throughout the epidermis (**Figure 28G,K**). Expression of these markers were present only 5%-10% of the embryos suggesting a failure to terminally differentiate in the absence of $\Delta Np63$. Given the apparent disorganization of the epidermis from the $\Delta Np63$ mutant mice, we investigated whether cells in the epidermis expressed multiple differentiation markers simultaneously. We performed double immunostaining for an early basal marker like K14 and a later spinous marker like K10 (**Figure 28Q-T**). Surprisingly we found that in the $\Delta Np63^{+/-}$ and $\Delta Np63^{-/-}$ embryos there was a high percentage cells demonstrating overlapping expression of the differentiation markers (**Figure 28B'-C'**). This indicates that $\Delta Np63$ is required for proper differentiation of the epidermis.

Because of the appearance of the basaloid cells in the skin from the $\Delta Np63^{+/-}$ and $\Delta Np63^{-/-}$ embryos, we investigated the expression of keratin 8(K8) and keratin 18(K18) markers of the simple epithelia. While we found very few positive cells in the wild-type skin (**Figure 28U&Y**), skin from the $\Delta Np63^{+/-}$ (**Figure 28V&Z**) and $\Delta Np63^{-/-}$ (**Figure W&A**) embryos had many areas of positive cells expressed in layers above the basal epithelium. The $p63^{-/-}$ embryos did not have any positively stained cells (**Figure 28X&B'**).

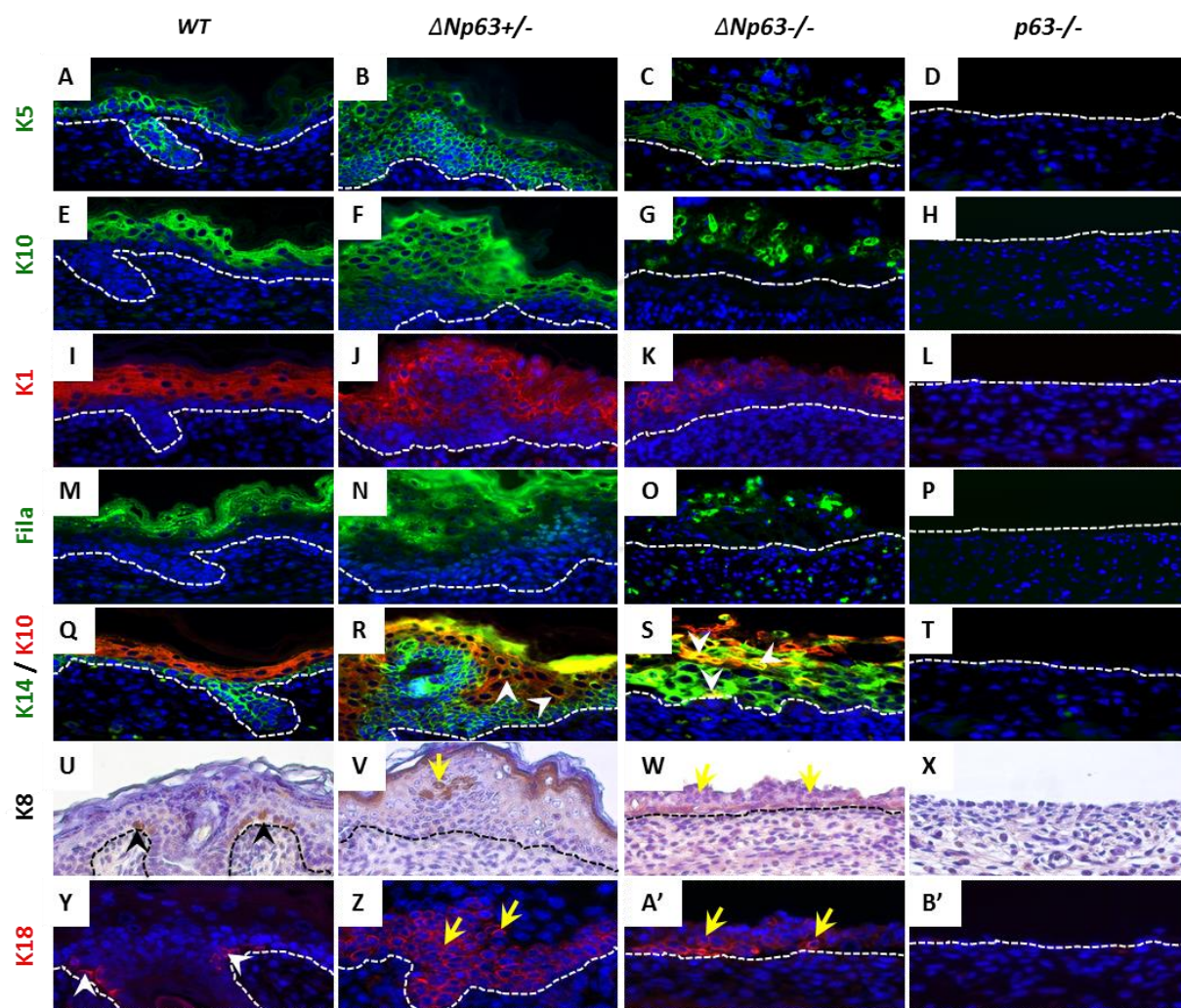


Figure 28: *Anp63* mutant mice exhibit epidermal abnormalities and defects in terminal differentiation

A-B') Immunofluorescence (IF) or immunohistochemistry (IHC) of skin from day E18.5 embryos of the indicated genotypes. Antibodies used are as follows: **(A-D)** keratin 5 (K5), **(E-H)** keratin 10 (K10), **(I-L)** keratin 1 (K1), **(M-P)** filaggrin (Fila), **(Q-T)** keratin 14 (K14) (green) and K10 (red), **(U-X)** keratin 8 (K8), and **(Y-B')** keratin 18 (K18). DAPI was used as a counterstain for IF and hematoxylin was used for IHC. Magnification 400X. Black arrowheads indicate examples of K8 positive cells in the basal layer (U). White arrowheads indicate examples of K18 positive cells in the basal layer (Y). Yellow arrows indicate examples of K8 or K18 positive cells in the spinous layer (**V, W, Z, & A'**). **C'-H')** Double immunofluorescence using skin from E18.5 day embryos of the indicated genotypes. Magnification 400X. Asterisks indicate statistical significance, ($p < 0.001$). The dashed lines denote the dermal/epidermal interface.

4.2.4. Loss of *ΔNp63* results in hyperproliferation of the epidermis

The presence of an expanded epidermis in *ΔNp63* mutant mice suggested that cells within this tissue are hyperproliferative. To determine whether there was an over proliferation of epidermal cells in the skin of *ΔNp63*^{+/−} and *ΔNp63*^{−/−} embryos, we injected pregnant *ΔNp63*^{+/−} female mice carrying *wild-type*, *ΔNp63*^{+/−} and *ΔNp63*^{−/−} embryos with bromodeoxyuridine (BrdU) to mark cells in S-phase of the cell cycle. By performing double immunofluorescence for BrdU and K5 (**Figures 29A-C**) or BrdU and K10 (**Figures 29D-F**), we found that the skin of E18.5 dpc *ΔNp63*^{+/−} and *ΔNp63*^{−/−} embryos have hyperproliferative and expanded basal and spinous layers as evidenced by the simultaneous expression of K5 and BrdU (**Figures 29G**) and K10 and BrdU (**Figures 29H**), respectively.

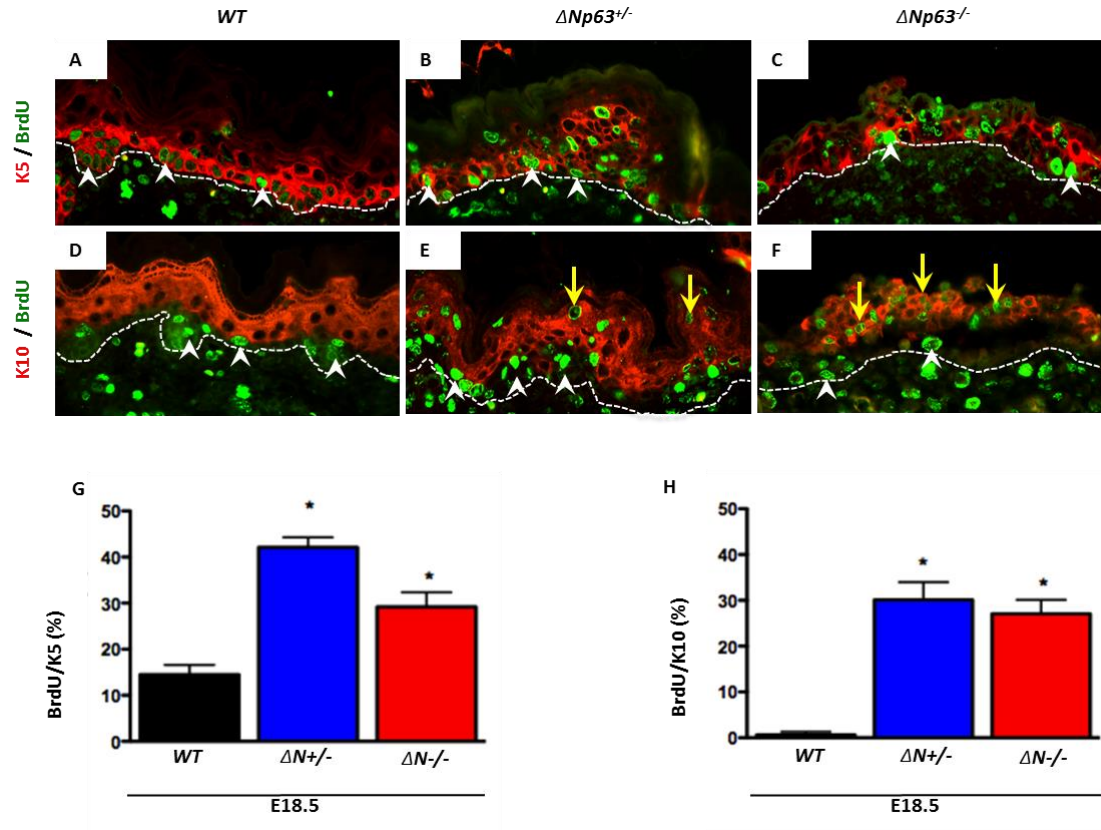


Figure 29: Loss of $\Delta Np63$ results in hyperproliferation of the epidermis

A-F) Immunofluorescence staining for anti-keratin 5, keratin 10 and bromodeoxyuridine. Antibodies used are as follows: **(A-C)** keratin 5 (K5, red) and bromodeoxyuridine (BrdU, green) and **(D-F)** keratin 10 (K10) (red) and bromodeoxyuridine (BrdU, green). DAPI was used as a counterstain. **A-C)** White arrowheads indicate examples of BrdU positive cells in the basal layer. **E&F)** Yellow arrows indicate examples of BrdU positive cells in the K10 expressing spinous layer **G)** Percentage of K5 positive cells expressing BrdU. **H)** Percentage of K10 positive cells expressing BrdU. Asterisks indicate statistical significance, ($p < 0.001$). The dashed lines denote the dermal/epidermal interface.

4.2.5. *ΔNp63* deficient epidermal cells can self-renew

Due to presence of an expanded basal layer and the expression of K8 and K18, which are one of the earliest embryonic genes expressed in both mouse ES cells and human ES cells, we investigated whether these cells can self-renew. *ΔNp63^{fl/fl}* (wild-type) and *ΔNp63Δ/Δ* (*ΔNp63* deficient) epidermal cells were serially passaged and stained with rhodamine B to score for the morphology of epidermal clones (**Figure 30A**). We scored for the shape, size, and number of clones formed by each genotype. Large, round clones are indicative of a more stem-like morphology. Indeed, the number of large, round clones was greater in *ΔNp63* deficient epidermal cells. To quantify the proliferative capacity of these clones, we labeled *wild-type* and *ΔNp63^{-/-}* clones with BrdU after serial passaging (passages 1 through 5). We then performed double immunofluorescence using anti-BrdU and anti-K5 antibodies (**Figure 30B**). Colonies of wild-type epidermal cells were initially proliferative (passage 1) but by passage 5 greater than 75% of these colonies incorporated very little BrdU (**Figures 30B & C**), indicating an inability to self-renew beyond passage 5. In contrast, colonies derived from *ΔNp63Δ/Δ* epidermal cells incorporated high levels of BrdU even at passage 5 (**Figures 30B & C**), indicating the ability to self-renew.

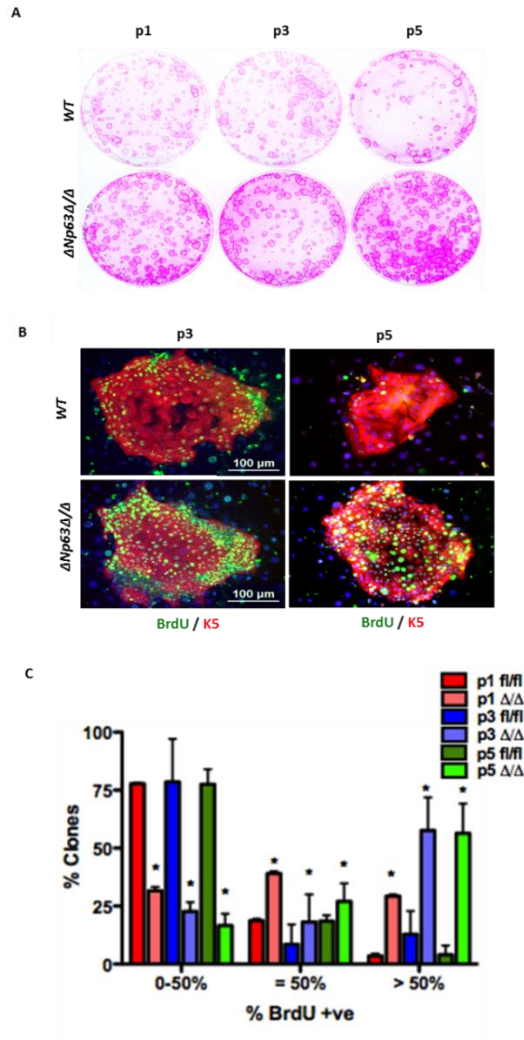


Figure 30: $\Delta Np63$ deficient epidermal cells can self-renew

A) Epidermal colonies from wild-type and $\Delta Np63$ deficient epidermal cells (Δ/Δ) cultured on J2 3T3 feeder layers and stained with rhodamine B. Passages 1 (P1), 3 (P3), and 5 (P5) are shown. **B)** Immunostaining for BrdU (green) and K5 (red) in passage 3 and 5 wild-type ($\Delta Np63^{fl/fl}$) and $\Delta Np63 \Delta/\Delta$ epidermal cells. DAPI (blue) was used as a counterstain. White bar indicates 100 μ m. **C)** Quantification of BrdU incorporation in colonies after 8 days in culture. Passages 1, 3, and 5 are shown. Experiments performed in triplicate. Asterisks indicate statistical significance (p-value <0.001).

4.2.6. *ΔNp63* deficient epidermal cells express high levels of factors associated with induced pluripotency

Based on the remarkable ability of the *ΔNp63*^{-/-} and *ΔNp63Δ/Δ* cells to proliferate over several serial passages and also based on the stem cell like morphology, we performed immunofluorescence staining for Oct-4, Nanog and stage specific embryonic antigen 1 (SSEA-1). Indeed we found that *ΔNp63*^{-/-} epidermal cells express Oct-4, Nanog and SSEA 1 at levels comparable to mouse induced pluripotent stem cells (miPS^{Yam}) generated by introduction of the Yamanaka factors while *wild-type* keratinocytes (WT-KC) do not express these markers (**Figure 31**). These data indicate that *ΔNp63*^{-/-} epidermal cells express factors associated with induced pluripotency.

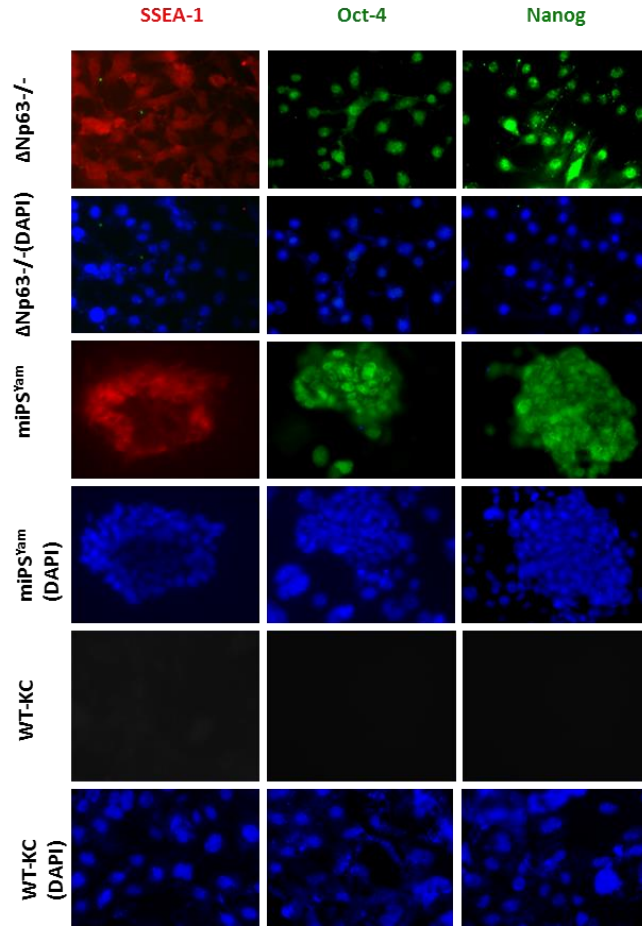


Figure 31: $\Delta Np63$ deficient epidermal cells express high levels of factors associated with induced pluripotency

Immunofluorescence (IF) performed with the indicated antibodies on mouse iPS cells (iPS^{Yam}), $\Delta Np63^{-/-}$ epidermal cells, or wild-type keratinocytes (WT-KC) using the indicated antibodies. DAPI (blue) was used as a counterstain. Magnification 400X. Experiments were done in triplicate.

4.2.7. DGCR8 expression is low in *ΔNp63* mutant cells and *ΔNp63*^{-/-} epidermis

Previously we have shown that *TAp63* transcriptionally regulates *Dicer*, which is a critical regulator of the microRNA biogenesis pathway. To investigate whether *ΔNp63* too plays a role in the regulation of the microRNA biogenesis pathway, we determined the mRNA levels of the three main important proteins in the microRNA pathway, Drosha, DGCR8 and *Dicer* (**Figure 32A**). We found *DGCR8* level was specifically downregulated in the *ΔNp63*^{-/-} epidermal cells compared to wild-type keratinocytes (**Figure 32A-B**). Interestingly we found the expression of *DGCR8* to be unaffected in the *TAp63*^{-/-} epidermal cells (**Figure 32B**).

We went on to test whether the epidermis from the *ΔNp63*^{-/-} embryos demonstrate a lack of *DGCR8* protein expression. We performed immunostaining for DGCR8 in the epidermal tissue of the *ΔNp63*^{-/-} and *wild-type* embryos and found the expression of DGCR8 to be absent in the epidermis of *ΔNp63*^{-/-} embryos (**Figure 32C**). In the *wild-type* embryos DGCR8 expression was high in the basal layer of the epidermis and in the hair follicles.

qRT-PCR and western blot analysis with anti *ΔNp63* or *DGCR8* antibody with RNA and protein lysates from wild-type, *ΔNp63*^{+/-} and *ΔNp63*^{-/-} epidermal cells showed low expression level of *ΔNp63* and DGCR8 in the *ΔNp63*^{+/-} and *ΔNp63*^{-/-} cells (**Figure 32D-F**).

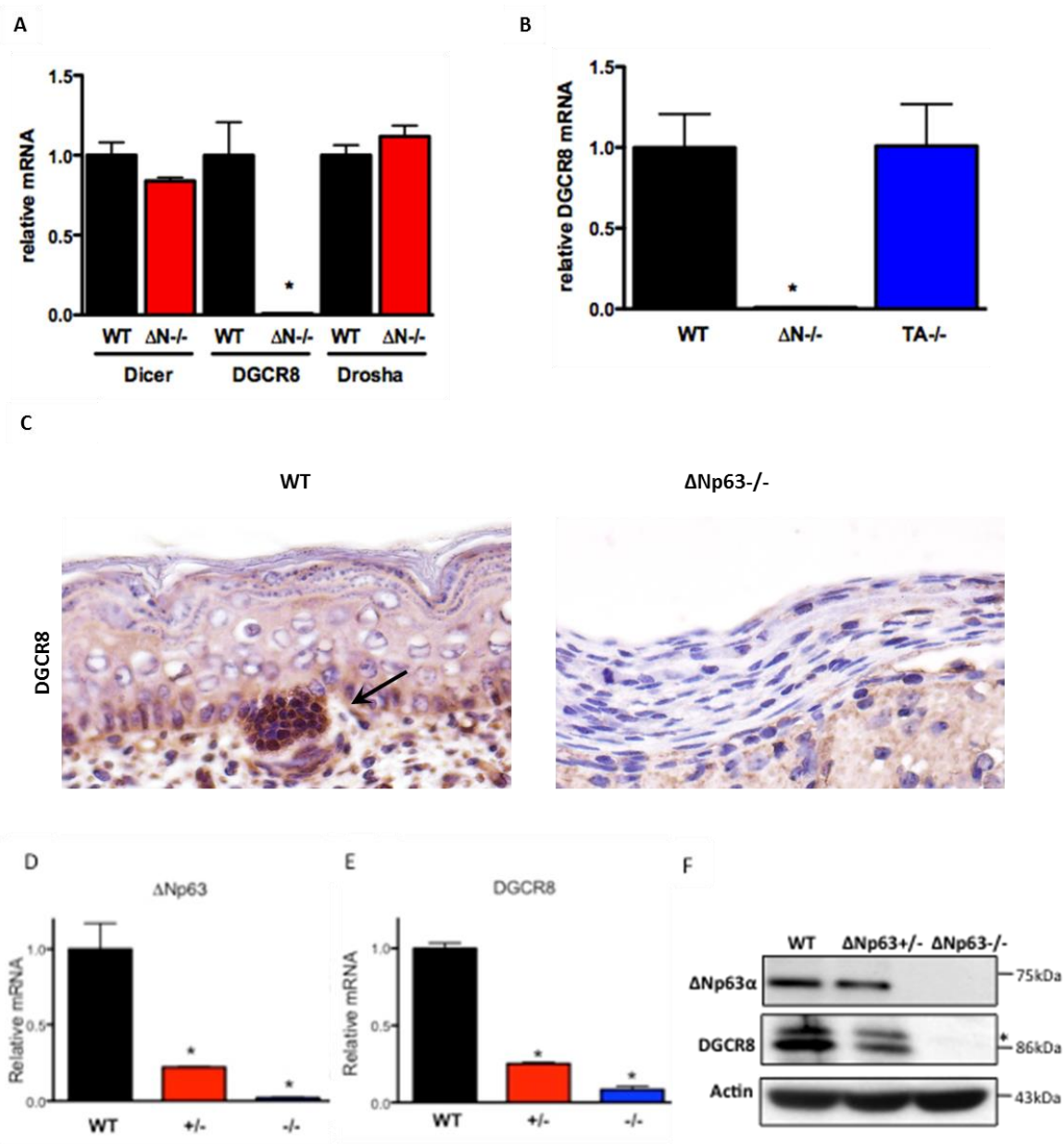


Figure 32: DGCR8 expression is low in $\Delta Np63$ mutant cells and $\Delta Np63^{-/-}$ epidermis

A) qRT-PCR for *Dicer*, *DGCR8* and *Drosha* using total RNA from wild-type (WT) and $\Delta Np63^{-/-}$ ($\Delta N^{-/-}$) epidermal cells. **B)** qRT-PCR for *DGCR8* using total RNA from wild-type (WT), $\Delta Np63^{-/-}$ ($\Delta N^{-/-}$) and *TAp63*^{-/-} epidermal cells. **C)** Immunohistochemistry using an antibody for DGCR8 on skin samples from day E18.5 wild-type and $\Delta Np63^{-/-}$ mouse embryos. **D)** qRT-PCR for *ΔNp63* in wild-type, $\Delta Np63^{+/-}$ and $\Delta Np63^{-/-}$ RNA from epidermal cells. **E)** qRT-PCR for *DGCR8* wild-type, $\Delta Np63^{+/-}$ and $\Delta Np63^{-/-}$ RNA from epidermal cells. **F)** Western blot analysis with anti *DGCR8* antibody with protein lysates from wild-type, $\Delta Np63^{+/-}$ and $\Delta Np63^{-/-}$ epidermal cells. Each bar represents the average of the fold activation of three independent experiments. The asterisks indicate statistical significance (p-value <0.001).

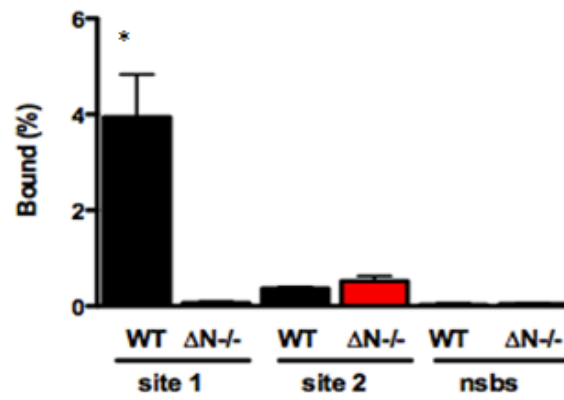
4.2.8. $\Delta Np63$ transcriptionally activates the DGCR8 promoter

To determine whether DGCR8 is a direct transcriptional target of $\Delta Np63$, we performed chromatin immunoprecipitation (ChIP) analysis using $p63$ antibodies and primers specific for two putative $p53/p63$ binding sites that we identified within intron 1 of the *DGCR8* promoter (**Figure 33B**). We found that $p63$ robustly binds to one of these sites (site 1) (**Figure 33A**). We also tested the ability of $p53$ to bind to site 1 and could not detect any significant binding, indicating that *DGCR8* is a unique $p63$ target gene.

To determine whether $p63$ isoforms can transactivate a *DGCR8-luciferase* reporter gene, we cloned the site bound to $p63$ in the ChIP assay (site 1) into a vector containing the luciferase reporter gene. We co-transfected the *DGCR8-luciferase* reporter gene (dgcr8 S-luc) (**Figure 33C**) and each $p63$ isoform individually (*TAp63* α , β , γ or $\Delta Np63$ α , β , γ) into $p53^{-/-};p63^{-/-}$ mouse embryonic fibroblasts (MEFs). Only the $\Delta Np63$ isoforms could transactivate the reporter gene with $\Delta Np63\alpha$ and β exhibiting the highest transactivation activity (**Figure 33C**). To determine whether the cloned $p63$ binding site is critical for transactivation of the *DGCR8-luciferase* reporter gene, we mutated the $p63$ consensus site from (ctgCATGtat ctctaaga agcCTTGcca) to (ctgTTTTtat ctctaaga agcTTTTcca) using site-directed mutagenesis (**Figure 33C**). None of the $p63$ isoforms transactivated the mutant *DGCR8* reporter gene (dgcr8 Sm-luc) (**Figure 33C**), indicating that $\Delta Np63$ transcriptionally activates *DGCR8* by binding to site 1.

A

DGCR8-p63 ChIP



B



C

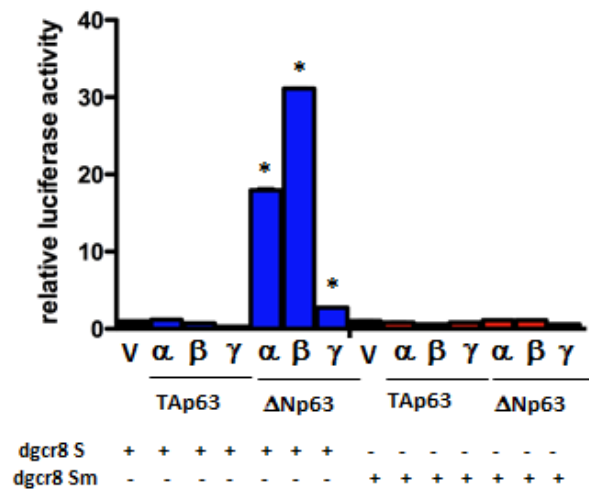


Figure 33: $\Delta Np63$ transcriptionally activates the DGCR8 promoter

A) qRT-PCR of ChIP assay using wild-type (WT) and $\Delta Np63^{-/-}$ ($\Delta N^{-/-}$) epidermal cells and indicating *p63*-binding site (site 1) or no binding of *p63* to site 2 or non-specific binding site (NSBS). **B)** Schematic showing *DGCR8*-site 1 (*dgcr8 S*) and *DGCR8*-mutant of site 1 (*dgcr8 Sm*) *luciferase* reporter genes. **C)** Luciferase assay for *DGCR8* in $p53^{-/-};p63^{-/-}$ MEFs transfected with the indicated *p63* isoforms and the indicated *luciferase* reporter gene. Each bar represents the average of the fold activation of three independent experiments. The asterisks indicate statistical significance (p-value <0.001).

4.2.9. $\Delta Np63$ represses Oct-4, Sox-2 and Nanog through transcriptional regulation of DGCR8

DGCR8 has been shown to be a critical repressor of *Oct-4*, *Sox-2* and *Nanog* expression, which are critical factors in the maintenance of pluripotency. To determine whether the $\Delta Np63^{-/-}$ epidermal cells regulate expression of *Oct-4*, *Sox-2* and *Nanog* through DGCR8, we performed immunoblotting using lysates from mouse induced pluripotent cells, reprogrammed with the Yamanaka factors (miPS^{Yam}), mouse embryonic stem cells (mES), wild-type keratinocytes (WT-KC) and $\Delta Np63^{-/-}$ cells infected with doxycycline inducible DGCR8 construct, with or without the induction of DGCR8 (**Figure 34**). We found significant levels of expression of Sox-2 and Nanog in the $\Delta Np63^{-/-}$, somewhat higher than the expression level in miPS cells and lower than the expression in mES cells. Expression of DGCR8 in the $\Delta Np63^{-/-}$ cells reduced the expression of Sox-2 and Nanog in these cells. Oct-4 expression level was much lower in the $\Delta Np63^{-/-}$ epidermal cells compared to mES and miPS^{Yam} cells. The expression of Oct-4 was also reduced on expressing DGCR8. This data indicates that $\Delta Np63^{-/-}$ epidermal cells express markers of pluripotency, which are under the regulation of DGCR8. This suggests the differentiation defects seen in these cells is possibly due to the lack of expression of DGCR8 in these cells, which maintains the cells in an undifferentiated state (**Figure 34**).

Because cells deficient for *p53* have been shown to have an enhanced ability to be reprogrammed, we investigated whether these cells have lower levels of *p53*. We found that *p53* expression in these cells remains undisturbed and the expression is comparable to *wild-type cells*, *mES* and *miPS^{Yam}* cells (**Figure 34**). This suggests that the expression of these pluripotency markers is not dependent on the *p53* status. We also assayed for the $\Delta Np63$ expression and found $\Delta Np63$ to be robustly expressed in the *wild-type* cells, but not in *mES* and *miPS^{Yam}* cells indicating that pluripotent stem cells do not express $\Delta Np63$ and further that $\Delta Np63$ is required for terminal differentiation.

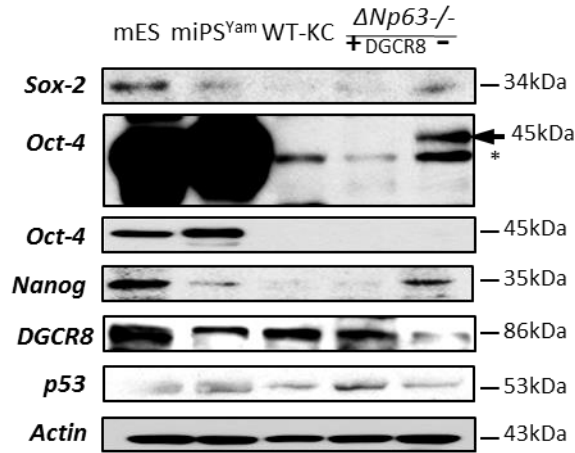


Figure 34: $\Delta Np63$ represses Oct-4, Sox-2 and Nanog through transcriptional regulation of DGCR8

Western blot analysis of mouse embryonic stem cells (mES), mouse induced pluripotent stem cells (miPS^{Yam}), wild type mouse keratinocytes (WT-KC) and $\Delta Np63^{-/-}$ epidermal cells infected with doxycycline inducible DGCR8 treated with doxycycline (+) or without doxycycline (-) using the indicated antibodies. Arrow indicates Oct4 specific band. Asterisk indicates non-specific band. Upper Oct4 blot is a longer exposure of the one immediately below it. Actin was used as loading control.

4.2.10. $\Delta Np63^{-/-}$ epidermal cells, iPS cells and mouse ES cells have a similar microRNA and mRNA signature

Because we found that $\Delta Np63$ transcriptionally activates *DGCR8*, we determined the expression of miRNAs and mRNAs in the $\Delta Np63^{-/-}$ epidermal cells using miRNA-Seq and RNA-Seq experiments. Importantly, there are critical microRNAs that have been shown to reprogram cells, such as miR-302 (249). To determine the miRNA signature of the $\Delta Np63^{-/-}$ epidermal cells, we performed miRNA-Seq experiments on RNA isolated from $\Delta Np63^{-/-}$ epidermal cells and compared them to wild-type keratinocytes, iPS^{Yam}, and mouse ES cells (**Figure 35**). Using Pearson's Correlation Analysis, we found that the $\Delta Np63^{-/-}$ epidermal cells clustered with mouse iPS^{Yam} and ES cells (**Figure 35 and Appendix 1**). We then identified an iPS signature, which included mouse iPS^{Yam}, ES, and $\Delta Np63^{-/-}$ epidermal cells (**Figure 36 and Appendix 2**) using supervised hierarchical clustering. We also performed mRNA-seq analysis with the same set of RNA from the same cell lines (**Figure 37 and Appendix 11**) We next performed miRNA-RNA functional pair analysis (**Figure 36 and Appendix 3 and 4**) using our miRNA-Seq and RNA-Seq data (184). Among the significantly upregulated miRNAs in $\Delta Np63^{-/-}$ epidermal cells, iPS^{Yam} and ES cells were miR-290, miR-295, and miR-302, miRNAs that have been found to be critical for reprogramming (191) or upregulated in iPS cells reprogrammed with the Yamanaka factors (250) (**Figure 36 and Appendix 2**). In addition, we found a number of miRNAs that were significantly down regulated in the $\Delta Np63^{-/-}$ epidermal cells, iPS^{Yam} and ES cells including miR-200a, miR-200b, miR-200c, miR-141, miR-203, miR-205, and miR-15b (**Figure 36 and Appendix 2**). We also found a set of eighteen miRNAs using miRNA-mRNA pair analysis (184) that were most significantly up or down regulated in the $\Delta Np63^{-/-}$ epidermal cells that also matched the expression pattern of miRNAs in mouse ES and mouse iPS^{Yam} cells (**Table 6. and Appendix 3 and 4**). Lastly, we performed Gene Ontology using the miRNA-mRNA pairs and DAVID software (**Figure 38 and Appendix 5**). We identified genes involved in multiple pathways including proliferation, differentiation, and development (**Figure 38**).

To determine whether these microRNAs are regulated in $\Delta Np63^{-/-}$ epidermal cells through DGCR8, we expressed DGCR8 in $\Delta Np63^{-/-}$ epidermal cells cultured in keratinocyte media (**Figure 36**). Importantly, we found that the miRNA signature from these cells

clustered with that of wild-type keratinocytes (**Figure 35 & 36 and Appendices 1 & 2**) indicating that the critical miRNAs for pluripotency in these cells is controlled through DGCR8.

There were also a number of miRNAs that were differentially regulated in $\Delta Np63^{-/-}$ epidermal cells that were distinct from the published ES and iPS miRNA profiles indicating that $\Delta Np63^{-/-}$ epidermal cells have a unique miRNA signature that poises them for pluripotency (**Figure 35, Figure 39 and Appendices 1 & 10**).

RNA-Seq using RNA isolated from wild-type mouse keratinocytes, $\Delta Np63^{-/-}$ epidermal cells, miPS^{Yam} and mES cells revealed that the gene expression signature of the $\Delta Np63^{-/-}$ epidermal cells most closely resembled the miPS^{Yam} and mES cells (**Figure 37 and Appendix 11**). These data suggest that factors other than high expression of Oct4, Sox2, and Nanog are critical for reprogramming in cells deficient for $\Delta Np63$.

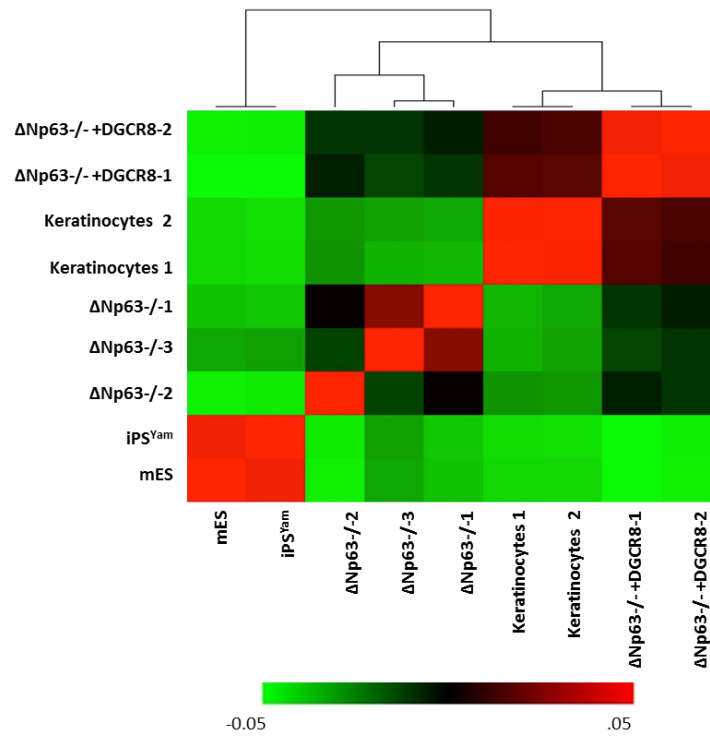
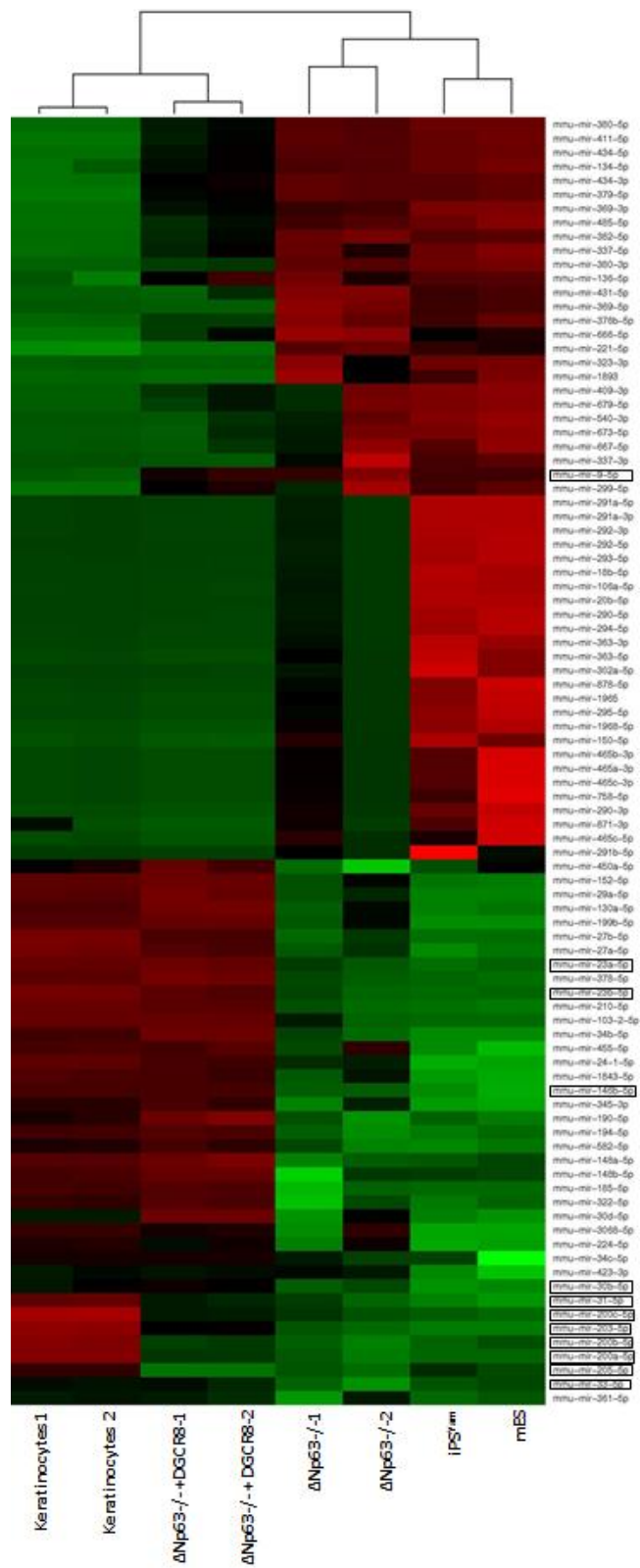


Figure 35: Pearson's Correlation Analysis from miRNA-Seq

Pearson's Correlation Analysis from miRNA-Seq performed using cells of the following genotypes: *wild-type* mouse keratinocytes (Keratinocytes 1, 2), mouse $\Delta Np63^{-/-}$ epidermal cells ($\Delta Np63^{-/-}$ 1, 2, 3), mouse $\Delta Np63^{-/-}$ epidermal cells expressing DGCR8 ($\Delta Np63^{-/-}$ 1 and 2 + DGCR8) mouse iPS cells generated from fibroblasts using the Yamanaka factors (miPS^{Yam}), and mouse embryonic stem cells (mES).



-2.69 0.0 2.88

Figure 36: Heat map showing supervised hierarchical clustering from mouse miRNA seq

Heat map showing supervised hierarchical clustering of the samples shown in (Figure 35). Low miRNA expression is indicated in green and high expression in red for both (Figure 35) and (Figure 36). Boxes marked in black indicate miRNAs that were most significantly up- or down- regulated in the $\Delta Np63/iPS$ cell signature. The signature that was found to be most highly significant is boxed in black.

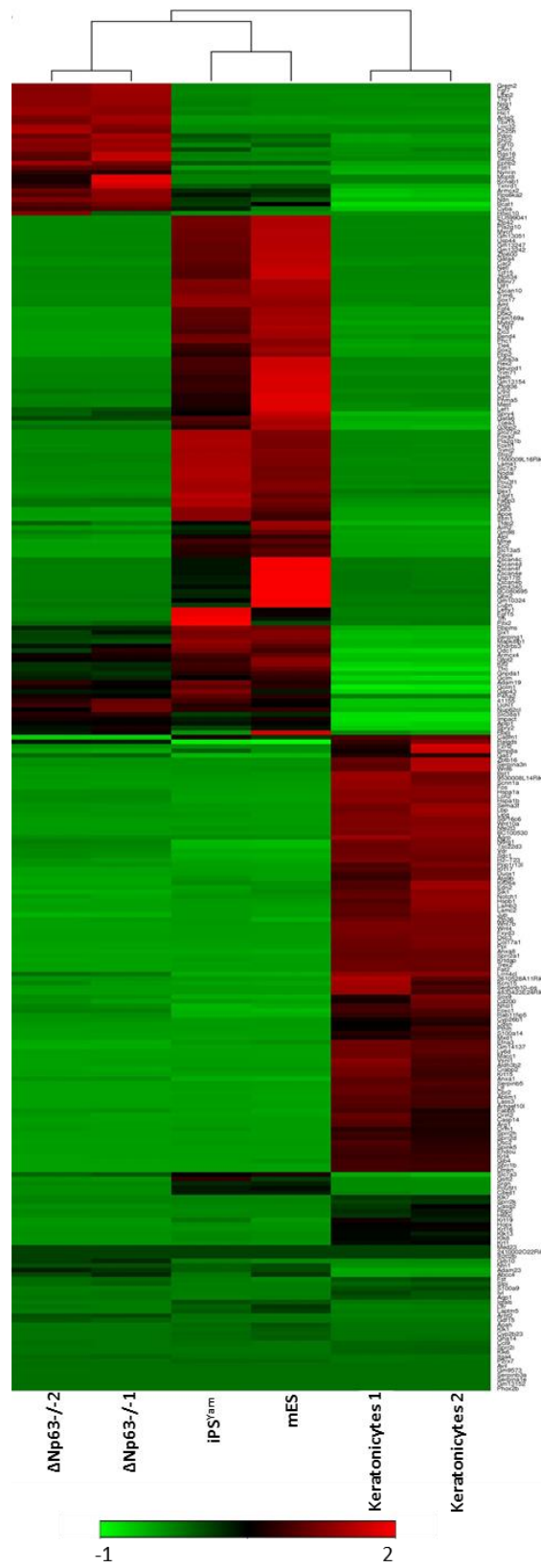


Figure 37: Unsupervised and supervised clustering for mRNA-seq mouse

Table 6: miRNA-mRNA functional pair analysis

miRNA-mRNA pair analysis

up-regulated miRs	Down-regulated genes	Enrichment P-value	Enrichment ratio
mmu-mir-9-5p	70	1.57902E-05	1.862543228
mmu-mir-125b-5p	63	8.36196E-10	2.545387556
mmu-mir-199a-5p	32	2.22547E-05	2.466661972
mmu-mir-145-5p	39	0.00010874	2.100954808
mmu-mir-100-5p	6	0.008425052	3.710047286

down-regulated miRs	Up-regulated Genes	Enrichment P-value	Enrichment ratio
mmu-mir-200b-5p	106	1.33959E-23	3.307980671
mmu-mir-200a-5p	62	2.46229E-11	2.836918151
mmu-mir-141-5p	62	2.46229E-11	2.836918151
mmu-mir-33-5p	39	6.74602E-11	3.693817182
mmu-mir-205-5p	38	4.01818E-09	3.267757846
mmu-mir-203-5p	56	8.29817E-09	2.571063711
mmu-let-7e-5p	63	5.68768E-05	1.869160502
mmu-mir-31-5p	23	0.001870575	2.186048531
mmu-mir-183-5p	43	3.9476E-11	3.508384592
mmu-mir-96-5p	81	4.72988E-11	2.443349005
mmu-mir-138-5p	40	6.47987E-06	2.391875732
mmu-mir-135b-5p	41	0.00062505	1.921466608
mmu-mir-335-3p	16	0.004954846	2.317689212

miRNA-mRNA functional pair analysis using the samples shown in (A).

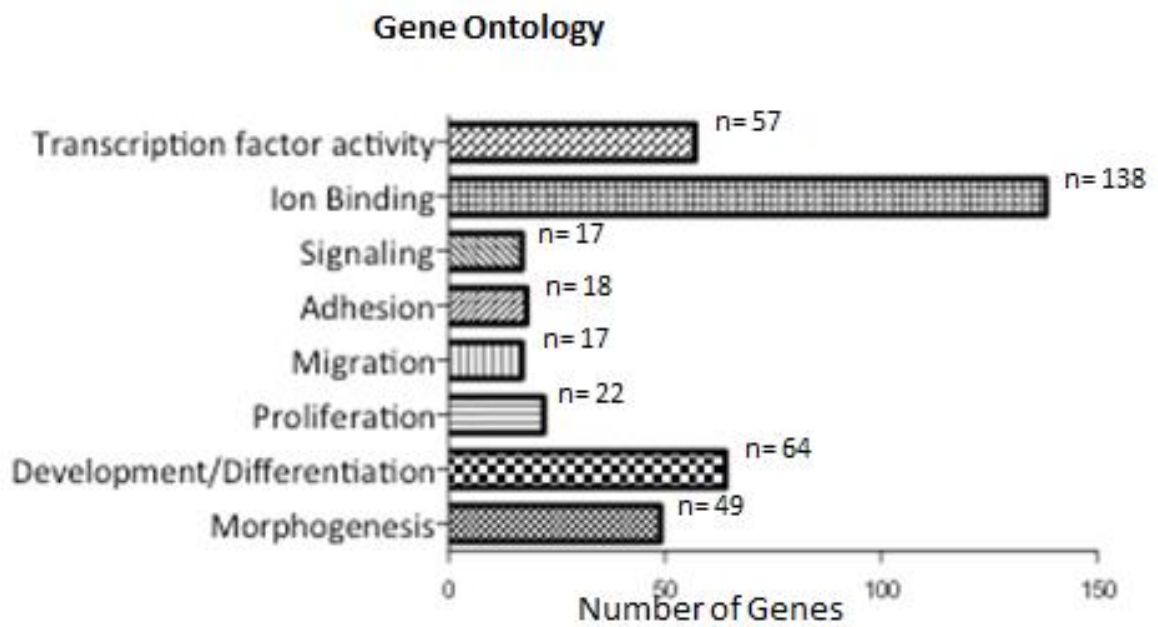


Figure 38: Gene Ontology using DAVID software

Gene Ontology using DAVID software of the miRNA-mRNA functional pair analysis shown in (Table 6).

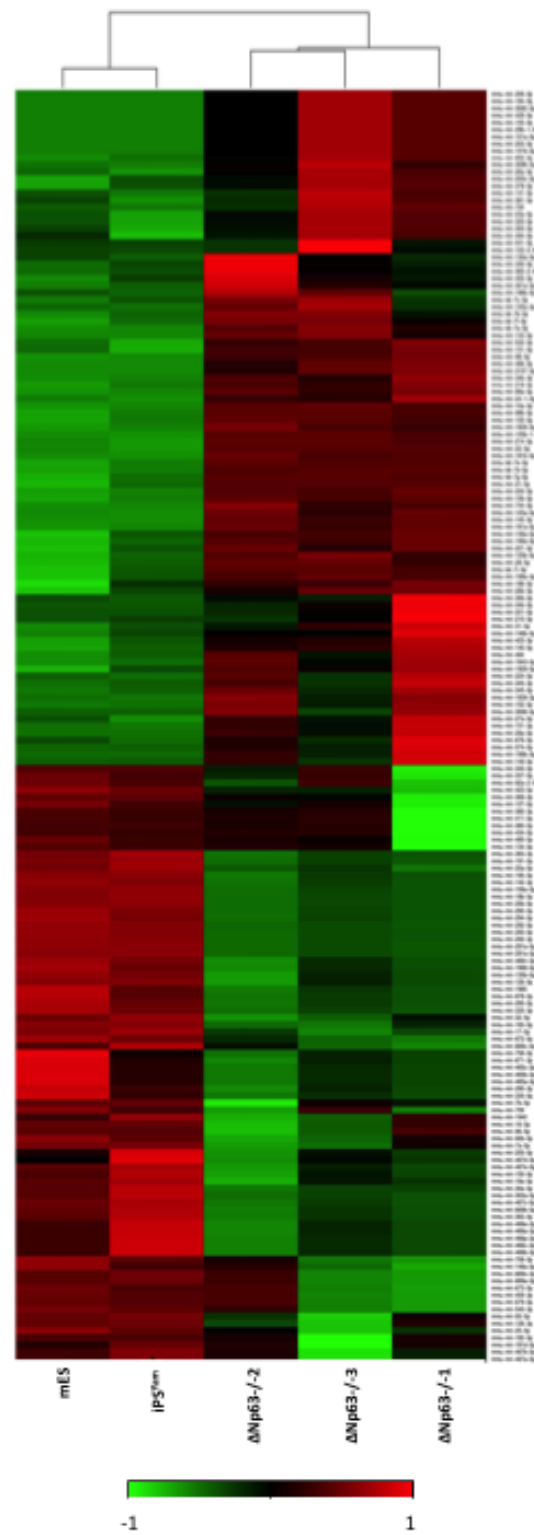


Figure 39: Supervised miR-seq clustering with the data from Figure 35 showing differences between $\Delta Np63^{-/-}$ and miPSYam.

4.2.11. *ΔNp63* deficient epidermal cells can be differentiated into multiple cell fates in vitro

High levels of Oct4, Sox2, and Nanog in *ΔNp63*^{-/-} and *ΔNp63Δ/Δ* epidermal cells and their apparent morphology suggested that these cells are pluripotent. To determine whether the epidermal cells deficient for *ΔNp63* are pluripotent and could differentiate into different cell fates, we cultured *ΔNp63Δ/Δ* cells under conditions permissive for keratinocyte or neuronal differentiation. Because differentiation of *ΔNp63* deficient epidermal cells is dependent on expression of DGCR8, we cultured *ΔNp63Δ/Δ* epidermal cells expressing DGCR8 in keratinocyte differentiation media and found that cells exhibited a differentiated morphology (compare **Figures 40A & B**) and expressed markers of keratinocyte differentiation, similar to levels expressed in wild-type keratinocytes (**Figure 40D**).

When we cultured *ΔNp63Δ/Δ* epidermal cells expressing DGCR8 in neuroectodermal media, these cells displayed a neuronal morphology (**Figure 40C**). Importantly, these cells expressed nestin and NeuN, markers of neuronal differentiation (**Figure 40E**).

Furthermore when the *ΔNp63Δ/Δ* cells and *ΔNp63*^{-/-} epidermal cells with or without the expression of DGCR8, were cultured under conditions permissive for embryoid body formation, they all formed embryoid body like structure (**Figure 41A-D**). On validation of the differentiation marker expression for ectoderm-nestin, mesoderm-brachyury and endoderm-alpha-feto protein (AFP), we found that the embryoid bodies expressing DGCR8 had a higher level of expression of these differentiation markers, compared to the *ΔNp63* deficient embryoid bodies which did not express DGCR8. Embryoid bodies from mES cells were used as positive control for these marker expressions (**Figure 41E-G**).

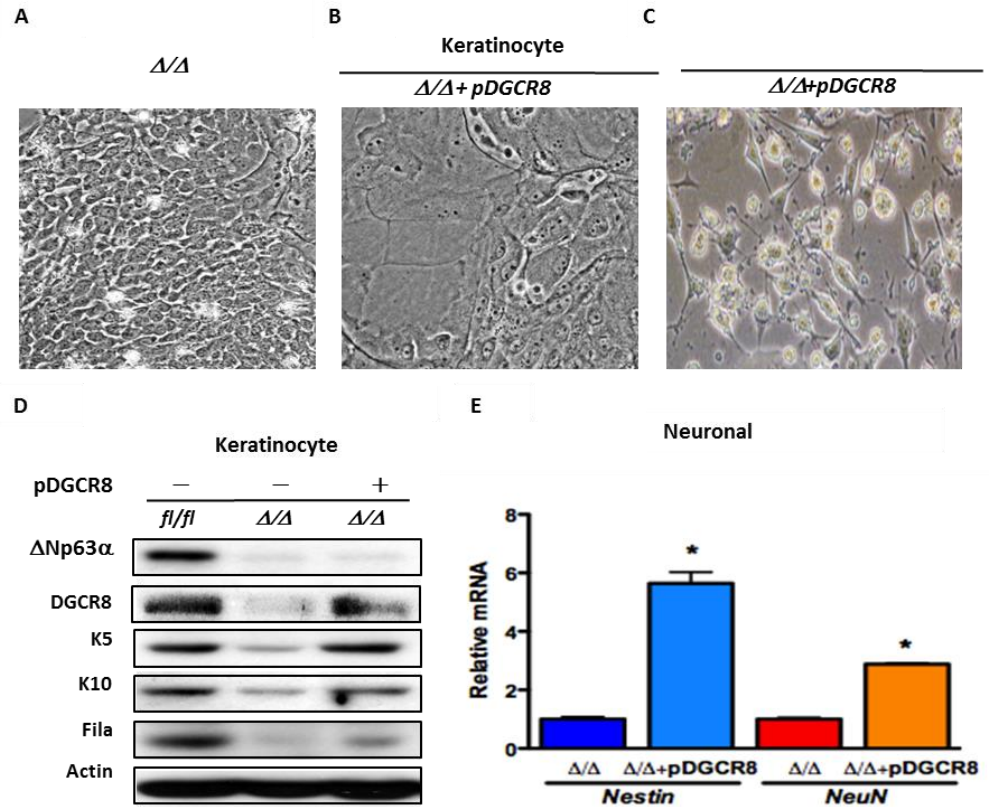


Figure 38: $\Delta Np63$ deficient epidermal cells are pluripotent

A-D) $\Delta Np63$ deficient epidermal cells (Δ/Δ with or without DGCR8 (pDGCR8) cultured under the following conditions: (A) keratinocyte media (Low Ca^{2+}), (B) keratinocyte differentiation media (High Ca^{2+}), and (C) neuroectodermal media. **D)** Western blot analysis of epidermal cells cultured in keratinocyte differentiation media of the indicated genotypes with (+pDGCR8) or without (-pDGCR8) DGCR8 and using the antibodies shown. Actin was used as a loading control. **E)** qRT-PCR for *nestin* and *NeuN* using total RNA from epidermal cells of the indicated genotypes cultured in neuroectodermal media. Magnification at 200x.

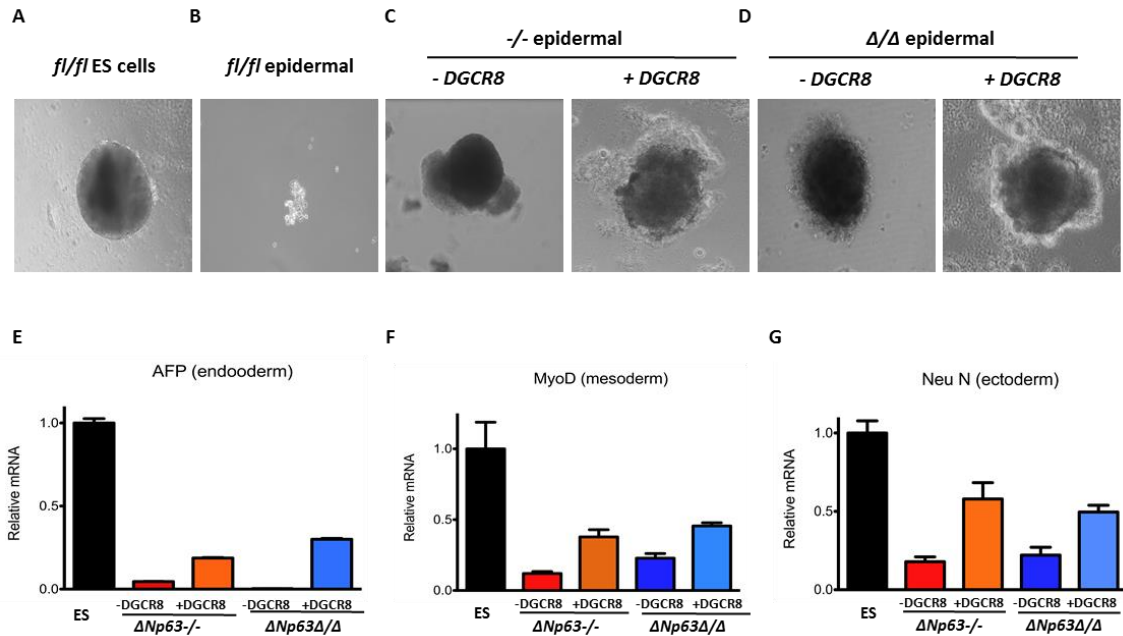


Figure 39: $\Delta Np63$ deficient cells can form embryoid bodies

A-D) Embryoid bodies from cells of the indicated genotypes: A) Embryoid body from mouse embryonic stem cells. B) Cell clump from murine keratinocytes. C) $\Delta Np63^{-/-}$ cells infected with lentiviral DGCR8 with (+DGCR8) or without doxycycline (-DGCR8) form embryoid bodies D) $\Delta Np63^{\Delta/\Delta}$ cells infected with lentiviral DGCR8 with or without DGCR8 form embryoid bodies. **E-G)** qRT-PCR for AFP from the embryoid bodies from mouse ES cells, $\Delta Np63^{-/-}$ cells and $\Delta Np63^{\Delta/\Delta}$ infected with lentiviral DGCR8 treated with (+DGCR8) or without (-DGCR8) doxycycline. Experiments were done in triplicates. The asterisks indicate statistical significance (p-value <0.001).

4.2.11. *ΔNp63* deficient epidermal cells are pluripotent and can differentiate into multiple cell fates in vivo

Our data thus far indicates that epidermal cells lacking *ΔNp63* have characteristics of induced pluripotent stem (iPS) cells. To further determine whether *ΔNp63*^{-/-} epidermal cells are iPS cells, we asked whether cells lacking *ΔNp63* could form teratomas after injection into mice. Indeed, we found that *ΔNp63*^{-/-} epidermal cells can form poorly differentiated teratomas in mice and express markers of the ectoderm, mesoderm, and endoderm (**Figure 42B,E,H**). Moreover, we found that these *ΔNp63*^{-/-} teratomas express low levels of mesoderm -brachyury (**Figure 42K**), ectoderm-nestin (**Figure 42N**), and AFP (**Figure 42Q**). Because we found that the terminal differentiation of *ΔNp63*^{-/-} epidermal cells depends on the expression of DGCR8 (**Figure 34**), we transduced *ΔNp63*^{-/-} epidermal cells with a tetracycline inducible DGCR8 vector. These cells were injected into mice, were allowed to form tumors for four weeks, and fed doxycycline for two weeks. The *ΔNp63*^{-/-} epidermal cells expressing DGCR8 form well-differentiated teratomas (**Figure 42B-H**) that express markers of the mesoderm (**Figure 42L**), ectoderm (**Figure 42O**), and endoderm (**Figure 42R**). Expression and structures apparent in *ΔNp63*^{-/-} epidermal cells expressing DGCR8 is similar to that of wild-type mES cells (**Figure 42A-P**). These data indicate that *ΔNp63*^{-/-} epidermal cells are iPS cells that can be reprogrammed into multiple cell fates.

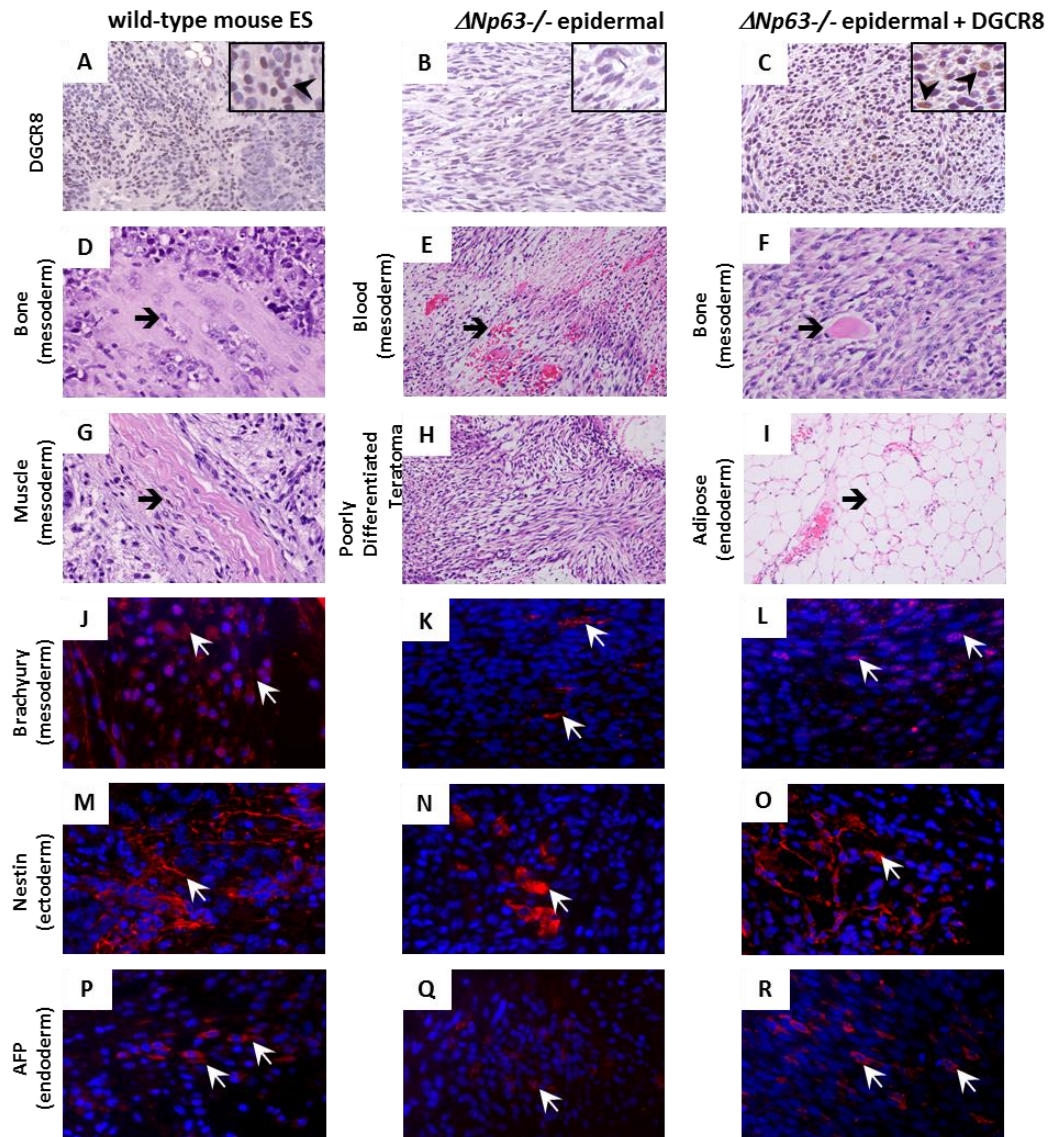


Figure 40: *ΔNp63* deficient epidermal cells can form teratomas

A-C) Immunohistochemistry (IHC) using an antibody for DGCR8 on teratomas of the indicated genotypes. (200X magnification) and insets (400X magnification). Arrows in insets point to examples of positive cells. **D-I)** Hematoxylin and eosin (H&E) stained cross sections of teratomas derived from wild-type mouse embryonic stem cells (**D & G**), *ΔNp63*^{-/-} epidermal cells (**E & H**), and *ΔNp63*^{-/-} epidermal cells expressing DGCR8 (**F & I**). (**J-R**) Immunofluorescence (IF) of teratomas of the indicated genotypes using the indicated antibodies. DAPI (blue) was used as counterstains. Magnification 200X

4.2.12. Generation of chimeric mouse embryos from $\Delta Np63^{-/-}$ epidermal cells

We next asked whether $\Delta Np63^{-/-}$ epidermal cells could contribute to tissues of the developing mouse. To determine this, we performed blastocyst injections using iPS^{Yam} expressing GFP and $\Delta Np63^{-/-}$ epidermal cells expressing GFP. Indeed we found that $\Delta Np63^{-/-}$ epidermal cells expressing GFP form high contribution chimeras (**Figure 43C,D,H,I**) comparable to what is seen with iPS cells created using the Yamanaka factors expressing GFP (**Figure 43A,B,F,G**). Cross sections through multiple tissues of chimeras generated from both iPS cell types revealed similar chimeric contribution (**Figure 43K-N**) as detected by anti-GFP immunostaining. The epidermis from the $\Delta Np63^{-/-}$ chimeric mice resembled the epidermis of $\Delta Np63^{-/-}$ and $\Delta Np63^{+/-}$ mice (**Figure 44A-C**). They showed hyperproliferation of K5 positive cells in the basal layer (**Figure 44D-F**). The epidermis also demonstrated overexpression of K8 and K18 positive cells similar to $\Delta Np63^{-/-}$ and $\Delta Np63^{+/-}$ mice epidermis (**Figure 44G-L**). We also performed a southern blot to eliminate the possibility of contamination of the $\Delta Np63^{-/-}$ epidermal cells with the miPS^{Yam} cells with a probe targeted towards the Klf4 exon (**Figure 44M**). The southern blot conclusively indicates that the $\Delta Np63^{-/-}$ cells are not contaminated. The chimeras generated from the $\Delta Np63^{-/-}$ epidermal cells exhibited post-natal lethality due to their similarity in phenotype to the $\Delta Np63^{-/-}$ mice. Like the $\Delta Np63^{-/-}$ mice, these chimeras also died few hours after birth due to the lack of proper skin formation from dehydration and desiccation. Table. 7. summarizes the number of chimeras generated from the $\Delta Np63^{-/-}$ epidermal cells and the control miPS cells generated by the Yamanaka factor infection of mouse fibroblasts.

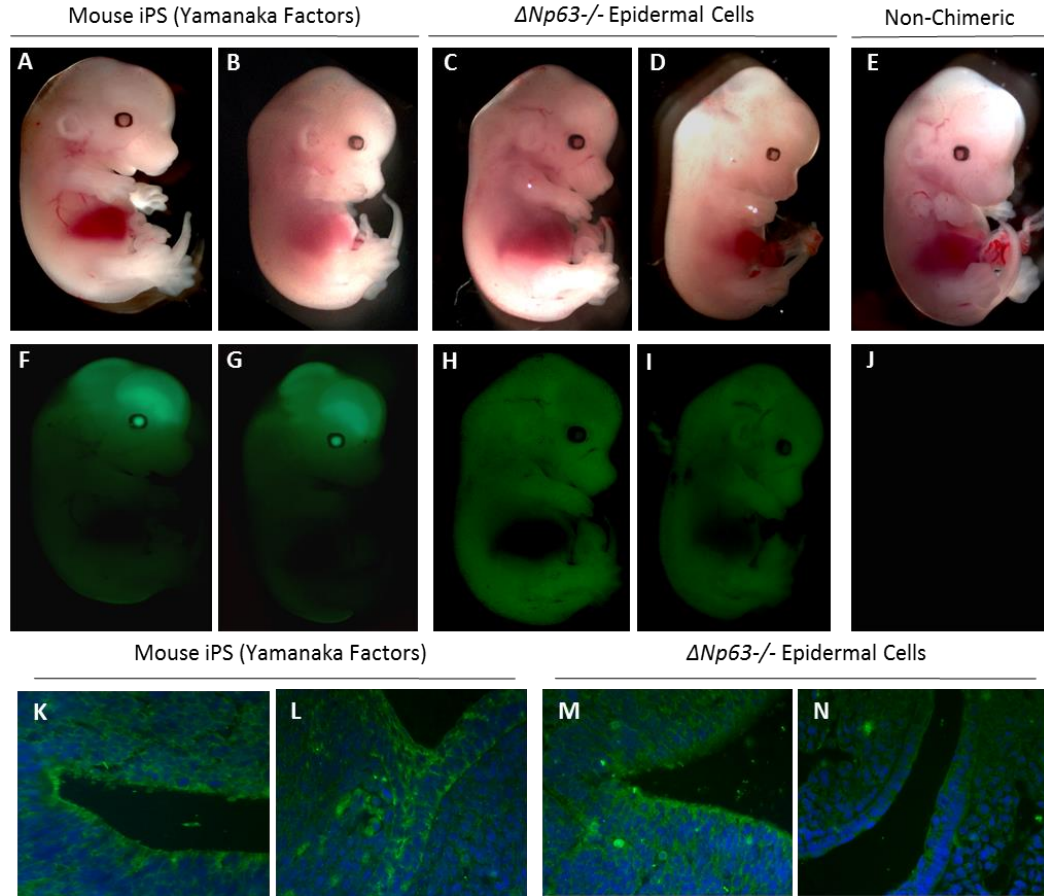


Figure 41: Generation of chimeric mouse embryos from $\Delta Np63^{-/-}$ epidermal cells

A-E) Brightfield images of chimeric embryos at day 13.5 (E13.5) generated from mouse induced pluripotent stem cells expressing the Yamanaka factors and GFP (iPS^{Yam}) (A&B) or $\Delta Np63$ deficient epidermal cells expressing GFP ($\Delta Np63^{-/-}$) (C&D). (E) E13.5 embryos from wild-type, non-chimeric mice. **F-J)** Fluorescent images of E13.5 chimeric embryos with GFP expressing tissues derived from the Yamanaka miPS cells (F & G) or $\Delta Np63^{-/-}$ epidermal cells (H&I). J) E13.5 embryos from wild-type, non-chimeric mice. **K-N)** Immunofluorescence for GFP (green) in the brain (K) and gut (L) of E13.5 embryos generated from Yamanaka miPS cells expressing GFP (Yamanaka Factors) or in the brain (M) and gut (N) of E13.5 embryos generated from $\Delta Np63^{-/-}$ epidermal cells. DAPI (blue) was used as counterstain. Magnification 200X

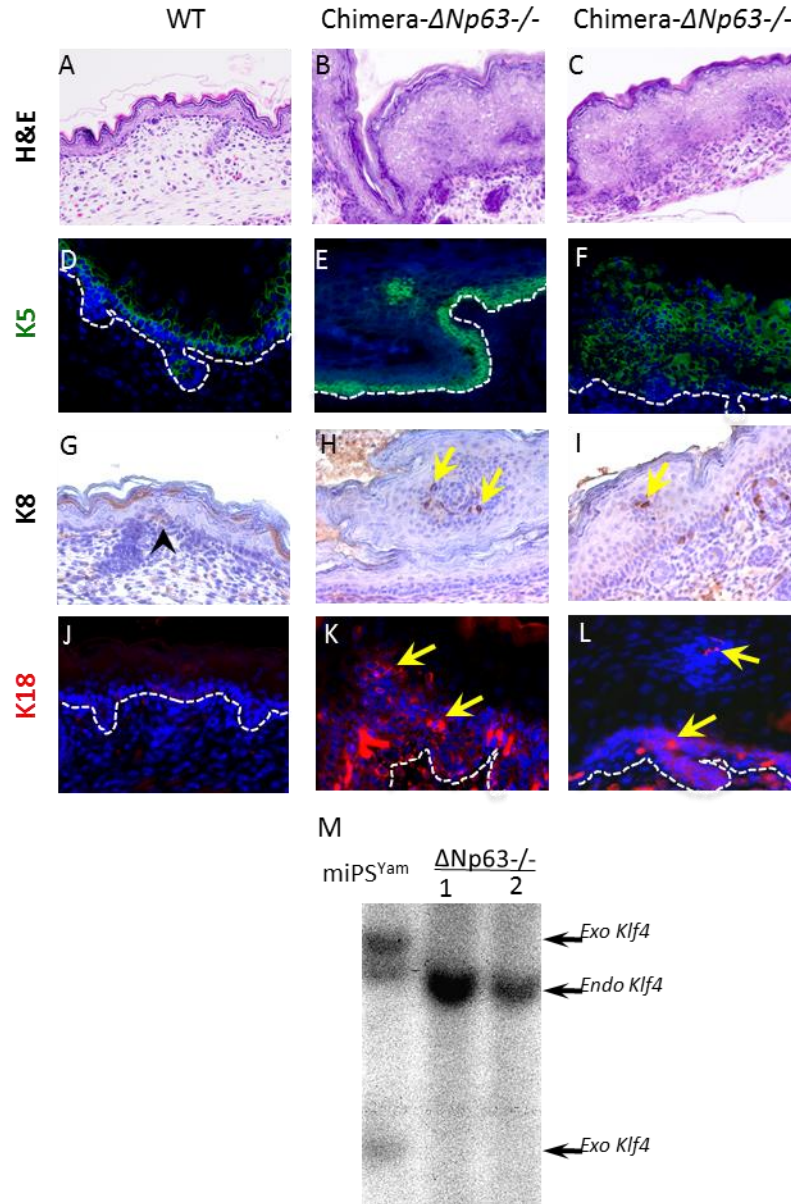


Figure 42: Analysis of $\Delta Np63^{-/-}$ chimeras

A-C) Hematoxylin and Eosin (H&E) stained cross sections of the epidermis from E18.5 embryos of wild-type mice and $\Delta Np63^{-/-}$ chimeric mice. **D-L)** Immunofluorescence (IF) or immunohistochemistry (IHC) of cross sections from wild-type and $\Delta Np63^{-/-}$ chimeras at day E18.5 stained with the indicated antibodies (200X magnification). **M)** Southern blot analysis using genomic DNA extracted from mouse iPS cells reprogrammed with the Yamanaka factors (iPS^{Yam}) and $\Delta Np63^{-/-}$ epidermal cells. A probe for Klf4 was used to indicate endogenous (endo) and exogenous (exo) Klf4 DNA.

Table 7: Embryos generated from iPS cells

iPS cells	# of blastocysts	# of embryos @ E13.5	# of GFP +ve
Δ Np63 ^{-/-} 1	17	4	2
Δ Np63 ^{-/-} 2	12	3	1
Δ Np63 ^{-/-} 3	14	0	N/A
Δ Np63 ^{-/-} 4	15	1	0
Δ Np63 ^{-/-} 5	15	4	2
Δ Np63 ^{-/-} 6	20	0	N/A
Δ Np63 ^{-/-} 7	21	0	N/A
iPS ^{Yam} -1	14	0	N/A
iPS ^{Yam} -2	12	2	1
iPS ^{Yam} -3	16	9	4
iPS ^{Yam} -4	16	9	3
iPS ^{Yam} -5	21	6	2
iPS ^{Yam} -6	21	7	3

Δ Np63^{-/-}: epidermal cells derived from Δ Np63^{-/-} mice

iPS^{Yam}: mouse fibroblasts reprogrammed with Yamanaka factors

E13.5: embryonic day 13.5

N/A: not applicable

4.2.13. Normal human epidermal keratinocytes can be induced to pluripotency by knockdown of *ΔNp63*

To determine whether knockdown of *ΔNp63* or DGCR8 could induce pluripotency in human epidermal keratinocytes. We knocked down *ΔNp63* or DGCR8 in normal human epidermal keratinocytes (NHEKs) (**Figure 45A & B**). NHEKs with knock down of *ΔNp63* or DGCR8 changed morphology (**Figure 45 E & F**). We started to notice small packed Tra-1-60 positive colonies at 6 days in the sh*ΔNp63* or shDGCR8. Colonies from NHEKs with knock down of *ΔNp63* or DGCR8 appeared more packed than colonies formed from NHEKs (**Figure 45A**) and more similar to human iPS colonies (hiPS) (**Figure 45D**). NHEKs with knock down of *ΔNp63* (**Figure 46A-E**) or DGCR8 (**Figure 46F-J**) also expressed SSEA-4, Tra-1-60, Oct4, Sox2, and Nanog similar to the expression in hiPS cells (**Figures K-O**) while NHEKs alone do not express these markers of pluripotency (**Figure P-T**).

Western blotting was performed on these cells with antibodies towards either *ΔNp63* or DGCR8 to determine whether the lentiviral silencing was still maintained (**Figure U&V**).

ΔNp63 and DGCR8 were still found to be down regulated. qRT-PCR was performed to verify levels of Oct-4, Sox-2 and Nanog in the NHEK-sh*ΔNp63* (**Figure W-Y**) and NHEK-shDGCR8 cells (**Figure Z-B'**). Levels of Oct-4 and Sox-2 and Nanog were found to high but varied in the different cell lines, suggesting that the reprogramming occurs at different levels in these different cell lines.

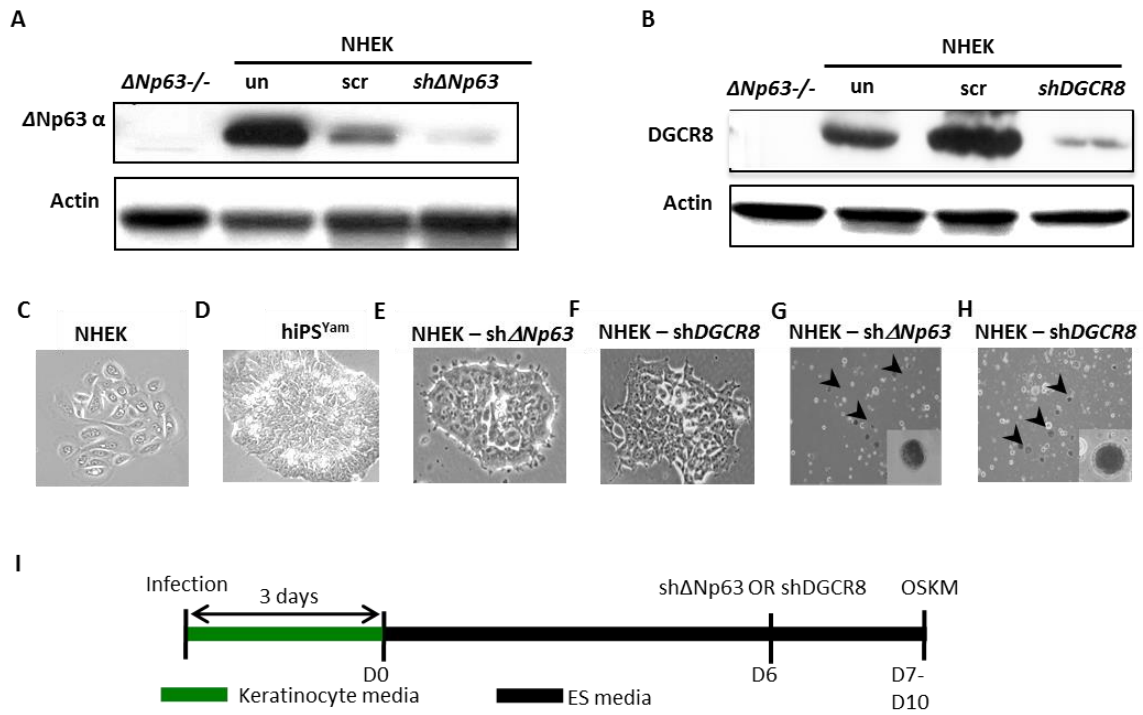


Figure 43: Reprogramming of NHEK cells by down regulation of $\Delta Np63$ or DGCR8

A-B) Western blot analysis of downregulation of $\Delta Np63$ or DGCR8 in the NHEK cells. Actin was used as a loading control **C-H)** Phenotypes of the colonies of cells of the indicated genotypes. Magnification 400x. **I)** A cartoon representing the timing of reprogramming of the NHEK cells after knock down of $\Delta Np63$ or DGCR8.

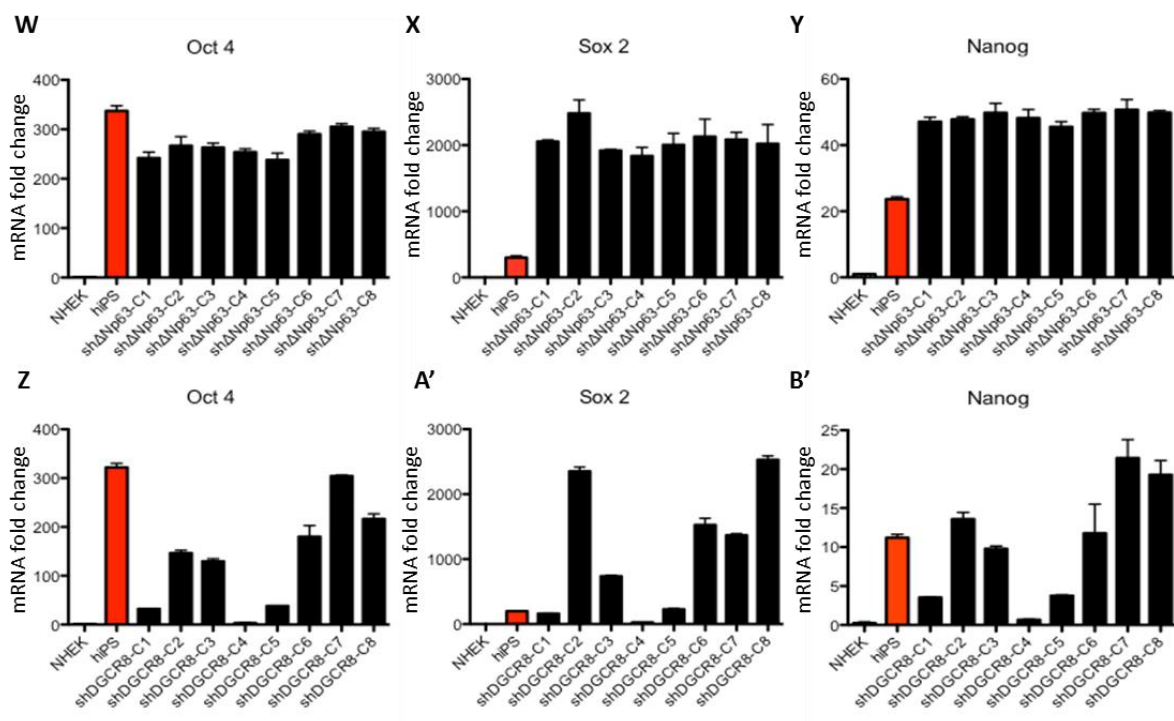
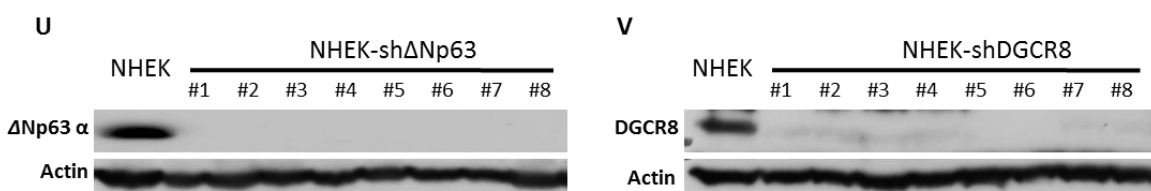
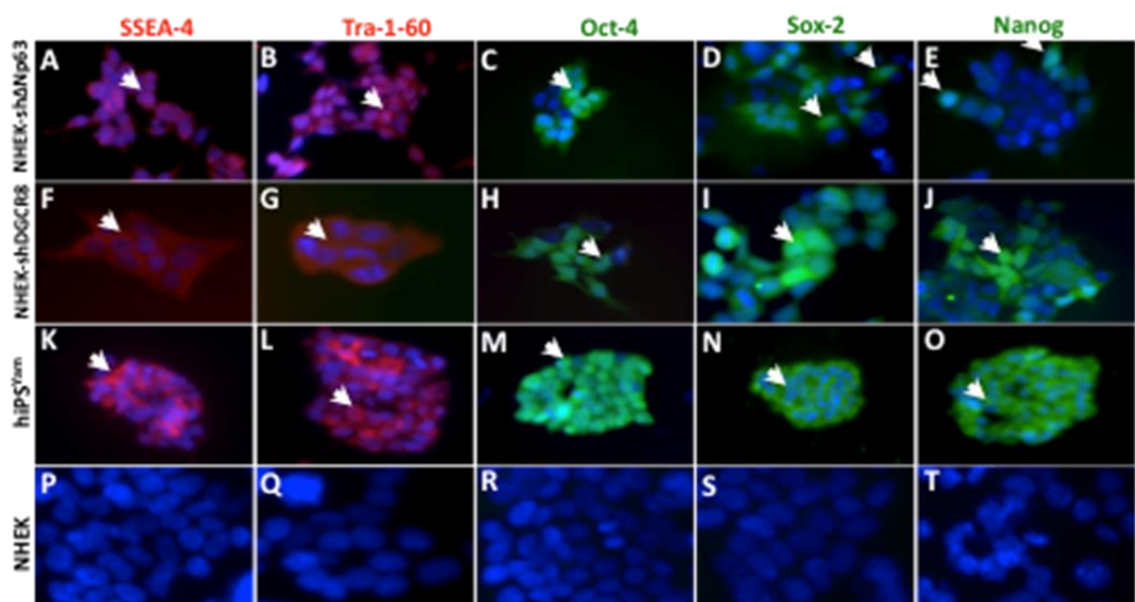


Figure 44: Characterization of NHEK-sh*ΔNp63*/*DGCR8* cells

A-T) Immunofluorescence (IF) using normal human epidermal keratinocytes (NHEK) infected with lentiviral shRNA for *ΔNp63* (NHEK-sh*ΔNp63*) (**A-E**) or *DGCR8* (NHEK-sh*DGCR8*) (**F-J**), fibroblasts infected with the Yamanaka Factors (Human iPS) (**K-O**), and NHEK cells and the indicated antibodies. DAPI (blue) was used as counterstain. Arrows indicate examples of positive nuclei. Magnification, 200X.

4.2.14. NHEK-Sh Δ Np63 /shDGCR8 cells can form teratomas

We next asked whether these cells could form teratomas in SCID mice. Indeed, we found that these cells form differentiated teratomas with structures representing the endoderm (**Figure 47A&E**), mesoderm (**Figure 47 B,C & F,G**), and ectoderm (**Figure 47D&H**). Additional immunofluorescence for marker analysis revealed robust expression of AFP, brachyury, E-cadherin, and keratin 5 (**Figure 47I-P**) comparable to the expression in human iPS cells generated using the Yamanaka factors (**Figure 47Q-T**). Taken together, these data indicate human keratinocytes can be reprogrammed to different cell fates by knock down of Δ Np63.

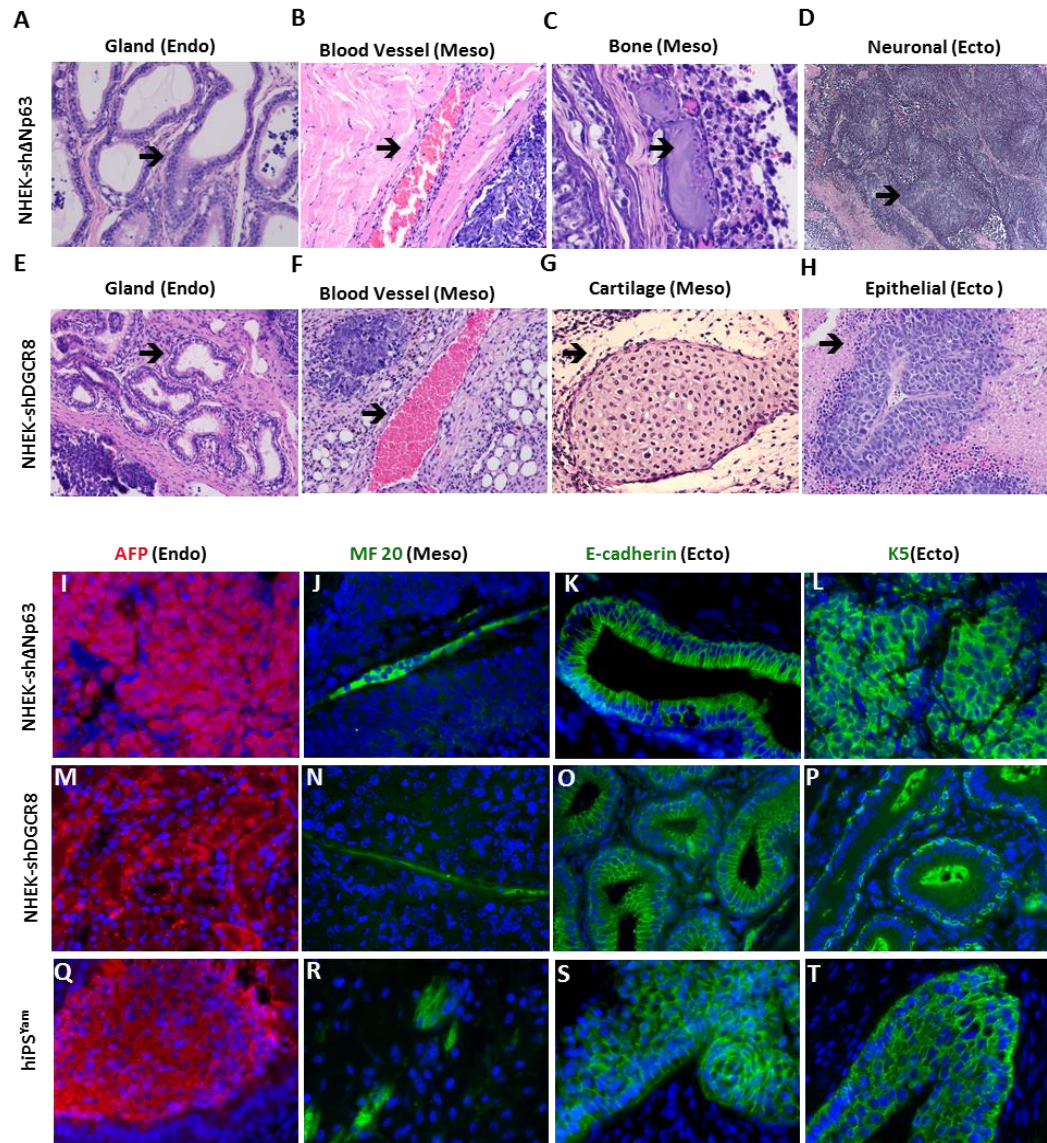


Figure 45: NHEK-shΔNp63 /shDGCR8 cells can form teratomas

A-H) Micrographs of hematoxylin and eosin stained cross-sections from teratomas generated using NHEK-shΔNp63 and NHEK-shDGCR8 cells indicating the structural diversity of the three embryonic layers as indicated. Magnification, 200X. **I-T)** IF performed on cross-sections of teratomas derived from NHEK-shΔNp63 cells (**I-L**), NHEK-shDGCR8 cells (**M-P**) or human iPS cells (**Q-T**) using the indicated antibodies. DAPI (blue) was used as counterstain. Magnification, 200X.

4.2.15. $\Delta Np63$ deficient mouse and human epidermal cells have a similar miRNA signature to mouse and human iPS cells reprogrammed with the Yamanaka factors

We performed microRNA-Seq using RNA isolated from NHEKs with knock down of $\Delta Np63$ or DGCR8 (**Figure 48A-C** and **Appendices 5,6** and **7**). Interestingly, we found that the microRNA expression signature of these cells clustered with $\Delta Np63^{-/-}$ epidermal cells, miPSYam, and mES cells indicating that pluripotency can be induced by acute knock down of $\Delta Np63$ or DGCR8 in human keratinocytes (**Figure 48A** and **48B** and **Appendices 5** and **6**). Additionally, NHEKs with knock down of $\Delta Np63$ or DGCR8 had a nearly identical microRNA expression signature, indicating that cells deficient for $\Delta Np63$ regulate the same genes in differentiation and stem cell specification as DGCR8 (**Figure 48C** and **Appendix 7**).

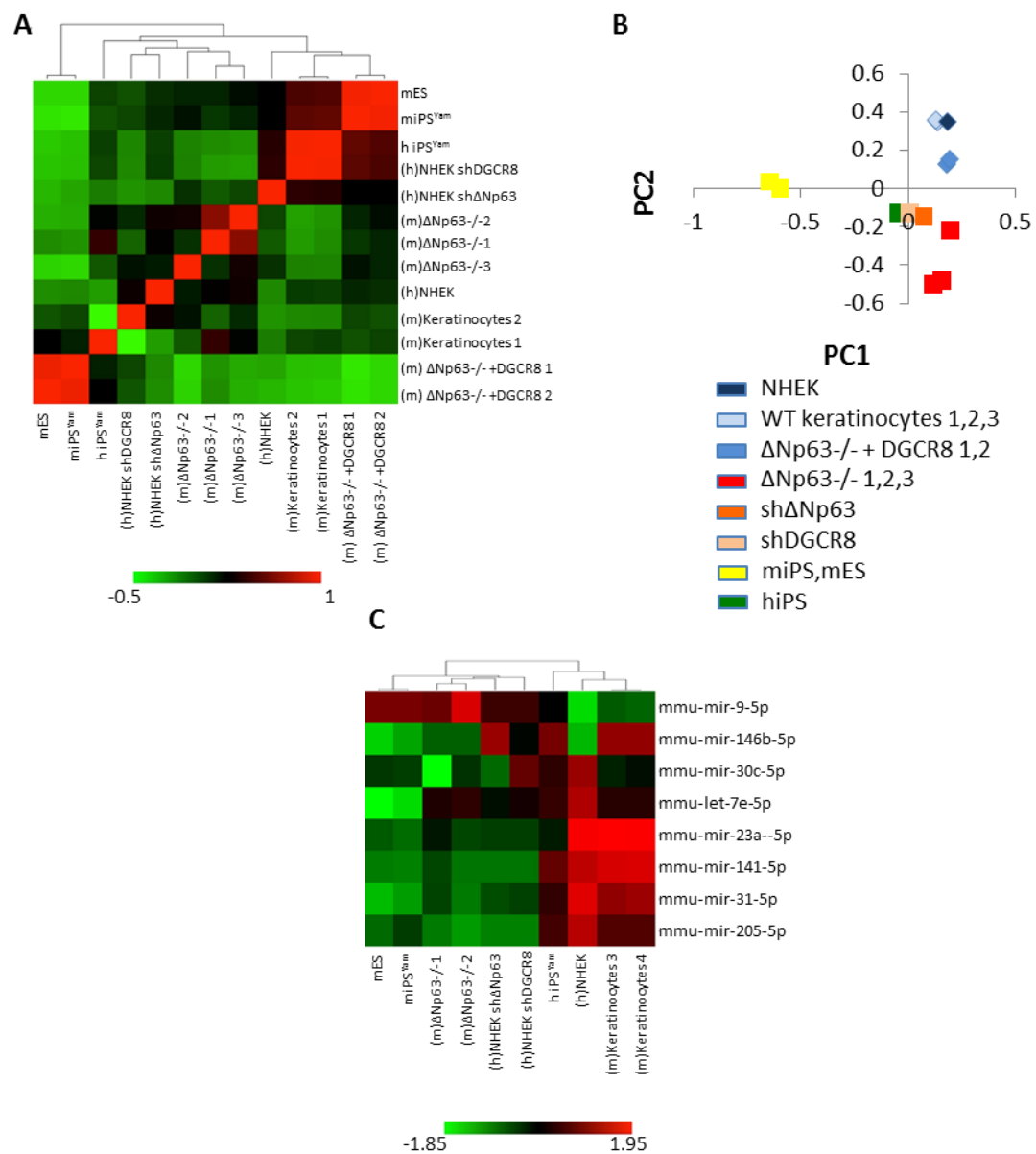


Figure 46: MicroRNA-seq data analysis in mouse and humans

A-C) Bioinformatic analysis of a human to mouse comparison of microRNA-Seq data of the following genotypes: mouse embryonic stem cells (mES), mouse iPS cells generated from fibroblasts using the Yamanaka factors (miPS^{Yam}), wild-type mouse keratinocytes ((m)Keratinocytes 1, 2), normal human epidermal keratinocytes transduced with shΔNp63 or shDGCR8 ((h)NHEKshΔNp63 or (h)NHEKshDGCR8), human iPS cells generated from fibroblasts using the Yamanaka factors (hiPS^{Yam}), and (h)NHEK cells. Low miRNA expression is indicated in green and high expression in red. Analyses shown are Pearson's correlation analysis (**A**), Principal component analysis (**B**), and supervised hierarchical clustering (**C**).

4.2.15. $\Delta Np63$ deficient mouse and human epidermal cells have a similar mRNA signature to mouse and human iPS cells reprogrammed with the Yamanaka factors

We also performed mRNA-Seq using RNA isolated from NHEKs with knock down of $\Delta Np63$ or DGCR8 (**Figure 50**). We performed Pearson's correlation analysis between the mouse and the human cells to identify common targets required for the reprogramming process (**Figure 49 A&B** and **Appendices 8** and **9**). Interestingly, we found that the gene expression signature of these cells clustered with $\Delta Np63^{-/-}$ epidermal cells, miPSYam, and mES cells indicating that pluripotency can be induced by acute knock down of $\Delta Np63$ or DGCR8 in human keratinocytes. Additionally, NHEKs with knock down of $\Delta Np63$ or DGCR8 had a nearly identical miRNA expression signature, indicating that cells deficient for $\Delta Np63$ regulate the same genes in differentiation and stem cell specification as DGCR8 as demonstrated by a cross-species comparison heat map analysis (**Figure 50** and **Appendix 12**).

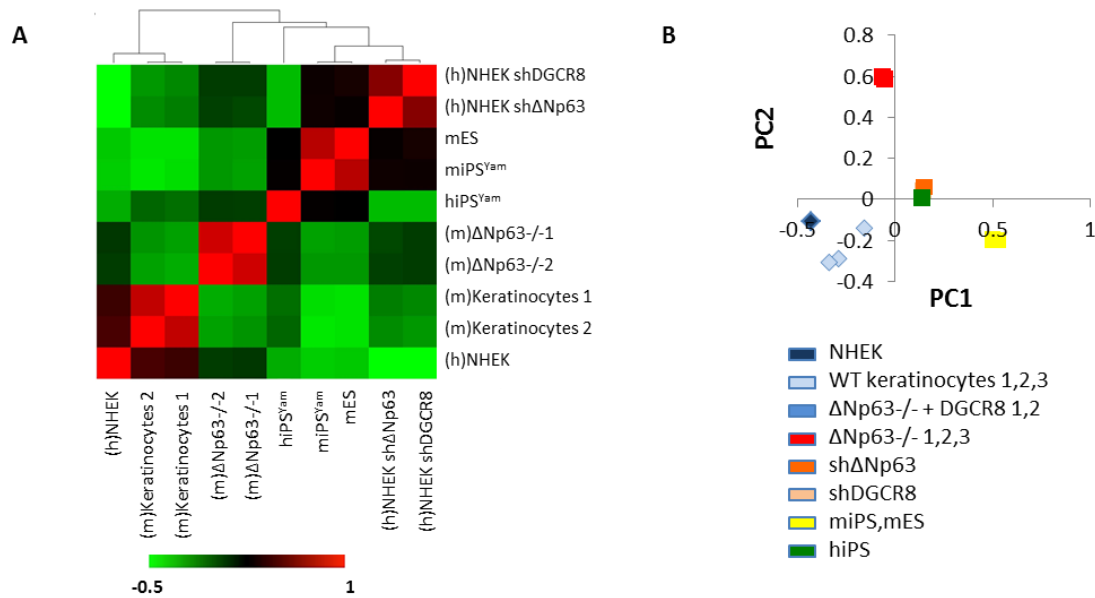


Figure 47: mRNA-seq data analysis in mouse and humans

A-B) Bioinformatic analysis of a human to mouse comparison of mRNA-Seq data of the following genotypes: mouse embryonic stem cells (mES), mouse iPS cells generated from fibroblasts using the Yamanaka factors (miPS^{Yam}), wild-type mouse keratinocytes ((m)Keratinocytes 1, 2), normal human epidermal keratinocytes transduced with sh Δ Np63 or shDGCR8 ((h)NHEKsh Δ Np63 or (h)NHEKshDGCR8), human iPS cells generated from fibroblasts using the Yamanaka factors (hiPS^{Yam}), and (h)NHEK cells. Low mRNA expression is indicated in green and high expression in red. Analyses shown are Pearson's correlation analysis (**A**), Principal component analysis (**B**).

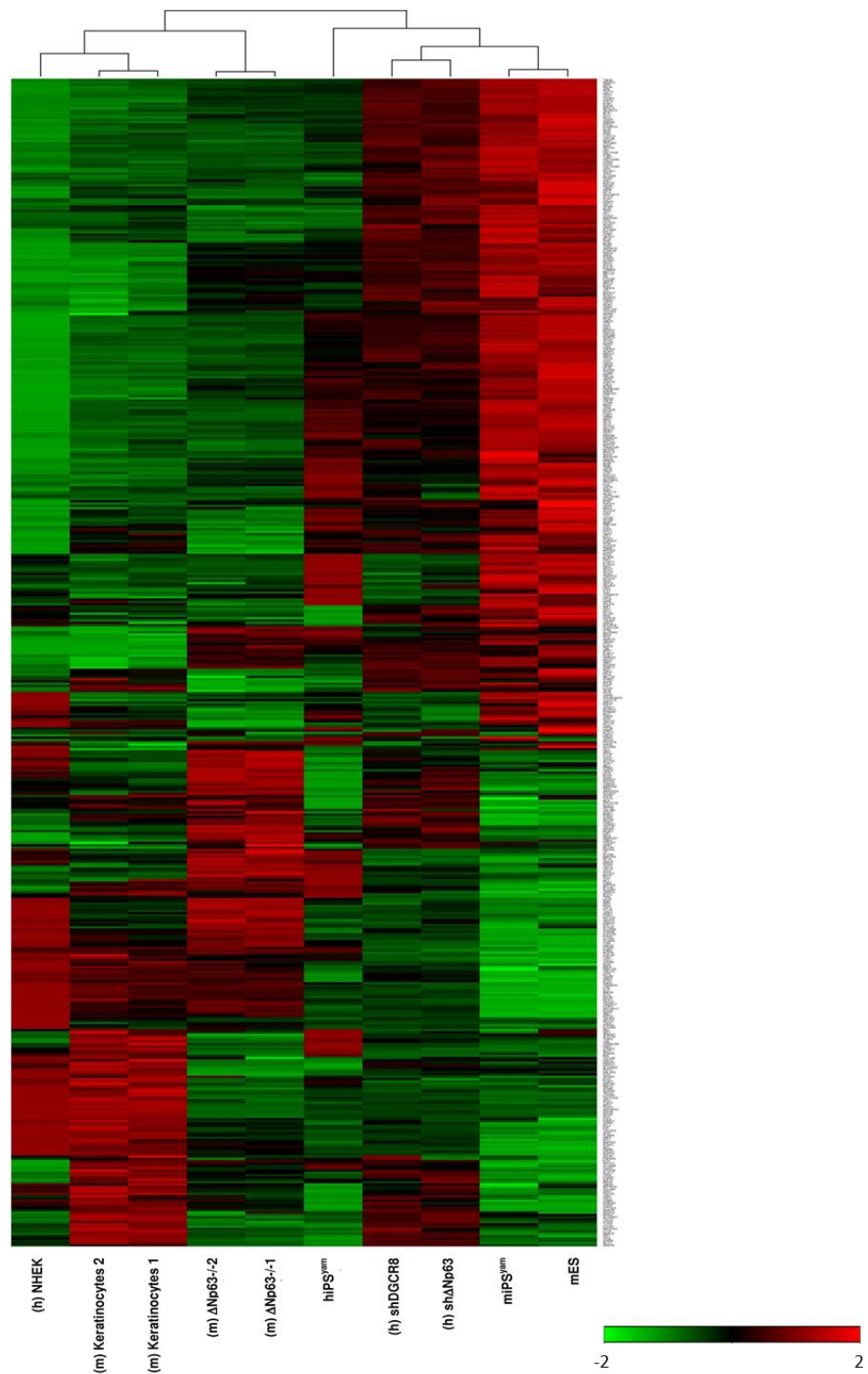


Figure 48: Unsupervised mRNA seq clustering comparing human and mouse cell line.

4.2.15. Deregulated microRNA processing in the NHEK-sh $\Delta Np63$ /shDGCR8 cells demonstrated by Northern blot analysis

We further validated miRNA expression using Northern blot analysis (**Figure 51A-C**) and found that there was an accumulation in the primary miRNAs in NHEKs expressing sh $\Delta Np63$ or shDGCR8 suggesting defects in miRNA processing to the precursor form due to low expression levels of DGCR8 in these cells.

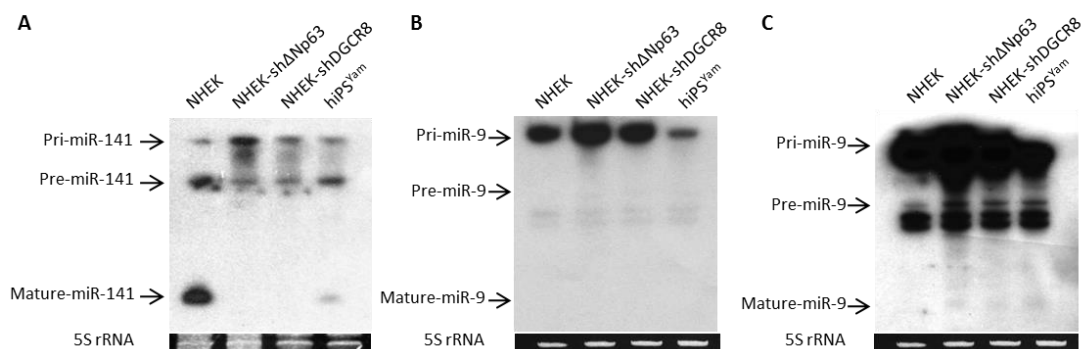


Figure 49: Northern blot analysis in the NHEK-sh $\Delta Np63$ /shDGCR8 cells

Northern blot analysis of RNA from cells of indicated genotypes showing expression of primary, precursor, and mature miRNA-141 (A) and a short (B) and long exposure of miR-9 (C).

4.3. Discussion

Here, we show that deletion or knock down of *ΔNp63* or *DGCR8* in primary mouse and human epidermal keratinocytes, respectively, results in efficient reprogramming of cells with remarkable plasticity that can differentiate into multiple lineages of the mesoderm, endoderm, and ectoderm. Mice with a germline deletion of *ΔNp63* have a rudimentary, disorganized epidermis that forms around the developing mouse embryo and fails to completely terminally differentiate. These epidermal phenotypes are reminiscent of mice lacking *DGCR8* and *Dicer* expression in the skin (159, 248). Accordingly, *ΔNp63* transcriptionally regulates *DGCR8* and modulation of *DGCR8* in *ΔNp63*^{-/-} epidermal cells represses the pluripotency factors, *Oct4*, *Sox2*, and *Nanog* (150, 251), and regulates a unique miRNA and mRNA signature in these cells. We also found that *ΔNp63*^{-/-} epidermal cells had a miRNA signature similar to that of ES cells and iPS cells (252-255). Importantly, we found that acute deletion of *ΔNp63* or *DGCR8* in human keratinocytes resulted in pluripotent stem cells that resemble ES and human iPS cells and can be differentiated *in vivo* to express genes representative of the three embryonic germ layers. This reprogramming occurs in 6 days and is highly efficient 0.07% for knock down of *ΔNp63* and 0.1% for knock down of *DGCR8* compared to 0.03% for expression of *Oct4*, *Sox2*, *Klf4*, and *c-myc*. These data have important implications for regenerative medicine and provide evidence that epidermal cells, which are readily accessible through the skin, can be reprogrammed to a pluripotent state without the addition of oncogenes.

The presence of a rudimentary epidermis in *ΔNp63*^{-/-} mouse embryos and the ability of *ΔNp63* deficient epidermal cells to hyperproliferate was quite surprising. The roles of *p63* in epidermal morphogenesis have been the subject of heated controversy. Experimental evidence supports a role for *p63* in both stem cell proliferation and in the initiation of differentiation (30, 66, 67, 241). Experiments using *p63* deficient epithelial cells demonstrated that *p63* is required for stem cell proliferation (67). Also, data from other studies using *p63*^{-/-} mice showed that *p63* is required for proper differentiation of epithelial tissues (241). Most of these studies were performed using mouse models that are deficient for all isoforms of *p63* making

the interpretation of the data difficult to decipher due to the existence of multiple *p63* isoforms. More recently, experiments have been performed using *in vivo* siRNA knock down of $\Delta Np63\alpha$, the isoform predominantly expressed in the skin (75), or germline deletion of the $\Delta Np63$ isoforms ($\Delta Np63^{gfp/gfp}$) (247). Both mouse models are consistent with our data in that $\Delta Np63$ is required for complete terminal differentiation. Moreover, the mouse model with *in vivo* siRNA knock down of $\Delta Np63\alpha$ also displayed hyperproliferation of the epidermis consistent with our results (75). Our mouse model has unveiled unknown functions of the $\Delta Np63$ isoforms in epidermal stem cell proliferation and in the induction of epidermal differentiation. Our $\Delta Np63$ conditional knockout allele has allowed for germline and acute deletion in epidermal cells of $\Delta Np63$. Importantly, we found that $\Delta Np63$ indirectly regulates the expression of the pluripotency factors, such as, *Oct4*, *Sox2*, *Nanog*, and a unique miRNA signature by direct transactivation of *DGCR8*. Our data demonstrate that $\Delta Np63$ is required for commitment to terminal differentiation through a unique miRNA and mRNA signature that is similar in both mouse and human cells. In line with our observations, recent evidence indicates that factors other than *Oct4*, *Sox2*, and *Nanog* are critical for appropriate reprogramming of differentiated cells to pluripotency (249).

Our data also show that re-expression of *DGCR8* in $\Delta Np63$ deficient epidermal cells can bypass the terminal differentiation defects and allows differentiation into multiple cell fates. The phenotype of $\Delta Np63^{+/-}$ and $\Delta Np63^{-/-}$ embryos is similar to that of mice with *DGCR8* ablated in K14 expressing cells within the epidermis. All three of these mouse models have a hyperproliferative epidermis (159, 194, 248). Moreover, *DGCR8*^{-/-} embryonic stem cells continue to self-renew and fail to undergo terminal differentiation. This is similar to what we found in mouse epidermal cells that were derived from $\Delta Np63$ germline deleted mice ($\Delta Np63^{-/-}$) as well as those with acutely deleted $\Delta Np63$ ($\Delta Np63\Delta/\Delta$). These cells express *DGCR8* at low levels, continue to proliferate beyond late passages in clonogenic assays, and continue to express markers of pluripotency, *Oct4*, *Sox2*, and *Nanog*, after multiple passages while wild-type epidermal cells senesce. We were able to terminally differentiate $\Delta Np63^{-/-}$ epidermal cells after re-expression of *DGCR8*. Although it has been suggested that $\Delta Np63$ induces pluripotency (67), our data supports a model whereby deletion of $\Delta Np63$ induces pluripotency in epidermal cells. These $\Delta Np63^{-/-}$ epidermal cells can differentiate into all

embryonic lineages *in vivo* but cannot contribute to the germline because resulting chimeric mice die at postnatal day 1 due to skin defects similar to those seen in $\Delta Np63^{-/-}$ mice (Tables 3 & 4). Because these cells could not give rise to a fully stratified epithelium, we have dubbed them induced multipotent stem cells (iMS) cells. These cells have remarkable plasticity and have the potential to be important for regenerative medicine.

Importantly, we further demonstrated the induction of pluripotency in normal human keratinocytes that were acutely knocked down for $\Delta Np63$ or $DGCR8$. Thus, knock down of either one of these two factors, $\Delta Np63$ or $DGCR8$, represents a new way to induce keratinocytes to a stem-like state without the expression of proto-oncogenes or deletion of tumor suppressor genes. Importantly, we found that loss of $\Delta Np63$ does not result in loss of $p53$ expression, which has been shown previously to result in efficient reprogramming (127, 237-240). This result is significant given that down regulation of tumor suppressor genes, like $p53$, while leading to the generation of cells that are pluripotent, can also lead to the production of tumorigenic cells (256).

The miRNA expression patterns of $\Delta Np63^{-/-}$ epidermal cells were similar to that of embryonic stem cells and induced pluripotent stem cells. Consistent with low levels of $DGCR8$ in $\Delta Np63^{-/-}$ epidermal cells, we found miR-203, miR-205, and the miR-200 family (miR-200a, miR-200b, miR-200c, miR-141, miR-145, miR-429) expressed at very low levels. Paradoxically, we found a large number of miRNAs that were upregulated. These included miR-290, miR-295, and miR-302, which have been found upregulated in both embryonic stem cells and/or induced pluripotent stem cells (249, 252-255), and miR-9. This result was further demonstrated by Northern blot analysis (**Figures 51A-C**). The high levels of some miRNA expression may be due to the fact that there is still a low level of $DGCR8$ expression present in $\Delta Np63^{-/-}$ epidermal cells. We also noted that cells deficient for $\Delta Np63$ or $DGCR8$ had higher levels of primary miRNAs compared to wild-type cells (**Figures 51A-C**) consistent with defects in processing to the precursor form. Another possibility is that these high expressing miRNAs may also be processed via $DGCR8$ independent mechanisms (257). Re-expression of $DGCR8$ in $\Delta Np63^{-/-}$ epidermal cells rescued expression of these miRNAs (Figure 4). Another striking finding was that the miRNA expression of $\Delta Np63^{-/-}$ epidermal cells clustered with mouse iPS cells generated with the Yamanaka factors (miPS^{Yam}) and mES cells while $\Delta Np63^{-/-}$

^{4/-} epidermal cells expressing DGCR8 clustered with wild-type keratinocytes. Importantly, the miRNA and gene expression patterns between both mouse and human epidermal cells deficient for $\Delta Np63$ clustered together and with human and mouse iPS and mouse ES cells, further indicating that $\Delta Np63$ is a key player in reprogramming cells to a stem-like state.

In summary, $\Delta Np63$ is required for transcriptional activation of *DGCR8* in epidermal cells leading to a stem-like phenotype. We have dubbed these cells iMS cells because of their remarkable plasticity and ability to differentiate into multiple cell lineages. $\Delta Np63$ is essential for epidermal morphogenesis; therefore, in the absence of $\Delta Np63$, the epidermal stem cells in the developing skin fail to suppress expression of *Oct4*, *Sox2*, *Nanog*, and regulate a unique miRNA signature critical for pluripotency through *DGCR8* transcriptional regulation. These findings have important implications for regenerative medicine. Based on our results using human keratinocytes, we predict that epidermal cells can be extracted from patient skin biopsies and reprogrammed into multipotent stem cells by knock down of $\Delta Np63$ or *DGCR8*. Indeed, inducible knock down of $\Delta Np63$ and/or *DGCR8* may be preferable to the overexpression of potentially oncogenic factors such as c-myc or the down regulation of the critical tumor suppressor gene, *p53*. In the future, understanding the mechanisms employed by the individual *p63* isoforms in maintaining progenitor and stem cells in various tissues is key to understanding its complex roles in stem cell maintenance as well as cancer development and metastasis.

5. Chapter 5: Induced multipotent (iMS) NHEK-sh *p63* /DGCR8 cells can be induced to differentiate into epidermal tissue

5.1. Introduction

Since the discovery of iPS cells in 2006 by Yamanaka's group, they have been used for many purposes, the most common purpose being to differentiate into various tissue types. iPS cells have been made to differentiate into cardiomyocytes (258), skin cells capable of forming functional three dimensional skin architecture with hair follicles and glands (259), pancreatic islets capable of producing insulin (260), adipocytes (261), neurons, hematopoietic cells (262) and hepatocytes (263). Skin is one of the most accessible tissues of the body. Therefore keratinocytes could serve as the most reasonable target for reprogramming. This could potentially reduce the chances of rejection in patients. Cells can be taken from patients reprogrammed and differentiated and transplanted back to the same individual. Genetic skin diseases are very common like psoriasis, epidermolysis bullosa and others. Skin grafting could be a probable treatment option for these diseases. This necessitates the excision of skin from certain areas and grafting fresh skin. This would be feasible if methods could be devised to differentiate the iPS cells or iMS cell into functional skin, which could differentiate into all the epidermal components. This would certainly circumvent the problem of graft versus host rejection. Skin transplants are also very important for burn victims. The artificial skin can cover the burnt area and protect from contamination and infections. Also this helps is burns to heal faster. If a method could be devised where cells could be taken from such patients and differentiated back into a limit less supply of skin that would certainly save lives. Also disease models for various types of skin diseases could be designed to be studied in petridishes and drugs to be tested on them. In this chapter we describe a method of differentiating NHEK-sh $\Delta Np63$ /shDGCR8 (induced multipotent cells) to skin cells with the help of an established method of in vitro raft culture ref. These cells were able to differentiate to certain extent and express cytokeratin 5 when cultured in keratinocyte specific media. They were also able to form multilayered sheath on raft cultures, which were cytokeratin 5 positive. Further work need to be done to investigate their differentiation potential and optimization of the raft culture conditions.

5.2. Results

5.2.1. NHEK-sh*ΔNp63*/shDGCR8 can be induced to differentiate to ectodermal lineage

NHEK-sh*ΔNp63* or the NHEK-shDGCR8 cells are grown in stem cell specific media containing LIF (leukemia inhibitory factor) and on 0.1% gelatin. This maintains the cells in their undifferentiated state. To investigate whether these cells could be differentiated into epidermal lineage, they were cultured in keratinocyte specific media containing EGF and insulin (called F-media). This media was formulated to grow differentiated keratinocytes. These cells were cultured in differentiating conditions for 3-4 days. At 4 days the cells were collected lysed and western blot was performed for cytokeratin 5 (K5). We also used lysates from NHEK cells as positive control for K5. This experiment showed that the NHEK-sh*ΔNp63*/shDGCR8 cells grown in stem cell specific media did not express K5. When grown in keratinocyte specific media for 4 days these cells started to express keratin 5 albeit at lower levels than the NHEK cells (**Figure 52**). This suggests that the NHEK-sh*ΔNp63*/shDGCR8 cells have potential to be differentiated into ectodermal lineage. The defect in keratin 5 expression could be attributed to the low levels of *ΔNp63* and DGCR8 in these cells which we have shown previously is required for terminal differentiation.

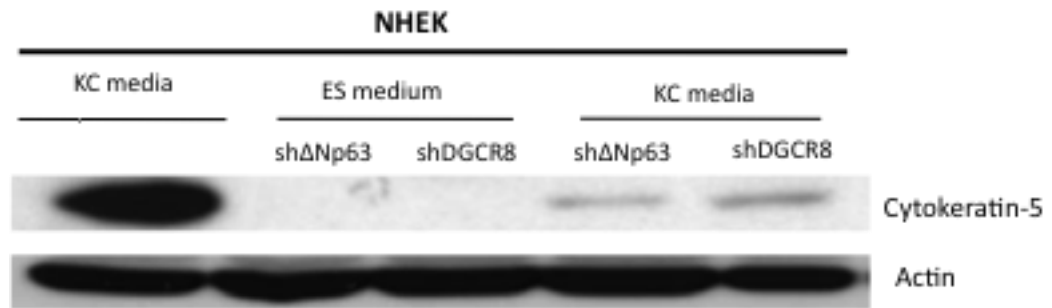


Figure 50: Cytokeratin 5 expression in NHEK-shΔNp63/ shDGCR8

Immunoblotting performed with NHEK cells grown in keratinocyte specific media (KC media), NHEK-shΔNp63/shDGCR8 grown in stem cell media (ES media) and NHEK-shΔNp63/shDGCR8 grown in keratinocyte media (KC media) for cytokeratin 5. Actin is used as loading control.

5.2.2. Loss of pluripotency marker expression in NHEK-sh*ΔNp63*/shDGCR8 cells under differentiating conditions

Immunofluorescence, with antibodies towards Oct-4, Sox-2, Nanog and cytokeratin5, was performed on the NHEK-sh*ΔNp63*/shDGCR8 colonies grown in either stem cell media or under differentiating conditions in F-media. Interestingly both the cell types show a decrease in the expression of the stem cell markers when grown in F-media (**Figure 52A-F & 53A-F**) and an increase in cytokeratin 5 expression (**Figure 53 G&H, 54 G&H**). Also the NHEK-shDGCR8 cells showed a much higher level of keratin 5 expression when grown in the F-media suggesting that loss of *ΔNp63* may regulate other factors which affect differentiation. On the other hand loss of DGCR8 seems to compromise differentiation to a lesser extent. And these cells can be induced to differentiate more promptly. Further work needs to be done to validate the level of the pluripotency markers and the differentiation markers in these cells. Quantitative assays like western blot analysis will also have to be performed to accurately assess the levels of these markers. Further characterization with other differentiation markers needs to be performed on these cells.

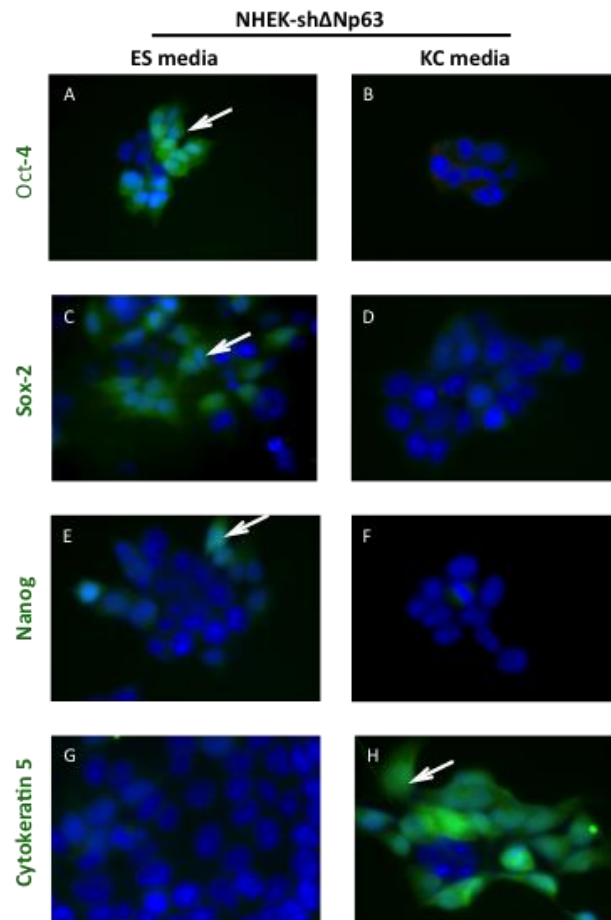


Figure 51: Differentiation of NHEK-shDNp63 towards ectodermal lineage

A-H) Immunostaining of colonies from NHEK-sh $\Delta Np63$ cells. **A,C,E)** Oct-4, Sox-2 and Nanog expression of colonies grown in stem cell (ES media) media. **G)** Cytokeratin-5 expression in stem cell media (ES media). **B,D,F)** Oct-4, Sox-2 and Nanog expression of colonies grown in keratinocyte media (F media). **H)** Cytokeratin-5 expression in colonies in keratinocyte media (KC media). White arrows denote positive cells. Magnification 400x

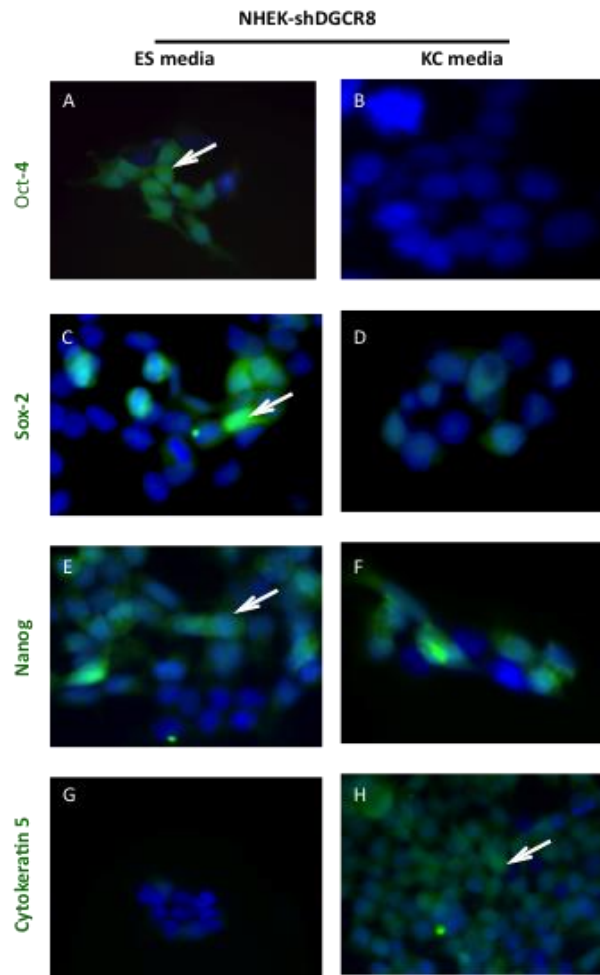


Figure 52: Differentiation of NHEK-shDGCR8 towards ectodermal lineage

A-H) Immunostaining of colonies from NHEK-shDGCR8 cells. **A,C,E)** Oct-4, Sox-2 and Nanog expression of colonies grown in stem cell (ES media) media. **G)** Cytokeratin-5 expression in stem cell media (ES media). **B,D,F)** Oct-4, Sox-2 and Nanog expression of colonies grown in keratinocyte media (F media). **H)** Cytokeratin-5 expression in colonies in keratinocyte media (KC media). White arrows denote positive cells. Magnification 400x

5.2.3. Defects in terminal differentiation of the NHEK-sh*ΔNp63*/shDGCR8 cells as demonstrated in raft culture assay

The NHEK-*ΔNp63* and NHEK-shDGCR8 cells were plated on collagen rafts. This method is an established method for differentiating keratinocytes to full thickness epidermis. The cells are plated onto the collagen rafts initially in a submerged culture followed by lifting them such that the cells are in a air-liquid interface. They get their media supplement only from the basal layer whereas their apical surface is in contact with air. This creates an artificial skin like environment. The basal cells at first proliferate but once lifted starts to differentiate into the epidermal layers, spinous, granular and finally gives rise to the cornified epithelium on the top surface.

When the NHEK-sh*ΔNp63* and NHEK-shDGCR8 cells were subjected to such an assay they could form a thin multilayer structure with a slight cornified upper layer (**Figure 54A-C**). Unfortunately our control experiment with BC-1-EP/SL (**Figure 54A**) did not work as well. Although when stained with cytokeratin 5 we saw a similar expression of keratin 5 as seen in the 2D culture method (**Figure 54D-F**), but conclusions could not be drawn from these assays as our control cells demonstrated defective stratification and no expression of further differentiation markers other than keratin 5. We are still optimizing this assay.

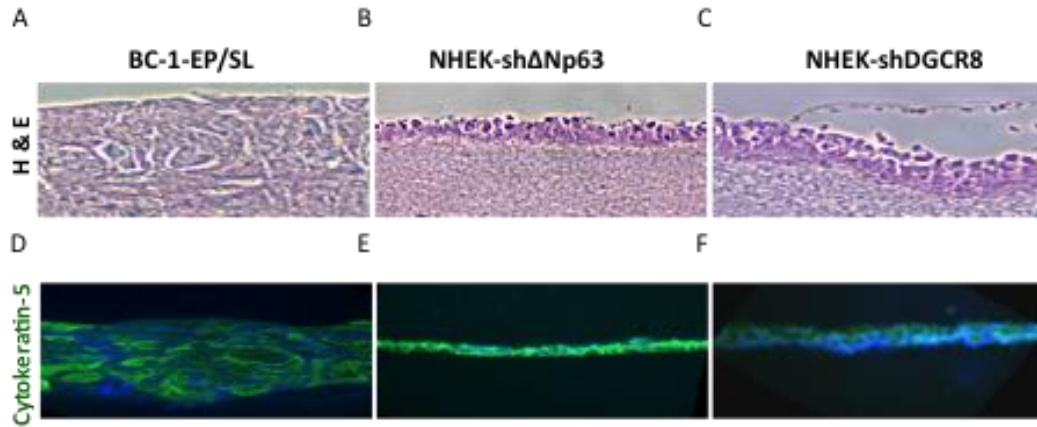


Figure 53: Raft culture assay to differentiate NHEK-shDNp63/shDGCR8 cells to full thickness epidermis

A-C) Hemtaoxylin staining of skin rafts from BC-1-EP/SL(A), NHEK-sh $\Delta Np63$ (B) and NHEK-shDGCR8 (C). **D-F)** Immunofluorescence staining of rafts with anti-keratin 5. Green (anti-FITC secondary antibody staining) staining denoting keratin 5 expression in the rafts from the indicated cell type.

5.3. Discussion

Here we show that the NHEK-sh*ΔNp63* and NHEK-shDGCR8 cells may be useful tools for the reconstruction of ectodermal tissues. Currently we are trying to optimize the raft culture protocol and devise a tool which can be used to generate functional epidermis. We are also currently working on the generation of other tissue lineages like the hematopoietic tissue. The complete differentiation of these cells may be difficult due to the absence of *ΔNp63* and DGCR8 based on our model. Therefore efforts are being made to generate an inducible and titratable DGCR8 vector. This will allow us to express sufficient levels of DGCR8 in these cells which will be enough to drive terminal differentiation in such tissue differentiation assays. We are also working on over-expressing or repressing the expression of the panel of microRNA as shown earlier to be a pluripotency signature in Figure 48C. Many of these microRNAs have been shown to be potent in inducing differentiation in tissues of embryos. The loss of these microRNAs leads to a loss in differentiation, for example let-7, miR-141 and miR-205. We are in the process of expressing these microRNAs in the NHEK-sh*ΔNp63* and NHEK-shDGCR8 cell and test their efficiency in driving differentiation in raft culture assays. We would also knock-down few of the over-expressed microRNAs like miR-9-5p and miR-146b-5p in the NHEK cells and test their potential to induce pluripotency. It is a possibility that both the differentiation assay and the induction of pluripotency by microRNAs, would require the modulation of several microRNAs from the cross-species microRNA analysis.

Differentiation of stem cells, iPS cells and iMS cells may be a valuable tool for treatment of various diseases. These methods have to be thoroughly validated. One of the common con of these methods are the undifferentiated stem like cells which are left behind after differentiation of the majority of the cells. This then could lead to the formation of tumors. Several trials have to be done to verify this. Also currently there is no method for validating the existence of these undifferentiated cells in a differentiated cell population. Methods have to be designed to calculate percentage of these cell types and what can be done to improve the technique so all cells are differentiated uniformly. Work is currently going on to assess the graft versus host rejection issue. More work needs to be done in this field.

6. Chapter 6: Role of $\Delta Np63$ in tumor suppression and oncogenesis is context dependent

6.1. Introduction

The role of *p63* in tumorigenesis has been a topic of constant debate. Previously we have shown that *TAp63* is a suppressor of tumorigenesis and metastasis through its regulation of *Dicer* and other microRNAs (65). We also found that *ΔNp63* regulates the microRNA biogenesis pathway by regulating DGCR8 and plays an important role in induced pluripotency of epidermal cells (Manuscript in Review at *PNAS*). Therefore we wanted to delineate the role of *ΔNp63* in tumorigenesis. *p63* has been shown to be highly expressed in human tumors (45, 46, 73). This together with the fact that expression of *p63* is hardly lost in tumors unlike *p53*, which is mutated or lost in 50% of all tumors (264, 265), led researchers to hypothesize that *p63* is an oncogene. In some tumors *p63* locus also demonstrates amplification (46), a characteristic of an oncogene like *MYC* (266-268). Although, there is contradictory literature demonstrating the loss of *p63* in certain tumor type (56). Recent accumulating sequencing data from the TCGA also suggests that *p63* undergoes point mutation in lung cancers (63). There are several independent case studies of CML and AML patients, where *p63* have been shown to have point mutations (60). This dual evidence further makes it very difficult to determine the role of *p63* in tumorigenesis. The other critical problem in the field is the lack of antibodies capable of detecting the different isoforms of *p63*. A lot of previous literature on *p63* is muddled due to the use of an antibody that detects primarily *ΔNp63* over the *TAp63* isoforms. This makes it hard to discern the true expression patterns (loss or gain) of the two different isoforms in tumors. *TAp63* expression pattern being similar to *p53* also creates difficulties in detecting *TAp63* in tissues and tumors under unstressed conditions. For a period of time it was believed that *TAp63* did not play any crucial role in the biological processes, as it could be hardly detected in adult tissues (except in female germ cells) (71). But now we know that the subtle expression of *TAp63* is sufficient to suppress tumorigenesis and metastasis in healthy tissues (65). We have shown that *TAp63* expression is certainly lost in a wide variety of aggressive metastatic tumors including head and neck squamous cell carcinomas, mammary adenocarcinomas and mammary adenocarcinoma (65). It has therefore become imperative to sort out the differences in the functions of the two isoforms in tumorigenesis. This is also now possible with the two conditional knock-out mouse models generated by our laboratory for the two different isoforms.

6.2. Results

6.2.1. *ΔNp63* heterozygous mice develop tumors of the epithelial origin

To investigate whether *ΔNp63* is a tumor suppressor or an oncogene, we generated a cohort of *ΔNp63*^{+/−} mice (30mice) and wild-type mice (30mice) and aged them to 3 years, since the *ΔNp63*^{−/−} mice die a few hours after birth as specified in section 4.2.2, **Figure 27C**. We found that the *ΔNp63*^{+/−} mice had a shorter survival compared to the WT mice. On analysis, we found that the *ΔNp63*^{+/−} mice develop mainly epidermal carcinomas (**Figure 56A**). We are currently analyzing more animals for this study.

To further understand the collaboration between *p53* and *ΔNp63* as mentioned earlier, we crossed these mice to *p53*^{−/−} and *p53*^{+/−} mice. We generated a cohort of (30 mice for each cohort) *ΔNp63*^{+/−};*p53*^{−/−} mice to be compared to *p53*^{−/−} mice and *ΔNp63*^{+/−};*p53*^{+/−} mice to be compared to *p53*^{+/−} mice. Interestingly we found that the *ΔNp63*^{+/−};*p53*^{−/−} mice develop a wide spectrum of tumors like thymic lymphomas, osteosarcomas, histiocytic squamous cell carcinoma, adenocarcinoma of the lungs and testicular adenocarcinoma. Surprisingly only 30% of the *ΔNp63*^{+/−};*p53*^{−/−} mice developed thymic lymphoma, compared to the 90% of the *p53*^{−/−} mice which developed thymic lymphomas. Curiously when we analyzed the survival curves of the *ΔNp63*^{+/−};*p53*^{−/−} mice and the *p53*^{−/−} mice, there was no difference between the survival of the animals (**Figure 56B**). We therefore went on to determine whether mortality was due to the other tumor types and not due to the thymic lymphomas. We found that if we plot the survival curves of the *ΔNp63*^{+/−};*p53*^{−/−} and *p53*^{−/−} mice with only thymic lymphomas (**Figure 56C**), the median survival time of the *ΔNp63*^{+/−};*p53*^{−/−} mice (6.7 months) was greater than the *p53*^{−/−} mice (4.5months). Also there were some mice, which lived until 8.2 months, while all the *p53*^{−/−} mice died at 6 months of age. This suggests that *ΔNp63* plays an oncogenic role atleast in the thymus, whereas in the other epidermal tissues it seems to be playing a more tumor suppressive function.

The *ΔNp63*^{+/−};*p53*^{+/−} mice on the other hand had similar survival curves to the *p53*^{+/−} mice. Although a cohort of these mice develop carcinomas too. These cohorts of mice are still under analysis.

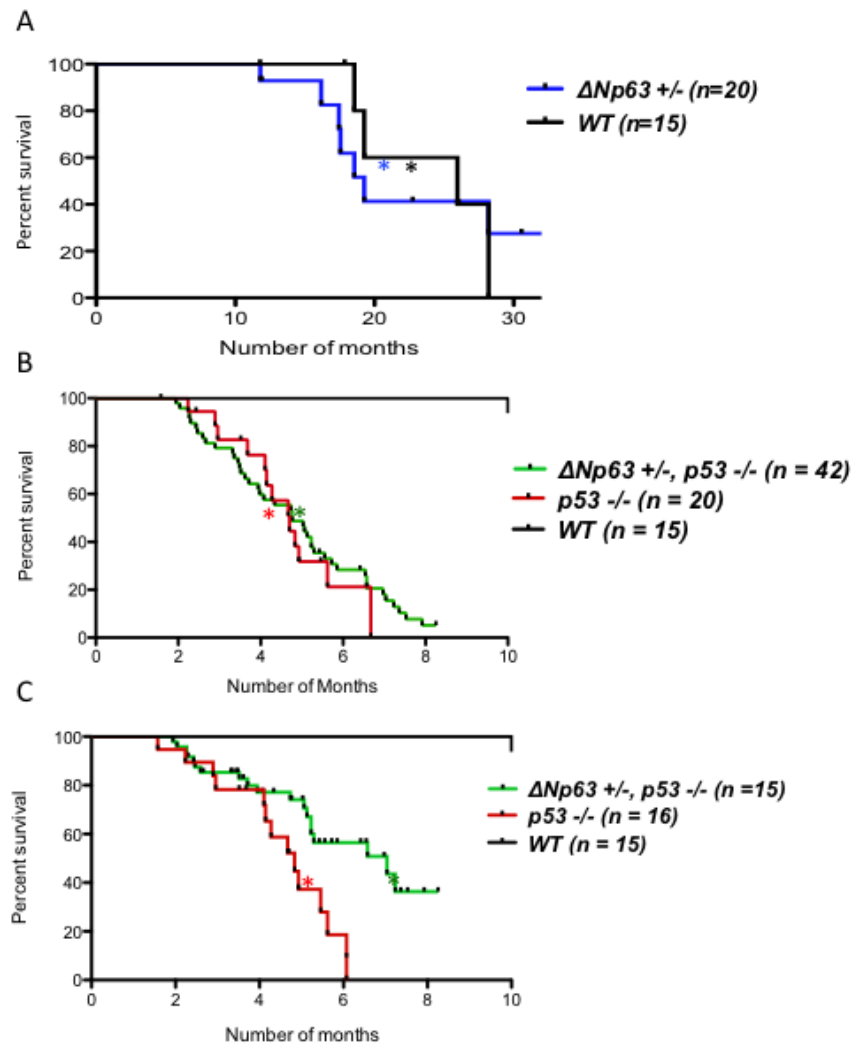


Table 8: Tumor spectrum of $\Delta Np63^{+/-}; p53^{-/-}$

	$p53^{-/-}$	$\Delta Np63^{+/-}; p53^{-/-}$
Lymphoma	85%	30%
Sarcoma	5%	14%
Carcinoma	0	40%
Others	10%	16%

Percentage of mice within each cohort of the indicated genotype with specific tumor types.

N=20 for $p53^{-/-}$, n=42 for $\Delta Np63^{+/-}; p53^{-/-}$

Figure 54: Loss of $\Delta Np63$ leads to a shortened life-span

A-C) Kaplan Meier survival curve for the indicated genotypes. **A)** Kaplan Meier survival curves of $\Delta Np63^{+/-}$ (n= 20) and wild-type (n=15). $\Delta Np63^{+/-}$ mice. The median survival time of the $\Delta Np63^{+/-}$ mice are significantly shorter than the survival curve for wild-type mice. Asterisk indicate significance . (p value ≤ 0.05). **B)** Kaplan Meier survival curves of $\Delta Np63^{+/-}; p53^{-/-}$ (n= 20) , $p53^{-/-}$ (n=20) mice, with a wide range of tumor spectrum, and wild-type (n=15) mice. The median survival time of the $\Delta Np63^{+/-}; p53^{-/-}$ mice are not different from the median survival time of the $p53^{-/-}$ mice. Asterisk indicate significance. . (p value ≤ 0.05). **C)** Kaplan Meier survival curves of $\Delta Np63^{+/-}; p53^{-/-}$ (n= 15) , $p53^{-/-}$ (n=16) mice with thymic lymphomas and wild-type (n=15) mice. The median survival time of the $\Delta Np63^{+/-}; p53^{-/-}$ mice are different from the median survival time of the $p53^{-/-}$ mice with thymic lymphomas. Asterisks indicate significance. P-value ≤ 0.05 .

6.2.2. Loss of *ΔNp63* is tumor protective in the thymus in vivo

We investigated this lack of thymic lymphomagenesis in these animals and further evaluated the function of *ΔNp63* in the thymus, by performing quantitative real time PCR for some of the well *p63* apoptotic targets like *Puma* and *Noxa*. We found that apoptotic targets like *PUMA* and *NOXA* was up regulated in the thymic lymphomas of the *ΔNp63*^{+/-};*p53*^{-/-} compared to the lymphomas from the *p53*^{-/-} mice (**Figure 57B,C**). We also validated the senescence targets of *p53/p63* like p21. We found that p21 was indeed up regulated in the *ΔNp63*^{+/-};*p53*^{-/-} tumors in comparison to the lymphomas from the *p53*^{-/-} mice (**Figure 57A**). *TAp63* has been shown to be a transcriptional activator of these apoptotic and senescence targets in others tissue. We performed a quantitative real-time PCR for *TAp63* from the thymic lymphoma tissue of these mice and found that *TAp63* was up regulated in these lymphomas to very high levels (36 folds higher), while the *p53*^{-/-} lymphomas showed no such upregulation of *TAp63* (**Figure 57D**).

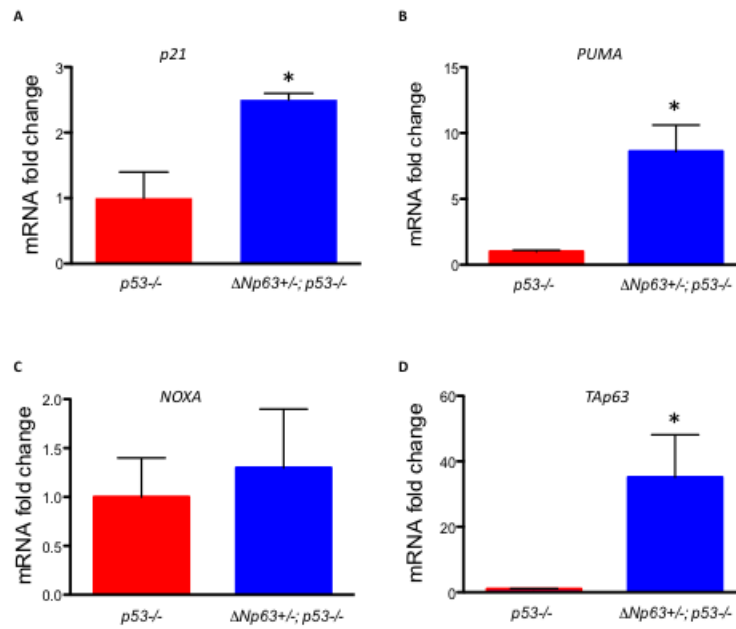


Figure 55: Loss of $\Delta Np63$ is tumor protective in the thymic lymphomas

A-D) Quantitative real-time PCR performed on thymic tumor tissues from $p53^{-/-}$ and $\Delta Np63^{+/-}; p53^{-/-}$ (n=3). mRNA levels for p21 (A), PUMA (B), NOXA (C) and TAp63 (D). Asterisk indicates significance. $P\text{-value} \leq 0.05$.

6.2.3. Loss of $\Delta Np63$ leads to increased apoptosis and reduced proliferation *in vivo*

In order to investigate the events leading upto the increase in the senescence and the apoptotic targets we analyzed the thymii from young mice for signs of apoptosis and senescence. We performed immunostaining for cleaved caspase-3 in the thymii of 3.5 month old $p53^{-/-}$ and $\Delta Np63^{+/-};p53^{-/-}$ mice in order to determine the difference in apoptosis during early lymphomagenesis (**Figure 58A**). Our goal was to determine whether a cohort of mice of the $\Delta Np63^{+/-};p53^{-/-}$ genotype exhibit more apoptosis at this early stage explaining the low percentage of thymic lymphomas in these mice. We found high number caspase positive cells in all the thymii that we tested (n=3). We also analyzed these thymii for PCNA staining to determine the proliferation rate of the thymocytes, We found that the $\Delta Np63^{+/-};p53^{-/-}$ thymus has a much lower proliferation rate than the thymus from the $p53^{-/-}$ animals (**Figure 58B**). Analysis remains to be done in more mice. The thymii from the $\Delta Np63^{+/-};p53^{-/-}$ mice were also phenotypically more ‘normal’ and retained its tissue architecture than the thymii from the $p53^{-/-}$ mice at this age (data not shown). This indicates that the $\Delta Np63^{+/-};p53^{-/-}$ mice positively have an upregulation of apoptotic and senescence pathways in the thymii.

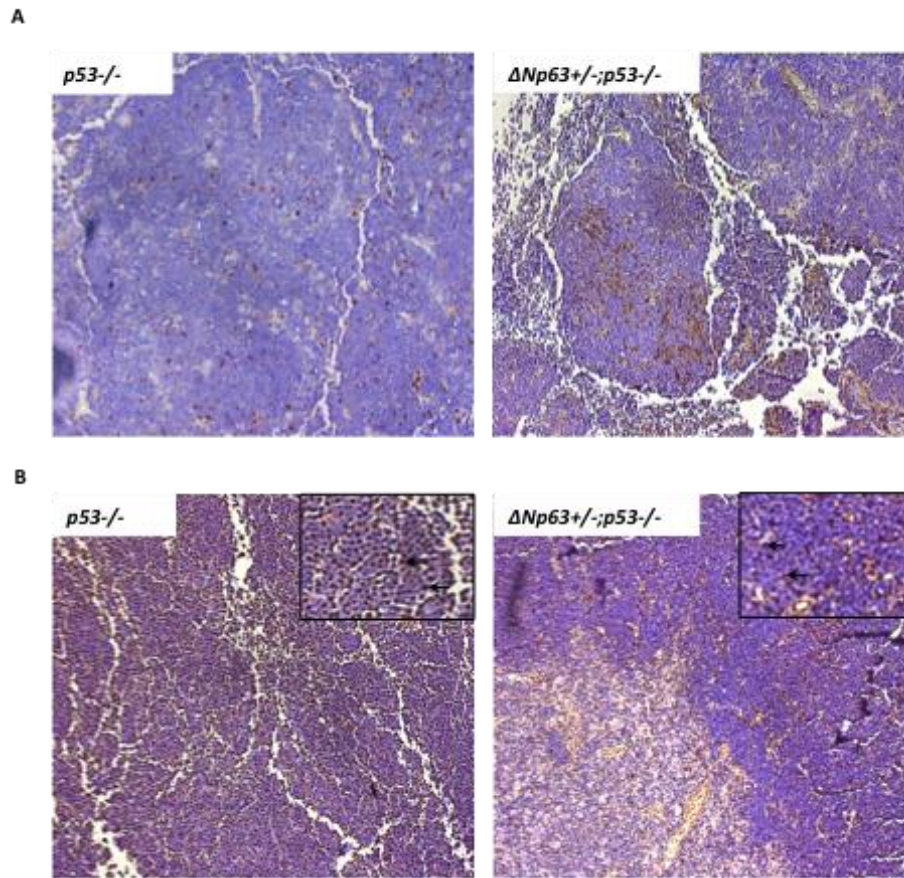


Figure 56: Loss of $\Delta Np63$ leads to increased apoptosis and reduced proliferation in vivo

A) Immunostaining for cleaved-caspase 3 in thymic lymphoma tissue from $\Delta Np63^{+/-};p53^{-/-}$ and *p53*^{-/-} mice (n=3). **B)** Immunostaining for PCNA in thymic lymphoma tissue from $\Delta Np63^{+/-};p53^{-/-}$ and *p53*^{-/-} (n=3) mice. Arrows indicate positive cells. Magnification 200x. Insets are 400X magnification.

6.2.4. Loss of $\Delta Np63$ induces apoptosis, senescence and cell cycle arrest in vitro

To further validate and emulate the events during thymic lymphomagenesis, we isolated thymocytes from untreated or γ -irradiated (10Gy) animals of the following genotypes, *wild-type*, $p53^{-/-}$ and $\Delta Np63^{+/-};p53^{-/-}$ at 6 weeks of age. We performed quantitative real-time PCR for the apoptotic targets, *Puma* and *Noxa* and senescence target *p21*. We observed a similar effect in the thymocytes. The γ -irradiated thymocytes from the $\Delta Np63^{+/-} p53^{-/-}$ mice had a higher level of expression of *Puma*, *Noxa* and *p21* two hours post-radiation with continued increase upto 6 hours post-radiation compared to the $p53^{-/-}$ irradiated thymocytes (**Figure 59A-F**), which showed almost no upregulation of these genes. This indicates loss of $\Delta Np63$ to be a major player in suppression of apoptosis and senescence in these cells. We also validated the expression level of *TAp63* and found that *TAp63* mRNA expression was 2.5 folds higher in the irradiated $\Delta Np63^{+/-};p53^{-/-}$ thymocytes compared to the $p53^{-/-}$ thymocytes, which showed no signs of *TAp63* induction (**Figure 59 G& H**).

$\Delta Np63$ mRNA levels was found to be low in the thymocytes and the level further went down after irradiation (data not shown).

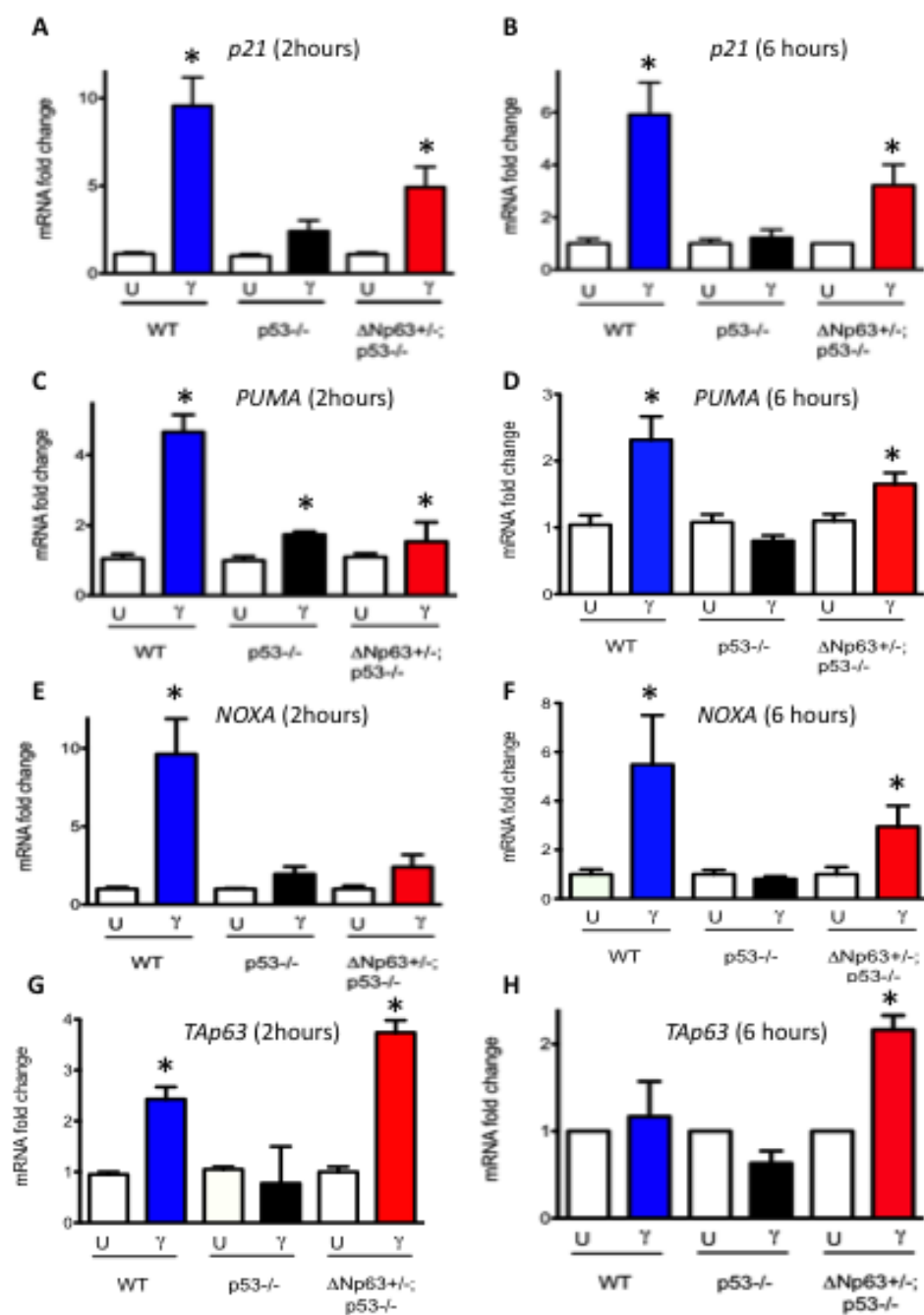


Figure 57: Loss of $\Delta Np63$ leads to increased apoptosis and senescence in vitro

A-H) Quantitative real-time PCR performed on RNA from $p53^{-/-}$ and $\Delta Np63^{+/-};p53^{-/-}$ (n=6) thymii treated with or without γ -radiation. **A,C,E,G)** mRNA levels of the indicated target genes at 2hours after γ -radiation. **B, D, F, H)** mRNA levels of the indicated target genes 6 hours after γ -radiation. Asterisk indicates significance. P-value \leq 0.05.

6.2.5. *ΔNp63* undergoes proteasomal degradation on γ -radiation

We were keen on determining the change in *ΔNp63* status after γ -radiation. We irradiated MEFs with 10Gy and verified the change in *ΔNp63* protein expression. Researchers have shown that *ΔNp63* undergoes proteasomal degradation after treatment with γ -radiation. We wanted to verify this in our system. We treated *wild-type* MEFs with 10 micromolar solution of MG-132 for one hour before irradiating them. 6 hours post radiation these cells were collected and immunoblotting was performed. There was degradation of the *ΔNp63* protein post radiation compared to the untreated cells. Also treating the cells with MG-132 inhibited this degradation stabilizing *ΔNp63* levels. *TAp63* protein levels were shown to be comparable in the untreated cells with or without the treatment of MG-132. Post-radiation the MG-132 treated cells showed a decrease in the level of *TAp63* compared to the MG-132 untreated cells, suggesting that when once *ΔNp63* is degraded post radiation, *TAp63* protein levels increase. But when MG-132 is added post-radiation, stabilizing *ΔNp63*, *TAp63* protein levels are further decreased due to the possible inhibition by *ΔNp63* (**Figure 60**). Therefore *ΔNp63* could be a negative regulator of *TAp63*.

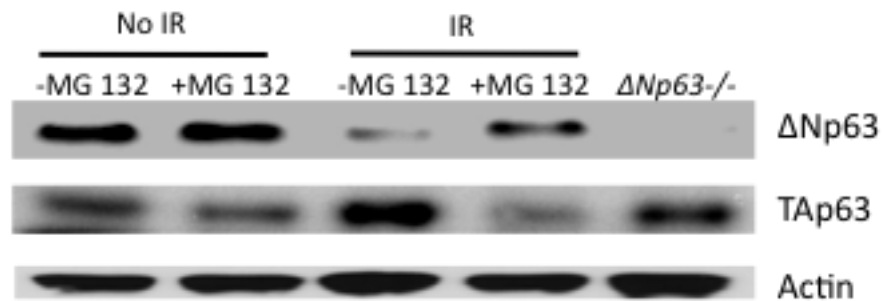


Figure 58: Loss of $\Delta Np63$ leads to upregulation of the TAp63 protein

Immunoblotting with lysates from wild-type MEFs treated or untreated with γ -radiation and MG-132 with antibodies against $\Delta Np63$ and TAp63. Lysate from $\Delta Np63^{-/-}$ MEF is used as control. Actin is used as a loading control.

6.2.6. *ΔNp63* transcriptionally represses the *TAp63* promoter

These data taken together indicated there was an inter-regulation between *ΔNp63* and *TAp63*. The loss of *ΔNp63* induces *TAp63* at the mRNA level. We therefore asked whether *ΔNp63* suppressed the expression of *TAp63* by binding to its promoter region. We searched for putative *p53/63* binding site in the *TAp63* promoter region. We performed chromatin immunoprecipitation analysis with *p63* antibody with either wild-type MEFs, *ΔNp63*^{-/-} MEFs or *p63*^{-/-} MEFs treated with or without γ -irradiation. We found that in control cells, *ΔNp63* binds strongly to the *TAp63* promoter region in the wild-type cells, under stress like γ -irradiation there is a reduction in binding to the *TAp63* upstream promoter site at -3515 upstream of the *TAp63* transcription start site as determined by a ChIP assay (**Figure 61** and **Table8**). In the *ΔNp63*^{-/-} and also in the *p63*^{-/-} MEFs cells we detected no binding at the *TAp63* promoter due to the lack of *ΔNp63* isoform. This also suggests that *TAp63* does not bind to its own promoter site.

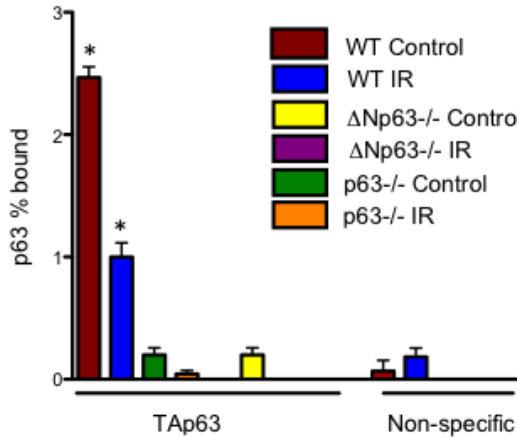


Table 9: *p53/p63* response element on the *TAp63* promoter

Element	Location	Sequence	MM/Spacer
<i>TAp63</i>	-3515 to -3436	ttgCAAGgcc tgcaagaa gctCAAGgtc	6/8

Figure 59: *ΔNp63* suppresses *TAp63* transcription by binding to its promoter

qRT-PCR of ChIP assay for *p63* on a specific binding site on *TAp63* promoter (*TAp63* specific) and non-specific binding site (Non-specific). Cells from the indicated genotypes were used. Experiments were done in triplicate. Asterisks indicate significance. p value ≤ 0.05 .

6.2.7. $\Delta Np63^{+/-};p53^{-/-}$ mice die of multiple metastatic tumors

We analyzed the cohort of $\Delta Np63^{+/-};p53^{-/-}$ mice which does not develop thymic lymphomas (70%) and found that they develop metastatic carcinomas like a metastatic lung adenocarcinoma which metastasized to the diaphragm (image not shown) . These carcinomas are highly aggressive. They are of various tissue origins. Interestingly unlike the $\Delta Np63^{+/-};p53^{-/-}$ mice which develop thymic lymphomas and have comparatively longer median life span (**Figure 56 C.**), these mice die earlier (**Figure 62 & Table 9**). Their median survival is similar to the $p53^{-/-}$ mice, suggesting that $\Delta Np63$ plays an oncogenic role in the thymus, whereas it may behave like a tumor suppressor in other tissues.

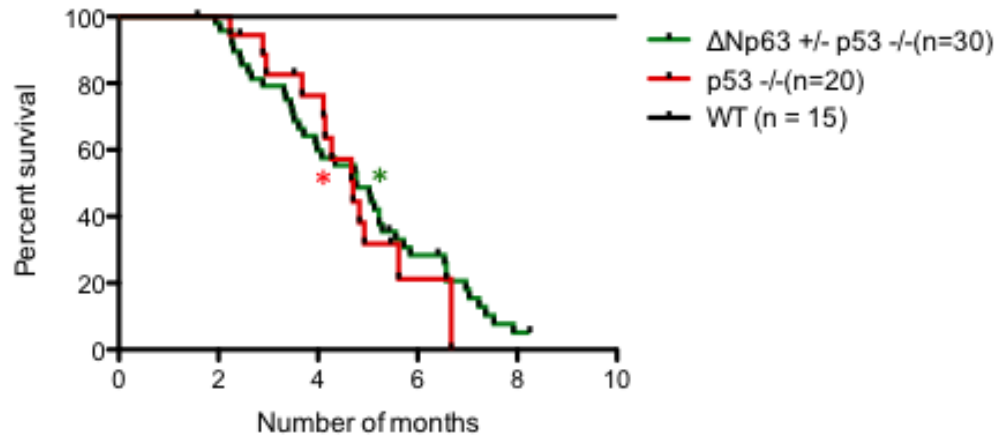


Table 10: Tumor spectrum of $\Delta Np63^{+/-}; p53^{-/-}$ mice

	$p53^{-/-}$	$\Delta Np63^{+/-}; p53^{-/-}$
Lymphoma	85%	30%
Sarcoma	5%	14%
Carcinoma	0	40%
Others	10%	16%

Percentage of mice with the indicated tumor types. N=20 for $p53^{-/-}$ cohort and n=42 for $\Delta Np63^{+/-}; p53^{-/-}$ cohort.

Figure 60: $\Delta Np63^{+/-}; p53^{-/-}$ mice die of multiple metastatic tumors

Kaplan Meier survival curves of $\Delta Np63^{+/-}; p53^{-/-}$ (n= 30) , $p53^{-/-}$ (n=20) mice, with a wide range of tumor spectrum, and wild-type (n=15) mice. The median survival time of the $\Delta Np63^{+/-}; p53^{-/-}$ mice are not different from the median survival time of the $p53^{-/-}$ mice. Asterisk indicate the median survival.

6.2.8. $\Delta Np63^{+/-};p53^{+/-}$ mice develop varied metastatic carcinomas

A cohort of $\Delta Np63^{+/-};p53^{+/-}$ mice we generated and aged for 2.5 years. These mice demonstrate similar survival to the $p53^{+/-}$ mice and earlier than the mice from the wild-type cohort (**Figure 63**). These mice developed various types of tumors. The moribund mice were euthanized and their tumors collected. On a detailed analysis it appears that the $\Delta Np63^{+/-};p53^{+/-}$ mice develop many different types of carcinomas along with sarcomas. These mice develop mammary adenocarcinomas, squamous cell carcinomas and ovarian carcinomas. Carcinomas were not found to be present in most of the $p53^{+/-}$ mice. Many of these carcinomas are aggressive and malignant. Further work has to be done for a detailed analysis of these tumors.

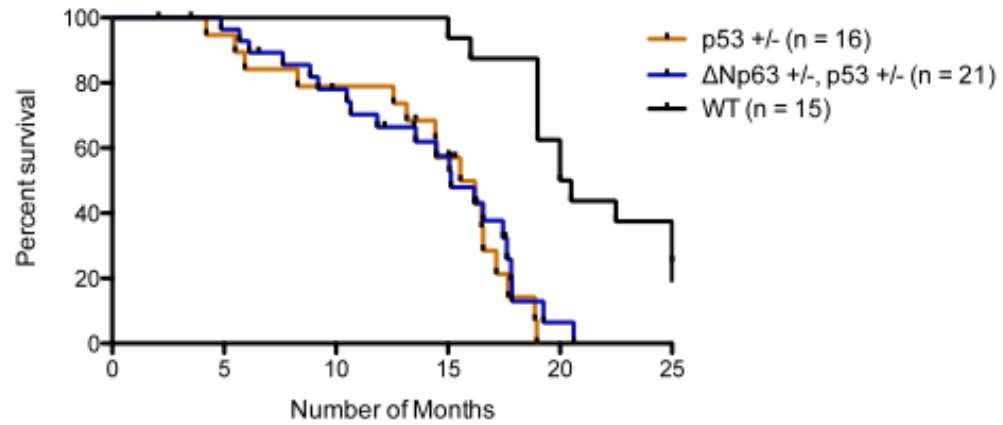


Figure 61: $\Delta Np63^{+/-};p53^{+/-}$ mice develop varied metastatic carcinomas

Kaplan Meier survival curves of $\Delta Np63^{+/-};p53^{+/-}$ (n= 21) , $p53^{+/-}$ (n=16) mice, with a wide range of tumor spectrum, and wild-type (n=15) mice. The median survival time of the $\Delta Np63^{+/-};p53^{+/-}$ mice are not different from the median survival time of the $p53^{+/-}$ mice.

6.2.9. $\Delta Np63^{-/-}$ MEFs and keratinocytes have high migration and invasion potential

We went on to characterize the invasive potential of $\Delta Np63^{-/-}$ MEFs and keratinocytes in vitro with a Boyden chamber assay. We found that the $\Delta Np63^{-/-}$ MEFs and keratinocytes are highly invasive when assayed by this method (**Figure 64 A-D**).

We also performed time-lapse microscopic imaging on scratch assays with the *wild-type* and $\Delta Np63^{-/-}$ keratinocytes. A scratch was made on a confluent plate of wild-type keratinocytes and $\Delta Np63^{-/-}$ epidermal cells with the tip of a 200um pipette. The $\Delta Np63^{-/-}$ cells were more migratory and could cover the scratch within 24 hours, while the wild-type keratinocytes took close to 48 hours to cover the scratch (**Figure 64E**). When the movement of these cells was analyzed, we found that the $\Delta Np63^{-/-}$ cells exhibited a loss of contact inhibition and loss of directional movement. While the wild-type cells all moved towards the scratch in a coordinated fashion, the $\Delta Np63^{-/-}$ keratinocytes showed a more rapid but random movement.

We determined the average path length covered by the $\Delta Np63^{-/-}$ cells (n=30) for a given time (12 hours) and compared this to the path length covered by the wild-type keratinocytes (n=30) in the same time. This showed that the $\Delta Np63^{-/-}$ cells covered a longer path in the same amount of time in comparison to the *wild-type* keratinocytes. Suggesting that these cells are highly migratory, but lack directionality (**Figure 64F**).

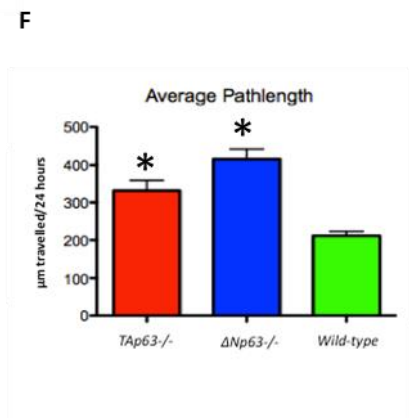
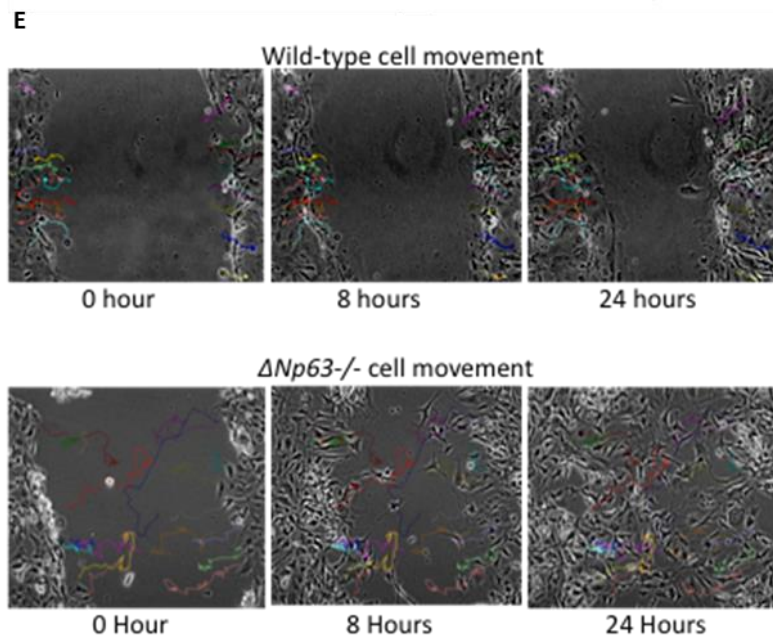
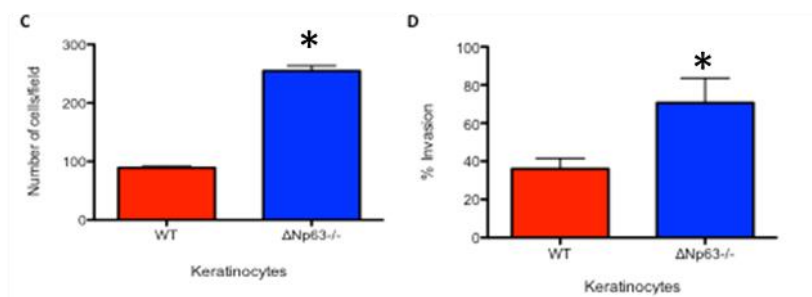
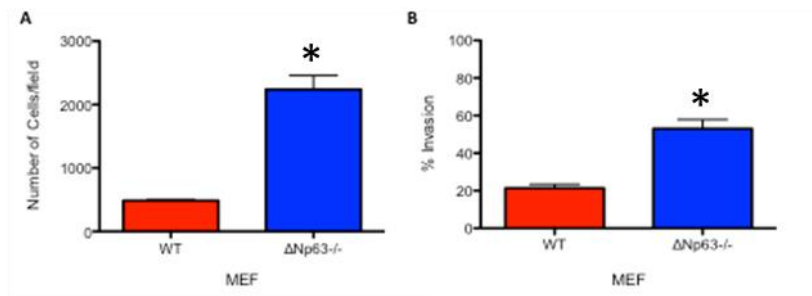


Figure 64: *ΔNp63* deficient keratinocytes and MEFs are highly migratory and invasive

A-D) Bargraphs indicating migration and invasion in MEFs and keratinocytes of the indicated genotypes. **E)** Real time-lapse scratch assay with keratinocytes of the indicated genotypes monitored over 24 hours. The colored lines indicate the path taken by each cell in closing the scratch. **F)** Calculation of the average pathlength travelled by 30 cells from the indicated genotypes over a period of 12 hours. (n=3). Magnification 200x. Asterisk indicate significance. p value ≤ 0.05 .

6.3. Discussion

For the past 12 or more years researchers have speculated about the role of *p63* in tumorigenesis. Since the construction of the *p63* knock-out mice, which are postnatally lethal and have developmental defects, *p63* have been thought to mainly play roles in development and not so much in the suppression of tumorigenesis. In 2005 Dr. Elsa Flores found that *p63*^{+/-} mice develop spontaneous tumors. Also when crossed to the *p53*^{+/-} mice, which mainly develop sarcomas and lymphomas, there was a significant reduction in the median survival (7 months compared to 10 months) of the *p63*^{+/-};*p53*^{+/-} mice primarily due to the development of spontaneous carcinomas which were highly aggressive. 50% of the mice got metastatic disease (ref). This led to a major shift in belief about the role of *p63* in suppression of tumorigenesis. The Flores lab along with other labs have shown that *p63* indeed has tumor suppressive roles (129-131). *TAp63* has been shown to be a tumor suppressor by the regulation of *Dicer* and microRNAs (65). The role of $\Delta Np63$ on the other hand has not been investigated in the suppression of tumorigenesis as much mainly due to the post-natal lethality of these mice, similar to the total *p63* knock-out mice (74). Thus the study of the $\Delta Np63$ mutant mice has to be performed in a heterozygous background. In spite of the retention of one allele of $\Delta Np63$ in these mice, they develop carcinomas and have a reduced median survival in comparison to the wild-type. Suggesting a role of $\Delta Np63$ in suppression of tumorigenesis. Interestingly in a *p53*^{-/-} background only 30% of these mice develop thymic lymphomas, a drastic reduction from 80-90% thymic lymphoma incidence in the *p53*^{-/-} mice suggesting, in thymus $\Delta Np63$ could potentially play a role as an oncogene. This could be explained by its ability to bind to the *TAp63* isoform and also *TAp73* isoforms (data not shown) and suppress their activity in inducing cell death.

Further analysis is going on to test this hypothesis in our lab. While the other $\Delta Np63$ ^{+/-} ; *p53*^{-/-} mice develop metastatic carcinomas and other aggressive tumor types which leads to the early death of these mice. This suggests that $\Delta Np63$ could play tumor suppressive role in other tissue types.

The phenotype of the $\Delta Np63^{+/-};p53^{-/-}$ mice suggests that $\Delta Np63$ could play oncogenic roles in certain tumor types. This finding is remarkable in that this could lead to therapies where the $p53$ protein is lost or mutated. The reduction in the levels of $\Delta Np63$ could lead to the upregulation of $TAp63$ (and possibly $TAp73$) causing critical apoptosis and senescence in Specific tumor types. This is reminiscent of the study by Leif W.Ellisen's group, where they demonstrated that in triple negative breast cancer overexpressing $\Delta Np63$, $\Delta Np63$ can specifically sequester $TAp73$ inhibiting apoptosis. This interaction is dissociated when platinum based chemotherapeutic agent, cisplatin is administered, releasing $TAp73$ to be able to induce apoptosis through Puma. When they knocked-down $\Delta Np63$ with siRNAs, liberating $TAp73$ in cells lines, there was an increase in apoptosis (ref). Taken together this could lead to specific and successful therapeutic strategies in $p53$ mutated or lost tumors. The fact that $p63$ is not so frequently mutated in tumors could be used towards advantage of such therapies.

7. Chapter 7. Conclusion and Future Direction

7. Conclusion and Future Directions

My thesis work demonstrates an intricate network of genes and microRNAs regulated by the *p63* isoforms that regulate various biological processes like tumorigenesis, metastasis, stem cell maintenance and the generation of stem like cells (iMS cells) from differentiated cells. For the first time I have shown that *p63*, both *TAp63* and $\Delta Np63$ can regulate the microRNA biogenesis network of proteins thereby placing *p63* in the center of the microRNA biogenesis network and various biological processes. We found that *TAp63* transcriptionally regulates *Dicer* and $\Delta Np63$ transcriptionally regulates *DGCR8*. *Dicer* and *DGCR8* are crucial to the microRNA biogenesis pathway. In the absence of these proteins there is a loss in the mature and precursor microRNA production.

The *TAp63* knock-out mice develop spontaneous highly metastatic carcinomas and sarcomas. These tumors metastasize to the liver bone, lungs and even to the brain, a rare occurrence in spontaneous mouse tumor models. Cells and cell lines from these mice express low levels of *Dicer* and microRNAs and this causes increased metastasis (65). We assayed for metastasis by *in vitro* Boyden chamber assay, which measures invasive potential of cells. This assay is correlative, but very useful in determining the metastatic potential of the cells *in vivo* since invasion is an early step of metastasis (65). Also this assay allows us to manipulate proteins and microRNAs in a system to assess their effects on invasion and therefore metastasis. We found that the *TAp63*^{-/-} MEFs are highly invasive *in vitro* which correlates with the *TAp63*^{-/-} metastatic tumor development in mice. Re-expression of *Dicer* in the MEFs from these mice rescues the invasive phenotype *in vitro* (65). We also found that *TAp63* can transcriptionally regulate *miR-130b*. Re-expression of this microRNA by itself did not affect the rate of invasion in these cells (65). Whereas co-expression of *Dicer* and *miR-130b* in MEFs reduced their invasive potential in a Boyden chamber assay, suggesting that there is co-operation between *Dicer* and *miR-130b* in the regulation of invasion *in vitro* (65).

Primary and metastatic human lung adenocarcinomas, mammary adenocarcinomas and head and neck squamous cell carcinomas were assayed for their metastatic potential. The high grade metastatic tumors exhibited a concomitant loss of *TAp63*, *Dicer* and *miR-130b* suggesting that the regulation of metastasis by these proteins are dependent upon *TAp63* status

in these tumors. The loss of TAp63 seems to be gradual in these tumors. The lower grades of tumors (Grade I & II) retain some expression of *TAp63*, *Dicer* and *miR-130b*, whereas total loss is seen in the higher grades of tumors (Grade II & III) (65). The *TAp63*^{-/-} mice develop metastases later in the tumor development course. Most of these mice start developing tumors at the age of 12 months and more (65). This could be due to the fact that the latency period for tumor development is longer in these mice, but once the tumors develop they become highly metastatic. This could be because with the loss of *TAp63* there is increased DNA damage and genomic instability. Genomic instability has been shown to be a precursor of cellular senescence. The primary tumors overcome this senescent phenotype by genomic instability and respond by further mutations in other pathways. This genetic makeover leads to aggressive metastasis of these tumors in the *TAp63*^{-/-} mice.

Interestingly the carcinomas from the *TAp63* mutant mice do exhibit high levels of metastases. This is also true when these mice are crossed to the *p53* mutant mice. Interestingly the level of senescence was to be higher in the *TAp63*^{-/-};*p53*^{+/-} and *TAp63*^{+/-};*p53*^{+/-} sarcomas than in the carcinomas (65). The sarcomas from these mice were found to have higher levels of age-related senescence. On the contrary the carcinomas from both these cohorts had a lower level of senescence and a higher level of metastasis (65). This could be explained by the fact that there is an increased level of genomic instability in the carcinomas from the *TAp63*^{-/-}, *TAp63*^{-/-};*p53*^{+/-} and *TAp63*^{+/-};*p53*^{+/-} mice when compared to the sarcomas from the same mice (65). This could be due to the fact that *TAp63* plays a more important role in the epithelial compartment than the mesenchymal compartment. Loss of *TAp63* in the epithelium is therefore more deleterious to the organism (65).

We found that *ΔNp63* transcriptionally regulates *DGCR8*. Loss of *ΔNp63* leads to a loss in terminal differentiation in the epidermis. We also found that re-expression of *DGCR8* in these isolated epidermal cells from the *ΔNp63* knock-out mice may be able to induce differentiation in these cells. These cells were shown to possess characters of stem cells. They can differentiate into multiple cells types *in vitro* and can even give rise to chimeras when injected into the blastocysts of a pseudopregnant mouse. Although the chimeras generated from these blastocysts look phenotypically similar to the *ΔNp63*^{-/-} embryos. They have a defect in the terminal differentiation of their epidermis and express some the markers of

epidermal stem cells like K8 and K18 in a similar manner to the epidermis of the *ΔNp63*^{-/-} embryos. These chimeras also die a few hours after birth. This defect in terminal differentiation can be partially rescued by the re-expression of *DGCR8* in these cells. Teratomas generated from the *ΔNp63*^{-/-} epidermal cells without the expression of *DGCR8* is extremely undifferentiated, whereas teratomas from these cells expressing *DGCR8* is well differentiated. This suggests that *DGCR8* plays an important role in the regulation of differentiation and that *ΔNp63* regulates differentiation through the regulation of *DGCR8* (in review, PNAS).

Moreover when *ΔNp63* or *DGCR8* is knocked down in normal human keratinocytes (NHEK) cells with the help of lentiviral shRNAs for *ΔNp63* or *DGCR8*, these cells behave in a stem like manner. They express stem cells markers like SSEA-1, Oct-4, Sox-2, Tra-1-81 and can form teratomas when injected into SCID mice. The cells deficient for *ΔNp63* form teratomas, which are less differentiated than the cells, which are deficient for *DGCR8*. This could be because *ΔNp63* regulates many other genes important for the regulation terminal differentiation like E-cadherin and keratin 14. This method could prove to be a robust method for the generation of multipotent stem cells as mentioned earlier in chapter 4.

Finally we also found, by cross-species microRNA comparison, a set of microRNAs which are common between the human shRNA knock-down cells and the murine *ΔNp63* deficient epidermal cells. These were in turn compared with the human iPS cells and mouse iPS cells generated by the introduction of the Yamanaka factors. These microRNAs as mentioned earlier could be the key microRNAs involved in the reprogramming potential of these cells. There has been an explosion in knowledgebase about the microRNAs and other proteins that are involved in reprogramming somatic cells to pluripotent stem cells. Research is still ongoing to identify the key factors and also to find a way of reducing the number of factors required for this purpose. My thesis work may facilitate refining the search for the core factors and indicating the most important microRNAs required to be modulated for this process.

7.1. *p63*, microRNAs and cancer

We found that *TAp63* transcriptionally regulates *Dicer* and *ΔNp63* transcriptionally regulates *DGCR8*. In many cancers there is a loss of these *p63* isoforms (56, 73). There is also a global downregulation of microRNAs in many cancers; therefore the regulation of *Dicer*, *Drosha*, *Ago2*, *TARBP* and the other proteins involved in the microRNA biogenesis pathway possibly plays a critical role in the regulation of tumorigenesis and metastasis of tumors (269, 270). Interestingly the loss of *Dicer* and *Drosha* has been shown to have prognostic value in ovarian, breast and colorectal cancers (271). Loss of these proteins is generally deleterious to the survival of patients with such diseases. Approaches are being made towards the re-expression of *Dicer*, *Drosha* or *TARBP* in some types of tumors. This may help in the increased microRNA biogenesis and the improvement in patient survival(270). There is evidence that *p63* is amplified and overexpressed in cancers (73). It would be intriguing to profile the microRNAs from those tumors and delineate the regulation of *Dicer* and *DGCR8*. *Dicer* and *DGCR8* have also been shown to be regulated by microRNAs themselves. Therefore it will be intriguing to delineate the network of these microRNAs and to determine whether *p63* plays any role in these interactions.

Recently there has been a lot of development of microRNA therapeutics. A number of tumor suppressor microRNAs have been shown to be lost in cancer. Attempts are being made to express some of these microRNAs. In 2009, Taulli et al. reexpressed miR-1/miR-206 in skeletal muscle. These microRNAs are shown to be lost in RMS. When expressed in these cells *in vitro* they led to loss of growth in soft agar assay and loss of proliferation and invasion. This also induced forced myogenic differentiation in these cells (272). Other microRNA like miR-375 can induce drug sensitivity and reduce EMT like properties in tamoxifen resistant MCF-7 cells *in vitro* (273). Several studies are underway which test whether the re-expression of different microRNAs can reduce proliferation, invasion, induce cell death or senescence in cells (274),(275). Recently a microRNA based drug was developed against the Hepatitis C viral antigen. This drug is in phase II clinical trial. The drug is based on microRNA 122 which have been modified by LNA insertion into its backbone. Some of the major problems with

microRNA based therapy is non-specific targeting, instability in body fluids and therefore high dose requirement, (276).

7.2. *p63* and EMT

Dicer has been shown to regulate many microRNAs which regulate EMT. miR-200 family of microRNAs has been demonstrated to be major regulators of EMT (203). These microRNAs can regulate E-cadherin, one of the main proteins in maintaining tissue integrity (277). Loss of miR-200 family is an early event in metastasis and is thought to mark the initiation of EMT events. Therefore the loss of *Dicer* and the other microRNA biogenesis pathway proteins may be investigated as a biomarker for cancer progression along with other proteins involved in EMT (Epithelial Mesenchymal Transition). EMT marks the first stages of metastasis, therefore it seems that loss of *TAp63* could potentially induce EMT in these tumors, which would then become highly metastatic. *Dicer* has also been implicated in this process of EMT, indirectly through the regulation of microRNA like the miR-200 family (278). It would be interesting to see whether re-expression of *Dicer* and *TAp63* or $\Delta Np63$ in tumor cells revert back their mesenchymal phenotype to a more epithelial phenotype. Some of the factors important in EMT are snail, slug, Twist and E-cadherin. It will be interesting to see whether the loss *TAp63* and $\Delta Np63$ can cooperate with any of these factors to induce EMT. It is possible that the loss of $\Delta Np63$ may make the cells more mesenchymal as seen in the epidermal cells from the $\Delta Np63^{-/-}$ mice. These cells are highly invasive in Boyden chamber assay. They seem to lose contact inhibition as they come in contact with other cells (unpublished work from Chakravarti and Flores, chapter 6). Further work needs to be done to demonstrate that.

7.3. *p63*, stem cell maintenance, differentiation and stratification

p63 has been shown to be important in differentiation. *TAp63* has been shown to be required to maintain homeostasis in the transiently amplifying stem cells of the epidermis (72), while $\Delta Np63$ maintains the stem cells in the basal layer of the epidermis in their stem like

state. $\Delta Np63$ has also been shown to be important in the induction of differentiation in the basal layer of the epidermis. Therefore there is a divide in thoughts over $\Delta Np63$'s role in stem cell maintenance or induction of terminal differentiation. Overexpression of $TAp63\alpha$ in the K14 cells of the basal layer in a induced mouse model leads to an expansion in the epidermal compartment and delayed differentiation as detected by keratin1 expression. This suggests that overexpression of $TAp63$ possibly leads to an expansion in the stem cells in the epidermis and in turn leads to hyperproliferation of these stem cells (78). Overexpression of $\Delta Np63a$ has also shown to be inhibitory in the induction of differentiation (98). Depletion of $\Delta Np63$ on the other hand as shown by others and us leads to a defect in the epidermis formation (247). Although the epidermal cells from the $\Delta Np63$ knock-out mice express all the differentiation markers, they do not undergo proper stratification. One explanation for this is that the cells in the epidermis receive signals from the dermis to differentiate, but they require $\Delta Np63$ for proper stratification and also to regulate the timing of differentiation. Since stratification and differentiation are two different aspects in the development of the epidermis, it is possible that $\Delta Np63$ is a major regulator of the stratification process. The current idea in the field is that $\Delta Np63$ is required to maintain the cells in their stem like state in the basal layer of the epidermis. But it could be a possibility that $\Delta Np63$ expression is really a signal for the cells in the basal layer to differentiate and stratify, since others and we have found that the stem cells in the skin are present even in the absence of $\Delta Np63$. Further work has to be done to test this hypothesis.

7.4. Role of $p63/p73$ in iPS cell generation

Recently there were few reports on the effects of $p63$ and $p73$ on iPS cell generation. Researchers found that overexpression of $\Delta Np73$ in human fibroblasts along with induction with the four Yamanaka factors increase the reprogramming potential of the cells by 12.67%. Also when injected into SCID mice these cells are resistant to differentiation. On analysis of 10 random microscopic fields (400x), they found that in the control iPS cell teratomas 100% of the field had differentiated cells with less than 30% of the fields showing non-specific cells. But in the $\Delta Np73$ overexpressing teratomas only 20% of the fields had differentiated cells and

30%-100% of the fields showed presence of non-specific or undifferentiated cells suggesting that overexpression of *ΔNp73* inhibits differentiation potential of the iPSCs in vivo. They further explained that this defect could be contributed to the repression of the Nanog promoter by *ΔNp73* as tested by luciferase assay (279).

Another paper reported that iPS cells generated from patients with EEC syndrome with 2 point mutations (R304W and R204W) in the DNA binding domain display defects in ectodermal differentiation. This paper showed that when these cells were infected with the Yamanaka factors and subjected to embryoid body formation assay, they could form embryoid bodies and on attachment give rise to cells from all three germ layer. On treatment with BMP4 and SB431542, which induce ectodermal differentiation in the iPSCs from wild-type fibroblasts evident by the expression of keratin 14 positive cells, the iPSCs from the EEC patient cells did not differentiate into keratin 14 expressing cells. Although a small percentage of cells expressed keratin 18, a marker of ectodermal progenitor. These cells demonstrated a similar defect to differentiate in to corneal epithelial cells when cultured on corneal fibroblasts and treated with BMP-4. Recently APR-246/PRIMA-1^{MET} has been shown to induce apoptosis through *p63*. In order to test whether this compound has effects on *p63*-mediated differentiation, the patient specific iPSCs were treated with APR-246/PRIMA-1^{MET}. This led to an increase in keratin 14 positive cells in the EEC patient specific cells from about $43 \pm 12\%$ in iPSC^{R304W/+} and to $24 \pm 15\%$ and iPSC^{R204W/+}, while the wild-type iPSCs remain unaffected at 27.5% (279, 280) .

7.5. *p63* and cancer stem cells

TAp63 has been shown to be important in maintaining stem cells homeostasis by Su et.al, 2009. Loss of *TAp63* leads to a hyperproliferation in the stem cell compartment. *TAp63* has also been shown to be important in the induction of senescence under oncogenic stress. The *TAp63*^{-/-} mice develop squamous cell carcinomas. This could possibly be due to a hyperproliferation in the SKP cells in the adult skin cell compartment. This demonstrates its role in tumor suppression to be varied. Therefore it would be interesting to identify its role in cancer stem cell regulation.

7.6. $\Delta Np63$ and tumor suppression

We have shown that $\Delta Np63$ heterozygote mice develop highly malignant tumors. These tumors are metastatic. Also $\Delta Np63$ mutant cells are highly invasive and migratory. Therefore it is tempting to speculate that $\Delta Np63$ has tissue tumor suppressive functions. This finding is significant because until now researchers believed $\Delta Np63$ is an oncogene based on its overexpression in human tumors. This is the first demonstration of tumor suppressive capability of $\Delta Np63$. It will be interesting to understand the co-operation of $\Delta Np63$ and $TAp63$ in this function. We have also shown that $TAp63$ is transcriptionally regulated by $\Delta Np63$. This regulation may be of prime importance in the regulation of tumorigenesis. $\Delta Np63$ has been shown to have a dominant negative effect on the entire $p53$ family. It may be worth speculating that it perhaps counteracts the effects of overactive $p53$, $TAp63$ and $TAp73$ after stress response and returns the cells to normalcy.

My work places $p63$ in an important junction of the microRNA biogenesis pathway. This sheds light on the previously unknown functions of this family of proteins and makes it an important regulator of biological processes which were seemingly unrelated to this protein. It is interesting that $p63$ and not $p53$ regulates these proteins by direct transcriptional activation at these sites. Although we do not know whether there is co-operation between the family members in this regulation. Furthermore $p63$ has always thought to be important in the epithelial morphogenesis. It is exciting to find that its regulatory effect on the microRNA biogenesis pathway is not restricted to the epithelium. The regulation of this pathway in the keratinocytes and fibroblasts suggest that it has a broader role than appreciated earlier. This also links $p63$ to a diverse range of biological processes, which were thought to be $p63$ independent. Finally we have shown conclusively that $TAp63$ suppresses tumorigenesis. It would be intriguing to investigate the role of $\Delta Np63$ in tumorigenesis. It appears from the preliminary data generated by our lab that $\Delta Np63$ could have dual role in both tumor suppression and oncogenesis.

Appendix 1: mouse miRNA Pearson's correlation analysis									
Sample	mES	miPS ^{Yam}	Δ Np63-/-1	Δ Np63-/-2	Δ Np63-/-3	Keratinocytes 1	Keratinocytes 2	Δ Np63-/- +DGCR8-1	Δ Np63-/- +DGCR8-2
mES1	1.000	0.951	-0.277	-0.353	-0.493	-0.427	-0.416	-0.490	-0.544
miPS ^{Yam}	0.951	1.000	-0.254	-0.367	-0.475	-0.448	-0.431	-0.490	-0.532
Δ Np63-/-1	-0.277	-0.254	1.000	0.633	0.026	-0.258	-0.308	0.068	0.013
Δ Np63-/-2	-0.353	-0.367	0.633	1.000	0.260	-0.277	-0.324	0.135	0.068
Δ Np63-/-3	-0.493	-0.475	0.026	0.260	1.000	-0.230	-0.222	0.070	0.125
Keratinocytes 1	-0.427	-0.448	-0.258	-0.277	-0.230	1.000	0.983	0.453	0.503
Keratinocytes 2	-0.416	-0.431	-0.308	-0.324	-0.222	0.983	1.000	0.431	0.487
Δ Np63-/- +DGCR8-1	-0.490	-0.490	0.068	0.135	0.070	0.453	0.431	1.000	0.961
Δ Np63-/- +DGCR8-2	-0.544	-0.532	0.013	0.068	0.125	0.503	0.487	0.961	1.000

Appendix 2 : mouse-miRNA heat map								
miRNA	mES	miPS ^{yam}	Δ Np63-/-1	Δ Np63-/-2	Keratinocytes 1	Keratinocytes 2	Δ Np63-/- +DGCR8-1	Δ Np63-/- +DGCR8-2
mmu-mir-205-5p	-0.670	-0.341	-0.770	-1.011	0.676	0.676	-1.109	-1.105
mmu-mir-666-5p	0.503	0.214	1.779	1.625	-1.121	-1.100	0.017	-0.490
mmu-mir-450a-5p	0.092	-0.707	-1.030	-2.010	0.210	0.453	0.820	1.237
mmu-mir-582-5p	-1.123	-1.327	-0.622	-1.257	0.465	0.510	0.638	0.896
mmu-mir-455-5p	-1.852	-1.370	-0.662	0.611	0.882	0.984	1.099	0.868
mmu-mir-465c-5p	2.402	0.414	0.622	-0.368	-0.684	-0.645	-0.773	-0.757
mmu-mir-337-3p	1.118	0.890	0.012	2.173	-0.740	-0.718	-0.792	-0.783
mmu-mir-369-5p	0.907	0.798	1.663	1.389	-0.809	-0.789	-0.857	-0.848
mmu-mir-150-5p	1.336	1.989	0.544	-0.424	-0.732	-0.694	-0.819	-0.803
mmu-mir-190-5p	-1.183	-0.894	-0.713	-1.420	0.412	0.566	1.550	1.266
mmu-mir-299-5p	1.135	0.816	-0.274	1.895	-1.059	-1.036	0.460	0.133
mmu-mir-290-3p	2.244	1.259	0.356	-0.433	-0.685	-0.654	-0.756	-0.743

mmu-mir-1968-5p	2.045	1.627	0.271	-0.448	-0.677	-0.649	-0.742	-0.730
mmu-mir-871-3p	2.373	0.968	0.323	-0.496	-0.045	-0.725	-0.831	-0.818
mmu-mir-431-5p	0.927	0.751	1.554	1.514	-0.885	-0.866	-0.337	-0.922
mmu-mir-376b-5p	1.214	0.814	1.576	1.191	-0.963	-0.941	-0.521	-0.521
mmu-mir-361-5p	-0.806	-0.999	-1.475	-0.140	-0.174	-0.099	-0.344	-0.174
mmu-mir-465a-3p	2.471	1.045	0.236	-0.428	-0.639	-0.613	-0.699	-0.688
mmu-mir-465b-3p	2.471	1.045	0.236	-0.428	-0.639	-0.613	-0.699	-0.688
mmu-mir-465c-3p	2.471	1.045	0.236	-0.428	-0.639	-0.613	-0.699	-0.688
mmu-mir-1843-5p	-1.673	-1.499	-0.802	-0.074	1.007	0.922	0.749	0.903
mmu-mir-758-5p	2.576	0.800	0.259	-0.413	-0.626	-0.600	-0.687	-0.676
mmu-mir-363-5p	1.552	2.214	0.135	-0.451	-0.638	-0.615	-0.691	-0.682
mmu-mir-1965	2.246	1.518	0.126	-0.451	-0.634	-0.612	-0.686	-0.677
mmu-mir-667-5p	1.674	1.070	-0.151	1.695	-0.790	-0.771	-0.433	-0.825
mmu-mir-673-5p	1.657	1.428	-0.181	1.396	-0.810	-0.792	-0.310	-0.846
mmu-mir-295-5p	2.178	1.672	0.046	-0.456	-0.616	-0.596	-0.661	-0.653
mmu-mir-224-5p	-1.565	-1.663	-1.200	0.302	0.473	0.531	0.357	-0.014

mmu-mir-1893	1.458	0.813	1.835	0.135	-0.954	-0.937	-0.993	-0.986
mmu-mir-136-5p	1.047	1.016	1.358	0.439	-0.770	-1.216	0.836	0.157
mmu-mir-194-5p	-0.983	-1.169	-0.878	-1.380	0.806	0.856	0.953	1.023
mmu-mir-540-3p	1.730	1.562	-0.218	1.209	-0.778	-0.762	-0.388	-0.810
mmu-mir-423-3p	-1.939	-1.329	0.023	-0.141	-0.141	0.035	-0.006	-0.079
mmu-mir-33-5p	-0.632	-0.768	-0.932	-1.428	-0.013	-0.066	-0.283	0.004
mmu-mir-679-5p	1.603	1.482	-0.323	1.419	-0.861	-0.845	-0.110	-0.539
mmu-mir-323-3p	1.405	1.317	1.635	0.152	-0.840	-0.825	-0.873	-0.867
mmu-mir-878-5p	2.303	1.530	0.020	-0.452	-0.603	-0.584	-0.645	-0.638
mmu-mir-3068-5p	-1.616	-1.619	-1.361	0.651	0.697	0.697	0.495	0.378
mmu-mir-23b-5p	-0.957	-1.024	-0.599	-0.969	1.390	1.374	1.016	1.126
mmu-mir-382-5p	1.090	1.010	1.238	1.391	-1.024	-1.010	0.053	-0.309
mmu-mir-34b-5p	-1.333	-1.333	-0.546	-0.982	0.873	0.857	1.308	1.308
mmu-mir-130a-5p	-1.133	-1.246	-0.848	0.015	0.910	0.958	1.423	1.357
mmu-mir-337-5p	1.538	1.271	1.215	0.447	-1.037	-1.021	0.215	-0.257
mmu-mir-345-3p	-1.647	-1.530	-1.251	-0.237	0.559	0.587	0.683	0.938

mmu-mir-409-3p	1.642	1.492	-0.365	1.372	-0.865	-0.850	-0.123	-0.412
mmu-mir-363-3p	1.775	2.140	-0.039	-0.458	-0.592	-0.576	-0.630	-0.623
mmu-mir-369-3p	1.494	1.459	0.715	0.849	-1.050	-1.036	0.091	-0.066
mmu-mir-291b-5p	0.008	2.876	0.150	-0.348	-0.507	-0.488	-0.552	-0.544
mmu-mir-380-3p	1.426	1.295	1.157	1.064	-0.913	-0.901	-0.455	-0.529
mmu-mir-294-5p	2.129	1.816	-0.090	-0.459	-0.577	-0.562	-0.610	-0.604
mmu-mir-200a-5p	-0.963	-0.963	-0.788	-1.170	1.546	1.546	-0.463	-0.444
mmu-mir-106a-5p	1.940	2.029	-0.122	-0.460	-0.567	-0.554	-0.598	-0.592
mmu-mir-322-5p	-0.929	-1.155	-1.906	-0.648	0.726	0.651	0.957	1.023
mmu-mir-290-5p	2.087	1.882	-0.130	-0.460	-0.564	-0.551	-0.594	-0.589
mmu-mir-200b-5p	-0.704	-0.927	-0.875	-1.245	1.575	1.537	-0.465	-0.561
mmu-mir-434-3p	1.155	1.065	1.172	1.030	-1.085	-1.075	0.323	0.163
mmu-mir-30b-5p	-1.319	-1.467	-0.864	-0.644	-0.111	0.161	0.198	0.319
mmu-mir-23a-5p	-0.920	-1.030	-0.507	-0.796	1.219	1.198	1.232	1.297
mmu-mir-380-5p	1.314	1.279	1.100	1.016	-1.024	-1.013	0.052	-0.171
mmu-mir-18b-5p	1.919	2.058	-0.143	-0.460	-0.560	-0.548	-0.589	-0.584

mmu-mir-302a-5p	1.541	2.355	-0.103	-0.452	-0.564	-0.550	-0.595	-0.590
mmu-mir-20b-5p	1.972	2.012	-0.154	-0.460	-0.557	-0.545	-0.585	-0.580
mmu-mir-9-5p	0.815	0.815	0.709	1.548	-0.801	-0.877	0.744	0.365
mmu-mir-210-5p	-1.164	-1.076	-0.714	-1.029	1.240	1.240	1.093	1.113
mmu-mir-185-5p	-0.985	-0.978	-1.833	-0.915	0.883	0.845	0.978	1.026
mmu-mir-27a-5p	-1.101	-1.355	-0.785	-0.379	1.391	1.340	0.939	1.045
mmu-mir-434-5p	1.292	1.190	1.060	1.060	-1.047	-1.037	0.210	-0.076
mmu-mir-199b-5p	-1.377	-1.377	-0.796	0.029	1.006	1.019	1.213	1.224
mmu-mir-485-5p	1.581	1.265	0.845	1.022	-1.064	-1.053	-0.014	-0.362
mmu-mir-292-3p	2.034	1.959	-0.180	-0.459	-0.548	-0.537	-0.574	-0.569
mmu-mir-291a-3p	1.998	1.998	-0.188	-0.459	-0.546	-0.535	-0.570	-0.566
mmu-mir-291a-5p	2.016	1.983	-0.193	-0.459	-0.544	-0.533	-0.568	-0.564
mmu-mir-200c-5p	-0.981	-0.853	-0.423	-0.732	1.910	1.939	-0.180	-0.145
mmu-mir-293-5p	2.076	1.918	-0.190	-0.459	-0.545	-0.534	-0.569	-0.565
mmu-mir-134-5p	1.390	1.234	0.925	1.015	-1.096	-0.815	0.210	-0.044
mmu-mir-27b-5p	-1.037	-1.066	-0.981	-0.460	1.447	1.409	0.889	0.922

mmu-mir-29a-5p	-1.231	-1.231	-0.727	-0.279	1.091	1.062	1.231	1.378
mmu-mir-31-5p	-1.470	-1.234	-0.534	-0.957	1.130	1.229	-0.281	-0.144
mmu-mir-411-5p	1.330	1.203	1.107	0.995	-1.134	-1.124	0.112	-0.195
mmu-mir-148b-5p	-0.618	-0.521	-2.081	-0.471	0.874	0.947	1.237	1.218
mmu-mir-24-1-5p	-1.617	-1.727	-0.336	-0.209	1.164	1.164	0.843	0.894
mmu-mir-221-5p	0.440	0.669	1.047	1.207	-1.359	-1.388	-1.052	-1.052
mmu-mir-152-5p	-1.170	-1.133	-0.734	0.043	1.135	1.135	1.241	1.271
mmu-mir-292-5p	2.062	1.942	-0.211	-0.459	-0.537	-0.528	-0.560	-0.556
mmu-mir-148a-5p	-0.611	-0.789	-1.251	-0.858	1.059	1.059	1.459	1.270
mmu-mir-203-5p	-1.185	-1.185	-0.764	-0.997	1.652	1.652	0.245	0.133
mmu-mir-379-5p	1.180	1.072	1.180	1.072	-1.159	-1.152	0.223	0.020
mmu-mir-378-5p	-1.051	-0.958	-0.630	-0.863	1.110	1.110	1.309	1.401
mmu-mir-30d-5p	-1.414	-1.224	-1.414	0.116	-0.154	-0.154	1.312	1.312
mmu-mir-103-2-5p	-0.983	-0.997	-0.133	-0.940	1.225	1.225	1.225	1.225
mmu-mir-34c-5p	-2.587	-0.582	-0.129	-0.582	0.392	0.392	0.392	0.392
mmu-mir-146b-5p	-1.696	-1.364	-0.866	-0.866	0.883	0.883	0.883	0.883

Appendix 3 : mouse up-regulated miRNAs and gene targets from mRNA-seq						
Category	Term	Count in Selected Genes	Count in Total Population	P-value	Gene	173 down-regulated genes
TargetScan6.0	mmu-mir-125b-5p	63	704	8.36196E-10	105732	Fam83h
TargetScan6.0	mmu-mir-125b-5p	63	704	8.36196E-10	106582	Nrm
TargetScan6.0	mmu-mir-125b-5p	63	704	8.36196E-10	107684	Coro2a
TargetScan6.0	mmu-mir-125b-5p	63	704	8.36196E-10	108150	Galnt7
TargetScan6.0	mmu-mir-125b-5p	63	704	8.36196E-10	116972	Fam57a
TargetScan6.0	mmu-mir-125b-5p	63	704	8.36196E-10	12142	Prdm1
TargetScan6.0	mmu-mir-125b-5p	63	704	8.36196E-10	13728	Mark2
TargetScan6.0	mmu-mir-125b-5p	63	704	8.36196E-10	15220	Foxq1
TargetScan6.0	mmu-mir-125b-5p	63	704	8.36196E-10	16848	Lfng
TargetScan6.0	mmu-mir-125b-5p	63	704	8.36196E-10	16969	Zbtb7a
TargetScan6.0	mmu-mir-125b-5p	63	704	8.36196E-10	170742	Sertad3

TargetScan6.0	mmu-mir-125b-5p	63	704	8.36196E-10	17122	Mxd4
TargetScan6.0	mmu-mir-125b-5p	63	704	8.36196E-10	17347	Mknk2
TargetScan6.0	mmu-mir-125b-5p	63	704	8.36196E-10	17920	Myo6
TargetScan6.0	mmu-mir-125b-5p	63	704	8.36196E-10	18003	Nedd9
TargetScan6.0	mmu-mir-125b-5p	63	704	8.36196E-10	18554	Pcsk7
TargetScan6.0	mmu-mir-125b-5p	63	704	8.36196E-10	18583	Pde7a
TargetScan6.0	mmu-mir-125b-5p	63	704	8.36196E-10	19340	Rab3d
TargetScan6.0	mmu-mir-125b-5p	63	704	8.36196E-10	195733	Grhl1
TargetScan6.0	mmu-mir-125b-5p	63	704	8.36196E-10	20111	Rps6ka1
TargetScan6.0	mmu-mir-125b-5p	63	704	8.36196E-10	20354	Sema4d
TargetScan6.0	mmu-mir-125b-5p	63	704	8.36196E-10	211945	Plekhh1
TargetScan6.0	mmu-mir-125b-5p	63	704	8.36196E-10	212168	Zswim4
TargetScan6.0	mmu-mir-125b-5p	63	704	8.36196E-10	214112	Nipal4
TargetScan6.0	mmu-mir-125b-5p	63	704	8.36196E-10	214531	Tmprss13
TargetScan6.0	mmu-mir-125b-5p	63	704	8.36196E-10	218215	Rnf144b

TargetScan6.0	mmu-mir-125b-5p	63	704	8.36196E-10	218442	Serinc5
TargetScan6.0	mmu-mir-125b-5p	63	704	8.36196E-10	22337	Vdr
TargetScan6.0	mmu-mir-125b-5p	63	704	8.36196E-10	228543	Rhov
TargetScan6.0	mmu-mir-125b-5p	63	704	8.36196E-10	230857	Ece1
TargetScan6.0	mmu-mir-125b-5p	63	704	8.36196E-10	231287	Atp10d
TargetScan6.0	mmu-mir-125b-5p	63	704	8.36196E-10	232146	Fam176a
TargetScan6.0	mmu-mir-125b-5p	63	704	8.36196E-10	235584	Dusp7
TargetScan6.0	mmu-mir-125b-5p	63	704	8.36196E-10	235627	Nbeal2
TargetScan6.0	mmu-mir-125b-5p	63	704	8.36196E-10	240505	Cdc42bpg
TargetScan6.0	mmu-mir-125b-5p	63	704	8.36196E-10	26403	Map3k11
TargetScan6.0	mmu-mir-125b-5p	63	704	8.36196E-10	26569	Slc27a4
TargetScan6.0	mmu-mir-125b-5p	63	704	8.36196E-10	269181	Mgat4a
TargetScan6.0	mmu-mir-125b-5p	63	704	8.36196E-10	30838	Fbxw4
TargetScan6.0	mmu-mir-125b-5p	63	704	8.36196E-10	330192	Vps37b
TargetScan6.0	mmu-mir-125b-5p	63	704	8.36196E-10	360013	Myo18a

TargetScan6.0	mmu-mir-125b-5p	63	704	8.36196E-10	52588	Tspan14
TargetScan6.0	mmu-mir-125b-5p	63	704	8.36196E-10	53883	Celsr2
TargetScan6.0	mmu-mir-125b-5p	63	704	8.36196E-10	53970	Rfx5
TargetScan6.0	mmu-mir-125b-5p	63	704	8.36196E-10	54325	Elovl1
TargetScan6.0	mmu-mir-125b-5p	63	704	8.36196E-10	57912	Cdc42se1
TargetScan6.0	mmu-mir-125b-5p	63	704	8.36196E-10	66451	2610528J11Rik
TargetScan6.0	mmu-mir-125b-5p	63	704	8.36196E-10	668158	Ccdc85c
TargetScan6.0	mmu-mir-125b-5p	63	704	8.36196E-10	67998	Fam134c
TargetScan6.0	mmu-mir-125b-5p	63	704	8.36196E-10	69727	Usp46
TargetScan6.0	mmu-mir-125b-5p	63	704	8.36196E-10	70737	Cgn
TargetScan6.0	mmu-mir-125b-5p	63	704	8.36196E-10	71145	Scara5
TargetScan6.0	mmu-mir-125b-5p	63	704	8.36196E-10	71653	4930506M07Rik
TargetScan6.0	mmu-mir-125b-5p	63	704	8.36196E-10	71911	Bdh1
TargetScan6.0	mmu-mir-125b-5p	63	704	8.36196E-10	74559	Elovl7
TargetScan6.0	mmu-mir-125b-5p	63	704	8.36196E-10	75146	Tmem180

TargetScan6.0	mmu-mir-125b-5p	63	704	8.36196E-10	76459	Car12
TargetScan6.0	mmu-mir-125b-5p	63	704	8.36196E-10	77053	Sun1
TargetScan6.0	mmu-mir-125b-5p	63	704	8.36196E-10	78255	Ralgps2
TargetScan6.0	mmu-mir-125b-5p	63	704	8.36196E-10	78334	Cdk19
TargetScan6.0	mmu-mir-125b-5p	63	704	8.36196E-10	79566	Sh3bp5l
TargetScan6.0	mmu-mir-125b-5p	63	704	8.36196E-10	83796	Smarcd2
TargetScan6.0	mmu-mir-125b-5p	63	704	8.36196E-10	97130	C77080
TargetScan6.0	mmu-mir-9-5p	70	1069	1.57902E-05	100532	Rell1
TargetScan6.0	mmu-mir-9-5p	70	1069	1.57902E-05	100737	Dcun1d4
TargetScan6.0	mmu-mir-9-5p	70	1069	1.57902E-05	101476	Plekha1
TargetScan6.0	mmu-mir-9-5p	70	1069	1.57902E-05	101772	Ano1
TargetScan6.0	mmu-mir-9-5p	70	1069	1.57902E-05	105445	Dock9
TargetScan6.0	mmu-mir-9-5p	70	1069	1.57902E-05	108100	Baiap2
TargetScan6.0	mmu-mir-9-5p	70	1069	1.57902E-05	114301	Palmd
TargetScan6.0	mmu-mir-9-5p	70	1069	1.57902E-05	11658	Alcam

TargetScan6.0	mmu-mir-9-5p	70	1069	1.57902E-05	12142	Prdm1
TargetScan6.0	mmu-mir-9-5p	70	1069	1.57902E-05	12224	Klf5
TargetScan6.0	mmu-mir-9-5p	70	1069	1.57902E-05	12227	Btg2
TargetScan6.0	mmu-mir-9-5p	70	1069	1.57902E-05	12306	Anxa2
TargetScan6.0	mmu-mir-9-5p	70	1069	1.57902E-05	12550	Cdh1
TargetScan6.0	mmu-mir-9-5p	70	1069	1.57902E-05	12822	Col18a1
TargetScan6.0	mmu-mir-9-5p	70	1069	1.57902E-05	13367	Diap1
TargetScan6.0	mmu-mir-9-5p	70	1069	1.57902E-05	13636	Efna1
TargetScan6.0	mmu-mir-9-5p	70	1069	1.57902E-05	14425	Galnt3
TargetScan6.0	mmu-mir-9-5p	70	1069	1.57902E-05	15205	Hes1
TargetScan6.0	mmu-mir-9-5p	70	1069	1.57902E-05	16403	Itga6
TargetScan6.0	mmu-mir-9-5p	70	1069	1.57902E-05	16480	Jup
TargetScan6.0	mmu-mir-9-5p	70	1069	1.57902E-05	16564	Kif21a
TargetScan6.0	mmu-mir-9-5p	70	1069	1.57902E-05	17691	Sik1
TargetScan6.0	mmu-mir-9-5p	70	1069	1.57902E-05	17761	Mtap7

TargetScan6.0	mmu-mir-9-5p	70	1069	1.57902E-05	17988	Ndrp1
TargetScan6.0	mmu-mir-9-5p	70	1069	1.57902E-05	20530	Slc31a2
TargetScan6.0	mmu-mir-9-5p	70	1069	1.57902E-05	20623	Snrk
TargetScan6.0	mmu-mir-9-5p	70	1069	1.57902E-05	208618	Etl4
TargetScan6.0	mmu-mir-9-5p	70	1069	1.57902E-05	20969	Sdc1
TargetScan6.0	mmu-mir-9-5p	70	1069	1.57902E-05	212531	Sh3bgrl2
TargetScan6.0	mmu-mir-9-5p	70	1069	1.57902E-05	212632	Iffo2
TargetScan6.0	mmu-mir-9-5p	70	1069	1.57902E-05	214230	Pak6
TargetScan6.0	mmu-mir-9-5p	70	1069	1.57902E-05	215819	Nhsl1
TargetScan6.0	mmu-mir-9-5p	70	1069	1.57902E-05	216551	1110067D22Rik
TargetScan6.0	mmu-mir-9-5p	70	1069	1.57902E-05	21810	Tgfb1
TargetScan6.0	mmu-mir-9-5p	70	1069	1.57902E-05	218442	Serinc5
TargetScan6.0	mmu-mir-9-5p	70	1069	1.57902E-05	22417	Wnt4
TargetScan6.0	mmu-mir-9-5p	70	1069	1.57902E-05	22779	Ikzf2
TargetScan6.0	mmu-mir-9-5p	70	1069	1.57902E-05	229658	Vangl1

TargetScan6.0	mmu-mir-9-5p	70	1069	1.57902E-05	230257	Rod1
TargetScan6.0	mmu-mir-9-5p	70	1069	1.57902E-05	231070	Insig1
TargetScan6.0	mmu-mir-9-5p	70	1069	1.57902E-05	231207	Cpeb2
TargetScan6.0	mmu-mir-9-5p	70	1069	1.57902E-05	233011	Itpkc
TargetScan6.0	mmu-mir-9-5p	70	1069	1.57902E-05	238988	Erc2
TargetScan6.0	mmu-mir-9-5p	70	1069	1.57902E-05	244049	Mctp2
TargetScan6.0	mmu-mir-9-5p	70	1069	1.57902E-05	26569	Slc27a4
TargetScan6.0	mmu-mir-9-5p	70	1069	1.57902E-05	27428	Shroom3
TargetScan6.0	mmu-mir-9-5p	70	1069	1.57902E-05	30945	Rnf19a
TargetScan6.0	mmu-mir-9-5p	70	1069	1.57902E-05	387524	Znrf2
TargetScan6.0	mmu-mir-9-5p	70	1069	1.57902E-05	52392	D1Ert622e
TargetScan6.0	mmu-mir-9-5p	70	1069	1.57902E-05	53883	Celsr2
TargetScan6.0	mmu-mir-9-5p	70	1069	1.57902E-05	64297	Gprc5b
TargetScan6.0	mmu-mir-9-5p	70	1069	1.57902E-05	66044	Dtd1
TargetScan6.0	mmu-mir-9-5p	70	1069	1.57902E-05	66540	Fam107b

TargetScan6.0	mmu-mir-9-5p	70	1069	1.57902E-05	668225	Figl12
TargetScan6.0	mmu-mir-9-5p	70	1069	1.57902E-05	67486	Polr3g
TargetScan6.0	mmu-mir-9-5p	70	1069	1.57902E-05	69354	Slc38a4
TargetScan6.0	mmu-mir-9-5p	70	1069	1.57902E-05	69386	Hist1h4h
TargetScan6.0	mmu-mir-9-5p	70	1069	1.57902E-05	70584	Pak4
TargetScan6.0	mmu-mir-9-5p	70	1069	1.57902E-05	71436	Flrt3
TargetScan6.0	mmu-mir-9-5p	70	1069	1.57902E-05	71720	Osbp13
TargetScan6.0	mmu-mir-9-5p	70	1069	1.57902E-05	71885	2310003H01Rik
TargetScan6.0	mmu-mir-9-5p	70	1069	1.57902E-05	72504	Taf4b
TargetScan6.0	mmu-mir-9-5p	70	1069	1.57902E-05	72549	Reep4
TargetScan6.0	mmu-mir-9-5p	70	1069	1.57902E-05	73102	Slc22a23
TargetScan6.0	mmu-mir-9-5p	70	1069	1.57902E-05	73469	Rnf38
TargetScan6.0	mmu-mir-9-5p	70	1069	1.57902E-05	75599	Pcdh1
TargetScan6.0	mmu-mir-9-5p	70	1069	1.57902E-05	78255	Ralgps2
TargetScan6.0	mmu-mir-9-5p	70	1069	1.57902E-05	83603	Elovl4

TargetScan6.0	mmu-mir-9-5p	70	1069	1.57902E-05	83796	Smarcd2
TargetScan6.0	mmu-mir-9-5p	70	1069	1.57902E-05	98878	Ehd4
TargetScan6.0	mmu-mir-199a-5p	32	369	2.22547E-05	103710	Slc35e4
TargetScan6.0	mmu-mir-199a-5p	32	369	2.22547E-05	108100	Baiap2
TargetScan6.0	mmu-mir-199a-5p	32	369	2.22547E-05	108902	B3gnt1
TargetScan6.0	mmu-mir-199a-5p	32	369	2.22547E-05	12305	Ddr1
TargetScan6.0	mmu-mir-199a-5p	32	369	2.22547E-05	12389	Cav1
TargetScan6.0	mmu-mir-199a-5p	32	369	2.22547E-05	14368	Fzd6
TargetScan6.0	mmu-mir-199a-5p	32	369	2.22547E-05	16477	Junb
TargetScan6.0	mmu-mir-199a-5p	32	369	2.22547E-05	211945	Plekhh1
TargetScan6.0	mmu-mir-199a-5p	32	369	2.22547E-05	22422	Wnt7b
TargetScan6.0	mmu-mir-199a-5p	32	369	2.22547E-05	226250	Afap1l2
TargetScan6.0	mmu-mir-199a-5p	32	369	2.22547E-05	230857	Ece1
TargetScan6.0	mmu-mir-199a-5p	32	369	2.22547E-05	232431	Gprc5a
TargetScan6.0	mmu-mir-199a-5p	32	369	2.22547E-05	26403	Map3k11

TargetScan6.0	mmu-mir-199a-5p	32	369	2.22547E-05	28075	Pppde2
TargetScan6.0	mmu-mir-199a-5p	32	369	2.22547E-05	50767	Pnpla6
TargetScan6.0	mmu-mir-199a-5p	32	369	2.22547E-05	50799	Slc25a13
TargetScan6.0	mmu-mir-199a-5p	32	369	2.22547E-05	50932	Mink1
TargetScan6.0	mmu-mir-199a-5p	32	369	2.22547E-05	54324	Arhgef5
TargetScan6.0	mmu-mir-199a-5p	32	369	2.22547E-05	54648	Ccdc120
TargetScan6.0	mmu-mir-199a-5p	32	369	2.22547E-05	56430	Clip1
TargetScan6.0	mmu-mir-199a-5p	32	369	2.22547E-05	56496	Tspan6
TargetScan6.0	mmu-mir-199a-5p	32	369	2.22547E-05	57278	Bcam
TargetScan6.0	mmu-mir-199a-5p	32	369	2.22547E-05	58235	Pvrl1
TargetScan6.0	mmu-mir-199a-5p	32	369	2.22547E-05	66540	Fam107b
TargetScan6.0	mmu-mir-199a-5p	32	369	2.22547E-05	66960	Fam188a
TargetScan6.0	mmu-mir-199a-5p	32	369	2.22547E-05	69727	Usp46
TargetScan6.0	mmu-mir-199a-5p	32	369	2.22547E-05	70178	Fam108c
TargetScan6.0	mmu-mir-199a-5p	32	369	2.22547E-05	70584	Pak4

TargetScan6.0	mmu-mir-199a-5p	32	369	2.22547E-05	71085	Arhgap19
TargetScan6.0	mmu-mir-199a-5p	32	369	2.22547E-05	71436	Flrt3
TargetScan6.0	mmu-mir-199a-5p	32	369	2.22547E-05	73469	Rnf38
TargetScan6.0	mmu-mir-199a-5p	32	369	2.22547E-05	77053	Sun1
TargetScan6.0	mmu-mir-145-5p	39	528	0.00010874	105445	Dock9
TargetScan6.0	mmu-mir-145-5p	39	528	0.00010874	110075	Bmp3
TargetScan6.0	mmu-mir-145-5p	39	528	0.00010874	12224	Klf5
TargetScan6.0	mmu-mir-145-5p	39	528	0.00010874	12388	Ctnnd1
TargetScan6.0	mmu-mir-145-5p	39	528	0.00010874	13512	Dsg3
TargetScan6.0	mmu-mir-145-5p	39	528	0.00010874	13638	Efna3
TargetScan6.0	mmu-mir-145-5p	39	528	0.00010874	14012	Mpzl2
TargetScan6.0	mmu-mir-145-5p	39	528	0.00010874	15402	Hoxa5
TargetScan6.0	mmu-mir-145-5p	39	528	0.00010874	16564	Kif21a
TargetScan6.0	mmu-mir-145-5p	39	528	0.00010874	17240	Mdfi
TargetScan6.0	mmu-mir-145-5p	39	528	0.00010874	18003	Nedd9

TargetScan6.0	mmu-mir-145-5p	39	528	0.00010874	18569	Pdcd4
TargetScan6.0	mmu-mir-145-5p	39	528	0.00010874	20166	Rtkn
TargetScan6.0	mmu-mir-145-5p	39	528	0.00010874	20682	Sox9
TargetScan6.0	mmu-mir-145-5p	39	528	0.00010874	211945	Plekhh1
TargetScan6.0	mmu-mir-145-5p	39	528	0.00010874	218215	Rnf144b
TargetScan6.0	mmu-mir-145-5p	39	528	0.00010874	218442	Serinc5
TargetScan6.0	mmu-mir-145-5p	39	528	0.00010874	226352	Epb4.115
TargetScan6.0	mmu-mir-145-5p	39	528	0.00010874	22779	Ikzf2
TargetScan6.0	mmu-mir-145-5p	39	528	0.00010874	230857	Ece1
TargetScan6.0	mmu-mir-145-5p	39	528	0.00010874	231070	Insig1
TargetScan6.0	mmu-mir-145-5p	39	528	0.00010874	26403	Map3k11
TargetScan6.0	mmu-mir-145-5p	39	528	0.00010874	26921	Map4k4
TargetScan6.0	mmu-mir-145-5p	39	528	0.00010874	27360	Add3
TargetScan6.0	mmu-mir-145-5p	39	528	0.00010874	382236	Brwd3
TargetScan6.0	mmu-mir-145-5p	39	528	0.00010874	53892	Ppm1d

TargetScan6.0	mmu-mir-145-5p	39	528	0.00010874	54648	Ccdc120
TargetScan6.0	mmu-mir-145-5p	39	528	0.00010874	56349	Net1
TargetScan6.0	mmu-mir-145-5p	39	528	0.00010874	56430	Clip1
TargetScan6.0	mmu-mir-145-5p	39	528	0.00010874	56496	Tspan6
TargetScan6.0	mmu-mir-145-5p	39	528	0.00010874	58235	Pvrl1
TargetScan6.0	mmu-mir-145-5p	39	528	0.00010874	66540	Fam107b
TargetScan6.0	mmu-mir-145-5p	39	528	0.00010874	69727	Usp46
TargetScan6.0	mmu-mir-145-5p	39	528	0.00010874	69743	Casz1
TargetScan6.0	mmu-mir-145-5p	39	528	0.00010874	70178	Fam108c
TargetScan6.0	mmu-mir-145-5p	39	528	0.00010874	70584	Pak4
TargetScan6.0	mmu-mir-145-5p	39	528	0.00010874	71889	Epn3
TargetScan6.0	mmu-mir-145-5p	39	528	0.00010874	75678	Ippk
TargetScan6.0	mmu-mir-145-5p	39	528	0.00010874	77053	Sun1
TargetScan6.0	mmu-mir-100-5p	6	46	0.008425052	15394	Hoxa1
TargetScan6.0	mmu-mir-100-5p	6	46	0.008425052	16969	Zbtb7a

TargetScan6.0	mmu-mir-100-5p	6	46	0.008425052	211770	Trib1
TargetScan6.0	mmu-mir-100-5p	6	46	0.008425052	232174	Cyp26b1
TargetScan6.0	mmu-mir-100-5p	6	46	0.008425052	69274	Ctdspl
TargetScan6.0	mmu-mir-100-5p	6	46	0.008425052	76787	Ppfia3

Appendix 4 : mouse down-regulated miRNA and their gene targets from mRNA-seq						
Category	Term	Count in Selected Genes	Count in Total Population	P-value	Gene	750 up-regulated genes
TargetScan6.0	mmu-mir-200b-5p	106	868	1.33959E-23	100515	Zfp518b
TargetScan6.0	mmu-mir-200b-5p	106	868	1.33959E-23	100710	Pds5b
TargetScan6.0	mmu-mir-200b-5p	106	868	1.33959E-23	104156	Etv5
TargetScan6.0	mmu-mir-200b-5p	106	868	1.33959E-23	108012	Ap1s2
TargetScan6.0	mmu-mir-200b-5p	106	868	1.33959E-23	108154	Adamts6
TargetScan6.0	mmu-mir-200b-5p	106	868	1.33959E-23	108797	Mex3b
TargetScan6.0	mmu-mir-200b-5p	106	868	1.33959E-23	108899	2700081O15Rik
TargetScan6.0	mmu-mir-200b-5p	106	868	1.33959E-23	108927	Lhfp
TargetScan6.0	mmu-mir-200b-5p	106	868	1.33959E-23	114715	Spred1
TargetScan6.0	mmu-mir-200b-5p	106	868	1.33959E-23	11641	Akap2
TargetScan6.0	mmu-mir-200b-5p	106	868	1.33959E-23	12151	Bmi1

TargetScan6.0	mmu-mir-200b-5p	106	868	1.33959E-23	12321	Calu
TargetScan6.0	mmu-mir-200b-5p	106	868	1.33959E-23	12361	Cask
TargetScan6.0	mmu-mir-200b-5p	106	868	1.33959E-23	13527	Dtna
TargetScan6.0	mmu-mir-200b-5p	106	868	1.33959E-23	13557	E2f3
TargetScan6.0	mmu-mir-200b-5p	106	868	1.33959E-23	14020	Evi5
TargetScan6.0	mmu-mir-200b-5p	106	868	1.33959E-23	14247	Fli1
TargetScan6.0	mmu-mir-200b-5p	106	868	1.33959E-23	14254	Flt1
TargetScan6.0	mmu-mir-200b-5p	106	868	1.33959E-23	14299	Ncs1
TargetScan6.0	mmu-mir-200b-5p	106	868	1.33959E-23	14360	Fyn
TargetScan6.0	mmu-mir-200b-5p	106	868	1.33959E-23	14461	Gata2
TargetScan6.0	mmu-mir-200b-5p	106	868	1.33959E-23	14745	Lpar1
TargetScan6.0	mmu-mir-200b-5p	106	868	1.33959E-23	15227	Foxf1a
TargetScan6.0	mmu-mir-200b-5p	106	868	1.33959E-23	15228	Foxg1
TargetScan6.0	mmu-mir-200b-5p	106	868	1.33959E-23	15476	Hs3st1
TargetScan6.0	mmu-mir-200b-5p	106	868	1.33959E-23	15526	Hspa9

TargetScan6.0	mmu-mir-200b-5p	106	868	1.33959E-23	16543	Mdfic
TargetScan6.0	mmu-mir-200b-5p	106	868	1.33959E-23	16565	Kif21b
TargetScan6.0	mmu-mir-200b-5p	106	868	1.33959E-23	16597	Klf12
TargetScan6.0	mmu-mir-200b-5p	106	868	1.33959E-23	16764	Aff3
TargetScan6.0	mmu-mir-200b-5p	106	868	1.33959E-23	16911	Lmo4
TargetScan6.0	mmu-mir-200b-5p	106	868	1.33959E-23	16971	Lrp1
TargetScan6.0	mmu-mir-200b-5p	106	868	1.33959E-23	170719	Oxr1
TargetScan6.0	mmu-mir-200b-5p	106	868	1.33959E-23	17698	Msn
TargetScan6.0	mmu-mir-200b-5p	106	868	1.33959E-23	17984	Ndn
TargetScan6.0	mmu-mir-200b-5p	106	868	1.33959E-23	18007	Neo1
TargetScan6.0	mmu-mir-200b-5p	106	868	1.33959E-23	18080	Nin
TargetScan6.0	mmu-mir-200b-5p	106	868	1.33959E-23	18383	Tnfrsf11b
TargetScan6.0	mmu-mir-200b-5p	106	868	1.33959E-23	19009	Pou6f1
TargetScan6.0	mmu-mir-200b-5p	106	868	1.33959E-23	19248	Ptpn12
TargetScan6.0	mmu-mir-200b-5p	106	868	1.33959E-23	193813	Mcf2

TargetScan6.0	mmu-mir-200b-5p	106	868	1.33959E-23	20112	Rps6ka2
TargetScan6.0	mmu-mir-200b-5p	106	868	1.33959E-23	20444	St3gal2
TargetScan6.0	mmu-mir-200b-5p	106	868	1.33959E-23	20471	Six1
TargetScan6.0	mmu-mir-200b-5p	106	868	1.33959E-23	20868	Stk10
TargetScan6.0	mmu-mir-200b-5p	106	868	1.33959E-23	208691	Eif5a2
TargetScan6.0	mmu-mir-200b-5p	106	868	1.33959E-23	209131	Snx30
TargetScan6.0	mmu-mir-200b-5p	106	868	1.33959E-23	209630	Frmd4a
TargetScan6.0	mmu-mir-200b-5p	106	868	1.33959E-23	21413	Tcf4
TargetScan6.0	mmu-mir-200b-5p	106	868	1.33959E-23	21417	Zeb1
TargetScan6.0	mmu-mir-200b-5p	106	868	1.33959E-23	215280	Wipf1
TargetScan6.0	mmu-mir-200b-5p	106	868	1.33959E-23	21676	Tead1
TargetScan6.0	mmu-mir-200b-5p	106	868	1.33959E-23	21807	Tsc22d1
TargetScan6.0	mmu-mir-200b-5p	106	868	1.33959E-23	22196	Ube2i
TargetScan6.0	mmu-mir-200b-5p	106	868	1.33959E-23	22339	Vegfa
TargetScan6.0	mmu-mir-200b-5p	106	868	1.33959E-23	225020	Fez2

TargetScan6.0	mmu-mir-200b-5p	106	868	1.33959E-23	226144	Erlin1
TargetScan6.0	mmu-mir-200b-5p	106	868	1.33959E-23	226178	D19Wsu162e
TargetScan6.0	mmu-mir-200b-5p	106	868	1.33959E-23	226841	Vash2
TargetScan6.0	mmu-mir-200b-5p	106	868	1.33959E-23	229706	Slc6a17
TargetScan6.0	mmu-mir-200b-5p	106	868	1.33959E-23	231380	Uba6
TargetScan6.0	mmu-mir-200b-5p	106	868	1.33959E-23	231912	Katnal1
TargetScan6.0	mmu-mir-200b-5p	106	868	1.33959E-23	234875	Ttc13
TargetScan6.0	mmu-mir-200b-5p	106	868	1.33959E-23	238130	Dock4
TargetScan6.0	mmu-mir-200b-5p	106	868	1.33959E-23	23821	Bace1
TargetScan6.0	mmu-mir-200b-5p	106	868	1.33959E-23	23893	Grem2
TargetScan6.0	mmu-mir-200b-5p	106	868	1.33959E-23	23908	Hs2st1
TargetScan6.0	mmu-mir-200b-5p	106	868	1.33959E-23	24136	Zeb2
TargetScan6.0	mmu-mir-200b-5p	106	868	1.33959E-23	242481	Palm2
TargetScan6.0	mmu-mir-200b-5p	106	868	1.33959E-23	242509	Bnc2
TargetScan6.0	mmu-mir-200b-5p	106	868	1.33959E-23	244895	C230081A13Rik

TargetScan6.0	mmu-mir-200b-5p	106	868	1.33959E-23	26564	Ror2
TargetScan6.0	mmu-mir-200b-5p	106	868	1.33959E-23	269713	Clip2
TargetScan6.0	mmu-mir-200b-5p	106	868	1.33959E-23	279653	Pcdh19
TargetScan6.0	mmu-mir-200b-5p	106	868	1.33959E-23	330627	Trim66
TargetScan6.0	mmu-mir-200b-5p	106	868	1.33959E-23	381560	Xkr8
TargetScan6.0	mmu-mir-200b-5p	106	868	1.33959E-23	382252	A830080D01Rik
TargetScan6.0	mmu-mir-200b-5p	106	868	1.33959E-23	50768	Dlc1
TargetScan6.0	mmu-mir-200b-5p	106	868	1.33959E-23	53614	Reck
TargetScan6.0	mmu-mir-200b-5p	106	868	1.33959E-23	53619	Blcap
TargetScan6.0	mmu-mir-200b-5p	106	868	1.33959E-23	54371	Chst2
TargetScan6.0	mmu-mir-200b-5p	106	868	1.33959E-23	56323	Dnajb5
TargetScan6.0	mmu-mir-200b-5p	106	868	1.33959E-23	56442	Serinc1
TargetScan6.0	mmu-mir-200b-5p	106	868	1.33959E-23	56542	Ick
TargetScan6.0	mmu-mir-200b-5p	106	868	1.33959E-23	56693	Crtap
TargetScan6.0	mmu-mir-200b-5p	106	868	1.33959E-23	56807	Scamp5

TargetScan6.0	mmu-mir-200b-5p	106	868	1.33959E-23	59036	Dact1
TargetScan6.0	mmu-mir-200b-5p	106	868	1.33959E-23	67468	Mmd
TargetScan6.0	mmu-mir-200b-5p	106	868	1.33959E-23	67916	Ppap2b
TargetScan6.0	mmu-mir-200b-5p	106	868	1.33959E-23	68178	Cgnl1
TargetScan6.0	mmu-mir-200b-5p	106	868	1.33959E-23	68337	Crip2
TargetScan6.0	mmu-mir-200b-5p	106	868	1.33959E-23	68606	Ppm1f
TargetScan6.0	mmu-mir-200b-5p	106	868	1.33959E-23	70097	Sash1
TargetScan6.0	mmu-mir-200b-5p	106	868	1.33959E-23	70533	Btf3l4
TargetScan6.0	mmu-mir-200b-5p	106	868	1.33959E-23	70549	Tln2
TargetScan6.0	mmu-mir-200b-5p	106	868	1.33959E-23	71323	Rassf8
TargetScan6.0	mmu-mir-200b-5p	106	868	1.33959E-23	71532	9030418K01Rik
TargetScan6.0	mmu-mir-200b-5p	106	868	1.33959E-23	71709	Syde1
TargetScan6.0	mmu-mir-200b-5p	106	868	1.33959E-23	71918	Zcchc24
TargetScan6.0	mmu-mir-200b-5p	106	868	1.33959E-23	72033	Tsc22d2
TargetScan6.0	mmu-mir-200b-5p	106	868	1.33959E-23	72611	Zfp655

TargetScan6.0	mmu-mir-200b-5p	106	868	1.33959E-23	72640	Mex3a
TargetScan6.0	mmu-mir-200b-5p	106	868	1.33959E-23	75717	Cul5
TargetScan6.0	mmu-mir-200b-5p	106	868	1.33959E-23	80892	Zfhx4
TargetScan6.0	mmu-mir-200b-5p	106	868	1.33959E-23	83767	Wasf1
TargetScan6.0	mmu-mir-200b-5p	106	868	1.33959E-23	83814	Nedd4l
TargetScan6.0	mmu-mir-141-5p	62	592	2.46229E-11	114249	Npnt
TargetScan6.0	mmu-mir-141-5p	62	592	2.46229E-11	11641	Akap2
TargetScan6.0	mmu-mir-141-5p	62	592	2.46229E-11	117160	Ttyh2
TargetScan6.0	mmu-mir-141-5p	62	592	2.46229E-11	12167	Bmpr1b
TargetScan6.0	mmu-mir-141-5p	62	592	2.46229E-11	12321	Calu
TargetScan6.0	mmu-mir-141-5p	62	592	2.46229E-11	12406	Serpinh1
TargetScan6.0	mmu-mir-141-5p	62	592	2.46229E-11	13401	Dmwd
TargetScan6.0	mmu-mir-141-5p	62	592	2.46229E-11	13557	E2f3
TargetScan6.0	mmu-mir-141-5p	62	592	2.46229E-11	13852	Stx2
TargetScan6.0	mmu-mir-141-5p	62	592	2.46229E-11	14465	Gata6

TargetScan6.0	mmu-mir-141-5p	62	592	2.46229E-11	14489	Mtpn
TargetScan6.0	mmu-mir-141-5p	62	592	2.46229E-11	14758	Gpm6b
TargetScan6.0	mmu-mir-141-5p	62	592	2.46229E-11	16565	Kif21b
TargetScan6.0	mmu-mir-141-5p	62	592	2.46229E-11	16597	Klf12
TargetScan6.0	mmu-mir-141-5p	62	592	2.46229E-11	17076	Ly75
TargetScan6.0	mmu-mir-141-5p	62	592	2.46229E-11	17967	Ncam1
TargetScan6.0	mmu-mir-141-5p	62	592	2.46229E-11	18208	Ntn1
TargetScan6.0	mmu-mir-141-5p	62	592	2.46229E-11	18491	Pappa
TargetScan6.0	mmu-mir-141-5p	62	592	2.46229E-11	19270	Ptprg
TargetScan6.0	mmu-mir-141-5p	62	592	2.46229E-11	20315	Cxcl12
TargetScan6.0	mmu-mir-141-5p	62	592	2.46229E-11	20358	Sema6a
TargetScan6.0	mmu-mir-141-5p	62	592	2.46229E-11	20441	St3gal3
TargetScan6.0	mmu-mir-141-5p	62	592	2.46229E-11	20471	Six1
TargetScan6.0	mmu-mir-141-5p	62	592	2.46229E-11	209630	Frmd4a
TargetScan6.0	mmu-mir-141-5p	62	592	2.46229E-11	211712	Pcdh9

TargetScan6.0	mmu-mir-141-5p	62	592	2.46229E-11	21413	Tcf4
TargetScan6.0	mmu-mir-141-5p	62	592	2.46229E-11	21417	Zeb1
TargetScan6.0	mmu-mir-141-5p	62	592	2.46229E-11	215280	Wipf1
TargetScan6.0	mmu-mir-141-5p	62	592	2.46229E-11	217869	Eif5
TargetScan6.0	mmu-mir-141-5p	62	592	2.46229E-11	229706	Slc6a17
TargetScan6.0	mmu-mir-141-5p	62	592	2.46229E-11	231380	Uba6
TargetScan6.0	mmu-mir-141-5p	62	592	2.46229E-11	235184	BC024479
TargetScan6.0	mmu-mir-141-5p	62	592	2.46229E-11	238130	Dock4
TargetScan6.0	mmu-mir-141-5p	62	592	2.46229E-11	23821	Bace1
TargetScan6.0	mmu-mir-141-5p	62	592	2.46229E-11	23908	Hs2st1
TargetScan6.0	mmu-mir-141-5p	62	592	2.46229E-11	24066	Spry4
TargetScan6.0	mmu-mir-141-5p	62	592	2.46229E-11	24136	Zeb2
TargetScan6.0	mmu-mir-141-5p	62	592	2.46229E-11	242509	Bnc2
TargetScan6.0	mmu-mir-141-5p	62	592	2.46229E-11	243931	Tshz3
TargetScan6.0	mmu-mir-141-5p	62	592	2.46229E-11	244668	Sipa1l2

TargetScan6.0	mmu-mir-141-5p	62	592	2.46229E-11	244895	C230081A13Rik
TargetScan6.0	mmu-mir-141-5p	62	592	2.46229E-11	270669	Mbtps2
TargetScan6.0	mmu-mir-141-5p	62	592	2.46229E-11	279653	Pcdh19
TargetScan6.0	mmu-mir-141-5p	62	592	2.46229E-11	319622	Itpripl2
TargetScan6.0	mmu-mir-141-5p	62	592	2.46229E-11	319939	Tns3
TargetScan6.0	mmu-mir-141-5p	62	592	2.46229E-11	319996	Casc4
TargetScan6.0	mmu-mir-141-5p	62	592	2.46229E-11	320827	C530008M17Rik
TargetScan6.0	mmu-mir-141-5p	62	592	2.46229E-11	329165	Abi2
TargetScan6.0	mmu-mir-141-5p	62	592	2.46229E-11	50768	Dlc1
TargetScan6.0	mmu-mir-141-5p	62	592	2.46229E-11	56741	Igdcc4
TargetScan6.0	mmu-mir-141-5p	62	592	2.46229E-11	629378	Dact3
TargetScan6.0	mmu-mir-141-5p	62	592	2.46229E-11	66573	Dzip1
TargetScan6.0	mmu-mir-141-5p	62	592	2.46229E-11	71918	Zcchc24
TargetScan6.0	mmu-mir-141-5p	62	592	2.46229E-11	72349	Dusp3
TargetScan6.0	mmu-mir-141-5p	62	592	2.46229E-11	72701	Zfp618

TargetScan6.0	mmu-mir-141-5p	62	592	2.46229E-11	74051	Steap2
TargetScan6.0	mmu-mir-141-5p	62	592	2.46229E-11	77579	Myh10
TargetScan6.0	mmu-mir-141-5p	62	592	2.46229E-11	78100	8430410K20Rik
TargetScan6.0	mmu-mir-141-5p	62	592	2.46229E-11	78428	Wibg
TargetScan6.0	mmu-mir-141-5p	62	592	2.46229E-11	83964	Jam3
TargetScan6.0	mmu-mir-141-5p	62	592	2.46229E-11	93759	Sirt1
TargetScan6.0	mmu-mir-141-5p	62	592	2.46229E-11	93834	Peli2
TargetScan6.0	mmu-mir-200a-5p	62	592	2.46229E-11	114249	Npnt
TargetScan6.0	mmu-mir-200a-5p	62	592	2.46229E-11	11641	Akap2
TargetScan6.0	mmu-mir-200a-5p	62	592	2.46229E-11	117160	Ttyh2
TargetScan6.0	mmu-mir-200a-5p	62	592	2.46229E-11	12167	Bmpr1b
TargetScan6.0	mmu-mir-200a-5p	62	592	2.46229E-11	12321	Calu
TargetScan6.0	mmu-mir-200a-5p	62	592	2.46229E-11	12406	Serpinh1
TargetScan6.0	mmu-mir-200a-5p	62	592	2.46229E-11	13401	Dmwd
TargetScan6.0	mmu-mir-200a-5p	62	592	2.46229E-11	13557	E2f3

TargetScan6.0	mmu-mir-200a-5p	62	592	2.46229E-11	13852	Stx2
TargetScan6.0	mmu-mir-200a-5p	62	592	2.46229E-11	14465	Gata6
TargetScan6.0	mmu-mir-200a-5p	62	592	2.46229E-11	14489	Mtpn
TargetScan6.0	mmu-mir-200a-5p	62	592	2.46229E-11	14758	Gpm6b
TargetScan6.0	mmu-mir-200a-5p	62	592	2.46229E-11	16565	Kif21b
TargetScan6.0	mmu-mir-200a-5p	62	592	2.46229E-11	16597	Klf12
TargetScan6.0	mmu-mir-200a-5p	62	592	2.46229E-11	17076	Ly75
TargetScan6.0	mmu-mir-200a-5p	62	592	2.46229E-11	17967	Ncam1
TargetScan6.0	mmu-mir-200a-5p	62	592	2.46229E-11	18208	Ntn1
TargetScan6.0	mmu-mir-200a-5p	62	592	2.46229E-11	18491	Pappa
TargetScan6.0	mmu-mir-200a-5p	62	592	2.46229E-11	19270	Ptprg
TargetScan6.0	mmu-mir-200a-5p	62	592	2.46229E-11	20315	Cxcl12
TargetScan6.0	mmu-mir-200a-5p	62	592	2.46229E-11	20358	Sema6a
TargetScan6.0	mmu-mir-200a-5p	62	592	2.46229E-11	20441	St3gal3
TargetScan6.0	mmu-mir-200a-5p	62	592	2.46229E-11	20471	Six1

TargetScan6.0	mmu-mir-200a-5p	62	592	2.46229E-11	209630	Frmd4a
TargetScan6.0	mmu-mir-200a-5p	62	592	2.46229E-11	211712	Pcdh9
TargetScan6.0	mmu-mir-200a-5p	62	592	2.46229E-11	21413	Tcf4
TargetScan6.0	mmu-mir-200a-5p	62	592	2.46229E-11	21417	Zeb1
TargetScan6.0	mmu-mir-200a-5p	62	592	2.46229E-11	215280	Wipf1
TargetScan6.0	mmu-mir-200a-5p	62	592	2.46229E-11	217869	Eif5
TargetScan6.0	mmu-mir-200a-5p	62	592	2.46229E-11	229706	Slc6a17
TargetScan6.0	mmu-mir-200a-5p	62	592	2.46229E-11	231380	Uba6
TargetScan6.0	mmu-mir-200a-5p	62	592	2.46229E-11	235184	BC024479
TargetScan6.0	mmu-mir-200a-5p	62	592	2.46229E-11	238130	Dock4
TargetScan6.0	mmu-mir-200a-5p	62	592	2.46229E-11	23821	Bace1
TargetScan6.0	mmu-mir-200a-5p	62	592	2.46229E-11	23908	Hs2st1
TargetScan6.0	mmu-mir-200a-5p	62	592	2.46229E-11	24066	Spry4
TargetScan6.0	mmu-mir-200a-5p	62	592	2.46229E-11	24136	Zeb2
TargetScan6.0	mmu-mir-200a-5p	62	592	2.46229E-11	242509	Bnc2

TargetScan6.0	mmu-mir-200a-5p	62	592	2.46229E-11	243931	Tshz3
TargetScan6.0	mmu-mir-200a-5p	62	592	2.46229E-11	244668	Sipa1l2
TargetScan6.0	mmu-mir-200a-5p	62	592	2.46229E-11	244895	C230081A13Rik
TargetScan6.0	mmu-mir-200a-5p	62	592	2.46229E-11	270669	Mbtps2
TargetScan6.0	mmu-mir-200a-5p	62	592	2.46229E-11	279653	Pcdh19
TargetScan6.0	mmu-mir-200a-5p	62	592	2.46229E-11	319622	Itpril2
TargetScan6.0	mmu-mir-200a-5p	62	592	2.46229E-11	319939	Tns3
TargetScan6.0	mmu-mir-200a-5p	62	592	2.46229E-11	319996	Casc4
TargetScan6.0	mmu-mir-200a-5p	62	592	2.46229E-11	320827	C530008M17Rik
TargetScan6.0	mmu-mir-200a-5p	62	592	2.46229E-11	329165	Abi2
TargetScan6.0	mmu-mir-200a-5p	62	592	2.46229E-11	50768	Dlc1
TargetScan6.0	mmu-mir-200a-5p	62	592	2.46229E-11	56741	Igdcc4
TargetScan6.0	mmu-mir-200a-5p	62	592	2.46229E-11	629378	Dact3
TargetScan6.0	mmu-mir-200a-5p	62	592	2.46229E-11	66573	Dzip1
TargetScan6.0	mmu-mir-200a-5p	62	592	2.46229E-11	71918	Zcchc24

TargetScan6.0	mmu-mir-200a-5p	62	592	2.46229E-11	72349	Dusp3
TargetScan6.0	mmu-mir-200a-5p	62	592	2.46229E-11	72701	Zfp618
TargetScan6.0	mmu-mir-200a-5p	62	592	2.46229E-11	74051	Steap2
TargetScan6.0	mmu-mir-200a-5p	62	592	2.46229E-11	77579	Myh10
TargetScan6.0	mmu-mir-200a-5p	62	592	2.46229E-11	78100	8430410K20Rik
TargetScan6.0	mmu-mir-200a-5p	62	592	2.46229E-11	78428	Wibg
TargetScan6.0	mmu-mir-200a-5p	62	592	2.46229E-11	83964	Jam3
TargetScan6.0	mmu-mir-200a-5p	62	592	2.46229E-11	93759	Sirt1
TargetScan6.0	mmu-mir-200a-5p	62	592	2.46229E-11	93834	Peli2
TargetScan6.0	mmu-mir-183-5p	43	332	3.9476E-11	114715	Spred1
TargetScan6.0	mmu-mir-183-5p	43	332	3.9476E-11	11852	Rhob
TargetScan6.0	mmu-mir-183-5p	43	332	3.9476E-11	12151	Bmi1
TargetScan6.0	mmu-mir-183-5p	43	332	3.9476E-11	12877	Cpeb1
TargetScan6.0	mmu-mir-183-5p	43	332	3.9476E-11	13527	Dtna
TargetScan6.0	mmu-mir-183-5p	43	332	3.9476E-11	14299	Ncs1

TargetScan6.0	mmu-mir-183-5p	43	332	3.9476E-11	15476	Hs3st1
TargetScan6.0	mmu-mir-183-5p	43	332	3.9476E-11	16563	Kif2a
TargetScan6.0	mmu-mir-183-5p	43	332	3.9476E-11	17912	Myo1b
TargetScan6.0	mmu-mir-183-5p	43	332	3.9476E-11	18227	Nr4a2
TargetScan6.0	mmu-mir-183-5p	43	332	3.9476E-11	19099	Mapk8ip1
TargetScan6.0	mmu-mir-183-5p	43	332	3.9476E-11	19165	Psen2
TargetScan6.0	mmu-mir-183-5p	43	332	3.9476E-11	20429	Shox2
TargetScan6.0	mmu-mir-183-5p	43	332	3.9476E-11	20742	Spnb2
TargetScan6.0	mmu-mir-183-5p	43	332	3.9476E-11	21413	Tcf4
TargetScan6.0	mmu-mir-183-5p	43	332	3.9476E-11	21417	Zeb1
TargetScan6.0	mmu-mir-183-5p	43	332	3.9476E-11	217340	Rnf157
TargetScan6.0	mmu-mir-183-5p	43	332	3.9476E-11	223527	Eny2
TargetScan6.0	mmu-mir-183-5p	43	332	3.9476E-11	233489	Picalm
TargetScan6.0	mmu-mir-183-5p	43	332	3.9476E-11	238871	Pde4d
TargetScan6.0	mmu-mir-183-5p	43	332	3.9476E-11	23893	Grem2

TargetScan6.0	mmu-mir-183-5p	43	332	3.9476E-11	24060	Slc35a1
TargetScan6.0	mmu-mir-183-5p	43	332	3.9476E-11	24064	Spry2
TargetScan6.0	mmu-mir-183-5p	43	332	3.9476E-11	24136	Zeb2
TargetScan6.0	mmu-mir-183-5p	43	332	3.9476E-11	242481	Palm2
TargetScan6.0	mmu-mir-183-5p	43	332	3.9476E-11	242509	Bnc2
TargetScan6.0	mmu-mir-183-5p	43	332	3.9476E-11	26611	Rcn2
TargetScan6.0	mmu-mir-183-5p	43	332	3.9476E-11	330267	Thsd7a
TargetScan6.0	mmu-mir-183-5p	43	332	3.9476E-11	382034	Gse1
TargetScan6.0	mmu-mir-183-5p	43	332	3.9476E-11	52592	Brms1l
TargetScan6.0	mmu-mir-183-5p	43	332	3.9476E-11	56542	Ick
TargetScan6.0	mmu-mir-183-5p	43	332	3.9476E-11	59046	Arpp19
TargetScan6.0	mmu-mir-183-5p	43	332	3.9476E-11	74480	Samd4
TargetScan6.0	mmu-mir-183-5p	43	332	3.9476E-11	93701	Pcdhgb4
TargetScan6.0	mmu-mir-183-5p	43	332	3.9476E-11	93706	Pcdhgc3
TargetScan6.0	mmu-mir-183-5p	43	332	3.9476E-11	93707	Pcdhgc4

TargetScan6.0	mmu-mir-183-5p	43	332	3.9476E-11	93708	Pcdhgc5
TargetScan6.0	mmu-mir-183-5p	43	332	3.9476E-11	93710	Pcdhga2
TargetScan6.0	mmu-mir-183-5p	43	332	3.9476E-11	93711	Pcdhga3
TargetScan6.0	mmu-mir-183-5p	43	332	3.9476E-11	93716	Pcdhga8
TargetScan6.0	mmu-mir-183-5p	43	332	3.9476E-11	93717	Pcdhga9
TargetScan6.0	mmu-mir-183-5p	43	332	3.9476E-11	93723	Pcdhga11
TargetScan6.0	mmu-mir-183-5p	43	332	3.9476E-11	93724	Pcdhga12
TargetScan6.0	mmu-mir-96-5p	81	898	4.72988E-11	108116	Slco3a1
TargetScan6.0	mmu-mir-96-5p	81	898	4.72988E-11	114249	Npnt
TargetScan6.0	mmu-mir-96-5p	81	898	4.72988E-11	11492	Adam19
TargetScan6.0	mmu-mir-96-5p	81	898	4.72988E-11	12631	Cfl1
TargetScan6.0	mmu-mir-96-5p	81	898	4.72988E-11	12831	Col5a1
TargetScan6.0	mmu-mir-96-5p	81	898	4.72988E-11	12877	Cpeb1
TargetScan6.0	mmu-mir-96-5p	81	898	4.72988E-11	13591	Ebf1
TargetScan6.0	mmu-mir-96-5p	81	898	4.72988E-11	13712	Elk1

TargetScan6.0	mmu-mir-96-5p	81	898	4.72988E-11	13823	Epb4.1l3
TargetScan6.0	mmu-mir-96-5p	81	898	4.72988E-11	14020	Evi5
TargetScan6.0	mmu-mir-96-5p	81	898	4.72988E-11	14254	Flt1
TargetScan6.0	mmu-mir-96-5p	81	898	4.72988E-11	14360	Fyn
TargetScan6.0	mmu-mir-96-5p	81	898	4.72988E-11	14389	Gab2
TargetScan6.0	mmu-mir-96-5p	81	898	4.72988E-11	14432	Gap43
TargetScan6.0	mmu-mir-96-5p	81	898	4.72988E-11	14573	Gdnf
TargetScan6.0	mmu-mir-96-5p	81	898	4.72988E-11	14758	Gpm6b
TargetScan6.0	mmu-mir-96-5p	81	898	4.72988E-11	14783	Grb10
TargetScan6.0	mmu-mir-96-5p	81	898	4.72988E-11	17532	Mras
TargetScan6.0	mmu-mir-96-5p	81	898	4.72988E-11	17698	Msn
TargetScan6.0	mmu-mir-96-5p	81	898	4.72988E-11	18015	Nf1
TargetScan6.0	mmu-mir-96-5p	81	898	4.72988E-11	18196	Nsg1
TargetScan6.0	mmu-mir-96-5p	81	898	4.72988E-11	18491	Pappa
TargetScan6.0	mmu-mir-96-5p	81	898	4.72988E-11	18595	Pdgfra

TargetScan6.0	mmu-mir-96-5p	81	898	4.72988E-11	19335	Rab23
TargetScan6.0	mmu-mir-96-5p	81	898	4.72988E-11	20163	Rsu1
TargetScan6.0	mmu-mir-96-5p	81	898	4.72988E-11	20358	Sema6a
TargetScan6.0	mmu-mir-96-5p	81	898	4.72988E-11	20429	Shox2
TargetScan6.0	mmu-mir-96-5p	81	898	4.72988E-11	20441	St3gal3
TargetScan6.0	mmu-mir-96-5p	81	898	4.72988E-11	20444	St3gal2
TargetScan6.0	mmu-mir-96-5p	81	898	4.72988E-11	207806	Gm608
TargetScan6.0	mmu-mir-96-5p	81	898	4.72988E-11	209131	Snx30
TargetScan6.0	mmu-mir-96-5p	81	898	4.72988E-11	209630	Frmd4a
TargetScan6.0	mmu-mir-96-5p	81	898	4.72988E-11	213760	Prepl
TargetScan6.0	mmu-mir-96-5p	81	898	4.72988E-11	21384	Tbx15
TargetScan6.0	mmu-mir-96-5p	81	898	4.72988E-11	21413	Tcf4
TargetScan6.0	mmu-mir-96-5p	81	898	4.72988E-11	21417	Zeb1
TargetScan6.0	mmu-mir-96-5p	81	898	4.72988E-11	215280	Wipf1
TargetScan6.0	mmu-mir-96-5p	81	898	4.72988E-11	21676	Tead1

TargetScan6.0	mmu-mir-96-5p	81	898	4.72988E-11	217869	Eif5
TargetScan6.0	mmu-mir-96-5p	81	898	4.72988E-11	223254	Farp1
TargetScan6.0	mmu-mir-96-5p	81	898	4.72988E-11	223732	Ldoc1l
TargetScan6.0	mmu-mir-96-5p	81	898	4.72988E-11	226144	Erlin1
TargetScan6.0	mmu-mir-96-5p	81	898	4.72988E-11	226432	Ipo9
TargetScan6.0	mmu-mir-96-5p	81	898	4.72988E-11	228602	4930402H24Rik
TargetScan6.0	mmu-mir-96-5p	81	898	4.72988E-11	228662	Btbd3
TargetScan6.0	mmu-mir-96-5p	81	898	4.72988E-11	229517	Slc25a44
TargetScan6.0	mmu-mir-96-5p	81	898	4.72988E-11	233115	Dpy19l3
TargetScan6.0	mmu-mir-96-5p	81	898	4.72988E-11	235431	Coro2b
TargetScan6.0	mmu-mir-96-5p	81	898	4.72988E-11	237782	Smcr8
TargetScan6.0	mmu-mir-96-5p	81	898	4.72988E-11	238130	Dock4
TargetScan6.0	mmu-mir-96-5p	81	898	4.72988E-11	24056	Sh3bp5
TargetScan6.0	mmu-mir-96-5p	81	898	4.72988E-11	24060	Slc35a1
TargetScan6.0	mmu-mir-96-5p	81	898	4.72988E-11	242509	Bnc2

TargetScan6.0	mmu-mir-96-5p	81	898	4.72988E-11	26949	Vat1
TargetScan6.0	mmu-mir-96-5p	81	898	4.72988E-11	27426	Nagpa
TargetScan6.0	mmu-mir-96-5p	81	898	4.72988E-11	319939	Tns3
TargetScan6.0	mmu-mir-96-5p	81	898	4.72988E-11	320150	Zdhhc17
TargetScan6.0	mmu-mir-96-5p	81	898	4.72988E-11	320165	Tacc1
TargetScan6.0	mmu-mir-96-5p	81	898	4.72988E-11	329165	Abi2
TargetScan6.0	mmu-mir-96-5p	81	898	4.72988E-11	360213	Trim46
TargetScan6.0	mmu-mir-96-5p	81	898	4.72988E-11	53614	Reck
TargetScan6.0	mmu-mir-96-5p	81	898	4.72988E-11	546336	Prrg1
TargetScan6.0	mmu-mir-96-5p	81	898	4.72988E-11	56428	Mtch2
TargetScan6.0	mmu-mir-96-5p	81	898	4.72988E-11	58194	Sh3kbp1
TargetScan6.0	mmu-mir-96-5p	81	898	4.72988E-11	59046	Arpp19
TargetScan6.0	mmu-mir-96-5p	81	898	4.72988E-11	64540	Tspan4
TargetScan6.0	mmu-mir-96-5p	81	898	4.72988E-11	68404	Nrn1
TargetScan6.0	mmu-mir-96-5p	81	898	4.72988E-11	68606	Ppm1f

TargetScan6.0	mmu-mir-96-5p	81	898	4.72988E-11	69219	Ddah1
TargetScan6.0	mmu-mir-96-5p	81	898	4.72988E-11	70546	Zdhhc2
TargetScan6.0	mmu-mir-96-5p	81	898	4.72988E-11	70676	Gulp1
TargetScan6.0	mmu-mir-96-5p	81	898	4.72988E-11	71093	Atoh8
TargetScan6.0	mmu-mir-96-5p	81	898	4.72988E-11	71323	Rassf8
TargetScan6.0	mmu-mir-96-5p	81	898	4.72988E-11	71914	Antxr2
TargetScan6.0	mmu-mir-96-5p	81	898	4.72988E-11	72543	Fam125b
TargetScan6.0	mmu-mir-96-5p	81	898	4.72988E-11	74136	Sec14l1
TargetScan6.0	mmu-mir-96-5p	81	898	4.72988E-11	75717	Cul5
TargetScan6.0	mmu-mir-96-5p	81	898	4.72988E-11	76438	Rftn1
TargetScan6.0	mmu-mir-96-5p	81	898	4.72988E-11	78339	Ttyh3
TargetScan6.0	mmu-mir-96-5p	81	898	4.72988E-11	78619	Zfp449
TargetScan6.0	mmu-mir-96-5p	81	898	4.72988E-11	80892	Zfhx4
TargetScan6.0	mmu-mir-33-5p	39	286	6.74602E-11	106585	Ankrd12
TargetScan6.0	mmu-mir-33-5p	39	286	6.74602E-11	11551	Adra2a

TargetScan6.0	mmu-mir-33-5p	39	286	6.74602E-11	11858	Rnd2
TargetScan6.0	mmu-mir-33-5p	39	286	6.74602E-11	12321	Calu
TargetScan6.0	mmu-mir-33-5p	39	286	6.74602E-11	12395	Runx1t1
TargetScan6.0	mmu-mir-33-5p	39	286	6.74602E-11	13591	Ebf1
TargetScan6.0	mmu-mir-33-5p	39	286	6.74602E-11	13821	Epb4.1l1
TargetScan6.0	mmu-mir-33-5p	39	286	6.74602E-11	14009	Etv1
TargetScan6.0	mmu-mir-33-5p	39	286	6.74602E-11	14573	Gdnf
TargetScan6.0	mmu-mir-33-5p	39	286	6.74602E-11	16497	Kcnab1
TargetScan6.0	mmu-mir-33-5p	39	286	6.74602E-11	16764	Aff3
TargetScan6.0	mmu-mir-33-5p	39	286	6.74602E-11	16923	Sh2b3
TargetScan6.0	mmu-mir-33-5p	39	286	6.74602E-11	17076	Ly75
TargetScan6.0	mmu-mir-33-5p	39	286	6.74602E-11	18032	Nfix
TargetScan6.0	mmu-mir-33-5p	39	286	6.74602E-11	18208	Ntn1
TargetScan6.0	mmu-mir-33-5p	39	286	6.74602E-11	18595	Pdgfra
TargetScan6.0	mmu-mir-33-5p	39	286	6.74602E-11	20346	Sema3a

TargetScan6.0	mmu-mir-33-5p	39	286	6.74602E-11	20361	Sema7a
TargetScan6.0	mmu-mir-33-5p	39	286	6.74602E-11	20444	St3gal2
TargetScan6.0	mmu-mir-33-5p	39	286	6.74602E-11	209683	Ttc28
TargetScan6.0	mmu-mir-33-5p	39	286	6.74602E-11	212712	Satb2
TargetScan6.0	mmu-mir-33-5p	39	286	6.74602E-11	21413	Tcf4
TargetScan6.0	mmu-mir-33-5p	39	286	6.74602E-11	22629	Ywhah
TargetScan6.0	mmu-mir-33-5p	39	286	6.74602E-11	228662	Btbd3
TargetScan6.0	mmu-mir-33-5p	39	286	6.74602E-11	235402	Lingo1
TargetScan6.0	mmu-mir-33-5p	39	286	6.74602E-11	238871	Pde4d
TargetScan6.0	mmu-mir-33-5p	39	286	6.74602E-11	53623	Gria3
TargetScan6.0	mmu-mir-33-5p	39	286	6.74602E-11	54216	Pcdh7
TargetScan6.0	mmu-mir-33-5p	39	286	6.74602E-11	56177	Olfm1
TargetScan6.0	mmu-mir-33-5p	39	286	6.74602E-11	56542	Ick
TargetScan6.0	mmu-mir-33-5p	39	286	6.74602E-11	58194	Sh3kbp1
TargetScan6.0	mmu-mir-33-5p	39	286	6.74602E-11	664994	Isoc2a

TargetScan6.0	mmu-mir-33-5p	39	286	6.74602E-11	665563	Mthfd2l
TargetScan6.0	mmu-mir-33-5p	39	286	6.74602E-11	71323	Rassf8
TargetScan6.0	mmu-mir-33-5p	39	286	6.74602E-11	71973	Rbpms2
TargetScan6.0	mmu-mir-33-5p	39	286	6.74602E-11	74480	Samd4
TargetScan6.0	mmu-mir-33-5p	39	286	6.74602E-11	76108	Rap2a
TargetScan6.0	mmu-mir-33-5p	39	286	6.74602E-11	78619	Zfp449
TargetScan6.0	mmu-mir-33-5p	39	286	6.74602E-11	80892	Zfhx4
TargetScan6.0	mmu-mir-181cd-5p	80	891	7.81212E-11	10003912 3	Gm14295
TargetScan6.0	mmu-mir-181cd-5p	80	891	7.81212E-11	105000	Dnalc1
TargetScan6.0	mmu-mir-181cd-5p	80	891	7.81212E-11	105245	Txndc5
TargetScan6.0	mmu-mir-181cd-5p	80	891	7.81212E-11	108099	Prkag2
TargetScan6.0	mmu-mir-181cd-5p	80	891	7.81212E-11	108797	Mex3b
TargetScan6.0	mmu-mir-181cd-5p	80	891	7.81212E-11	11864	Arnt2
TargetScan6.0	mmu-mir-181cd-5p	80	891	7.81212E-11	12831	Col5a1

TargetScan6.0	mmu-mir-181cd-5p	80	891	7.81212E-11	14225	Fkbp1a
TargetScan6.0	mmu-mir-181cd-5p	80	891	7.81212E-11	14254	Flt1
TargetScan6.0	mmu-mir-181cd-5p	80	891	7.81212E-11	14465	Gata6
TargetScan6.0	mmu-mir-181cd-5p	80	891	7.81212E-11	14489	Mtpn
TargetScan6.0	mmu-mir-181cd-5p	80	891	7.81212E-11	14681	Gnao1
TargetScan6.0	mmu-mir-181cd-5p	80	891	7.81212E-11	14696	Gnb4
TargetScan6.0	mmu-mir-181cd-5p	80	891	7.81212E-11	14702	Gng2
TargetScan6.0	mmu-mir-181cd-5p	80	891	7.81212E-11	14783	Grb10
TargetScan6.0	mmu-mir-181cd-5p	80	891	7.81212E-11	15111	Hand2
TargetScan6.0	mmu-mir-181cd-5p	80	891	7.81212E-11	16201	Ilf3
TargetScan6.0	mmu-mir-181cd-5p	80	891	7.81212E-11	16443	Itsn1
TargetScan6.0	mmu-mir-181cd-5p	80	891	7.81212E-11	16948	Lox
TargetScan6.0	mmu-mir-181cd-5p	80	891	7.81212E-11	16978	Lrrfip1
TargetScan6.0	mmu-mir-181cd-5p	80	891	7.81212E-11	17690	Msi1
TargetScan6.0	mmu-mir-181cd-5p	80	891	7.81212E-11	17754	Mtap1a

TargetScan6.0	mmu-mir-181cd-5p	80	891	7.81212E-11	17755	Mtap1b
TargetScan6.0	mmu-mir-181cd-5p	80	891	7.81212E-11	18007	Neo1
TargetScan6.0	mmu-mir-181cd-5p	80	891	7.81212E-11	18383	Tnfrsf11b
TargetScan6.0	mmu-mir-181cd-5p	80	891	7.81212E-11	18595	Pdgfra
TargetScan6.0	mmu-mir-181cd-5p	80	891	7.81212E-11	18787	Serpine1
TargetScan6.0	mmu-mir-181cd-5p	80	891	7.81212E-11	208440	Dip2c
TargetScan6.0	mmu-mir-181cd-5p	80	891	7.81212E-11	20868	Stk10
TargetScan6.0	mmu-mir-181cd-5p	80	891	7.81212E-11	21676	Tead1
TargetScan6.0	mmu-mir-181cd-5p	80	891	7.81212E-11	21814	Tgfbr3
TargetScan6.0	mmu-mir-181cd-5p	80	891	7.81212E-11	22221	Ubp1
TargetScan6.0	mmu-mir-181cd-5p	80	891	7.81212E-11	224860	Plcl2
TargetScan6.0	mmu-mir-181cd-5p	80	891	7.81212E-11	225358	Fam13b
TargetScan6.0	mmu-mir-181cd-5p	80	891	7.81212E-11	226778	Mark1
TargetScan6.0	mmu-mir-181cd-5p	80	891	7.81212E-11	228662	Btbd3
TargetScan6.0	mmu-mir-181cd-5p	80	891	7.81212E-11	229521	Syt11

TargetScan6.0	mmu-mir-181cd-5p	80	891	7.81212E-11	233489	Picalm
TargetScan6.0	mmu-mir-181cd-5p	80	891	7.81212E-11	233545	2210018M11Rik
TargetScan6.0	mmu-mir-181cd-5p	80	891	7.81212E-11	23794	Adamts5
TargetScan6.0	mmu-mir-181cd-5p	80	891	7.81212E-11	238130	Dock4
TargetScan6.0	mmu-mir-181cd-5p	80	891	7.81212E-11	23881	G3bp2
TargetScan6.0	mmu-mir-181cd-5p	80	891	7.81212E-11	239393	Lrp12
TargetScan6.0	mmu-mir-181cd-5p	80	891	7.81212E-11	24066	Spry4
TargetScan6.0	mmu-mir-181cd-5p	80	891	7.81212E-11	24136	Zeb2
TargetScan6.0	mmu-mir-181cd-5p	80	891	7.81212E-11	242481	Palm2
TargetScan6.0	mmu-mir-181cd-5p	80	891	7.81212E-11	242509	Bnc2
TargetScan6.0	mmu-mir-181cd-5p	80	891	7.81212E-11	244668	Sipa1l2
TargetScan6.0	mmu-mir-181cd-5p	80	891	7.81212E-11	244895	C230081A13Rik
TargetScan6.0	mmu-mir-181cd-5p	80	891	7.81212E-11	319996	Casc4
TargetScan6.0	mmu-mir-181cd-5p	80	891	7.81212E-11	328949	Mcc
TargetScan6.0	mmu-mir-181cd-5p	80	891	7.81212E-11	333433	Gpd1l

TargetScan6.0	mmu-mir-181cd-5p	80	891	7.81212E-11	382034	Gse1
TargetScan6.0	mmu-mir-181cd-5p	80	891	7.81212E-11	382793	Mtx3
TargetScan6.0	mmu-mir-181cd-5p	80	891	7.81212E-11	434215	Lrrc32
TargetScan6.0	mmu-mir-181cd-5p	80	891	7.81212E-11	53614	Reck
TargetScan6.0	mmu-mir-181cd-5p	80	891	7.81212E-11	55992	Trim3
TargetScan6.0	mmu-mir-181cd-5p	80	891	7.81212E-11	56323	Dnajb5
TargetScan6.0	mmu-mir-181cd-5p	80	891	7.81212E-11	66262	Ing5
TargetScan6.0	mmu-mir-181cd-5p	80	891	7.81212E-11	67299	Dock7
TargetScan6.0	mmu-mir-181cd-5p	80	891	7.81212E-11	67897	Rnmt
TargetScan6.0	mmu-mir-181cd-5p	80	891	7.81212E-11	67916	Ppap2b
TargetScan6.0	mmu-mir-181cd-5p	80	891	7.81212E-11	68617	1110012J17Rik
TargetScan6.0	mmu-mir-181cd-5p	80	891	7.81212E-11	69976	Galk2
TargetScan6.0	mmu-mir-181cd-5p	80	891	7.81212E-11	70292	Afap1
TargetScan6.0	mmu-mir-181cd-5p	80	891	7.81212E-11	71323	Rassf8
TargetScan6.0	mmu-mir-181cd-5p	80	891	7.81212E-11	71738	Mamdc2

TargetScan6.0	mmu-mir-181cd-5p	80	891	7.81212E-11	72033	Tsc22d2
TargetScan6.0	mmu-mir-181cd-5p	80	891	7.81212E-11	72611	Zfp655
TargetScan6.0	mmu-mir-181cd-5p	80	891	7.81212E-11	72640	Mex3a
TargetScan6.0	mmu-mir-181cd-5p	80	891	7.81212E-11	72701	Zfp618
TargetScan6.0	mmu-mir-181cd-5p	80	891	7.81212E-11	73467	1700066M21Rik
TargetScan6.0	mmu-mir-181cd-5p	80	891	7.81212E-11	75717	Cul5
TargetScan6.0	mmu-mir-181cd-5p	80	891	7.81212E-11	77579	Myh10
TargetScan6.0	mmu-mir-181cd-5p	80	891	7.81212E-11	78339	Ttyh3
TargetScan6.0	mmu-mir-181cd-5p	80	891	7.81212E-11	78619	Zfp449
TargetScan6.0	mmu-mir-181cd-5p	80	891	7.81212E-11	80892	Zfhx4
TargetScan6.0	mmu-mir-181cd-5p	80	891	7.81212E-11	81703	Jdp2
TargetScan6.0	mmu-mir-181cd-5p	80	891	7.81212E-11	83435	Plekha3
TargetScan6.0	mmu-mir-181cd-5p	80	891	7.81212E-11	93759	Sirt1
TargetScan6.0	mmu-mir-205-5p	38	315	4.01818E-09	100515	Zfp518b
TargetScan6.0	mmu-mir-205-5p	38	315	4.01818E-09	109676	Ank2

TargetScan6.0	mmu-mir-205-5p	38	315	4.01818E-09	12167	Bmpr1b
TargetScan6.0	mmu-mir-205-5p	38	315	4.01818E-09	12321	Calu
TargetScan6.0	mmu-mir-205-5p	38	315	4.01818E-09	12977	Csf1
TargetScan6.0	mmu-mir-205-5p	38	315	4.01818E-09	14389	Gab2
TargetScan6.0	mmu-mir-205-5p	38	315	4.01818E-09	14783	Grb10
TargetScan6.0	mmu-mir-205-5p	38	315	4.01818E-09	15476	Hs3st1
TargetScan6.0	mmu-mir-205-5p	38	315	4.01818E-09	16323	Inhba
TargetScan6.0	mmu-mir-205-5p	38	315	4.01818E-09	16597	Klf12
TargetScan6.0	mmu-mir-205-5p	38	315	4.01818E-09	16971	Lrp1
TargetScan6.0	mmu-mir-205-5p	38	315	4.01818E-09	18576	Pde3b
TargetScan6.0	mmu-mir-205-5p	38	315	4.01818E-09	20868	Stk10
TargetScan6.0	mmu-mir-205-5p	38	315	4.01818E-09	212712	Satb2
TargetScan6.0	mmu-mir-205-5p	38	315	4.01818E-09	21417	Zeb1
TargetScan6.0	mmu-mir-205-5p	38	315	4.01818E-09	21676	Tead1
TargetScan6.0	mmu-mir-205-5p	38	315	4.01818E-09	217340	Rnf157

TargetScan6.0	mmu-mir-205-5p	38	315	4.01818E-09	217351	Tnrc6c
TargetScan6.0	mmu-mir-205-5p	38	315	4.01818E-09	21843	Tial1
TargetScan6.0	mmu-mir-205-5p	38	315	4.01818E-09	22339	Vegfa
TargetScan6.0	mmu-mir-205-5p	38	315	4.01818E-09	228662	Btbd3
TargetScan6.0	mmu-mir-205-5p	38	315	4.01818E-09	234839	Fam38a
TargetScan6.0	mmu-mir-205-5p	38	315	4.01818E-09	24060	Slc35a1
TargetScan6.0	mmu-mir-205-5p	38	315	4.01818E-09	246154	Vasn
TargetScan6.0	mmu-mir-205-5p	38	315	4.01818E-09	269152	Kif26b
TargetScan6.0	mmu-mir-205-5p	38	315	4.01818E-09	269424	Phf17
TargetScan6.0	mmu-mir-205-5p	38	315	4.01818E-09	319996	Casc4
TargetScan6.0	mmu-mir-205-5p	38	315	4.01818E-09	320184	Lrrc58
TargetScan6.0	mmu-mir-205-5p	38	315	4.01818E-09	50493	Txnrd1
TargetScan6.0	mmu-mir-205-5p	38	315	4.01818E-09	54598	Calcr1
TargetScan6.0	mmu-mir-205-5p	38	315	4.01818E-09	56386	B4galt6
TargetScan6.0	mmu-mir-205-5p	38	315	4.01818E-09	66725	Lrrk2

TargetScan6.0	mmu-mir-205-5p	38	315	4.01818E-09	67468	Mmd
TargetScan6.0	mmu-mir-205-5p	38	315	4.01818E-09	71330	Rcbtb1
TargetScan6.0	mmu-mir-205-5p	38	315	4.01818E-09	71752	Gtf3c2
TargetScan6.0	mmu-mir-205-5p	38	315	4.01818E-09	71973	Rbpms2
TargetScan6.0	mmu-mir-205-5p	38	315	4.01818E-09	73230	Bmper
TargetScan6.0	mmu-mir-205-5p	38	315	4.01818E-09	94223	Dgcr8
TargetScan6.0	mmu-mir-203-5p	56	590	8.29817E-09	105000	Dnalc1
TargetScan6.0	mmu-mir-203-5p	56	590	8.29817E-09	108012	Ap1s2
TargetScan6.0	mmu-mir-203-5p	56	590	8.29817E-09	108099	Prkag2
TargetScan6.0	mmu-mir-203-5p	56	590	8.29817E-09	108154	Adamts6
TargetScan6.0	mmu-mir-203-5p	56	590	8.29817E-09	108927	Lhfp
TargetScan6.0	mmu-mir-203-5p	56	590	8.29817E-09	11737	Anp32a
TargetScan6.0	mmu-mir-203-5p	56	590	8.29817E-09	11858	Rnd2
TargetScan6.0	mmu-mir-203-5p	56	590	8.29817E-09	12151	Bmi1
TargetScan6.0	mmu-mir-203-5p	56	590	8.29817E-09	12361	Cask

TargetScan6.0	mmu-mir-203-5p	56	590	8.29817E-09	12395	Runx1t1
TargetScan6.0	mmu-mir-203-5p	56	590	8.29817E-09	13591	Ebf1
TargetScan6.0	mmu-mir-203-5p	56	590	8.29817E-09	13617	Ednra
TargetScan6.0	mmu-mir-203-5p	56	590	8.29817E-09	14009	Etv1
TargetScan6.0	mmu-mir-203-5p	56	590	8.29817E-09	14299	Ncs1
TargetScan6.0	mmu-mir-203-5p	56	590	8.29817E-09	15904	Id4
TargetScan6.0	mmu-mir-203-5p	56	590	8.29817E-09	16011	Igfbp5
TargetScan6.0	mmu-mir-203-5p	56	590	8.29817E-09	16563	Kif2a
TargetScan6.0	mmu-mir-203-5p	56	590	8.29817E-09	16911	Lmo4
TargetScan6.0	mmu-mir-203-5p	56	590	8.29817E-09	170625	Snx18
TargetScan6.0	mmu-mir-203-5p	56	590	8.29817E-09	17527	Mpv17
TargetScan6.0	mmu-mir-203-5p	56	590	8.29817E-09	18196	Nsg1
TargetScan6.0	mmu-mir-203-5p	56	590	8.29817E-09	18595	Pdgfra
TargetScan6.0	mmu-mir-203-5p	56	590	8.29817E-09	20346	Sema3a
TargetScan6.0	mmu-mir-203-5p	56	590	8.29817E-09	20358	Sema6a

TargetScan6.0	mmu-mir-203-5p	56	590	8.29817E-09	20692	Sparc
TargetScan6.0	mmu-mir-203-5p	56	590	8.29817E-09	20742	Spnb2
TargetScan6.0	mmu-mir-203-5p	56	590	8.29817E-09	208968	Zfp280c
TargetScan6.0	mmu-mir-203-5p	56	590	8.29817E-09	21386	Tbx3
TargetScan6.0	mmu-mir-203-5p	56	590	8.29817E-09	21413	Tcf4
TargetScan6.0	mmu-mir-203-5p	56	590	8.29817E-09	22196	Ube2i
TargetScan6.0	mmu-mir-203-5p	56	590	8.29817E-09	22339	Vegfa
TargetScan6.0	mmu-mir-203-5p	56	590	8.29817E-09	228071	Sestd1
TargetScan6.0	mmu-mir-203-5p	56	590	8.29817E-09	23794	Adamts5
TargetScan6.0	mmu-mir-203-5p	56	590	8.29817E-09	238871	Pde4d
TargetScan6.0	mmu-mir-203-5p	56	590	8.29817E-09	240427	Setbp1
TargetScan6.0	mmu-mir-203-5p	56	590	8.29817E-09	242481	Palm2
TargetScan6.0	mmu-mir-203-5p	56	590	8.29817E-09	26564	Ror2
TargetScan6.0	mmu-mir-203-5p	56	590	8.29817E-09	26611	Rcn2
TargetScan6.0	mmu-mir-203-5p	56	590	8.29817E-09	269023	Zfp608

TargetScan6.0	mmu-mir-203-5p	56	590	8.29817E-09	279653	Pcdh19
TargetScan6.0	mmu-mir-203-5p	56	590	8.29817E-09	320827	C530008M17Rik
TargetScan6.0	mmu-mir-203-5p	56	590	8.29817E-09	330267	Thsd7a
TargetScan6.0	mmu-mir-203-5p	56	590	8.29817E-09	50706	Postn
TargetScan6.0	mmu-mir-203-5p	56	590	8.29817E-09	56542	Ick
TargetScan6.0	mmu-mir-203-5p	56	590	8.29817E-09	67916	Ppap2b
TargetScan6.0	mmu-mir-203-5p	56	590	8.29817E-09	69675	Pxdn
TargetScan6.0	mmu-mir-203-5p	56	590	8.29817E-09	71323	Rassf8
TargetScan6.0	mmu-mir-203-5p	56	590	8.29817E-09	71566	9030425E11Rik
TargetScan6.0	mmu-mir-203-5p	56	590	8.29817E-09	71914	Antxr2
TargetScan6.0	mmu-mir-203-5p	56	590	8.29817E-09	73230	Bmper
TargetScan6.0	mmu-mir-203-5p	56	590	8.29817E-09	76108	Rap2a
TargetScan6.0	mmu-mir-203-5p	56	590	8.29817E-09	77057	Ston1
TargetScan6.0	mmu-mir-203-5p	56	590	8.29817E-09	80892	Zfhx4
TargetScan6.0	mmu-mir-203-5p	56	590	8.29817E-09	81904	Cacng7

TargetScan6.0	mmu-mir-203-5p	56	590	8.29817E-09	83814	Nedd4l
TargetScan6.0	mmu-mir-203-5p	56	590	8.29817E-09	93683	Glce
TargetScan6.0	mmu-mir-138-5p	40	453	6.47987E-06	105727	Slc38a1
TargetScan6.0	mmu-mir-138-5p	40	453	6.47987E-06	108116	Slco3a1
TargetScan6.0	mmu-mir-138-5p	40	453	6.47987E-06	11853	Rhoc
TargetScan6.0	mmu-mir-138-5p	40	453	6.47987E-06	13591	Ebf1
TargetScan6.0	mmu-mir-138-5p	40	453	6.47987E-06	14585	Gfra1
TargetScan6.0	mmu-mir-138-5p	40	453	6.47987E-06	14702	Gng2
TargetScan6.0	mmu-mir-138-5p	40	453	6.47987E-06	16210	Impact
TargetScan6.0	mmu-mir-138-5p	40	453	6.47987E-06	16565	Kif21b
TargetScan6.0	mmu-mir-138-5p	40	453	6.47987E-06	16597	Klf12
TargetScan6.0	mmu-mir-138-5p	40	453	6.47987E-06	16764	Aff3
TargetScan6.0	mmu-mir-138-5p	40	453	6.47987E-06	16800	Arhgef2
TargetScan6.0	mmu-mir-138-5p	40	453	6.47987E-06	16923	Sh2b3
TargetScan6.0	mmu-mir-138-5p	40	453	6.47987E-06	17690	Msi1

TargetScan6.0	mmu-mir-138-5p	40	453	6.47987E-06	18032	Nfix
TargetScan6.0	mmu-mir-138-5p	40	453	6.47987E-06	18111	Nnat
TargetScan6.0	mmu-mir-138-5p	40	453	6.47987E-06	18412	Sqstm1
TargetScan6.0	mmu-mir-138-5p	40	453	6.47987E-06	18491	Pappa
TargetScan6.0	mmu-mir-138-5p	40	453	6.47987E-06	20441	St3gal3
TargetScan6.0	mmu-mir-138-5p	40	453	6.47987E-06	209131	Snx30
TargetScan6.0	mmu-mir-138-5p	40	453	6.47987E-06	209630	Frmd4a
TargetScan6.0	mmu-mir-138-5p	40	453	6.47987E-06	20970	Sdc3
TargetScan6.0	mmu-mir-138-5p	40	453	6.47987E-06	21413	Tcf4
TargetScan6.0	mmu-mir-138-5p	40	453	6.47987E-06	218952	Fermt2
TargetScan6.0	mmu-mir-138-5p	40	453	6.47987E-06	22221	Ubp1
TargetScan6.0	mmu-mir-138-5p	40	453	6.47987E-06	228602	4930402H24Rik
TargetScan6.0	mmu-mir-138-5p	40	453	6.47987E-06	229706	Slc6a17
TargetScan6.0	mmu-mir-138-5p	40	453	6.47987E-06	230753	Thrap3
TargetScan6.0	mmu-mir-138-5p	40	453	6.47987E-06	24136	Zeb2

TargetScan6.0	mmu-mir-138-5p	40	453	6.47987E-06	270669	Mbtps2
TargetScan6.0	mmu-mir-138-5p	40	453	6.47987E-06	320706	9830001H06Rik
TargetScan6.0	mmu-mir-138-5p	40	453	6.47987E-06	380686	Cnrip1
TargetScan6.0	mmu-mir-138-5p	40	453	6.47987E-06	53619	Blcap
TargetScan6.0	mmu-mir-138-5p	40	453	6.47987E-06	56316	Ggcx
TargetScan6.0	mmu-mir-138-5p	40	453	6.47987E-06	594844	Tceal3
TargetScan6.0	mmu-mir-138-5p	40	453	6.47987E-06	629059	Fam124a
TargetScan6.0	mmu-mir-138-5p	40	453	6.47987E-06	70551	Tmtc4
TargetScan6.0	mmu-mir-138-5p	40	453	6.47987E-06	71566	9030425E11Rik
TargetScan6.0	mmu-mir-138-5p	40	453	6.47987E-06	72640	Mex3a
TargetScan6.0	mmu-mir-138-5p	40	453	6.47987E-06	78752	Csgalnact2
TargetScan6.0	mmu-mir-138-5p	40	453	6.47987E-06	93759	Sirt1
TargetScan6.0	mmu-let-7e-5p	63	913	5.68768E-05	105000	Dnalc1
TargetScan6.0	mmu-let-7e-5p	63	913	5.68768E-05	108078	Olr1
TargetScan6.0	mmu-let-7e-5p	63	913	5.68768E-05	12035	Bcat1

TargetScan6.0	mmu-let-7e-5p	63	913	5.68768E-05	12321	Calu
TargetScan6.0	mmu-let-7e-5p	63	913	5.68768E-05	12361	Cask
TargetScan6.0	mmu-let-7e-5p	63	913	5.68768E-05	12395	Runx1t1
TargetScan6.0	mmu-let-7e-5p	63	913	5.68768E-05	12832	Col5a2
TargetScan6.0	mmu-let-7e-5p	63	913	5.68768E-05	12877	Cpeb1
TargetScan6.0	mmu-let-7e-5p	63	913	5.68768E-05	14489	Mtpn
TargetScan6.0	mmu-let-7e-5p	63	913	5.68768E-05	14600	Ghr
TargetScan6.0	mmu-let-7e-5p	63	913	5.68768E-05	14852	Gspt1
TargetScan6.0	mmu-let-7e-5p	63	913	5.68768E-05	15248	Hic1
TargetScan6.0	mmu-let-7e-5p	63	913	5.68768E-05	15277	Hk2
TargetScan6.0	mmu-let-7e-5p	63	913	5.68768E-05	16193	Il6
TargetScan6.0	mmu-let-7e-5p	63	913	5.68768E-05	16565	Kif21b
TargetScan6.0	mmu-let-7e-5p	63	913	5.68768E-05	16886	Limk2
TargetScan6.0	mmu-let-7e-5p	63	913	5.68768E-05	16923	Sh2b3
TargetScan6.0	mmu-let-7e-5p	63	913	5.68768E-05	170676	Peg10

TargetScan6.0	mmu-let-7e-5p	63	913	5.68768E-05	18208	Ntn1
TargetScan6.0	mmu-let-7e-5p	63	913	5.68768E-05	18414	Osmr
TargetScan6.0	mmu-let-7e-5p	63	913	5.68768E-05	18491	Pappa
TargetScan6.0	mmu-let-7e-5p	63	913	5.68768E-05	18933	Prrx1
TargetScan6.0	mmu-let-7e-5p	63	913	5.68768E-05	19734	Rgs16
TargetScan6.0	mmu-let-7e-5p	63	913	5.68768E-05	209131	Snx30
TargetScan6.0	mmu-let-7e-5p	63	913	5.68768E-05	214642	A430107O13Rik
TargetScan6.0	mmu-let-7e-5p	63	913	5.68768E-05	21814	Tgfbr3
TargetScan6.0	mmu-let-7e-5p	63	913	5.68768E-05	21825	Thbs1
TargetScan6.0	mmu-let-7e-5p	63	913	5.68768E-05	22240	Dpysl3
TargetScan6.0	mmu-let-7e-5p	63	913	5.68768E-05	223254	Farp1
TargetScan6.0	mmu-let-7e-5p	63	913	5.68768E-05	226841	Vash2
TargetScan6.0	mmu-let-7e-5p	63	913	5.68768E-05	228071	Sestd1
TargetScan6.0	mmu-let-7e-5p	63	913	5.68768E-05	228602	4930402H24Rik
TargetScan6.0	mmu-let-7e-5p	63	913	5.68768E-05	228662	Btbd3

TargetScan6.0	mmu-let-7e-5p	63	913	5.68768E-05	229521	Syt11
TargetScan6.0	mmu-let-7e-5p	63	913	5.68768E-05	230233	Ikbpap
TargetScan6.0	mmu-let-7e-5p	63	913	5.68768E-05	235402	Lingo1
TargetScan6.0	mmu-let-7e-5p	63	913	5.68768E-05	23794	Adamts5
TargetScan6.0	mmu-let-7e-5p	63	913	5.68768E-05	242509	Bnc2
TargetScan6.0	mmu-let-7e-5p	63	913	5.68768E-05	244895	C230081A13Rik
TargetScan6.0	mmu-let-7e-5p	63	913	5.68768E-05	270669	Mbtps2
TargetScan6.0	mmu-let-7e-5p	63	913	5.68768E-05	277154	Nynrin
TargetScan6.0	mmu-let-7e-5p	63	913	5.68768E-05	279653	Pcdh19
TargetScan6.0	mmu-let-7e-5p	63	913	5.68768E-05	320024	Nceh1
TargetScan6.0	mmu-let-7e-5p	63	913	5.68768E-05	330222	Sdk1
TargetScan6.0	mmu-let-7e-5p	63	913	5.68768E-05	380785	Begain
TargetScan6.0	mmu-let-7e-5p	63	913	5.68768E-05	381560	Xkr8
TargetScan6.0	mmu-let-7e-5p	63	913	5.68768E-05	433926	Lrrc8b
TargetScan6.0	mmu-let-7e-5p	63	913	5.68768E-05	50768	Dlc1

TargetScan6.0	mmu-let-7e-5p	63	913	5.68768E-05	52187	Rragd
TargetScan6.0	mmu-let-7e-5p	63	913	5.68768E-05	56741	Igdcc4
TargetScan6.0	mmu-let-7e-5p	63	913	5.68768E-05	59046	Arpp19
TargetScan6.0	mmu-let-7e-5p	63	913	5.68768E-05	66573	Dzip1
TargetScan6.0	mmu-let-7e-5p	63	913	5.68768E-05	68178	Cgnl1
TargetScan6.0	mmu-let-7e-5p	63	913	5.68768E-05	68606	Ppm1f
TargetScan6.0	mmu-let-7e-5p	63	913	5.68768E-05	69675	Pxdn
TargetScan6.0	mmu-let-7e-5p	63	913	5.68768E-05	72033	Tsc22d2
TargetScan6.0	mmu-let-7e-5p	63	913	5.68768E-05	72543	Fam125b
TargetScan6.0	mmu-let-7e-5p	63	913	5.68768E-05	72640	Mex3a
TargetScan6.0	mmu-let-7e-5p	63	913	5.68768E-05	74136	Sec14l1
TargetScan6.0	mmu-let-7e-5p	63	913	5.68768E-05	75612	Gns
TargetScan6.0	mmu-let-7e-5p	63	913	5.68768E-05	77889	Lbh
TargetScan6.0	mmu-let-7e-5p	63	913	5.68768E-05	78923	Chsy3
TargetScan6.0	mmu-let-7e-5p	63	913	5.68768E-05	83814	Nedd4l

TargetScan6.0	mmu-mir-135b-5p	41	578	0.00062505	105245	Txndc5
TargetScan6.0	mmu-mir-135b-5p	41	578	0.00062505	11551	Adra2a
TargetScan6.0	mmu-mir-135b-5p	41	578	0.00062505	12831	Col5a1
TargetScan6.0	mmu-mir-135b-5p	41	578	0.00062505	12890	Cplx2
TargetScan6.0	mmu-mir-135b-5p	41	578	0.00062505	13527	Dtna
TargetScan6.0	mmu-mir-135b-5p	41	578	0.00062505	13591	Ebf1
TargetScan6.0	mmu-mir-135b-5p	41	578	0.00062505	13712	Elk1
TargetScan6.0	mmu-mir-135b-5p	41	578	0.00062505	14020	Evi5
TargetScan6.0	mmu-mir-135b-5p	41	578	0.00062505	14225	Fkbp1a
TargetScan6.0	mmu-mir-135b-5p	41	578	0.00062505	14489	Mtpn
TargetScan6.0	mmu-mir-135b-5p	41	578	0.00062505	16323	Inhba
TargetScan6.0	mmu-mir-135b-5p	41	578	0.00062505	16800	Arhgef2
TargetScan6.0	mmu-mir-135b-5p	41	578	0.00062505	16978	Lrrfip1
TargetScan6.0	mmu-mir-135b-5p	41	578	0.00062505	170625	Snx18
TargetScan6.0	mmu-mir-135b-5p	41	578	0.00062505	17532	Mras

TargetScan6.0	mmu-mir-135b-5p	41	578	0.00062505	18196	Nsg1
TargetScan6.0	mmu-mir-135b-5p	41	578	0.00062505	18577	Pde4a
TargetScan6.0	mmu-mir-135b-5p	41	578	0.00062505	20315	Cxcl12
TargetScan6.0	mmu-mir-135b-5p	41	578	0.00062505	20742	Spnb2
TargetScan6.0	mmu-mir-135b-5p	41	578	0.00062505	208440	Dip2c
TargetScan6.0	mmu-mir-135b-5p	41	578	0.00062505	209630	Frmd4a
TargetScan6.0	mmu-mir-135b-5p	41	578	0.00062505	218952	Fermt2
TargetScan6.0	mmu-mir-135b-5p	41	578	0.00062505	23821	Bace1
TargetScan6.0	mmu-mir-135b-5p	41	578	0.00062505	240427	Setbp1
TargetScan6.0	mmu-mir-135b-5p	41	578	0.00062505	24060	Slc35a1
TargetScan6.0	mmu-mir-135b-5p	41	578	0.00062505	269424	Phf17
TargetScan6.0	mmu-mir-135b-5p	41	578	0.00062505	330222	Sdk1
TargetScan6.0	mmu-mir-135b-5p	41	578	0.00062505	330627	Trim66
TargetScan6.0	mmu-mir-135b-5p	41	578	0.00062505	433375	Creg1
TargetScan6.0	mmu-mir-135b-5p	41	578	0.00062505	53614	Reck

TargetScan6.0	mmu-mir-135b-5p	41	578	0.00062505	53623	Gria3
TargetScan6.0	mmu-mir-135b-5p	41	578	0.00062505	58193	Extl2
TargetScan6.0	mmu-mir-135b-5p	41	578	0.00062505	70676	Gulp1
TargetScan6.0	mmu-mir-135b-5p	41	578	0.00062505	73230	Bmper
TargetScan6.0	mmu-mir-135b-5p	41	578	0.00062505	74136	Sec14l1
TargetScan6.0	mmu-mir-135b-5p	41	578	0.00062505	75292	Prkd3
TargetScan6.0	mmu-mir-135b-5p	41	578	0.00062505	76108	Rap2a
TargetScan6.0	mmu-mir-135b-5p	41	578	0.00062505	81703	Jdp2
TargetScan6.0	mmu-mir-135b-5p	41	578	0.00062505	93759	Sirt1
TargetScan6.0	mmu-mir-135b-5p	41	578	0.00062505	93834	Peli2
TargetScan6.0	mmu-mir-135b-5p	41	578	0.00062505	94332	Cadm3
TargetScan6.0	mmu-mir-31-5p	23	285	0.001870575	114715	Spred1
TargetScan6.0	mmu-mir-31-5p	23	285	0.001870575	12831	Col5a1
TargetScan6.0	mmu-mir-31-5p	23	285	0.001870575	13992	Khdrbs3
TargetScan6.0	mmu-mir-31-5p	23	285	0.001870575	14783	Grb10

TargetScan6.0	mmu-mir-31-5p	23	285	0.001870575	14852	Gspt1
TargetScan6.0	mmu-mir-31-5p	23	285	0.001870575	208968	Zfp280c
TargetScan6.0	mmu-mir-31-5p	23	285	0.001870575	212712	Satb2
TargetScan6.0	mmu-mir-31-5p	23	285	0.001870575	213760	Prepl
TargetScan6.0	mmu-mir-31-5p	23	285	0.001870575	215280	Wipf1
TargetScan6.0	mmu-mir-31-5p	23	285	0.001870575	217869	Eif5
TargetScan6.0	mmu-mir-31-5p	23	285	0.001870575	22240	Dpysl3
TargetScan6.0	mmu-mir-31-5p	23	285	0.001870575	223527	Eny2
TargetScan6.0	mmu-mir-31-5p	23	285	0.001870575	233115	Dpy19l3
TargetScan6.0	mmu-mir-31-5p	23	285	0.001870575	24066	Spry4
TargetScan6.0	mmu-mir-31-5p	23	285	0.001870575	320165	Tacc1
TargetScan6.0	mmu-mir-31-5p	23	285	0.001870575	320827	C530008M17Rik
TargetScan6.0	mmu-mir-31-5p	23	285	0.001870575	330812	Rnf150
TargetScan6.0	mmu-mir-31-5p	23	285	0.001870575	57752	Tacc2
TargetScan6.0	mmu-mir-31-5p	23	285	0.001870575	71709	Syde1

TargetScan6.0	mmu-mir-31-5p	23	285	0.001870575	72543	Fam125b
TargetScan6.0	mmu-mir-31-5p	23	285	0.001870575	75717	Cul5
TargetScan6.0	mmu-mir-31-5p	23	285	0.001870575	80892	Zfhx4
TargetScan6.0	mmu-mir-31-5p	23	285	0.001870575	83814	Nedd4l
TargetScan6.0	mmu-mir-335-3p	16	187	0.004954846	104111	Adcy3
TargetScan6.0	mmu-mir-335-3p	16	187	0.004954846	12321	Calu
TargetScan6.0	mmu-mir-335-3p	16	187	0.004954846	12832	Col5a2
TargetScan6.0	mmu-mir-335-3p	16	187	0.004954846	14020	Evi5
TargetScan6.0	mmu-mir-335-3p	16	187	0.004954846	14173	Fgf2
TargetScan6.0	mmu-mir-335-3p	16	187	0.004954846	14254	Flt1
TargetScan6.0	mmu-mir-335-3p	16	187	0.004954846	14260	Fmn1
TargetScan6.0	mmu-mir-335-3p	16	187	0.004954846	14852	Gspt1
TargetScan6.0	mmu-mir-335-3p	16	187	0.004954846	18760	Prkd1
TargetScan6.0	mmu-mir-335-3p	16	187	0.004954846	207806	Gm608
TargetScan6.0	mmu-mir-335-3p	16	187	0.004954846	211712	Pcdh9

TargetScan6.0	mmu-mir-335-3p	16	187	0.004954846	228598	Ebf4
TargetScan6.0	mmu-mir-335-3p	16	187	0.004954846	238130	Dock4
TargetScan6.0	mmu-mir-335-3p	16	187	0.004954846	24136	Zeb2
TargetScan6.0	mmu-mir-335-3p	16	187	0.004954846	56693	Crtap
TargetScan6.0	mmu-mir-335-3p	16	187	0.004954846	76156	Fam131b

Appendix 5 : mouse-human.miRNA Pearson's correlation analysis													
Sample	mES	miPS ^{Yam}	Δ Np63-/-1	Δ Np63-/-2	Δ Np63-/-3	Keratinocytes 1	Keratinocytes 2	Δ Np63-/- +DGCR8-1	Δ Np63-/- +DGCR8-2	hiPS ^{Yam}	NHEK	NHEK_Sh DGCR8	NHEK_Sh Δ Np63
mES	1.0000	0.9506	-0.2767	-0.3525	-0.4930	-0.4272	-0.4156	-0.4897	-0.5437	0.0784	-0.3340	-0.0358	-0.2432
miPS ^{Yam}	0.9506	1.0000	-0.2544	-0.3668	-0.4751	-0.4476	-0.4309	-0.4895	-0.5319	0.1954	-0.3957	-0.0851	-0.2627
Δ Np63-/-1	-0.2767	-0.2544	1.0000	0.6332	0.0259	-0.2583	-0.3078	0.0676	0.0132	0.3572	-0.1043	-0.1247	0.2052
Δ Np63-/-2	-0.3525	-0.3668	0.6332	1.0000	0.2597	-0.2772	-0.3241	0.1351	0.0681	0.1681	-0.0321	0.0499	0.2464
Δ Np63-/-3	-0.4930	-0.4751	0.0259	0.2597	1.0000	-0.2301	-0.2216	0.0698	0.1247	-0.0915	0.0316	0.1260	0.0963
Keratinocytes 1	-0.4272	-0.4476	-0.2583	-0.2772	-0.2301	1.0000	0.9832	0.4535	0.5033	-0.0219	0.3206	-0.2418	-0.0180
Keratinocytes 2	-0.4156	-0.4309	-0.3078	-0.3241	-0.2216	0.9832	1.0000	0.4314	0.4867	-0.0365	0.3295	-0.2432	-0.0020
Δ Np63-/- +DGCR8-1	-0.4897	-0.4895	0.0676	0.1351	0.0698	0.4535	0.4314	1.0000	0.9607	-0.0267	0.1837	-0.0742	0.0357
Δ Np63-/- +DGCR8-2	-0.5437	-0.5319	0.0132	0.0681	0.1247	0.5033	0.4867	0.9607	1.0000	-0.0784	0.1933	-0.0383	0.0585
hiPS ^{Yam}	0.0784	0.1954	0.3572	0.1681	-0.0915	-0.0219	-0.0365	-0.0267	-0.0784	1.0000	-0.2064	-0.6249	-0.3147
NHEK	-0.3340	-0.3957	-0.1043	-0.0321	0.0316	0.3206	0.3295	0.1837	0.1933	-0.2064	1.0000	-0.2788	-0.2502
NHEK_ShDGCR8	-0.0358	-0.0851	-0.1247	0.0499	0.1260	-0.2418	-0.2432	-0.0742	-0.0383	-0.6249	-0.2788	1.0000	0.2433
NHEK_Sh Δ Np63	-0.2432	-0.2627	0.2052	0.2464	0.0963	-0.0180	-0.0020	0.0357	0.0585	-0.3147	-0.2502	0.2433	1.0000

Appendix 6 : mouse-human miRNA Principal component analysis plot		
Samples	PC1	PC2
mES	-0.647453275	0.036247611
miPS ^{yam}	-0.596911562	0.001834562
Δ Np63-/-1	0.118460771	-0.502636132
Δ Np63-/-2	0.158769753	-0.483563594
Δ Np63-/-3	0.198706084	-0.218191284
Keratinocytes 1	0.136683214	0.34770748
Keratinocytes 2	0.129638738	0.357601714
Δ Np63-/- +DGCR8-1	0.179837435	0.127427349
Δ Np63-/- +DGCR8-2	0.192831842	0.153209111
hiPSYam	-0.044529441	-0.128145687
NHEK	0.182937225	0.34928618
NHEK_shDGCR8	0.008526762	-0.127011174
NHEK_shDNp63	0.072389336	-0.146813651

Appendix 7 : mouse-human miRNA signature										
miRNA	mES	miPS ^{yam}	Δ Np63-/-1	Δ Np63-/-2	Keratinocytes 1	Keratinocytes 2	hiPS ^{yam}	NHEK	NHEK_Sh DGCR8	NHEK_Sh Δ Np63
mmu-let-7e-5p	-1.955	-1.675	0.189	0.291	0.239	0.239	0.332	1.257	0.102	-0.185
mmu-mir-141-5p	-0.968	-1.017	-0.585	-0.925	1.533	1.581	0.681	1.342	-0.923	-0.923
mmu-mir-146b-5p	-1.612	-1.271	-0.759	-0.759	1.039	1.039	0.805	-1.408	-0.100	1.097
mmu-mir-205-5p	-0.847	-0.501	-0.953	-1.207	0.570	0.570	0.447	1.309	-1.006	-1.006
mmu-mir-23a-5p	-0.729	-0.862	-0.231	-0.580	1.850	1.824	-0.249	1.777	-0.509	-0.509
mmu-mir-30c-5p	-0.467	-0.520	-1.940	-0.429	-0.319	-0.162	0.303	1.094	0.682	-0.833
mmu-mir-31-5p	-1.451	-1.226	-0.558	-0.961	1.030	1.125	0.314	1.621	-0.538	-0.642
mmu-mir-9-5p	0.846	0.846	0.743	1.557	-0.722	-0.795	-0.069	-1.671	0.398	0.399

Appendix 8 : mouse-human mRNA Pearson's correlation analysis										
Sample	NHEK	NHEK_sh DGCR8	NHEK_sh ΔNp63	hiPSYam	Keratinocytes 1	Keratinocytes 2	miPS^{yam}	mES	ΔNp63-/-2	ΔNp63-/-1
NHEK	1.000	-0.614	-0.613	-0.352	0.386	0.423	-0.454	-0.444	0.023	0.001
NHEK_shDGCR8	-0.614	1.000	0.616	-0.399	-0.206	-0.248	0.246	0.223	-0.033	-0.010
NHEK_shDNp63	-0.613	0.616	1.000	-0.400	-0.241	-0.286	0.234	0.267	0.001	0.005
hiPS^{yam}	-0.352	-0.399	-0.400	1.000	-0.156	-0.137	0.215	0.195	-0.005	0.001
Keratinocytes 1	0.386	-0.206	-0.241	-0.156	1.000	0.803	-0.506	-0.517	-0.314	-0.349
Keratinocytes 2	0.423	-0.248	-0.286	-0.137	0.803	1.000	-0.541	-0.525	-0.277	-0.318
miPS^{yam}	-0.454	0.246	0.234	0.215	-0.506	-0.541	1.000	0.773	-0.318	-0.283
mES	-0.444	0.223	0.267	0.195	-0.517	-0.525	0.773	1.000	-0.301	-0.290
ΔNp63-/-2	0.023	-0.033	0.001	-0.005	-0.314	-0.277	-0.318	-0.301	1.000	0.842
ΔNp63-/-1	0.001	-0.010	0.005	0.001	-0.349	-0.318	-0.283	-0.290	0.842	1.000

Appendix 9 : mouse-human mRNA Principal component analysis plot		
Samples	PC1	PC2
NHEK	-0.42794346	-0.109069577
NHEK_shDGCR8	0.14228023	0.042429771
NHEK_shDNp63	0.1502105	0.059231079
hiPS ^{Yam}	0.13545272	0.007408728
Keratinocytes 1	-0.29061823	-0.289488466
Keratinocytes 3	-0.33900544	-0.30777434
Keratinocytes 2	-0.15839084	-0.14042462
miPS ^{Yam}	0.49921979	-0.196523198
mES	0.5242491	-0.199355859
Δ Np63-/-2	-0.06710176	0.599467252
Δ Np63-/-1	-0.05175552	0.588869705

Appendix 10 : mouse-differentially expressed miRNA in null vs. ips cells					
miRNA	mES	miPS^{yam}	ΔNp63-/-1	ΔNp63-/-2	ΔNp63-/-3
mmu-mir-330-5p	-0.859480032	-0.599228492	0.056537231	1.679855452	-0.277684159
mmu-mir-1839-3p	-0.877676735	-0.942556401	-0.301193989	1.073493244	1.047933881
mmu-mir-574-5p	-0.832995553	-0.792672909	-0.282420208	0.330495737	1.577592933
mmu-mir-201-5p	-0.685225118	-0.685225118	0.027056098	-0.367015388	1.710409526
mmu-mir-455-5p	-1.050513568	-0.534849248	0.223078987	1.584658565	-0.222374736
mmu-mir-126-5p	1.066205393	1.013129269	-0.281228587	-1.164658854	-0.633447221
mmu-mir-125a-3p	-0.803898973	-0.885139532	1.289615562	0.84290538	-0.443482438
mmu-mir-3107-5p	-1.059874736	-1.059874736	0.808771955	0.309159443	1.001818074
mmu-mir-486-5p	-1.059874736	-1.059874736	0.808771955	0.309159443	1.001818074
mmu-mir-467d-5p	0.028046456	1.61090862	-0.079189213	-1.08111466	-0.478651203
mmu-mir-300-5p	-0.574665464	-1.25480715	1.257982759	-0.132224971	0.703714826
mmu-mir-150-5p	0.644470584	1.328778155	-0.185004531	-1.19897529	-0.589268918
mmu-mir-467e-5p	0.764853612	1.278162943	-0.272033443	-1.149220261	-0.62176285

mmu-mir-676-5p	-0.633164487	-0.870882714	-0.39477627	0.285313685	1.613509786
mmu-mir-290-3p	1.456742386	0.531116718	-0.316940662	-1.058372939	-0.612545503
mmu-mir-1968-5p	1.246838976	0.860757032	-0.392696971	-1.05724896	-0.657650078
mmu-mir-345-5p	-0.945421349	-0.800113023	-0.375444445	0.865857039	1.255121778
mmu-mir-871-3p	1.569739575	0.301941223	-0.279210117	-1.018507066	-0.573963615
mmu-mir-466n-3p	1.177722434	0.939078637	-0.386458373	-1.070972447	-0.65937025
mmu-mir-365-2-5p	-0.850240765	-0.675370786	0.023760162	1.670877215	-0.169025826
mmu-mir-301a-5p	-0.981628752	-0.784171351	0.318945829	1.521255501	-0.074401227
mmu-mir-184-5p	-0.98581515	-0.98581515	1.228336864	0.003351347	0.73994209
mmu-mir-652-5p	-1.070012452	-0.873969019	1.245184502	-0.035704397	0.734501367
mmu-mir-494-5p	-0.360270816	-1.356421412	1.242643363	-0.195296167	0.669345032
mmu-mir-465a-3p	1.579347951	0.336157497	-0.368799941	-0.947272028	-0.599433479
mmu-mir-465b-3p	1.579347951	0.336157497	-0.368799941	-0.947272028	-0.599433479
mmu-mir-465c-3p	1.579347951	0.336157497	-0.368799941	-0.947272028	-0.599433479
mmu-mir-1843-5p	-1.070005039	-0.868356361	-0.062164057	0.781024245	1.219501212
mmu-mir-466a-3p	0.539133686	1.45887459	-0.338336967	-1.041133395	-0.618537914

mmu-mir-466e-3p	0.539133686	1.45887459	-0.338336967	-1.041133395	-0.618537914
mmu-mir-758-5p	1.656638628	0.134693773	-0.328861778	-0.904217702	-0.55825292
mmu-mir-466b-3p	0.528852321	1.474387193	-0.368469295	-1.010376261	-0.624393959
mmu-mir-466c-3p	0.528852321	1.474387193	-0.368469295	-1.010376261	-0.624393959
mmu-mir-466p-3p	0.528852321	1.474387193	-0.368469295	-1.010376261	-0.624393959
mmu-mir-669b-5p	0.796161503	1.314855919	-0.448505792	-0.995801961	-0.666709669
mmu-mir-335-5p	1.519791727	0.470877912	-0.411970387	-0.951586846	-0.627112407
mmu-mir-1929-5p	-1.314562181	-0.64048103	0.086754696	0.700763714	1.167524801
mmu-mir-125b-1-3p	-1.076280589	-1.110844898	0.791073755	0.758712772	0.637338961
mmu-mir-363-5p	0.766292574	1.341604426	-0.464865942	-0.974840968	-0.668190091
mmu-mir-1965	1.364980274	0.735268762	-0.467750909	-0.966070159	-0.666427966
mmu-mir-195-5p	1.069263899	1.093680246	-0.51275689	-0.959368751	-0.690818504
mmu-mir-3086-5p	-0.920062235	-0.990749997	1.398577586	0.050340142	0.461894504
mmu-mir-673-5p	0.891966007	0.657274406	-0.989510219	0.624736357	-1.18446655
mmu-mir-206-5p	-0.98581515	-0.98581515	1.228336864	0.003351347	0.73994209
mmu-mir-1940	0.503245945	1.140833798	-0.78197301	-1.286081426	0.423974694

mmu-mir-295-5p	1.283648837	0.856786765	-0.51591659	-0.939658805	-0.684860207
mmu-mir-224-5p	-0.776377901	-0.855491178	-0.480617751	0.737591198	1.374895632
mmu-mir-181d-5p	0.342660853	0.85249792	-1.734308959	0.306056651	0.233093534
mmu-mir-467c-5p	0.865325139	1.277385655	-0.518761473	-0.938028474	-0.685920847
mmu-mir-532-5p	-0.867789916	-1.254921723	0.621696224	0.468477305	1.032538111
mmu-mir-3082-5p	-0.98581515	-0.98581515	1.228336864	0.003351347	0.73994209
mmu-mir-149-5p	-0.773153606	-0.763083444	-0.472257364	0.465784005	1.542710408
mmu-mir-142-3p	1.1306458	1.039485233	-0.548524296	-0.923558452	-0.698048285
mmu-mir-709	1.031537577	0.591271173	0.516955422	-1.191927902	-0.94783627
mmu-mir-720	-0.749915316	-0.950656605	1.302097226	-0.416810869	0.815285564
mmu-mir-381-5p	-0.577380188	-1.091011818	1.371056902	-0.376843734	0.674178838
mmu-mir-140-5p	-1.203907864	-0.790756602	0.412034929	0.289727814	1.292901722
mmu-mir-540-3p	0.944279425	0.777003443	-0.990137167	0.427189216	-1.158334918
mmu-mir-423-3p	-1.186088102	-0.718220927	0.318938321	0.193130552	1.392240156
mmu-mir-99a-5p	-1.113090369	-1.0387352	0.434414226	0.762288774	0.955122569
mmu-mir-669c-5p	0.694827875	1.321410231	-0.831933502	-0.157590928	-1.026713676

mmu-mir-679-5p	0.824579791	0.709465983	-1.013998126	0.649181655	-1.169229304
mmu-mir-878-5p	1.377209228	0.734249138	-0.520817398	-0.913330732	-0.677310237
mmu-mir-3068-5p	-0.794250577	-0.797020884	-0.589654209	1.027164899	1.15376077
mmu-mir-34b-5p	-0.7264461	-0.7264461	0.123566661	-0.346705169	1.676030708
mmu-mir-130a-5p	-0.558150472	-0.780184986	0.0063819	1.713041383	-0.381087824
mmu-mir-484	-1.082065736	-0.760729354	-0.190385491	0.745235985	1.287944596
mmu-mir-92b-5p	1.079758214	0.781651748	-0.807504617	-1.239595921	0.185690575
mmu-mir-92a-2-5p	0.895213486	0.643648885	0.573589104	-0.72150283	-1.390948645
mmu-mir-337-5p	0.867061716	0.569965774	0.507186346	-0.349161781	-1.595052055
mmu-mir-345-3p	-0.876443569	-0.749698625	-0.450046087	0.64313954	1.433048741
mmu-mir-222-5p	-1.178489848	-0.999433566	0.605270598	0.71805017	0.854602646
mmu-mir-409-3p	0.857708196	0.717017814	-1.019071681	0.604595395	-1.160249724
mmu-mir-126-3p	0.828545555	0.914826709	-1.405927945	-0.639379484	0.301935165
mmu-mir-363-3p	0.931106117	1.230812345	-0.559987464	-0.904563159	-0.697367838
mmu-mir-28-5p	-1.348688713	-0.773415843	0.844876893	0.802006724	0.475220938
mmu-mir-34b-3p	-1.084723442	-1.013581956	0.309248915	0.670887648	1.118168836

mmu-mir-218-5p	-1.173214698	-0.961554815	0.441457305	0.658983595	1.034328613
mmu-mir-214-5p	-1.032612924	-1.153467334	0.767797646	0.772179585	0.646103027
mmu-mir-369-3p	0.819625189	0.781160181	-0.053047074	0.097176893	-1.644915189
mmu-mir-18a-5p	0.746220992	1.224820383	-0.203372725	-1.29570965	-0.471959
mmu-mir-708-5p	1.101763741	0.741676358	-0.942318904	0.235755007	-1.136876202
mmu-mir-429-5p	-0.98581515	-0.98581515	1.228336864	0.003351347	0.73994209
mmu-mir-380-3p	0.668480485	0.511711683	0.347536421	0.237016846	-1.764745434
mmu-mir-320-5p	-0.679690865	-1.196074522	1.258361716	-0.099561689	0.71696536
mmu-mir-294-5p	1.211421847	0.95818742	-0.583871158	-0.882718294	-0.703019815
mmu-mir-340-5p	0.69550888	0.672056407	0.54078614	-0.264518061	-1.643833365
mmu-mir-145-5p	-1.09963732	-1.075772515	0.532399269	0.834162668	0.808847898
mmu-mir-32-5p	0.891877522	1.147065976	-0.786891288	-1.118864245	-0.133187964
mmu-mir-96-5p	0.776588809	0.715423795	-0.752451342	-1.381071925	0.641510663
mmu-mir-125a-5p	-1.059450744	-1.094186567	0.420109913	0.891952186	0.841575212
mmu-mir-181b-5p	-1.082584528	-1.101841221	0.641169425	0.849211637	0.694044687
mmu-mir-1839-5p	-1.1465305	-1.013238759	0.665048427	0.970329511	0.524391321

mmu-mir-335-3p	1.264028168	0.896200956	-0.583447318	-0.876497174	-0.700284633
mmu-mir-196b-5p	-0.690162682	-0.811353009	0.80418794	1.342527681	-0.64519993
mmu-mir-669a-3p	0.726714353	0.906622602	-1.023749396	0.53665152	-1.146239079
mmu-mir-669o-3p	0.726714353	0.906622602	-1.023749396	0.53665152	-1.146239079
mmu-mir-106a-5p	1.054224831	1.125753371	-0.600370568	-0.871242117	-0.708365517
mmu-mir-672-5p	1.215956416	0.908228177	-0.822297148	-0.35688292	-0.945004525
mmu-mir-467a-5p	0.558787915	1.011932252	-1.5793724	0.295268185	-0.286615953
mmu-mir-467b-5p	0.558787915	1.011932252	-1.5793724	0.295268185	-0.286615953
mmu-mir-26b-5p	-1.411837546	-0.598910902	0.85293046	0.225172612	0.932645377
mmu-mir-141-5p	-0.683124919	-0.949821936	1.408749497	-0.445337982	0.669535341
mmu-mir-744-5p	-1.085120231	-1.049781908	0.417927051	1.047970105	0.669004984
mmu-mir-290-5p	1.170712894	1.006818247	-0.602974493	-0.866511461	-0.708045187
mmu-mir-25-5p	1.085125299	0.803254538	-1.400935606	-0.024788652	-0.462655579
mmu-mir-22-5p	-1.037835797	-1.151227053	0.738144724	0.733638023	0.717280104
mmu-mir-151-5p	-0.851092325	-1.289492081	0.602870246	0.585667185	0.952046975
mmu-mir-155-5p	-0.98581515	-0.98581515	1.228336864	0.003351347	0.73994209

mmu-mir-30b-5p	-0.618767879	-0.73124891	-0.273615253	-0.107271986	1.730904029
mmu-mir-23a-5p	-0.679690865	-1.196074522	1.258361716	-0.099561689	0.71696536
mmu-mir-186-5p	-1.541821219	-0.427485567	0.542695481	0.460407329	0.966203977
mmu-mir-7b-5p	0.826763385	0.826763385	0.153515356	-1.602326123	-0.204716003
mmu-let-7d-5p	-1.203884051	-0.979387439	0.739354117	0.687533155	0.756384218
mmu-mir-380-5p	0.598227515	0.558247561	0.354959944	0.259730428	-1.771165448
mmu-mir-181a-5p	-1.127928639	-1.04047363	0.49627515	0.857253589	0.814873529
mmu-mir-18b-5p	1.034624059	1.14572758	-0.609237978	-0.861357186	-0.709756475
mmu-mir-135b-5p	1.14045334	0.947155791	-0.308678931	-1.139147974	-0.639782226
mmu-mir-302a-5p	0.735559299	1.385537086	-0.576783657	-0.856148067	-0.688164662
mmu-mir-127-5p	0.9613894	0.597485102	0.204764599	-0.132953075	-1.630686026
mmu-mir-20b-5p	1.075561941	1.106996325	-0.614331957	-0.857102939	-0.71112337
mmu-let-7b-5p	-1.066897099	-0.813260898	1.03943512	1.03943512	-0.198712242
mmu-mir-100-5p	-1.219127381	-0.953594186	0.774566972	0.815297837	0.582856758
mmu-mir-98-5p	-1.107001214	-1.062574038	0.664492906	0.56373245	0.941349897
mmu-mir-210-5p	-0.684066985	-0.55285817	-0.010726861	-0.482511952	1.730163968

mmu-mir-27a-5p	-0.67767914	-1.087949457	-0.16767361	0.486977354	1.446324852
mmu-let-7i-5p	-1.389599384	-0.738349655	0.770770215	0.744919781	0.612259043
mmu-mir-541-5p	-0.504606806	-0.581060065	1.77048965	-0.481365432	-0.203457348
mmu-mir-16-5p	0.822611165	0.822611165	-0.752960422	-1.363084249	0.470822341
mmu-mir-29b-1-5p	-0.98581515	-0.98581515	1.228336864	0.003351347	0.73994209
mmu-mir-434-5p	0.605008535	0.490010264	0.341412624	0.341412624	-1.777844047
mmu-mir-199b-5p	-0.842720743	-0.842720743	-0.296814442	0.477866136	1.504389791
mmu-mir-101a-5p	-0.98581515	-0.98581515	1.228336864	0.003351347	0.73994209
mmu-mir-146a-5p	-1.390470708	-0.730450445	0.609265397	0.65765081	0.854004946
mmu-mir-485-5p	0.861852819	0.520607946	0.067344699	0.257612875	-1.707418339
mmu-mir-199a-3p	-1.407392385	-0.709879868	0.82330762	0.659423717	0.634540915
mmu-mir-292-3p	1.121258388	1.062389781	-0.625026501	-0.845638439	-0.712983229
mmu-mir-26a-5p	-0.830297047	-1.126720967	1.274323702	0.037892039	0.644802273
mmu-mir-291a-3p	1.092272756	1.092272756	-0.628574468	-0.842218081	-0.713752964
mmu-mir-291a-5p	1.105212865	1.079518508	-0.63082806	-0.83977092	-0.714132393
mmu-mir-200c-5p	-1.215084391	-0.646893281	1.258776203	-0.109893779	0.713095248

mmu-let-7e-5p	-1.215284582	-0.965558401	0.696887576	0.787067832	0.696887576
mmu-mir-17-5p	0.977440373	1.167725205	-1.021181393	-0.504779754	-0.61920443
mmu-mir-199a-5p	-1.319036373	-0.822211066	0.542679196	0.722144354	0.876423889
mmu-mir-293-5p	1.153430098	1.029092692	-0.628697284	-0.840631323	-0.713194183
mmu-mir-134-5p	0.710219381	0.539909413	0.202042066	0.300770245	-1.752941106
mmu-let-7g-5p	-1.292363053	-0.873880565	0.7400009	0.7400009	0.686241819
mmu-mir-151-3p	-0.88412563	-0.930078105	-0.114386927	0.474162058	1.454428604
mmu-mir-29a-5p	-0.901595368	-0.901595368	-0.153521812	0.511279918	1.445432629
mmu-mir-423-5p	1.108862953	0.861815565	-0.307328283	-0.307328283	-1.356021953
mmu-mir-31-5p	-1.053952595	-0.670203131	0.469000265	-0.218691383	1.473846844
mmu-mir-205-5p	0.244694415	1.550427178	-0.153173944	-1.108064327	-0.533883321
mmu-mir-30e-5p	0.719803136	1.383467051	-0.576376699	-0.950516789	-0.576376699
mmu-mir-411-5p	0.626926222	0.490171878	0.388004116	0.268105912	-1.773208129
mmu-mir-191-5p	0.987192255	1.184675213	-0.558651293	-0.872454924	-0.74076125
mmu-mir-93-5p	0.833517295	0.961958181	-1.471294349	-0.447249829	0.123068702
mmu-mir-24-1-5p	-0.974537103	-1.089211277	0.352617392	0.48436974	1.226761248

mmu-mir-221-5p	-1.377087489	-0.71134813	0.386565446	0.850935086	0.850935086
mmu-mir-20a-5p	0.925809899	1.224524063	-0.481638827	-0.736446689	-0.932248446
mmu-mir-125b-5p	-1.310836886	-0.805372541	0.978205517	0.688729239	0.449274671
mmu-mir-10b-5p	-1.212217844	-0.963762002	0.600441047	0.787769399	0.787769399
mmu-mir-152-5p	-0.955124441	-0.895736336	-0.253773935	0.996420704	1.108214008
mmu-let-7c-5p	-0.973808336	-0.709670569	1.167276121	0.98346296	-0.467260176
mmu-mir-292-5p	1.139099545	1.045383642	-0.637963419	-0.83142451	-0.715095258
mmu-mir-183-5p	1.065325947	1.065325947	-0.956751309	-0.837716013	-0.336184573
mmu-mir-148a-5p	1.130934866	0.582334924	-0.842815071	0.368728302	-1.239183021
mmu-mir-99b-5p	-1.209238526	-0.969722518	0.775913156	0.775913156	0.627134733
mmu-let-7a-5p	-1.077520721	-1.03625814	1.069364182	0.717370602	0.327044076
mmu-mir-203-5p	-0.98581515	-0.98581515	1.228336864	0.003351347	0.73994209
mmu-mir-378-5p	-1.206254077	-0.662261248	1.258643455	-0.10506769	0.71493956
mmu-mir-101b-5p	-0.98581515	-0.98581515	1.228336864	0.003351347	0.73994209
mmu-mir-10a-5p	-1.133709768	-1.049987201	0.820644632	0.751581831	0.611470507
mmu-mir-103-2-5p	-0.575018947	-0.614724049	1.752660862	-0.456400629	-0.106517238

mmu-mir-143-5p	-1.045425556	-1.045425556	1.021322666	0.850299703	0.219228742
mmu-let-7f-5p	-1.185270703	-0.844410222	0.96779423	0.96779423	0.094092465
mmu-mir-7a-5p	0.956115329	0.956115329	-0.886332793	-1.168642428	0.142744562
mmu-mir-146b-5p	-1.002326176	-0.604291396	-0.007564157	-0.007564157	1.621745885
mmu-mir-182-5p	0.653560195	0.653560195	-1.746227534	0.219553572	0.219553572
mmu-mir-21-5p	-1.317874511	-0.841751398	0.719875303	0.719875303	0.719875303

Appendix 11 : mouse mRNA heat map						
gene_Name	Keratinocytes 1	miPS^{yam}	Keratinocytes 2	mES	ΔNp63-/-2	ΔNp63-/-1
Atg9b	0.941095982	-0.638169181	1.331344809	-0.714579917	-0.777433955	-0.774623836
Rab11fip5	0.898817111	-0.862972475	1.035336778	-0.838292611	-0.612829849	-0.591556738
Slc13a5	-0.708459579	0.820541211	-0.716276687	1.23407858	-0.716461843	-0.713369744
BC080695	-0.418774042	0.204377529	-0.411019187	2.411686279	-0.446567645	-0.446567645
Cdsn	0.499235746	-0.692895928	0.760569512	-0.683373047	-0.669679101	-0.679496586
Ppp1r13l	1.094484909	-0.713277701	1.464029063	-0.742331577	-0.650151367	-0.630131869
Mdk	-0.5567058	1.823087285	-0.554514901	1.395405623	-0.525740905	-0.496513945
Lrrn4cl	1.593031607	-0.818831771	1.570596229	-0.823649711	-0.363498385	-0.419293774
Trim6	-0.548380717	1.533632919	-0.535988116	1.703342008	-0.54387307	-0.544873282
Zscan4c	-0.434770372	0.336806661	-0.440532612	2.378464598	-0.460695206	-0.460695206
Aim2	-0.676190231	0.155420948	-0.680178291	1.664199257	-0.658488857	-0.682220844
Amt	-0.581620646	1.655363565	-0.531185326	1.583823882	-0.530848974	-0.531429547
Gm13154	-0.506487753	0.889020144	-0.515714351	2.158513501	-0.519612322	-0.522108253

Shc2	-0.719994269	-0.270554815	-0.699427833	-0.403074714	1.57113998	1.630439963
Cadm1	1.064519227	0.719101524	1.244631773	0.057131312	-1.117551787	-1.114772944
Fat2	1.328607267	-0.709557508	1.290497521	-0.703193637	-0.729016487	-0.731982181
Krtdap	1.307365699	-0.674489106	1.353968363	-0.722215645	-0.751595495	-0.744097177
Zbtb16	1.279994175	-0.626165703	1.843559118	-0.623173396	-0.628839131	-0.625853687
Zscan10	-0.564090185	1.441584472	-0.565294056	1.780009731	-0.56533824	-0.566086251
Gm98	-0.749991711	0.249086941	-0.751770683	1.261641186	-0.489254371	-0.528661526
Zfp936	-0.514036658	0.936104339	-0.512228542	2.133764719	-0.513436719	-0.513174636
Golm1	-1.300720229	1.235413236	-1.28963945	0.83679283	0.644822778	0.485143964
Gm13051	-0.533211379	1.3161847	-0.534639956	1.886339655	-0.534970259	-0.535072318
Klk13	0.425643472	-0.552594843	0.228300369	-0.55592801	-0.601286861	-0.601286861
Kcnj15	1.736519775	-0.745111521	0.966090707	-0.757658366	-0.546995016	-0.678141924
Gm13152	-0.353553391	-0.353553391	-0.353553391	-0.353553391	-0.353553391	-0.353553391
Gm14137	1.365935645	-0.738708376	1.182342299	-0.746276509	-0.810440101	-0.794973278
Nynrin	-0.87581302	-0.391987277	-0.863201742	-0.422501924	0.856209276	0.788152111
Mtmr7	-0.538628835	1.479696426	-0.538628835	1.752076583	-0.538628835	-0.538628835

Trim71	-0.579171922	0.972057082	-0.577905039	2.101315316	-0.524160029	-0.52923168
Pitx2	-0.461068821	2.44909245	-0.421308735	-0.083757848	-0.315268329	-0.205054064
Txnrd1	-0.794560423	-0.25532281	-0.797573121	-0.101094726	0.880467745	2.068433611
Rbpms	-0.79444892	1.548950719	-0.827636139	1.338713292	0.207979944	0.204193115
Sdr16c6	1.481695187	-0.684040756	1.510601139	-0.684040756	-0.684040756	-0.684040756
G3bp2	-0.880765236	0.803904905	-0.919104855	1.862381487	-0.371743352	-0.3447307
Rbpj	-0.558388351	-0.627029509	-0.70083511	2.166501054	0.290183497	0.578089214
Cubn	-0.432309899	0.034361058	-0.434888813	2.443941833	-0.410847145	-0.416583874
Lrp2	-0.560803854	0.918936743	-0.561176483	2.13720264	-0.385514259	-0.432767039
Cyp2b23	-0.382667867	-0.312325823	-0.383507754	-0.24344385	-0.383507754	-0.383507754
Spink5	1.034734272	-0.708438755	0.853883075	-0.707784702	-0.705719591	-0.707065743
L1td1	-0.662824347	1.147063867	-0.664018257	1.837490564	-0.664018257	-0.664018257
4833423E24Rik	1.668480508	-0.704681173	1.00783983	-0.704681173	-0.704681173	-0.704681173
Nup62cl	-0.891561862	0.840027584	-0.880777421	0.901573476	0.55486641	1.355268488
BC100530	1.419802039	-0.678898385	1.591475313	-0.678898385	-0.678898385	-0.678898385
2410002O22Rik	0	0	0	0	0	0

Kif26a	1.122429888	-0.569399051	1.707205461	-0.608452203	-0.77218655	-0.783980161
Hic1	-0.57265527	-0.476496887	-0.576971875	-0.544836484	1.664367421	1.573130961
Duox1	0.961500663	-0.706174469	1.325919798	-0.72022412	-0.723599307	-0.726388794
Zscan4d	-0.430341415	0.33205933	-0.445504631	2.379779171	-0.459754034	-0.459754034
Pnma5	-0.504047921	0.767545994	-0.48470734	2.218860072	-0.507953944	-0.507953944
Foxi3	-0.57816554	1.726821895	-0.57816554	1.496088924	-0.57816554	-0.57816554
Gm13242	-0.534595998	1.273635276	-0.534076285	1.918216476	-0.537987616	-0.537612863
Ablim1	1.172997334	-0.70880142	1.046331549	-0.755586283	-0.713283056	-0.741523861
Zscan4f	-0.433944582	0.324549807	-0.43817706	2.381850706	-0.45929004	-0.45929004
Ifitm1	-0.711787871	1.559339116	-0.71941954	0.979720524	-0.715193116	-0.71941954
Arhgef10l	1.142237355	-0.71937561	1.009195374	-0.71937561	-0.71937561	-0.71937561
Lrrc32	-0.528075554	-0.54892479	-0.520756129	-0.549785345	1.756086395	1.47495337
Zfp534	-0.520611569	1.143719205	-0.52485038	2.008837732	-0.527367863	-0.528341867
P4ha2	-0.493727044	1.211946547	-0.479370776	0.844704165	0.657044499	0.454018385
1500009L16Rik	-0.575108135	1.777595518	-0.540263885	1.448463338	-0.497985222	-0.482499475
Ralgds	0.902146342	-1.315682454	1.463624877	-1.451189174	0.301794659	0.242888246

9530008L14Rik	1.681565561	-0.670195448	1.350971224	-0.670195448	-0.670195448	-0.670195448
Fam169a	-0.663667229	1.249398446	-0.663667229	1.774901482	-0.663667229	-0.663667229
Hopx	0.525011234	-0.586689433	0.534091313	-0.6134014	-0.654711171	-0.65754198
Serpinb10-ps	1.724526401	-0.686587148	1.111592167	-0.698309081	-0.685639393	-0.698309081
Triml2	-0.534337857	1.737681363	-0.539850991	1.495911451	-0.539850991	-0.539850991
Zscan4e	-0.414812234	0.325368172	-0.441981796	2.381408435	-0.463286119	-0.463286119
Macc1	1.349310634	-0.711976415	1.119539676	-0.724173939	-0.726271095	-0.72707007
S100a14	0.7974865	-0.694032502	0.890223666	-0.691197658	-0.694032502	-0.694032502
Nhs1	1.002912701	-0.901579301	1.310119151	-0.793098279	-0.519447926	-0.57914153
Abcc4	-0.776950861	-0.401501984	-0.724499823	0.104132719	-0.063111738	0.19180664
Lass3	1.198592754	-0.720382991	1.010616979	-0.724142279	-0.721055379	-0.722508523
Bend4	-0.64883416	1.354280306	-0.589470316	1.709204254	-0.706084325	-0.690716216
Dmkn	1.033815565	-0.707700414	0.94950233	-0.710380062	-0.722757723	-0.722093826
Armcx2	-0.974343315	0.164118764	-0.922823897	0.165521508	1.292588538	1.592746174
Med23	0	0	0	0	0	0
Slc38a1	-1.209261848	0.018149215	-1.20043588	0.186471654	0.810179131	0.873739434

Endou	0.997155488	-0.706792017	0.860159316	-0.706792017	-0.697714349	-0.706792017
Aldh3b2	1.490089448	-0.70616625	1.056767409	-0.709282498	-0.728336294	-0.725690211
EU599041	-0.533484506	1.365180717	-0.532345138	1.848080591	-0.536128743	-0.537833461
Gm4340	-0.417554311	0.399814426	-0.455122716	2.35977565	-0.472862779	-0.472862779
Zfp600	-0.534327271	1.240029879	-0.534327271	1.942597676	-0.534327271	-0.534327271
Grb10	-0.556705447	-0.43375287	-0.5425412	-0.537129072	0.026683641	0.16824617
Cyp26b1	0.599080368	-0.699820845	0.837192229	-0.697725347	-0.625923761	-0.645828377
Rex2	-0.52001371	1.041341401	-0.522242387	2.073272586	-0.524988926	-0.5253308
Gm10324	-0.471354929	0.496143716	-0.468253509	2.328884437	-0.471354929	-0.471354929
Tfdp2	-0.872526098	0.403675142	-0.892697442	1.692038274	-0.280819836	-0.47725291
Zscan4b	-0.412420396	0.257522518	-0.436106032	2.399172734	-0.45296302	-0.45296302
Armcx4	-0.989928521	1.041573905	-0.978522747	1.251615911	0.651343557	0.716061012
H60c	0.081794082	-0.541527231	0.3295911	-0.549614283	-0.563169348	-0.561380379
2610528A11Rik	1.839690437	-0.669623185	1.194189773	-0.674143174	-0.641998647	-0.637079922
Usp44	-0.541807245	1.320923754	-0.549548281	1.88222031	-0.549548281	-0.527924513
Gm13247	-0.532786998	1.277512705	-0.533580087	1.915404722	-0.535564625	-0.535564625

Gm9573	-0.340345898	-0.357013491	-0.349778036	-0.355703855	-0.359419261	-0.358126557
Slc7a7	-0.535859847	1.840497334	-0.535859847	1.374661745	-0.535859847	-0.535859847
Agrp	1.728375969	-0.557285186	1.502347115	-0.556840656	-0.568408801	-0.556486223
Alpl	-0.729307529	0.657074979	-0.747144644	0.941516825	-0.597712487	-0.697605605
Aplp1	-1.150904274	0.358573459	-1.066993483	0.469384177	0.443152825	0.550691488
Aqp1	-0.110390712	-0.480163301	-0.177016492	-0.439644545	-0.396547671	-0.395474325
Arg1	1.167001362	-0.709255898	0.774292245	-0.707658636	-0.706974798	-0.709681807
Arnt2	-0.492094548	-0.363737991	-0.48660586	-0.408451545	-0.143680383	-0.07337922
Slc7a3	-0.823828524	0.480522954	-0.933671465	0.733632228	-0.266858307	-0.178847699
Bcat1	-1.16176139	0.014067438	-1.16176139	0.480029273	1.170691026	1.404704895
Bmp8a	0.634363125	-0.245962615	2.043167965	-0.607111021	-0.732769273	-0.805856401
Cbr2	1.282982671	-0.73714777	0.96933341	-0.731603941	-0.710136545	-0.729484761
Cited1	-0.55349626	0.302150996	-0.575133754	0.275762054	-0.584263989	-0.575695073
Col17a1	1.305072606	-0.710439165	1.43205906	-0.70869074	-0.719663676	-0.719301137
Crabp2	1.360157114	-0.656406881	0.995735126	-0.670365788	-0.745489867	-0.771347416
Ctsk	-0.540299495	-0.540168637	-0.541649911	-0.536480231	1.682251945	1.556277818

Cyba	-1.002784804	0.231447921	-0.993775608	-0.463780576	0.987251075	1.129897459
Twist2	-0.539154618	-0.528290126	-0.543081188	-0.543758374	1.159495412	1.997831993
Dsc3	1.367083888	-0.698972901	1.473344585	-0.706539696	-0.708129896	-0.707922215
Edn2	1.08905372	-0.720674717	1.727486058	-0.622292948	-0.729300773	-0.729300773
Phc1	-0.722218913	1.385028803	-0.66966778	1.542299033	-0.700497249	-0.743372707
Foxh1	-0.551361332	1.793526056	-0.554511526	1.42998569	-0.554511526	-0.55275506
Fbp2	-0.709763599	0.777054633	-0.709763599	1.571385635	-0.709763599	-0.709763599
Fgf10	-0.627202291	-0.527212556	-0.615049729	-0.2334674	1.506499825	1.702346641
Fgf15	-0.483369821	2.28291282	-0.482436901	0.61972797	-0.488287791	-0.482796435
Fgf7	-0.575660802	-0.540059014	-0.570523858	-0.576769107	1.530637464	1.703782533
Fst	-0.16278318	-0.446553285	-0.058359298	-0.550516534	-0.322892513	-0.290381806
Fstl1	-0.810339592	-0.684277016	-0.810242877	-0.704495495	1.212149415	1.183432924
Gap43	-1.118097936	1.503411578	-1.118097936	0.297227599	0.277414943	0.359123181
Gas7	0.758645702	-0.917607514	0.857239286	-0.896567125	-0.357687143	-0.267068215
Gata4	-0.566834307	1.281233041	-0.574511565	1.908771462	-0.57558571	-0.565669543
Gdf3	-0.71081046	1.553275836	-0.71081046	1.19916851	-0.709359046	-0.71081046

Gjb4	1.00897024	-0.708568321	0.932324974	-0.650925993	-0.717090426	-0.737459364
Gclm	-1.154966273	0.513722913	-1.172394452	0.875114763	0.26077208	0.170644474
Gna14	-0.383655886	-0.323612057	-0.37782818	-0.230332745	-0.400482351	-0.398029006
Ifi202b	0	0	0	0	0	0
Igfals	-0.425477346	-0.117133027	-0.417232669	-0.174919978	-0.442384635	-0.442384635
Impact	-1.198416628	0.24651951	-1.231319637	0.678742847	0.676535505	0.59160574
Ivl	-0.021879664	-0.475112785	-0.174834273	-0.473797264	-0.430893842	-0.396635335
Klf2	-1.098784352	0.993230307	-1.038619258	1.545137167	0.109386645	0.175843675
Krt15	1.40678147	-0.718382538	0.96259278	-0.718970848	-0.721830658	-0.722588259
Krt16	0.455622147	-0.629625557	0.600532029	-0.632122949	-0.636562548	-0.635722644
Krt19	0.678327919	-0.409658176	0.256375097	-0.695469563	-0.658197321	-0.660281906
Krt1	0.374389895	-0.579470308	0.431839087	-0.607992125	-0.625969105	-0.625969105
Krt4	0.935139042	-0.701353707	0.96552777	-0.706795288	-0.712589295	-0.706554823
Lama1	-0.558561929	1.780493787	-0.557376826	1.446195714	-0.497144611	-0.523925866
Lamb3	1.202220257	-0.671999071	1.574336734	-0.715303336	-0.726562856	-0.729086963
Lamc2	1.252637149	-0.689529986	1.522976421	-0.740323259	-0.746012246	-0.74901837

Lbp	1.362503147	-0.67145067	1.716250201	-0.696561709	-0.63181848	-0.669232943
Lcn2	1.528790887	-0.724300549	1.541956307	-0.72822588	-0.592474682	-0.548570969
Ltf	1.274663628	-0.708996243	1.031511821	-0.726501759	-0.73053875	-0.728434701
Fxyd3	1.382727686	-0.67221684	1.389461721	-0.704198747	-0.728601332	-0.727716768
Mcpt8	-0.493427018	-0.493427018	-0.493427018	-0.493427018	0.69609313	2.251135939
Mest	-0.583681257	0.737098115	-0.533784832	2.229401268	-0.476543416	-0.51952987
Foxc1	1.007779568	-0.858704978	1.09189953	-0.913149464	-0.489272901	-0.486368149
Mme	-0.743835546	1.029758286	-0.747180796	1.218231186	-0.710496878	-0.7401278
Mybl2	-0.75722612	1.198788609	-0.750582123	1.7336928	-0.661577442	-0.657862596
Ndrg1	1.367879429	-0.906563605	1.436664028	-0.926409437	-0.459887033	-0.508497026
Nid2	-0.635747617	1.877237672	-0.635747617	1.309198849	-0.392613227	-0.40941979
Mycn	-0.530492068	1.316949147	-0.53423115	1.885751306	-0.537640668	-0.534046292
Notch1	1.275228271	-0.62555917	1.62107282	-0.643817223	-0.683201539	-0.754091589
Ntn1	-0.624420094	-0.212490031	-0.625900165	-0.096733601	-0.11802255	-0.109330059
Orm1	0.816374525	-0.647860757	0.728435646	-0.706736363	-0.664317987	-0.706736363
Phox2b	-0.354314263	-0.352719627	-0.354314263	-0.351575218	-0.354314263	-0.354314263

Ppl	1.307062273	-0.721312923	1.409728289	-0.727488984	-0.742832711	-0.743461923
Klk8	0.455679447	-0.528838221	0.383362751	-0.58682178	-0.641662738	-0.635273986
Pipox	-0.708326401	0.776969232	-0.704946542	1.155864061	-0.710776854	-0.710776854
Pthlh	0.579160392	-0.676971893	1.061570239	-0.691565311	-0.691565311	-0.685688905
Rbp2	0.142891964	-0.561480236	0.336649575	-0.542131553	-0.550876505	-0.570610684
Bex1	-0.447051712	1.782484343	-0.398762103	1.43310929	-0.615651603	-0.611427509
S100a9	-0.135303636	-0.452303174	-0.050591133	-0.452303174	-0.452303174	-0.452303174
Serpina3a	-0.348725933	-0.356857222	-0.351844558	-0.355726715	-0.356771421	-0.357918991
Sfrp2	-0.551011498	1.771552958	-0.558634659	1.454673938	-0.478675959	-0.484506235
Six1	-0.906895511	1.417623974	-0.889846836	1.495148082	-0.01063756	0.32926831
Serpina1e	-0.350463584	-0.355595511	-0.351935177	-0.350085706	-0.355595511	-0.355595511
Serpina3n	1.229655775	-0.648279398	1.860179609	-0.649391579	-0.608378557	-0.626832401
Serpina5	1.226578851	-0.708287481	1.135642	-0.719365177	-0.732775892	-0.731953758
Sprp1b	1.018249624	-0.714735191	1.003599953	-0.714820371	-0.71762863	-0.716957041
Tbx15	-0.682421778	-0.648247329	-0.673969345	-0.666880847	1.402483698	1.697739806
Tcf15	-0.533939952	1.15969499	-0.537151481	1.997693955	-0.537151481	-0.537151481

Thy1	-0.583772628	-0.495696149	-0.574205735	-0.54987645	1.555696375	1.681401764
Trh	-0.452032672	2.378991716	-0.45305686	0.335343465	-0.45305686	-0.45305686
Tuba3a	-0.5093723	1.037489652	-0.52672128	2.075596561	-0.52672128	-0.517040311
Utf1	-0.538071724	1.446463663	-0.538785091	1.780931705	-0.539086467	-0.539086467
Vdr	1.334791532	-0.798538306	1.406316238	-0.799380034	-0.566245717	-0.585370331
Wnt10a	1.436813083	-0.693312448	1.498836796	-0.694840284	-0.692916955	-0.695577778
Wnt4	1.43078486	-0.675907816	1.377876199	-0.70743916	-0.720660043	-0.721073294
Wnt6	1.218256725	-0.620229966	1.87751918	-0.58454617	-0.652880948	-0.646970761
Wnt7b	1.431841715	-0.658493689	1.422728434	-0.684933349	-0.728587878	-0.727738994
Zfp42	-0.533945127	1.377710876	-0.536528756	1.838041543	-0.536528756	-0.536528756
Zic2	-0.706401285	0.859134629	-0.707478564	0.992372855	-0.699000081	-0.70386656
Zic3	-0.69393384	1.082610216	-0.694565993	1.736673864	-0.691011454	-0.691032134
Actg2	-0.640583784	-0.657952047	-0.631101156	-0.659787863	1.398148636	1.717400601
Adam19	-0.955458445	1.371256368	-0.945510023	0.753566336	0.895315851	0.63486883
Avil	-0.357425346	-0.348877485	-0.361242557	-0.353004676	-0.347642086	-0.353212798
Apoe	-0.732000401	1.542457596	-0.736374851	0.984765093	-0.680752344	-0.68879633

Bst1	1.6901419	-0.62661501	1.363850898	-0.66833152	-0.680999509	-0.678350498
Serping1	-0.968231153	1.454597261	-0.925418302	1.504379585	0.010659182	0.039802891
Car2	-0.601789634	1.22769138	-0.591046318	1.930075016	-0.60477225	-0.609305973
Casp14	1.213135328	-0.683161545	0.754816313	-0.67905195	-0.724566687	-0.719588536
Casq2	0.055224733	-0.54559364	0.546826857	-0.543686388	-0.601153497	-0.595172858
Ch25h	-0.528528339	-0.534050986	-0.532734673	-0.543195146	1.835310488	1.381049539
Cnn1	-0.608680797	-0.067167016	-0.478809376	-0.567318093	1.487623259	1.678073092
Cyct	-0.499559426	0.759574694	-0.484502383	2.222724819	-0.499559426	-0.499559426
Dok2	-0.695868422	1.225524325	-0.693269303	1.684992115	-0.694173969	-0.675135325
Usp17l5	-0.394247267	0.276917343	-0.419411959	2.393712413	-0.467025175	-0.462962701
Lefty1	-0.484815149	2.295694283	-0.490299034	0.586792478	-0.469658379	-0.462630007
Efna3	1.388153063	-0.669926384	1.166433755	-0.609305771	-0.79264085	-0.817902456
Ephb2	-0.74873626	-0.177533491	-0.725301042	-0.208434193	1.733787071	1.414412729
Khdrbs3	-0.90092311	1.498593066	-0.871103651	1.154899563	0.318556497	0.519468332
F2rl2	0.761704044	-0.598360151	2.159637779	-0.592815279	-0.592546963	-0.598360151
Fabp3	-0.611182739	1.79758335	-0.618742908	1.406550598	-0.398383113	-0.347437501

Fgf4	-0.675745327	1.275608215	-0.676914794	1.711769404	-0.676914794	-0.676914794
Fos	1.616773846	-0.691242463	1.512678301	-0.698222057	-0.687798296	-0.680232469
Gata6	-0.792158328	1.153612333	-0.789438539	1.878485729	-0.085994363	-0.062091487
Gbx2	-0.439975888	0.209817301	-0.439975888	2.410689949	-0.433973188	-0.434010179
Tsc22d3	1.301217582	-0.895760555	1.444978886	-0.908952872	-0.531412265	-0.544060927
Pdpr	-0.719180641	-0.151560616	-0.658251762	-0.281528333	1.343569382	1.802395107
Gstt2	-0.562732163	0.868278841	-0.59483155	0.023539722	-0.612398497	-0.649108226
H2-T23	1.441330526	-0.78645999	1.304792861	-0.795553468	-0.638196411	-0.687305288
Foxa2	-0.537829462	1.774078794	-0.54634646	1.454102845	-0.54634646	-0.54634646
Hoxc10	-0.602075472	-0.584451444	-0.59743353	-0.596417143	1.498583166	-0.225963808
Hspa1b	1.571792745	-0.735123381	1.407466429	-0.74246642	-0.565484238	-0.578293866
Hspa1a	1.542906513	-0.697962666	1.520086454	-0.712310615	-0.579024242	-0.581111627
Itga4	-0.387447692	-0.360788879	-0.387845133	-0.364727028	-0.324249026	-0.268488683
Jup	1.164452314	-0.674396421	1.404256828	-0.72264228	-0.871678101	-0.858915736
Kcnab1	-0.498573048	-0.484932723	-0.492987112	-0.493761443	0.678474879	2.258666453
Fabp5	1.05363755	-0.695337653	0.702395367	-0.765312122	-0.617324939	-0.594101515

Klk1	-0.385391807	-0.341834269	-0.385391807	-0.213401091	-0.385391807	-0.385391807
Krt17	1.148818126	-0.712431339	1.28530709	-0.722449591	-0.731403705	-0.731950479
Laptn5	-0.448870998	-0.189624906	-0.449581239	-0.013625371	-0.447401334	-0.447855927
Lef1	-0.58237781	0.658935971	-0.608210388	2.20693956	-0.207265157	-0.115949824
Lipg	1.435080685	-0.618148042	1.628286051	-0.704925378	-0.657841831	-0.607620884
Anxa1	1.177370276	-0.81391491	1.021499134	-0.84783331	-0.599559489	-0.611025886
Ly6d	1.374182261	-0.718922607	1.218439815	-0.721252825	-0.722899995	-0.723773757
Mxd1	0.688164261	-0.729682106	0.971172213	-0.72461821	-0.697541091	-0.684932132
Cd200	0.693787682	-0.690408764	1.335091387	-0.730837399	-0.622166208	-0.710801586
Sik1	1.238107466	-0.687476606	1.537178447	-0.558447476	-0.83944718	-0.82587225
Ndn	-0.888090225	0.083831301	-0.880749558	-0.185755521	1.46640738	1.583138781
Neurod1	-0.516791409	1.01941978	-0.51860588	2.08640509	-0.51860588	-0.51860588
Nfe2l3	1.48670887	-0.644620848	1.559875485	-0.664113392	-0.690421488	-0.693576539
Nefh	-0.5058944	0.862816597	-0.5058944	2.172549805	-0.5058944	-0.5058944
Nefl	-0.531446643	1.17256907	-0.526942848	1.989588498	-0.52719319	-0.522992571
Nsg1	-0.586211818	-0.460311453	-0.601921812	-0.561921325	1.555562485	1.678521555

Orm2	1.297183158	-0.730474811	0.797456475	-0.730474811	-0.670263102	-0.730474811
P2rx7	-0.382594163	-0.282120221	-0.37599294	-0.306720425	-0.376032446	-0.373432234
Pla2g1b	-0.53360526	1.804016519	-0.540924507	1.419141948	-0.540924507	-0.540924507
Pou3f1	-0.521604508	1.756902599	-0.476597048	1.472711445	-0.562697109	-0.562721617
Srgn	-0.55667233	0.183821185	-0.557630428	0.25522529	-0.551718594	-0.549093524
Mapk8ip1	-0.901582695	1.630433665	-0.857108914	1.40245616	-0.064079215	-0.144386181
Klk6	-0.281013254	-0.384566159	-0.252672708	-0.387826064	-0.390594397	-0.390594397
Rgs16	-0.58610727	-0.461880444	-0.5841665	-0.492497981	1.205455757	1.964598739
Rps6ka2	-1.039819724	0.324008645	-0.979589747	0.084924672	1.157743421	1.565385791
Scnn1a	1.619589962	-0.682642498	1.393219535	-0.700937354	-0.680916655	-0.693315865
Ccl9	-0.295280075	-0.356877546	-0.299834271	-0.388181351	-0.374244163	-0.390161391
Sema3f	1.394132189	-0.661579794	1.681748873	-0.683778895	-0.646756488	-0.636741118
Slpi	-0.284862564	-0.468996537	-0.219281944	-0.474503728	-0.336831469	-0.241230635
Sox17	-0.540812735	1.605320008	-0.540812735	1.634944673	-0.540812735	-0.540812735
Sox2	-0.701260243	0.892105592	-0.70161243	1.712178473	-0.70161243	-0.70161243
Sox9	0.765154411	-0.824890268	1.43761933	-0.838814735	-0.585935429	-0.601156589

Spr2a1	1.260815141	-0.722220488	1.273660681	-0.722439929	-0.725244995	-0.724913857
Spr2d	0.906126676	-0.696125871	0.774044777	-0.696125871	-0.690775918	-0.696125871
Spr2h	0.975846873	-0.69433429	0.75909311	-0.696700887	-0.702022609	-0.697900589
Spr2i	-0.29300693	-0.387443361	-0.246628246	-0.387191669	-0.386949061	-0.383721569
Spr2k	-0.03158762	-0.489869227	0.067931462	-0.494977489	-0.486697034	-0.484028646
Sdc1	1.36731704	-0.839221963	1.337546591	-0.848542783	-0.549885005	-0.59742844
Tcea3	-0.828706013	1.046978827	-0.824635753	1.749320572	-0.449910226	-0.440550326
Tdgf1	-0.530554109	1.944184397	-0.532343463	1.237925523	-0.532343463	-0.532343463
Tle4	-0.756431117	1.02101106	-0.747716943	1.57099382	-0.701543103	-0.679671706
Tfrc	-1.200770932	0.909955754	-1.213331957	1.271673301	0.070897194	0.223184292
Uchl1	-0.984838846	0.802129918	-0.984441684	0.470687374	0.984609728	1.3528062
Zfp36	1.303046465	-0.678254301	1.421908168	-0.838587842	-0.737838682	-0.672664499
Adam23	-0.785020121	-0.240629095	-0.760765066	-0.068763909	0.243171603	0.10430855
Gdf15	-0.430731239	-0.379584642	-0.428289397	-0.388632635	-0.177338464	-0.245252433
Grem2	-0.551102452	-0.531604936	-0.545825423	-0.54162802	1.524028223	1.712123603
Klk7	0.057637128	-0.512201218	0.138312161	-0.516121402	-0.517100838	-0.518177352

41155	-0.987211488	1.022044402	-0.964422285	0.583600822	0.802941872	1.257113804
Spry2	-1.057133092	-0.039351558	-1.062399062	0.328383581	0.352333252	0.727005569
Spry4	-0.906417551	0.492048278	-0.910346916	2.007350879	-0.268086985	-0.019888386
Trex2	1.346600666	-0.717224094	1.316127591	-0.707125313	-0.723583708	-0.723583708
Gnpda1	-0.937730316	0.81466611	-0.916846504	1.01991408	0.185983026	0.081868559
Slc27a2	-0.537557233	1.771052531	-0.539888968	1.457946533	-0.539888968	-0.539888968
Pla2g10	-0.542494251	1.365476291	-0.542494251	1.847775604	-0.542494251	-0.521494116
Vsnl1	1.535536551	-0.704940416	1.037930172	-0.722830861	-0.722830861	-0.708418988
Aoah	-0.402456927	-0.309051123	-0.402456927	-0.147592093	-0.402456927	-0.402456927
Anxa8	1.286484614	-0.76820255	1.313896146	-0.791109417	-0.754085208	-0.780809575
Dsc2	1.11152791	-0.662928169	0.844764937	-0.689433906	-0.72280742	-0.727616911
Gfpt2	-0.932012054	0.896508974	-0.936526519	1.553619239	0.468163345	0.62811861
Hspb1	1.106815924	-0.679427325	1.585611538	-0.681084674	-0.764638897	-0.737621637
Lifr	-0.484676201	-0.272286096	-0.47111999	0.082755468	-0.41386805	-0.429194708
Ltbp2	-0.558467951	-0.540512103	-0.547930391	-0.554308102	1.564976562	1.673137783
Nodal	-0.533073869	1.834111887	-0.53658307	1.382569188	-0.538890513	-0.538890513

Odc1	-1.117191322	1.408708376	-1.135620405	0.986189639	-0.017885904	0.836963826
Pou5f1	-0.58616316	0.297134115	-0.587042393	0.387177906	-0.587042393	-0.587042393

Appendix 12 : mouse-human mRNA heat map										
Gene	NHEK	NHEK_s hDGCR8	NHEK_sh Δ Np63	hiPS ^{Yam}	Keratinocytes 1	Keratinocytes 2	miPS ^{Yam}	mES	Δ Np63-/- 2	Δ Np63-/- 1
SEMA4D	-0.815	-0.296	-0.348	1.459	0.986	1.301	0.266	0.526	-1.583	-1.573
CKS2	-1.489	0.329	0.542	0.618	-0.968	-0.772	1.914	1.333	-0.730	-0.701
FURIN	1.499	-0.534	-0.460	-0.505	-0.222	0.658	-1.460	-1.576	1.103	1.281
MRPL51	-1.437	0.881	0.313	0.243	-0.586	-0.982	1.672	1.387	-1.037	-0.849

PIGG	1.432	-0.409	-0.151	-0.871	1.371	1.040	-0.410	0.289	-1.441	-1.517
SNAPIN	-0.508	0.855	0.814	-1.161	0.615	0.296	-0.466	-0.802	-0.954	-0.884
WDR60	-0.960	1.252	0.337	-0.630	0.096	0.748	-1.562	-1.530	1.008	1.278
WBP11	-1.464	0.225	0.480	0.759	-0.995	-1.029	1.023	2.073	-0.591	-0.507
UBE2W	1.344	-0.772	-0.752	0.180	0.267	-0.051	-1.512	-1.472	1.243	1.384
CNTLN	-1.183	0.001	-0.080	1.262	-0.375	-0.185	-1.261	-1.022	1.682	1.490
RAD54B	-1.479	0.499	0.693	0.287	-0.734	-0.734	1.495	1.865	-0.642	-0.765
ALDH3B1	1.482	-0.481	-0.314	-0.688	-0.617	-0.273	-0.794	-0.919	0.336	-0.136
RRP1B	-1.212	0.742	0.894	-0.424	-1.280	-1.160	1.398	1.637	-0.385	-0.412
KLHL17	-0.906	1.018	0.697	-0.809	1.364	1.550	-1.314	-1.286	0.210	0.081
TULP4	1.483	-0.470	-0.326	-0.687	-0.599	-0.187	-1.186	-1.197	1.333	1.720
PJA2	1.468	-0.567	-0.693	-0.209	0.683	1.003	-1.587	-1.648	0.843	0.759
SECISBP2	-1.132	-0.003	-0.165	1.300	-0.654	-0.872	1.133	1.983	-0.294	-0.045
GPATCH4	-1.312	0.451	1.024	-0.163	-1.402	-1.637	0.836	1.548	-0.008	0.498
PDK2	0.009	0.925	0.457	-1.391	1.469	1.661	-0.856	-0.803	-0.745	-1.018
HOXA7	0.479	0.765	0.219	-1.462	1.074	1.135	-1.485	-1.539	-0.107	-0.067

SLC25A5	-0.818	0.556	1.128	-0.866	-0.773	-1.094	1.301	1.936	-0.581	-0.602
AQP3	1.500	-0.491	-0.497	-0.511	1.773	1.575	-0.739	-0.718	-0.798	-0.791
BRD9	-0.940	-0.567	0.180	1.327	-1.819	-1.352	0.591	0.992	0.452	1.148
NUP188	-0.997	0.849	0.872	-0.725	-0.533	-0.626	1.001	2.210	-0.565	-0.734
GALNT2	1.293	-0.485	0.216	-1.023	-0.221	0.132	-1.178	-1.160	1.971	1.033
MBD1	1.498	-0.561	-0.426	-0.510	0.341	0.408	-1.705	-1.544	0.556	0.947
SDF4	1.481	-0.313	-0.471	-0.697	1.573	1.353	-1.001	-1.620	-0.196	-0.100
RNASEH1	-1.323	-0.148	0.464	1.007	-0.772	-0.821	1.763	1.598	-0.564	-0.507
GNPAT	-0.794	1.339	0.191	-0.735	-0.252	-0.327	1.789	1.460	-1.040	-1.003
ANKRD49	-0.803	0.785	0.942	-0.923	-0.197	-0.871	1.571	1.574	-1.099	-1.010
PRKRIP1	-1.335	0.499	0.974	-0.138	-1.064	-1.819	1.406	0.861	0.805	0.261
PPME1	0.684	0.071	0.681	-1.436	-0.994	-0.941	-0.483	-0.590	1.610	1.678
KIF1B	0.484	-0.686	-0.965	1.167	-0.325	-0.184	-1.604	-0.698	1.835	1.190
SH2D4A	1.465	-0.752	-0.227	-0.486	2.057	1.175	-0.870	-0.590	-0.756	-0.763
CASC5	-1.339	0.740	0.790	-0.191	-0.762	-0.774	1.106	2.169	-0.504	-0.605
CDCA3	-1.455	0.564	0.735	0.157	-0.864	-0.753	1.582	1.614	-0.893	-0.872

ASPM	-1.236	0.783	0.842	-0.389	-0.599	-0.473	0.905	2.181	-0.934	-0.952
NAA15	-1.482	0.619	0.584	0.279	-1.255	-1.526	0.065	1.328	0.565	1.345
FANCA	-1.377	0.746	0.733	-0.101	-1.082	-1.082	1.613	1.621	-0.393	-0.342
PECR	-1.466	0.283	0.403	0.780	-0.436	-0.692	1.842	1.528	-0.836	-0.833
METTL1	-1.454	0.484	0.785	0.185	-0.944	-1.539	1.264	1.531	0.176	0.374
TOPBP1	-1.158	1.015	0.628	-0.484	-1.082	-1.117	1.526	1.704	-0.251	-0.343
KDM5C	-0.573	0.662	1.011	-1.100	-0.175	1.717	-0.051	0.994	-1.358	-1.417
DCAF5	1.444	-0.314	-0.267	-0.863	0.693	0.654	-1.649	-1.620	1.014	0.808
OSTC	-1.299	0.106	0.054	1.139	-0.678	-0.916	1.798	1.554	-0.671	-0.626
ANAPC4	-1.435	0.356	0.199	0.880	-1.664	-1.376	0.944	1.182	0.715	0.540
MND1	-1.482	0.359	0.416	0.707	-0.676	-0.695	1.595	1.772	-0.775	-0.845
DNAJC3	1.343	-0.760	0.183	-0.766	-0.089	-0.241	-1.413	-0.946	1.693	1.374
ERBB2IP	0.501	1.029	-0.255	-1.275	1.164	1.570	-1.343	-1.481	0.029	-0.184
TREX1	1.486	-0.632	-0.543	-0.311	-0.367	-0.820	-0.750	-0.519	-0.063	-0.048
KLC1	1.491	-0.648	-0.412	-0.432	0.790	1.161	-1.546	-1.560	0.824	0.687
MLLT3	-0.201	0.828	0.706	-1.333	1.131	1.648	-1.078	-1.106	-0.696	-0.766

RPS27A	-1.196	-0.272	0.277	1.191	-0.948	-1.187	2.067	0.730	-0.715	-0.465
SLC25A22	-0.903	-0.293	-0.233	1.430	-0.916	-1.623	0.314	0.294	1.488	1.215
MRPS18A	-1.474	0.240	0.554	0.680	-0.558	-0.770	2.219	0.753	-0.774	-0.962
ING4	1.496	-0.413	-0.581	-0.502	1.320	1.539	-0.603	-1.098	-0.920	-0.980
ARF4	1.371	-1.027	-0.233	-0.111	-0.466	-0.477	-0.978	-1.002	1.718	1.599
SF3A1	-1.017	0.437	1.186	-0.606	-1.160	-1.277	0.923	2.006	-0.055	-0.133
SRRM1	-1.492	0.350	0.548	0.594	-0.156	-2.126	0.934	1.307	-0.340	-0.418
LGALS8	1.449	-0.739	-0.581	-0.129	0.427	1.968	-1.250	-1.457	0.484	-0.081
BAG2	-1.450	0.193	0.438	0.818	-0.593	-0.826	-0.868	-0.954	1.409	1.814
LRIG1	-1.030	-0.191	-0.151	1.371	-0.453	-0.224	-1.302	-1.275	1.439	1.506
ALG6	-1.311	0.852	0.704	-0.245	-0.693	-0.984	1.423	1.869	-0.758	-0.611
LMNB2	-1.391	-0.029	0.879	0.540	-0.912	-0.999	1.331	1.935	-0.426	-0.465
XRCC1	-0.720	-0.429	-0.330	1.479	-0.874	-0.478	1.761	1.645	-0.673	-0.630
CDKN2C	-0.862	0.916	0.814	-0.868	-0.139	0.030	-1.653	-1.365	1.009	1.370
RAB12	1.404	-0.736	-0.698	0.031	1.145	0.852	-1.329	-1.642	0.685	0.847
RPS8	-1.458	0.819	0.319	0.319	0.720	0.135	1.390	1.233	-1.292	-1.136

TERC	-0.450	0.788	0.860	-1.199	-0.272	-0.267	1.755	1.435	-0.923	-1.066
KLHL20	1.491	-0.535	-0.349	-0.607	-0.596	-0.758	-1.639	-0.187	1.530	1.405
PUSL1	-1.051	0.890	0.819	-0.658	-1.693	-1.326	0.388	1.523	0.633	0.672
BDP1	-1.066	0.779	0.923	-0.637	0.529	0.256	0.300	2.092	-1.094	-1.110
ZFP91	1.165	-0.129	0.220	-1.256	0.617	0.399	-1.885	-1.498	0.518	0.839
RPS6KA1	0.964	-0.548	-1.126	0.710	-0.143	0.007	0.835	1.939	-1.335	-1.299
TMEM132B	-0.462	-0.504	-0.533	1.499	2.094	1.200	-0.807	-0.790	-0.472	-0.491
NOC4L	-1.346	0.618	0.884	-0.157	-0.749	-1.436	1.542	1.623	-0.269	-0.092
CAPN10	-1.398	0.909	0.468	0.021	-0.829	-0.853	1.878	1.492	-0.548	-0.417
KDELR2	0.004	0.700	0.711	-1.416	-0.797	-0.224	-1.022	-1.140	1.520	1.623
CLSPN	-1.454	0.630	0.684	0.140	-1.364	-1.264	1.366	1.612	-0.058	0.110
ATXN1L	1.456	-0.469	-0.200	-0.787	1.165	1.295	-1.540	-1.473	0.541	0.153
DGCR6	-0.447	0.814	0.834	-1.201	1.173	1.532	-0.431	-0.970	-1.245	-0.986
ERLIN1	0.330	1.253	-0.975	-0.609	2.152	0.825	-0.639	-1.347	-0.138	-0.435
CIB2	-1.188	0.181	-0.220	1.227	1.380	1.710	-0.740	-0.995	-0.873	-0.894
CHD7	-1.418	0.330	0.164	0.924	-0.578	-0.209	0.970	2.150	-1.013	-0.976

SHCBP1	-1.204	0.373	1.145	-0.315	-0.950	-1.103	1.824	1.443	-0.506	-0.376
DPYSL3	-0.515	-0.503	-0.482	1.500	-0.837	-0.560	-0.869	-0.780	1.323	1.962
EXPH5	1.484	-0.499	-0.316	-0.669	1.530	1.669	-0.840	-0.842	-0.845	-0.848
PHF11	1.387	-0.796	-0.661	0.069	-0.882	-0.882	0.142	2.278	-0.375	-0.882
SLC35E2	1.468	-0.312	-0.380	-0.776	-1.259	-0.770	-0.187	2.331	0.047	0.389
MKI67IP	-1.491	0.648	0.439	0.404	-0.666	-1.086	1.391	1.876	-0.737	-0.596
DCAF17	-0.020	-0.594	-0.802	1.416	-0.603	-0.714	1.550	1.870	-0.682	-0.682
KIF15	-1.397	0.104	0.329	0.964	-0.820	-0.817	1.514	1.868	-0.604	-0.566
RPL27A	-0.934	-0.249	-0.235	1.418	0.482	-0.061	1.962	0.792	-1.354	-1.046
SNHG3	-1.449	0.837	0.226	0.386	-1.407	-1.061	0.951	1.941	-0.434	0.071
EIF2B5	-1.204	-0.225	0.224	1.205	-0.461	-0.804	1.429	1.730	-1.087	-0.948
MRPS17	-1.377	0.836	0.630	-0.090	-0.807	-1.681	1.844	0.999	-0.198	0.062
EIF1AD	0.056	0.440	0.910	-1.406	-0.543	-1.457	1.301	1.714	-0.633	-0.627
BNIP3L	1.427	-0.580	-0.790	-0.058	1.338	1.441	-0.563	-1.360	-0.794	-0.771
PLXNA2	1.493	-0.478	-0.387	-0.628	1.470	1.300	-1.424	-1.395	-0.077	-0.292
ANKHD1	1.082	0.398	-0.204	-1.276	1.356	1.714	-0.914	0.361	-1.015	-1.050

SAT1	1.500	-0.505	-0.491	-0.504	1.121	1.144	-1.448	-1.729	0.133	0.471
DHX34	-1.425	0.639	0.748	0.039	0.039	0.524	1.130	0.465	-1.550	-1.730
CDK2AP1	-1.042	-0.147	-0.176	1.364	-1.056	-1.187	1.483	1.689	-0.379	-0.416
IQGAP1	0.900	-0.784	-0.944	0.827	0.889	0.859	-1.082	-1.643	1.233	0.511
PRCC	-1.116	0.799	0.888	-0.571	-0.050	0.142	1.062	1.882	-1.283	-1.242
CKS1B	-1.243	0.180	-0.123	1.186	-1.067	-1.030	2.034	1.141	-0.372	-0.380
CCZ1	-1.279	0.195	-0.065	1.150	-1.129	-0.632	1.726	1.631	-0.542	-0.514
NCAPG	-1.384	0.808	0.653	-0.076	-0.887	-0.815	1.724	1.675	-0.589	-0.519
KIF22	-1.495	0.484	0.402	0.608	-0.850	-0.827	1.577	1.779	-0.636	-0.661
TCTN1	-0.403	0.894	0.734	-1.225	1.236	1.742	0.384	-0.811	-0.875	-1.212
CALHM2	-0.569	1.498	-0.471	-0.457	-0.229	-0.003	-1.462	-1.511	1.376	0.912
RAB17	-0.461	-0.512	-0.526	1.499	1.243	1.236	-0.986	-0.747	-0.915	-0.915
NEK2	-1.260	0.814	0.794	-0.347	-0.949	-0.842	1.469	1.744	-0.754	-0.769
KPNA4	0.562	-1.112	-0.530	1.080	-0.351	-1.137	-0.802	-0.479	1.748	1.470
ITM2C	-0.595	-0.493	-0.408	1.496	0.502	0.734	-1.263	-1.698	1.078	1.187
MLPH	0.163	-0.757	-0.757	1.351	1.387	1.134	-0.964	-0.926	-0.897	-0.932

RNASEH2B	-1.500	0.503	0.511	0.486	-1.279	-1.048	1.346	1.758	-0.038	-0.311
COMMD10	0.122	-0.699	-0.791	1.368	-0.980	-1.427	1.990	0.888	-0.020	0.213
MTX1	-1.273	0.992	0.563	-0.281	-0.878	-0.871	1.647	1.616	-0.785	-0.273
TOB2	1.225	-0.753	-0.877	0.405	0.856	1.398	-1.725	-1.452	0.098	0.212
METAP2	-1.493	0.496	0.379	0.617	-0.498	-1.273	1.548	1.319	-1.009	-0.832
DEPDC7	0.628	0.331	0.530	-1.489	1.445	1.805	-0.469	-0.432	-1.001	-1.024
DPP8	1.149	0.271	-0.164	-1.256	0.790	0.894	-1.642	-1.649	0.762	0.737
HTATSF1	-1.183	0.778	0.878	-0.474	0.227	-2.127	0.667	-0.650	0.615	1.421
ABL2	1.188	-0.088	0.148	-1.248	-1.046	-0.979	-0.918	0.215	1.333	1.792
NME1	-1.242	0.877	0.741	-0.376	-1.484	-1.711	1.366	0.579	0.571	0.555
ARL8B	1.469	-0.254	-0.466	-0.749	0.902	0.819	-1.634	-1.685	0.729	0.595
SMC4	-1.352	1.024	0.353	-0.025	-1.072	-0.871	1.422	1.738	-0.874	-0.496
UBR2	-0.351	0.694	0.909	-1.252	0.592	2.033	-0.828	-1.454	0.476	-0.577
NR1D1	1.479	-0.585	-0.637	-0.257	0.470	1.508	-1.516	-1.531	0.747	0.423
EIF2D	-0.875	0.604	1.093	-0.822	-0.146	-0.195	1.472	1.524	-1.356	-1.218
RPN2	-1.395	-0.047	0.644	0.798	-1.471	-1.524	0.698	-0.040	1.478	0.890

LRRC40	-1.287	0.992	0.546	-0.251	-0.604	-0.577	1.499	1.914	-0.684	-0.730
RPL36AL	-1.399	0.970	0.147	0.283	-0.228	-0.854	1.724	1.429	-1.157	-0.904
ATP11B	1.414	-0.279	-0.195	-0.940	0.735	0.469	1.068	1.011	-1.592	-1.582
ARHGEF17	1.453	-0.367	-0.257	-0.829	0.278	0.593	-1.534	-1.724	1.174	0.913
FUBP1	-1.398	0.213	0.207	0.978	-0.526	-0.680	1.580	1.754	-0.767	-0.845
NUP214	-1.453	0.712	0.602	0.139	-0.947	-1.000	0.513	2.318	0.073	-0.088
MOB1B	1.039	-0.957	-0.749	0.667	0.531	0.727	-1.762	-1.392	1.168	0.856
PSME3	-1.182	1.014	0.613	-0.445	-0.864	-1.727	0.615	1.930	0.058	0.236
WLS	-0.065	0.587	0.861	-1.382	0.482	0.283	-1.458	-1.536	1.424	1.051
SLC39A6	1.293	0.222	-0.503	-1.013	0.278	0.286	-1.456	-1.434	1.306	1.369
ST6GALNAC2	1.500	-0.492	-0.501	-0.507	-0.790	-0.876	1.878	1.468	-0.704	-0.620
LBR	-0.978	0.609	1.080	-0.711	-0.632	-0.617	1.877	1.480	-0.837	-0.716
XPO7	-0.078	0.024	1.250	-1.196	-0.252	-0.260	1.078	2.156	-0.803	-0.809
BRIP1	-1.431	0.874	0.411	0.146	-1.617	-1.507	0.334	1.467	0.665	0.594
ECD	-1.484	0.696	0.370	0.419	-0.748	-1.390	1.198	1.913	-0.387	-0.392
GHDC	-0.116	1.049	0.385	-1.318	0.420	1.298	-1.002	-1.553	-0.200	-0.358

SMARCE1	-1.498	0.424	0.534	0.540	-0.736	-0.972	-0.701	-0.992	1.525	1.620
SPAG5	-1.486	0.656	0.320	0.509	-1.136	-1.082	1.301	1.870	-0.332	-0.448
FKTN	0.345	0.260	0.844	-1.449	-0.385	-0.529	-1.107	-0.223	1.699	1.582
PPCS	1.408	-0.528	-0.860	-0.020	-0.610	-0.909	1.437	1.944	-0.696	-0.570
ACER3	-1.309	0.131	1.126	0.052	1.896	0.894	-0.984	-1.473	-0.147	-0.409
NT5DC1	-1.413	0.910	0.098	0.405	-0.366	-0.794	1.714	1.642	-0.810	-0.817
EXOSC4	-0.749	0.528	1.144	-0.923	-0.195	-0.692	1.834	1.223	-0.999	-1.223
TNRC18	1.365	-0.217	-0.111	-1.037	0.676	1.079	-1.635	-1.492	1.013	0.515
CHAF1A	-1.451	0.360	0.252	0.838	-1.055	-1.115	1.353	1.876	-0.284	-0.260
OSBPL9	-0.723	0.280	-0.851	1.294	1.331	0.898	-1.805	-1.204	-0.162	0.803
GAR1	-1.387	0.496	0.911	-0.019	-0.765	-1.093	1.833	1.427	-0.519	-0.546
LSM3	-1.476	0.617	0.618	0.240	-0.938	-0.908	1.819	1.528	-0.631	-0.434
RIPK1	0.129	-0.287	1.281	-1.122	-0.058	-0.307	-1.744	-1.212	1.272	1.167
ATF7	1.470	-0.316	-0.387	-0.767	0.807	1.687	-1.629	-1.302	0.317	-0.135
NDUFA10	0.700	-0.714	1.007	-0.993	-0.321	-0.723	2.131	0.931	-0.146	-0.304
FOXRED1	-1.345	-0.178	0.770	0.753	-0.215	-0.459	1.792	1.294	-1.161	-1.199

TGOLN2	1.334	-0.708	0.199	-0.825	1.091	1.407	-0.339	0.246	0.445	-1.950
HMMR	-1.434	0.279	0.264	0.892	-0.780	-0.724	1.435	1.830	-0.864	-0.818
HOXB7	-0.825	1.059	0.648	-0.882	0.544	0.549	-1.663	-1.633	0.181	1.273
IFNAR2	-1.029	0.630	1.055	-0.656	1.391	1.040	-1.351	-1.675	-0.084	0.108
ZZEF1	0.535	0.172	0.750	-1.457	1.267	1.824	-1.297	-1.015	-0.259	-0.334
ZWILCH	-1.416	0.470	0.067	0.878	-0.779	-0.818	1.627	1.784	-0.630	-0.588
MARCKS	0.551	-0.986	-0.685	1.120	-0.159	-0.018	-1.415	-1.471	1.320	1.422
LZIC	1.398	-0.224	-0.197	-0.977	-1.491	-1.640	1.106	0.399	0.576	-0.205
TSTD2	-0.783	-0.313	-0.372	1.467	-0.782	-1.138	-1.157	0.182	1.428	1.593
NOM1	-1.149	1.064	0.564	-0.479	-0.665	-1.202	1.621	1.722	-0.359	-0.366
H2AFX	-1.433	0.082	0.792	0.559	-0.690	-0.670	1.422	1.977	-0.694	-0.667
HIST1H2AD	-1.030	0.767	0.943	-0.680	-0.840	-0.697	1.743	1.539	-0.711	-0.731
STRADB	-1.366	0.910	0.544	-0.088	1.016	2.056	-1.025	-1.068	-0.354	0.051
ICMT	-1.482	0.310	0.689	0.483	-0.241	-0.164	-1.213	-1.178	1.524	1.549
ZBED4	1.460	-0.518	-0.193	-0.749	-0.469	-0.400	1.116	2.104	-0.937	-1.007
HIST1H2AE	-0.541	0.196	-0.970	1.315	-0.834	-0.713	1.925	1.312	-0.736	-0.752

PFKFB4	1.498	-0.477	-0.443	-0.578	-0.338	0.104	-1.209	-1.134	0.261	0.365
SPC24	-1.377	0.631	0.835	-0.089	-0.683	-0.620	1.752	1.638	-0.770	-0.844
BCL6	1.500	-0.503	-0.520	-0.476	1.269	1.736	-1.277	-1.268	-0.103	-0.217
NDUFV2	-0.301	-0.578	-0.606	1.486	-0.449	-1.174	2.063	0.978	-0.944	-0.457
CSE1L	-1.482	0.502	0.300	0.679	-0.921	-1.110	1.536	1.776	-0.265	-0.435
FEN1	-1.494	0.444	0.626	0.424	-0.968	-0.979	1.434	1.854	-0.528	-0.537
NDST2	0.161	0.648	0.651	-1.460	0.608	1.181	-1.421	-1.679	0.968	0.489
ALDH3A2	1.495	-0.393	-0.601	-0.500	0.352	0.345	-1.424	-1.170	1.442	1.363
PIK3CA	1.479	-0.502	-0.692	-0.285	0.373	0.885	-1.544	-1.486	1.097	1.097
FAM136A	-1.494	0.500	0.390	0.604	-0.042	-0.539	1.099	2.067	-1.009	-1.018
LRP12	1.477	-0.574	-0.250	-0.652	-0.233	-0.330	-1.155	-1.228	1.735	1.384
RABAC1	1.324	0.204	-0.626	-0.902	1.274	1.832	-0.637	-1.510	-0.390	-0.318
PHF7	-0.430	0.380	1.180	-1.130	0.856	1.112	0.997	0.680	-1.548	-1.405
ELF2	-1.469	0.491	0.738	0.239	1.056	0.766	-1.412	-1.742	0.823	0.701
FXR2	0.094	0.960	0.344	-1.397	-0.919	-0.262	0.982	2.233	-0.634	-0.481
MSN	1.449	-0.839	-0.381	-0.228	-0.180	0.155	-1.210	-1.226	1.577	1.517

TBC1D22A	1.474	-0.500	-0.714	-0.260	1.093	1.728	-0.881	-0.892	-0.966	-0.884
PDZD2	1.496	-0.533	-0.562	-0.402	1.653	1.672	-0.678	-0.648	-0.877	-0.869
DAGLB	1.019	-0.880	-0.837	0.698	0.126	-0.353	-1.524	-1.182	1.574	1.268
SNRPB	-1.443	0.534	0.787	0.122	-1.266	-1.506	1.616	1.132	-0.029	0.298
HTRA2	-0.950	0.684	1.026	-0.760	1.309	0.862	-0.855	-0.398	-1.093	-1.370
HMGB3	-1.480	0.264	0.591	0.625	-1.507	-1.424	1.622	-0.066	0.643	0.771
PUF60	-1.085	0.129	1.300	-0.344	-0.689	-0.607	1.880	1.492	-0.718	-0.888
USP10	-1.454	0.139	0.646	0.670	-0.555	-0.817	1.788	1.642	-0.641	-0.553
TMUB2	1.230	0.036	-0.047	-1.218	0.724	0.735	-1.532	-1.743	0.802	0.854
TSC22D4	1.468	-0.229	-0.512	-0.728	1.109	1.638	-1.192	-1.349	-0.532	-0.404
ATG12	0.005	-0.736	-0.681	1.412	1.398	1.187	-1.456	-1.529	0.285	0.142
MAPRE3	1.373	-0.034	-0.340	-1.000	0.757	1.595	-1.357	-1.546	-0.095	0.175
ATP5O	-1.230	1.005	0.587	-0.362	-1.151	-1.322	2.043	0.571	-0.387	0.464
RUNX2	1.486	-0.546	-0.309	-0.631	0.214	0.611	-1.599	-1.611	0.922	0.741
PPIB	-1.293	-0.191	0.435	1.050	-1.243	-1.366	1.317	0.911	0.648	0.832
DLGAP4	1.395	-0.729	-0.721	0.055	0.211	0.454	-1.394	-1.564	1.188	1.376

KDELR1	1.491	-0.444	-0.647	-0.400	1.095	1.404	-1.533	-1.515	-0.183	0.148
MOCS1	-1.370	0.079	0.268	1.022	0.668	0.972	-1.537	-1.434	1.032	0.967
RPL36	-1.030	0.881	0.834	-0.684	0.542	0.343	1.858	0.160	-1.568	-1.187
MTG1	-1.294	0.914	0.647	-0.267	-0.601	-0.339	1.823	1.212	-1.145	-1.170
SNRPD3	-1.253	0.619	0.968	-0.334	-0.744	-1.031	1.687	1.680	-0.632	-0.493
DOLK	1.332	-0.075	-0.166	-1.092	-0.583	-0.727	-0.982	-0.917	1.229	1.937
HGSNAT	1.337	-0.012	-0.256	-1.070	0.195	0.248	-1.520	-1.475	1.027	1.512
ABL1	0.099	-0.757	-0.720	1.378	0.999	1.376	-1.578	0.602	0.529	-0.262
MYBBP1A	-1.254	0.719	0.887	-0.352	-0.553	-0.944	1.348	1.949	-0.756	-0.696
MED27	-1.262	0.840	0.765	-0.343	-1.319	-1.726	1.422	0.781	0.379	0.617
KDM5A	-0.361	0.758	0.855	-1.251	1.374	1.601	-0.942	-0.652	-0.873	-0.948
PA2G4	-1.296	0.580	0.961	-0.245	-0.812	-1.138	1.630	1.699	-0.469	-0.339
YWHAЕ	-1.461	0.695	0.595	0.171	-0.626	-0.851	1.005	2.132	-0.975	-0.561
FANCI	-1.246	0.862	0.753	-0.369	-0.878	-0.878	1.530	1.866	-0.454	-0.473
FAM54A	-1.287	0.981	0.563	-0.257	-1.028	-0.915	1.138	2.078	-0.573	-0.270
NCAPD2	-1.444	0.613	0.727	0.104	-0.815	-0.611	1.365	2.015	-0.659	-0.679

CDCA2	-1.234	0.032	-0.014	1.215	-0.758	-0.441	0.924	2.122	-0.783	-1.043
FOXO3	1.466	-0.377	-0.304	-0.785	1.579	1.543	-1.012	-0.948	-0.579	-0.841
GLT25D1	0.685	0.056	0.691	-1.432	0.767	-1.133	-0.293	-0.840	1.560	1.310
LSM12	-1.405	0.962	0.250	0.194	-1.093	-1.301	-0.663	0.570	0.871	1.869
TOR1A	0.246	0.480	0.743	-1.469	0.171	0.764	-2.368	0.634	0.357	0.858
ANGEL2	-1.124	0.723	0.953	-0.552	1.261	1.175	-0.170	-1.487	-1.487	0.710
KCTD3	-1.293	0.491	1.020	-0.218	-0.033	-0.289	1.380	1.723	-1.151	-1.048
RNMTL1	-0.979	1.085	0.602	-0.709	-0.996	-1.919	0.613	0.396	1.066	1.261
PSME1	0.307	-0.179	-1.261	1.133	-0.132	-0.249	2.278	-0.681	-1.188	-0.646
PPP1R12B	0.153	0.840	0.446	-1.439	-0.134	0.286	-1.504	-1.188	1.917	0.698
MTMR9	0.122	-0.840	-0.646	1.364	-0.709	-0.956	1.601	1.726	-0.610	-0.407
MRPS34	-1.424	0.595	0.785	0.045	0.468	0.084	1.496	0.847	-1.420	-1.655
TOP2A	-1.445	0.836	0.423	0.185	-0.949	-0.806	1.501	1.747	-0.719	-0.716
SNW1	-1.395	0.011	0.474	0.910	-0.574	-0.511	1.220	1.566	-1.354	-1.120
RB1CC1	-1.474	0.682	0.238	0.553	1.118	1.300	-1.616	-1.417	0.551	0.233
PEF1	-0.350	0.713	0.892	-1.254	1.352	1.498	-0.719	-1.540	-0.573	-0.649

TSEN34	0.668	0.676	0.101	-1.445	-1.032	-1.010	1.836	1.331	-0.536	-0.270
CDCA7	-1.477	0.355	0.385	0.737	-0.772	-0.826	1.541	1.830	-0.626	-0.607
ADRB2	1.500	-0.493	-0.495	-0.512	1.477	1.586	-0.794	-0.837	-0.921	-0.905
CHCHD5	-1.387	0.566	-0.048	0.868	0.556	0.534	1.259	0.987	-1.655	-1.351
BUB3	-1.131	0.860	0.823	-0.552	-1.024	-1.220	1.845	1.339	-0.370	-0.204
NPRL2	-1.009	0.654	1.041	-0.686	1.332	1.645	0.151	0.338	-1.240	-0.872
CYP2W1	1.500	-0.518	-0.485	-0.497	1.871	1.189	-0.835	-0.835	-0.835	-0.835
ECHS1	-1.123	0.985	0.685	-0.547	1.330	0.957	0.611	0.102	-1.521	-1.584
PARP2	-1.459	0.580	0.711	0.168	-0.687	-0.659	1.953	1.368	-0.812	-0.518
BAP1	0.131	0.316	0.956	-1.403	-0.429	-0.527	1.796	1.637	-0.686	-0.687
ZMPSTE24	-0.089	1.184	0.156	-1.251	-0.572	-0.956	-1.085	-0.946	1.426	1.565
RFTN1	1.434	-0.065	-0.646	-0.723	-0.642	-0.575	-0.735	-0.719	1.504	1.892
BMP2K	1.494	-0.519	-0.381	-0.594	0.578	1.026	-1.715	-1.626	0.541	0.666
AGPAT6	-1.150	-0.083	1.291	-0.058	-0.619	-0.859	-0.605	-0.901	1.573	1.747
ANKMY2	-1.162	1.022	0.615	-0.475	-0.835	-1.332	1.226	1.834	-0.266	0.210
MACROD1	-0.627	1.392	0.051	-0.817	1.461	1.916	-0.762	-0.967	-0.396	-0.568

FAM49B	-1.148	-0.206	0.076	1.278	-0.598	-0.899	1.751	1.591	-0.855	-0.540
RPS4X	-0.861	0.779	0.949	-0.867	0.095	-0.220	1.811	1.221	-1.411	-0.849
CCDC18	-1.370	0.871	0.595	-0.096	-0.590	-0.518	1.652	1.797	-0.769	-0.635
ARFGEF2	0.498	-0.204	1.008	-1.302	1.089	1.713	-1.781	-0.041	0.239	-0.148
FIP1L1	-1.385	0.867	-0.056	0.573	-0.511	0.315	0.669	1.654	-1.220	-1.590
ABCE1	-1.428	0.457	0.859	0.112	-0.817	-1.484	1.193	1.875	-0.080	0.011
HN1L	-0.767	-0.923	0.588	1.102	-0.894	-0.869	1.366	1.982	-0.499	-0.490
SLC39A1	-1.181	0.123	-0.190	1.247	0.612	0.444	-1.381	-1.912	0.975	0.923
NEDD4L	1.139	-0.788	-0.890	0.539	-0.590	-0.216	-0.557	-0.889	1.442	1.939
MAD2L1	-1.390	0.896	0.515	-0.021	-1.011	-0.983	1.535	1.700	-0.588	-0.584
RNF7	-0.171	-0.740	-0.546	1.458	-0.350	-1.318	1.650	1.562	-0.746	-0.452
LIG3	-1.086	-0.178	-0.072	1.336	0.366	0.041	0.690	1.885	-1.288	-1.373
PSENN	-0.443	1.217	-1.103	0.329	0.792	0.206	-0.642	-1.314	-1.156	-0.172
KIF14	-1.385	0.752	0.714	-0.081	-0.733	-0.560	0.948	2.132	-0.830	-0.913
IPO11	-1.228	0.839	0.791	-0.403	-0.804	-1.049	1.281	2.013	-0.176	-0.312
PPP2R1A	1.027	-1.159	-0.478	0.611	-1.326	-1.279	0.200	0.797	1.393	1.166

INPP5E	-0.057	0.557	0.882	-1.382	0.919	0.668	-1.965	-1.333	0.639	0.774
TRNAU1AP	-1.380	0.767	-0.092	0.706	-0.692	-0.946	1.716	1.369	-0.917	-0.935
LIF	0.322	-0.688	-0.902	1.268	-0.683	-0.729	-0.611	-0.632	0.902	2.278
CCNA2	-1.498	0.455	0.466	0.577	-0.819	-0.839	0.997	2.052	-0.800	-0.842
SLC37A1	-0.735	-0.373	-0.370	1.478	1.715	1.370	-0.318	-0.261	-1.204	-1.204
LARP4	-1.271	0.489	1.039	-0.257	-0.691	-0.387	0.006	2.510	-0.765	-0.633
ZFAND6	0.465	-0.829	-0.825	1.190	0.924	1.017	-0.255	-1.090	-0.973	-1.001
IFT27	-1.478	0.473	0.293	0.712	-1.534	-1.464	1.582	0.565	0.154	0.329
USE1	-0.800	1.004	0.714	-0.918	-0.769	-0.769	1.455	1.856	0.047	-0.769
HIST1H2AI	-1.217	0.533	1.049	-0.366	-0.843	-0.714	1.806	1.439	-0.723	-0.749
ALDH9A1	-1.345	0.876	0.632	-0.163	-0.515	-0.600	2.108	1.226	-0.679	-0.629
DDX59	-1.067	1.049	-0.609	0.626	-0.771	-0.947	1.750	1.482	-0.840	-0.351
RNF26	-0.167	-1.186	0.107	1.246	-1.965	-0.946	-0.540	1.321	0.727	0.638
METTL3	-1.482	0.655	0.540	0.287	-1.179	-1.179	1.285	1.362	0.324	0.374
CCDC115	1.441	-0.826	-0.467	-0.149	-1.070	-1.403	1.075	1.771	0.122	0.239
PSMC3IP	-1.446	0.842	0.209	0.395	-1.046	-1.046	1.505	1.712	-0.474	-0.536

NUP85	-1.225	1.014	0.579	-0.368	-0.891	-1.064	1.698	1.655	-0.456	-0.369
EXOSC5	-1.428	0.338	0.189	0.900	-0.456	-0.766	1.809	1.592	-0.633	-0.861
FZR1	0.491	0.308	0.683	-1.482	-0.552	-0.390	1.233	1.941	-1.065	-1.016
DDX41	0.078	-1.251	-0.022	1.195	-0.592	-0.781	1.548	1.744	-0.822	-0.895
CDC7	-1.233	0.792	0.835	-0.394	-0.935	-0.866	1.762	1.621	-0.301	-0.322
TSN	-1.486	0.617	0.566	0.303	-1.406	-1.492	0.520	1.337	0.699	0.904
MTPN	0.796	-0.029	0.634	-1.401	-0.348	-0.484	-0.958	-0.993	1.738	1.613
DST	1.500	-0.484	-0.536	-0.480	1.293	1.843	-1.092	-1.092	-0.555	-0.106
TRAPPC4	-0.532	-0.565	-0.400	1.496	-0.536	-0.862	2.086	1.259	-0.479	-0.524
PSMB1	-1.463	0.799	0.316	0.348	-0.041	0.207	2.094	0.480	-1.198	-1.347
KATNB1	-0.981	0.879	0.845	-0.742	-0.992	-0.739	1.077	2.107	-0.511	-0.661
FNTA	0.939	-0.421	-1.209	0.692	-0.388	-0.541	2.089	0.693	-0.987	-1.134
MCL1	1.087	-0.776	-0.920	0.609	-0.380	-0.359	1.014	1.968	-1.166	-1.174
C1D	-1.324	1.102	0.174	0.047	-0.919	-1.432	1.861	1.161	0.131	-0.129
SAC3D1	-1.229	1.018	0.569	-0.358	-0.614	-0.605	1.840	1.341	-0.949	-0.993
EIF3B	-1.361	0.235	1.042	0.084	-0.892	-1.027	1.333	1.970	-0.335	-0.458

MRPL12	-1.180	0.929	0.722	-0.471	-0.733	-1.321	1.522	1.638	-0.677	-0.415
HIST1H2AH	-1.256	0.169	1.177	-0.090	-0.866	-0.645	1.688	1.606	-0.669	-0.701
NUP37	-1.486	0.313	0.534	0.640	-0.563	-0.670	2.449	0.478	-0.689	-0.657
KLF6	1.498	-0.423	-0.524	-0.551	0.838	0.993	-1.363	-1.799	0.753	0.753
BTF3	-1.454	0.623	0.693	0.138	0.009	-0.176	1.756	1.161	-1.360	-1.253
MRPL16	-1.435	0.074	0.616	0.745	-0.678	-0.964	2.184	1.063	-0.555	-0.565
TMEM127	1.497	-0.481	-0.583	-0.433	0.321	0.479	-1.587	-1.602	1.062	1.050
SRGAP1	1.459	-0.690	-0.608	-0.160	1.652	0.653	-1.114	-1.114	0.898	-1.114
SLC5A3	1.489	-0.498	-0.346	-0.645	-0.226	0.676	-1.557	-1.565	0.912	1.243
GGCX	0.650	0.734	0.043	-1.427	-0.643	-0.209	-1.074	-0.798	1.704	1.634
USP21	-0.920	0.641	1.062	-0.783	-0.115	0.174	0.442	2.136	-1.175	-1.085
ALYREF	-1.273	1.020	0.519	-0.266	-1.331	-1.406	1.302	1.491	-0.266	-0.355
SUB1	-1.344	0.280	0.007	1.057	-0.360	-0.584	2.131	1.180	-0.822	-0.846
RALGDS	1.447	-0.394	-0.214	-0.839	1.223	1.528	-0.073	-0.502	-1.364	-1.364
XRCC4	-1.165	0.104	-0.200	1.261	0.008	-0.425	1.139	-1.218	-0.816	-0.856
TUBE1	-1.190	0.839	0.815	-0.464	-0.817	-0.869	1.706	1.598	-0.634	-0.688

RBM27	-0.521	-1.150	0.899	0.772	-0.749	-0.570	-0.036	2.534	-0.175	-0.266
ELOVL6	-0.199	-0.675	-0.594	1.467	-0.593	-0.664	1.183	2.093	-0.780	-0.717
TMOD3	1.500	-0.503	-0.519	-0.477	1.841	1.350	-0.977	-0.979	-0.598	-0.608
FIG4	-0.808	0.499	-0.858	1.167	-0.848	-1.225	1.148	2.008	-0.132	0.018
MKLN1	-1.046	-0.538	1.217	0.367	1.224	1.144	-1.256	-0.973	-0.684	-0.742
GPR19	-0.536	-0.463	-0.501	1.499	-0.450	-0.626	1.736	1.338	-1.564	-0.260
RAD51	-1.278	0.037	0.075	1.166	-0.967	-1.012	1.692	1.657	-0.417	-0.308
FBL	-1.461	0.438	0.785	0.239	-0.978	-1.288	1.912	1.147	0.030	0.131
NOLC1	-1.168	1.058	0.560	-0.450	-0.673	-1.017	1.964	1.123	-1.114	-0.248
MRPL2	-1.125	0.570	1.070	-0.515	-0.994	-1.049	1.974	1.156	-0.135	0.066
SMG5	-1.474	0.671	0.565	0.238	-0.986	-1.196	1.415	1.713	0.069	0.081
MAP4K2	1.194	-0.646	-0.983	0.436	0.978	2.120	-1.043	-0.403	-0.480	-0.896
MED4	-1.492	0.577	0.347	0.567	-0.633	-0.691	1.896	1.523	-0.619	-0.659
PTRH1	1.491	-0.644	-0.377	-0.470	-0.475	-0.558	-0.773	-1.187	1.595	1.650
NHP2	-1.099	1.020	0.651	-0.572	-0.524	-0.866	1.544	1.858	-0.747	-0.684
ANKRD52	0.237	0.264	0.922	-1.423	-0.242	-0.045	-1.390	-1.283	1.539	1.347

AIF1	-0.518	-0.463	-0.518	1.499	1.467	-1.232	-1.060	-1.232	1.169	0.133
NUP205	-1.492	0.641	0.449	0.402	-0.733	-0.805	1.292	2.087	-0.440	-0.573
GAMT	0.160	0.412	0.863	-1.435	-0.895	-0.926	-0.146	-0.451	0.441	2.417
FBXO8	1.270	0.027	-0.126	-1.171	2.214	0.664	-0.039	-0.507	-0.916	-1.090
FAM172A	1.465	-0.265	-0.420	-0.779	0.780	0.748	-2.265	-0.905	0.562	0.451
WTAP	-1.497	0.543	0.539	0.415	-0.713	-0.084	0.251	2.358	-0.168	-0.258
POLR2K	-1.460	0.600	0.694	0.166	-1.173	-1.433	1.817	1.047	0.221	-0.152
CALR	-0.291	-0.998	-0.094	1.382	-1.550	-1.254	1.441	1.184	0.146	0.307
TSEN2	-1.200	0.700	0.937	-0.437	-0.763	-0.855	1.639	1.792	-0.563	-0.464
KIFC1	-1.464	0.263	0.416	0.784	-0.964	-0.878	1.441	1.907	-0.478	-0.456
TOMM34	-1.250	0.540	1.024	-0.314	-1.111	-1.325	1.476	1.611	0.156	-0.123
PGLS	1.489	-0.340	-0.633	-0.515	1.435	1.326	-0.098	-1.983	-0.263	-0.030
ZCCHC8	-1.289	0.134	0.006	1.149	-0.562	0.031	1.096	2.039	-0.875	-0.975
RAB5B	1.496	-0.505	-0.580	-0.411	1.044	1.024	-1.645	-1.662	0.311	0.118
ELAVL1	-1.471	0.377	0.766	0.327	-1.443	-1.480	0.277	1.700	0.236	0.697
CDK1	-1.415	0.933	0.320	0.161	-1.098	-0.938	1.531	1.604	-0.675	-0.671

CKAP2	-0.995	0.579	1.099	-0.683	-1.099	-0.740	1.881	1.249	-0.661	-0.671
HDAC6	-0.156	0.840	0.667	-1.351	-1.777	0.573	1.271	1.278	0.078	-1.063
PFN2	0.075	-0.654	-0.806	1.385	0.473	-0.072	-1.507	-1.574	0.285	0.342
SGPP1	1.344	0.020	-0.321	-1.043	1.442	1.176	-1.467	-1.499	-0.026	-0.140
ACSL4	-0.564	0.731	0.950	-1.116	-0.308	-0.239	-1.206	-1.206	0.388	2.164
LCOR	-0.556	1.178	0.434	-1.056	1.714	1.543	-1.127	-0.591	-0.701	-0.680
MCM4	-1.446	0.690	0.648	0.108	-1.130	-1.142	1.439	1.778	-0.142	-0.170
TRAIP	-1.402	0.605	0.817	-0.019	-1.211	-1.177	1.287	1.752	-0.228	-0.116
UBE2S	-1.497	0.594	0.437	0.466	-0.867	-0.842	1.502	1.825	-0.661	-0.612
SDHD	-0.378	-1.014	0.040	1.352	-0.725	-0.817	2.067	1.272	-0.542	-0.396
ETV4	-0.294	-0.606	-0.585	1.485	-1.153	-1.225	0.537	2.181	-0.136	0.073
TRIP13	-1.320	0.800	0.751	-0.231	-0.957	-0.993	1.457	1.883	-0.447	-0.293
EIF2B1	-0.461	0.814	0.839	-1.192	-0.715	-1.030	1.642	1.721	-0.573	-0.539
MBD5	1.419	-0.083	-0.459	-0.877	0.879	1.337	-1.908	-0.825	0.909	0.280
CHCHD6	-1.321	0.104	1.110	0.107	-0.371	-1.441	1.929	1.147	-0.219	-0.640
TTF2	-1.491	0.640	0.485	0.366	-0.851	-0.871	1.602	1.815	-0.399	-0.423

USP33	-1.274	0.757	0.837	-0.320	-0.901	-0.901	-0.901	0.646	0.561	-0.901
UBE2A	0.979	0.078	0.331	-1.388	1.823	0.320	-2.050	-0.441	0.171	0.131
NUDCD1	-0.931	-0.249	-0.238	1.419	-0.832	-1.247	1.822	1.444	-0.200	-0.310
SNAP47	-0.876	0.965	0.761	-0.850	1.448	1.291	-1.203	-1.199	-0.537	-0.789
FPGS	-0.335	-0.708	-0.438	1.481	-0.743	-1.091	1.590	1.790	-0.392	-0.357
FANCD2	-1.468	0.544	0.710	0.214	-0.807	-0.818	1.601	1.803	-0.573	-0.615
HJURP	-1.308	0.059	0.121	1.128	1.641	1.014	-1.297	-1.297	-0.319	-0.300
CSTF2	-0.993	-0.076	1.382	-0.313	-1.061	-1.555	1.156	1.705	0.206	0.182
GMPS	-1.438	0.302	0.255	0.881	-0.863	-1.127	1.504	1.817	-0.252	-0.227
PDDC1	1.306	-0.381	0.138	-1.063	1.056	1.781	0.218	-0.016	-1.289	-1.171
SLC38A9	-1.363	0.350	0.004	1.009	1.286	1.429	-1.730	-1.051	0.129	-0.296
RPS7	-1.361	0.780	0.720	-0.139	0.246	-0.676	2.185	0.860	-1.015	-0.780
ECH1	1.112	-0.160	-1.277	0.326	1.617	1.805	-0.638	-0.481	-0.839	-0.605
EMP2	1.482	-0.519	-0.294	-0.670	1.528	1.373	-1.243	-1.309	-0.508	-0.383
LITAF	1.366	-0.703	-0.790	0.126	0.086	0.304	-1.292	-1.593	1.068	1.537
TMED9	1.167	-0.730	0.491	-0.929	-0.786	-0.861	-0.025	-1.393	1.752	1.216

CAND1	-1.384	0.477	0.926	-0.020	-0.346	-0.235	0.913	2.136	-0.685	-0.746
CDK17	1.389	-0.039	-0.393	-0.957	-1.020	-0.892	-0.325	-0.016	1.484	1.831
MAML1	-1.225	0.404	1.117	-0.297	0.542	0.525	-1.739	-1.285	1.208	1.086
PALB2	-0.776	0.208	-0.764	1.331	-0.698	-0.767	1.597	1.857	-0.494	-0.612
CASP1	1.500	-0.500	-0.500	-0.500	0.049	-0.315	-1.065	-1.065	1.309	1.794
UHMK1	0.883	0.387	0.160	-1.430	0.885	1.456	-1.701	-1.258	0.667	-0.130
MOCS2	-0.793	0.712	1.005	-0.924	-1.305	-1.423	-0.278	-0.341	0.210	1.003
PASK	-1.314	0.150	0.047	1.117	-0.862	-0.869	1.279	2.064	-0.336	-0.344
MUM1	-1.342	0.373	-0.058	1.027	-0.848	-0.913	1.491	1.873	-0.207	-0.311
ARPC1B	1.488	-0.665	-0.466	-0.357	-0.223	-0.448	-1.059	-1.551	1.451	1.423
VPS4B	1.481	-0.612	-0.600	-0.268	1.696	0.974	-0.605	-0.599	-1.110	-1.184
TSEN15	-1.217	0.788	0.850	-0.420	-0.973	-1.353	1.951	0.924	-0.072	-0.267
PRMT5	-0.774	0.363	1.251	-0.840	-0.800	-1.073	0.931	2.206	-0.359	-0.378
GART	-1.283	0.649	0.922	-0.288	-0.717	-0.847	1.524	1.909	-0.515	-0.509
MOSPD3	1.314	-0.201	-1.111	-0.001	-0.474	0.031	1.182	1.503	-1.545	-1.037
TTF1	-1.387	0.113	0.280	0.993	-0.431	-0.171	1.265	1.978	-0.888	-1.158

CEP70	-1.205	0.481	-0.364	1.088	-0.525	-0.475	1.920	1.478	-0.586	-0.923
SENP1	-1.375	0.925	0.502	-0.052	-0.580	-0.762	1.545	1.519	-1.106	-0.993
CREBL2	0.235	-0.612	-0.930	1.306	1.649	1.499	-1.014	-0.857	-0.715	-0.745
RAB14	1.204	0.207	-0.198	-1.212	0.846	1.031	-1.786	-1.511	0.602	0.460
EMG1	-0.417	-0.748	-0.309	1.474	-0.617	-0.648	1.800	1.658	-0.692	-0.702
AGGF1	-0.640	1.281	0.290	-0.931	-0.334	-0.581	1.503	1.822	-0.779	-0.990
PTPN4	-0.162	-0.662	-0.636	1.460	0.587	0.368	-0.305	2.148	-0.716	-0.844
CHD4	-1.248	0.491	-0.297	1.055	-0.070	0.755	0.320	2.133	-0.843	-1.267
LATS2	1.406	-0.756	-0.670	0.020	-0.105	-0.058	-1.086	-1.118	1.587	1.629
TMEM87B	1.485	-0.379	-0.694	-0.413	0.648	1.075	-1.469	-1.532	0.822	0.971
CYP4B1	1.500	-0.500	-0.500	-0.500	1.339	0.788	-1.499	-1.385	1.026	-0.122
TNFSF9	1.446	-0.234	-0.359	-0.852	0.199	0.333	-0.889	-1.027	-0.446	-0.379
RSAD1	-0.832	1.162	0.507	-0.837	0.196	-0.269	-1.690	-1.390	1.170	1.236
CNOT6L	1.104	-0.034	0.242	-1.312	1.803	1.398	-1.155	-0.727	-0.633	-0.487
CIRBP	-1.154	0.930	0.735	-0.511	-0.464	-0.170	1.600	1.673	-1.102	-1.036
SNAP29	-0.273	1.069	0.458	-1.254	1.315	1.064	-1.452	-1.368	-0.358	-0.379

CARS2	1.338	-0.832	-0.694	0.187	-1.072	-1.093	1.505	1.686	-0.495	-0.260
TAF1C	-1.055	0.082	1.325	-0.352	-0.872	-0.855	1.127	2.164	-0.244	-0.460
VPS37C	1.476	-0.591	-0.241	-0.644	1.181	1.344	-1.418	-1.461	-0.301	0.143
NCK1	1.481	-0.588	-0.271	-0.622	1.073	0.302	-1.082	-2.093	0.450	0.087
TBC1D8	1.348	-0.781	-0.738	0.171	0.588	0.906	1.264	0.486	-1.544	-1.570
DPY19L4	0.141	0.587	0.725	-1.453	1.420	0.994	-1.554	-1.522	0.398	-0.108
GTF3C2	-1.383	0.213	0.162	1.008	-0.570	-0.793	1.383	1.968	-0.795	-0.460
DONSON	-1.423	0.751	0.641	0.031	-1.064	-1.191	1.730	1.494	-0.166	-0.095
CXCL1	1.210	-0.749	-0.889	0.429	0.348	0.916	-1.546	-1.745	0.126	0.557
GBE1	1.147	0.469	-0.527	-1.089	-0.512	-0.610	-0.824	-0.585	1.812	1.647
CEP170	-1.258	0.743	0.863	-0.348	-0.597	-0.436	-0.773	-0.714	1.836	1.587
TNKS2	0.305	-0.316	-1.179	1.190	-0.165	0.101	1.571	1.535	-1.122	-1.314
THOC2	-1.047	0.664	1.025	-0.642	1.663	1.679	-0.676	-0.146	-1.086	-0.635
IMPDH2	-1.120	0.596	1.054	-0.530	-0.547	-0.603	1.933	1.494	-0.729	-0.797
THRA	-1.021	0.781	0.932	-0.692	1.064	1.561	-1.186	-1.542	-0.032	-0.407
MGAT2	-0.542	0.362	1.221	-1.041	-0.445	-0.721	-1.002	-0.927	1.790	1.420

ALAS1	0.351	0.435	0.697	-1.484	-0.376	0.809	-0.216	1.054	-1.606	-1.343
ZMYND19	-1.246	0.934	0.669	-0.357	-0.537	-0.913	1.716	1.709	-0.505	-0.599
CSAD	1.458	-0.166	-0.573	-0.719	0.244	0.663	0.255	1.491	-1.673	-1.471
AKT2	1.497	-0.579	-0.475	-0.443	1.482	1.806	-0.914	-0.664	-0.346	-1.012
PGAP3	1.200	-0.950	-0.684	0.435	1.666	1.608	-0.762	-0.485	-0.886	-0.675
RPRD1B	0.059	1.050	0.245	-1.354	-0.088	-0.478	0.583	1.911	-1.123	-1.506
SLC25A28	0.848	0.423	0.168	-1.440	1.523	1.523	-0.265	-0.287	-1.243	-1.242
CEP57	-1.329	0.066	0.167	1.096	-1.055	-1.032	1.515	1.685	-0.124	-0.034
MDC1	-1.113	0.857	0.833	-0.577	-1.117	-1.116	1.149	1.920	-0.151	-0.383
PLA2G12A	-1.313	-0.101	0.342	1.072	-1.199	-1.530	1.069	0.140	0.928	1.373
NIPA1	1.460	-0.454	-0.222	-0.783	-0.335	-0.320	-1.160	-0.762	1.723	1.585
METTL5	-0.633	0.699	0.994	-1.059	0.456	-0.217	1.056	1.443	-2.086	-0.301
ARPC2	1.496	-0.598	-0.467	-0.431	0.504	0.454	-1.635	-1.714	0.224	0.834
PPAN	-1.144	0.794	0.882	-0.532	-0.686	-0.858	1.799	1.637	-0.574	-0.534
MAGED1	-0.233	0.443	1.063	-1.273	-0.754	-0.201	-0.929	-0.877	1.721	1.574
WFDC5	1.500	-0.501	-0.499	-0.501	-0.185	-0.168	-0.498	-0.500	-0.500	-0.500

SOCS5	0.444	-0.723	-0.919	1.198	-0.247	-0.266	-1.011	-1.077	1.652	1.663
ZUFSP	-0.555	1.098	0.547	-1.090	1.332	1.012	-1.294	-0.048	0.569	0.486
GJA1	-0.097	-0.677	-0.670	1.444	-0.804	-0.820	0.517	2.260	-0.741	-0.809
GNL2	-1.484	0.535	0.649	0.300	-0.540	-0.956	1.649	1.730	-0.779	-0.543
ARHGAP27	1.498	-0.453	-0.567	-0.479	1.698	1.401	-0.743	-0.945	-0.860	-0.857
CENPI	-1.227	0.373	1.131	-0.278	-1.300	-1.326	1.169	1.714	-0.312	-0.178
ODF2	-0.791	0.835	0.894	-0.938	-0.836	-0.658	1.524	1.872	-0.451	-0.579
SND1	-0.818	-0.566	-0.034	1.418	0.576	2.112	-0.998	0.689	-0.320	-0.557
KLHL11	-0.496	0.935	0.725	-1.164	-0.442	0.920	-1.242	1.746	0.209	-1.485
MX2	0.803	-0.862	-0.868	0.927	0.884	1.482	-0.911	-1.212	-0.403	-1.228
PHB2	-1.357	0.767	0.740	-0.150	-0.313	-0.816	1.238	2.004	-0.687	-0.944
RPN1	-0.747	0.431	1.208	-0.893	-0.578	-0.811	1.904	1.381	-0.726	-0.912
CCNB1	-1.477	0.264	0.521	0.692	-0.759	-0.750	1.741	1.683	-0.693	-0.627
ISY1	-0.903	0.863	0.868	-0.828	-0.580	-0.845	1.686	1.697	-0.810	-0.660
RNF111	1.490	-0.651	-0.471	-0.367	-0.565	0.158	-1.560	-0.558	1.429	1.645
NPPB	-0.500	-0.500	-0.500	1.500	-0.678	0.904	1.681	1.118	-1.022	-0.784

POP1	-0.635	0.079	1.382	-0.826	-0.781	-0.924	0.995	2.226	-0.411	-0.467
RGMB	0.711	-0.578	-1.104	0.971	0.392	0.820	-1.350	-1.822	0.887	1.061
ACTR10	1.087	0.352	-0.146	-1.293	-0.489	-0.288	-0.906	-1.372	1.387	1.697
SGSH	0.668	0.128	0.656	-1.452	-0.216	-0.168	-1.127	-1.272	1.748	1.305
NOL10	-1.228	0.712	0.910	-0.394	-1.014	-1.285	1.597	1.455	0.026	0.332
BMPR1A	-0.765	-0.274	-0.429	1.468	0.905	0.251	-1.530	-1.455	1.177	0.857
SRM	-1.339	0.823	0.704	-0.188	-0.862	-1.050	1.448	1.883	-0.326	-0.262
ZMAT2	-1.422	0.682	0.025	0.715	-0.901	-1.078	1.654	1.656	-0.512	-0.420
SNRNP70	-1.368	0.818	0.667	-0.118	-1.142	-1.145	1.394	1.587	0.034	-0.315
ARHGAP19	-1.324	0.567	0.944	-0.186	-0.457	-0.405	1.369	1.943	-0.909	-0.940
PRPS1	-1.147	0.681	0.979	-0.513	-0.482	-0.669	1.562	1.887	-0.697	-0.738
RPS14	-1.339	0.004	1.066	0.269	0.213	-0.052	1.642	1.078	-1.328	-1.447
PRPSAP1	-1.009	1.144	0.509	-0.644	-0.653	-0.555	1.634	1.806	-0.781	-0.690
CSNK1E	0.089	0.528	0.815	-1.432	-0.486	0.295	-1.155	-1.370	1.176	1.700
SETD4	-0.590	-0.600	-0.295	1.485	-0.832	-0.625	1.239	1.951	-0.635	-0.745
PIGU	-0.857	-0.462	-0.110	1.429	-0.742	-1.059	-0.631	-0.955	1.185	1.068

MCM6	-1.498	0.426	0.512	0.560	-1.059	-1.043	1.549	1.742	-0.051	-0.245
TMPO	-1.459	0.640	0.660	0.159	1.088	-0.040	0.845	1.328	-1.123	-0.703
GPS2	-0.973	1.304	0.221	-0.551	0.804	0.856	0.327	0.326	-1.933	-1.459
MKKS	-1.489	0.411	0.413	0.665	-0.376	-1.321	0.013	1.809	0.381	-1.321
TRMT112	-0.997	-0.011	-0.361	1.369	-0.445	-0.757	2.090	1.199	-0.806	-0.755
MPDZ	-0.892	-0.281	-0.260	1.434	-0.710	-0.602	-0.517	-0.750	1.924	1.513
THAP4	-1.176	0.015	-0.107	1.267	1.820	1.429	-0.487	-0.682	-0.791	-1.090
GOLGA4	0.736	-0.203	0.801	-1.333	1.354	1.868	-1.298	-0.813	-0.194	-0.251
GCN1L1	1.358	-0.492	-0.952	0.087	-0.407	0.413	1.075	1.820	-0.919	-1.062
UCHL5	-0.846	0.894	0.837	-0.886	-0.540	-0.798	1.845	1.507	-0.824	-0.763
NDUFS8	-0.932	0.897	0.832	-0.797	-1.242	-1.617	1.541	0.140	0.768	0.614
PPRC1	-0.962	-0.235	-0.209	1.406	-0.783	-1.013	0.973	2.233	-0.281	-0.337
SLC25A27	-0.878	0.687	1.028	-0.837	1.563	1.763	-0.227	-0.470	-0.585	-1.144
PCCA	-0.560	-0.577	-0.356	1.492	-0.001	0.426	1.563	0.926	-0.679	-0.901
RPUSD4	-1.056	-0.651	0.827	0.881	-0.324	-0.740	1.583	1.842	-0.477	-0.548

Bibliography

1. Linzer, D. I., and A. J. Levine. 1979. Characterization of a 54K dalton cellular SV40 tumor antigen present in SV40-transformed cells and uninfected embryonal carcinoma cells. *Cell* 17:43-52.
2. Lane, D. P., and L. V. Crawford. 1979. T antigen is bound to a host protein in SV40-transformed cells. *Nature* 278:261-263.
3. DeLeo, A. B., G. Jay, E. Appella, G. C. Dubois, L. W. Law, and L. J. Old. 1979. Detection of a transformation-related antigen in chemically induced sarcomas and other transformed cells of the mouse. *Proc Natl Acad Sci U S A* 76:2420-2424.
4. Pinhasi, O., and M. Oren. 1984. Expression of the mouse p53 cellular tumor antigen in monkey cells. *Mol Cell Biol* 4:2180-2186.
5. Bienz, B., R. Zakut-Houri, D. Givol, and M. Oren. 1984. Analysis of the gene coding for the murine cellular tumour antigen p53. *EMBO J* 3:2179-2183.
6. Zakut-Houri, R., M. Oren, B. Bienz, V. Lavie, S. Hazum, and D. Givol. 1983. A single gene and a pseudogene for the cellular tumour antigen p53. *Nature* 306:594-597.
7. Oren, M., and A. J. Levine. 1983. Molecular cloning of a cDNA specific for the murine p53 cellular tumor antigen. *Proc Natl Acad Sci U S A* 80:56-59.
8. Reich, N. C., M. Oren, and A. J. Levine. 1983. Two distinct mechanisms regulate the levels of a cellular tumor antigen, p53. *Mol Cell Biol* 3:2143-2150.
9. Crawford, L. V., D. C. Pim, E. G. Gurney, P. Goodfellow, and J. Taylor-Papadimitriou. 1981. Detection of a common feature in several human tumor cell lines--a 53,000-dalton protein. *Proc Natl Acad Sci U S A* 78:41-45.
10. Jenkins, J. R., K. Rudge, and G. A. Currie. 1984. Cellular immortalization by a cDNA clone encoding the transformation-associated phosphoprotein p53. *Nature* 312:651-654.
11. Jenkins, M. K., H. Y. Lei, C. Waltenbaugh, and S. D. Miller. 1984. Immunoregulatory pathways in adult responder mice. I. Induction of GAT-specific tolerance and suppressor T cells for cellular and humoral responses. *Scand J Immunol* 19:501-512.
12. Finlay, C. A., P. W. Hinds, and A. J. Levine. 1989. The p53 proto-oncogene can act as a suppressor of transformation. *Cell* 57:1083-1093.
13. Hinds, P., C. Finlay, and A. J. Levine. 1989. Mutation is required to activate the p53 gene for cooperation with the ras oncogene and transformation. *J Virol* 63:739-746.
14. Ozaki, T., and A. Nakagawara. p53: the attractive tumor suppressor in the cancer research field. *J Biomed Biotechnol* 2011:603925.
15. Donehower, L. A., M. Harvey, B. L. Slagle, M. J. McArthur, C. A. Montgomery, Jr., J. S. Butel, and A. Bradley. 1992. Mice deficient for p53 are developmentally normal but susceptible to spontaneous tumours. *Nature* 356:215-221.
16. Aliouat-Denis, C. M., N. Dendouga, I. Van den Wyngaert, H. Goehlmann, U. Steller, I. van de Weyer, N. Van Slycken, L. Andries, S. Kass, W. Luyten, M. Janicot, and J. E. Vialard. 2005. p53-independent regulation of p21Waf1/Cip1 expression and senescence by Chk2. *Mol Cancer Res* 3:627-634.
17. Qin, J. Z., L. Stennett, P. Bacon, B. Bodner, M. J. Hendrix, R. E. Seftor, E. A. Seftor, N. V. Margaryan, P. M. Pollock, A. Curtis, J. M. Trent, F. Bennett, L. Miele, and B. J.

- Nickoloff. 2004. p53-independent NOXA induction overcomes apoptotic resistance of malignant melanomas. *Mol Cancer Ther* 3:895-902.
18. Lanni, J. S., S. W. Lowe, E. J. Licitra, J. O. Liu, and T. Jacks. 1997. p53-independent apoptosis induced by paclitaxel through an indirect mechanism. *Proc Natl Acad Sci U S A* 94:9679-9683.
 19. Ollmann, M., L. M. Young, C. J. Di Como, F. Karim, M. Belvin, S. Robertson, K. Whittaker, M. Demsky, W. W. Fisher, A. Buchman, G. Duyk, L. Friedman, C. Prives, and C. Kopczynski. 2000. *Drosophila* p53 is a structural and functional homolog of the tumor suppressor p53. *Cell* 101:91-101.
 20. Aguinaldo, A. M., J. M. Turbeville, L. S. Linford, M. C. Rivera, J. R. Garey, R. A. Raff, and J. A. Lake. 1997. Evidence for a clade of nematodes, arthropods and other moulting animals. *Nature* 387:489-493.
 21. Derry, W. B., A. P. Putzke, and J. H. Rothman. 2001. *Caenorhabditis elegans* p53: role in apoptosis, meiosis, and stress resistance. *Science* 294:591-595.
 22. Jin, S., S. Martinek, W. S. Joo, J. R. Wortman, N. Mirkovic, A. Sali, M. D. Yandell, N. P. Pavletich, M. W. Young, and A. J. Levine. 2000. Identification and characterization of a p53 homologue in *Drosophila melanogaster*. *Proc Natl Acad Sci U S A* 97:7301-7306.
 23. Belyi, V. A., P. Ak, E. Markert, H. Wang, W. Hu, A. Puzio-Kuter, and A. J. Levine. The origins and evolution of the p53 family of genes. *Cold Spring Harb Perspect Biol* 2:a001198.
 24. Pankow, S., and C. Bamberger. 2007. The p53 tumor suppressor-like protein nvp63 mediates selective germ cell death in the sea anemone *Nematostella vectensis*. *PLoS One* 2:e782.
 25. Fan, Y., T. V. Lee, D. Xu, Z. Chen, A. F. Lamblin, H. Steller, and A. Bergmann. Dual roles of *Drosophila* p53 in cell death and cell differentiation. *Cell Death Differ* 17:912-921.
 26. Schumacher, B., M. Hanazawa, M. H. Lee, S. Nayak, K. Volkmann, E. R. Hofmann, M. Hengartner, T. Schedl, and A. Gartner. 2005. Translational repression of *C. elegans* p53 by GLD-1 regulates DNA damage-induced apoptosis. *Cell* 120:357-368.
 27. Talos, F., A. Nemajero, E. R. Flores, O. Petrenko, and U. M. Moll. 2007. p73 suppresses polyploidy and aneuploidy in the absence of functional p53. *Mol Cell* 27:647-659.
 28. Amelio, I., F. Grespi, M. Annicchiarico-Petruzzelli, and G. Melino. p63 the guardian of human reproduction. *Cell Cycle* 11:4545-4551.
 29. Augustin, M., C. Bamberger, D. Paul, and H. Schmale. 1998. Cloning and chromosomal mapping of the human p53-related KET gene to chromosome 3q27 and its murine homolog Ket to mouse chromosome 16. *Mamm Genome* 9:899-902.
 30. Yang, A., R. Schweitzer, D. Sun, M. Kaghad, N. Walker, R. T. Bronson, C. Tabin, A. Sharpe, D. Caput, C. Crum, and F. McKeon. 1999. p63 is essential for regenerative proliferation in limb, craniofacial and epithelial development. *Nature* 398:714-718.
 31. Osada, M., M. Ohba, C. Kawahara, C. Ishioka, R. Kanamaru, I. Katoh, Y. Ikawa, Y. Nimura, A. Nakagawara, M. Obinata, and S. Ikawa. 1998. Cloning and functional analysis of human p51, which structurally and functionally resembles p53. *Nat Med* 4:839-843.

32. Madhumalar, A., L. H. Jun, D. P. Lane, and C. S. Verma. 2009. Dimerization of the core domain of the p53 family: a computational study. *Cell Cycle* 8:137-148.
33. Roelfsema, N. M., and J. M. Cobben. 1996. The EEC syndrome: a literature study. *Clin Dysmorphol* 5:115-127.
34. Cole, P., D. A. Hatef, Y. Kaufman, A. Magruder, A. Bree, E. Friedman, R. Sindwani, and L. H. Hollier, Jr. 2009. Facial clefting and orofacial pathway manifestations in ankyloblepharon-ectodermal defects-cleft lip/palate (AEC) syndrome. *Am J Med Genet A* 149A:1910-1915.
35. Siegfried, E., A. Bree, M. Fete, and V. P. Sybert. 2005. Skin erosions and wound healing in ankyloblepharon-ectodermal defect-cleft lip and/or palate. *Arch Dermatol* 141:1591-1594.
36. van Bokhoven, H., M. Jung, A. P. Smits, S. van Beersum, F. Ruschendorf, M. van Steensel, M. Veenstra, J. H. Tuerlings, E. C. Mariman, H. G. Brunner, T. F. Wienker, A. Reis, H. H. Ropers, and B. C. Hamel. 1999. Limb mammary syndrome: a new genetic disorder with mammary hypoplasia, ectrodactyly, and other Hand/Foot anomalies maps to human chromosome 3q27. *Am J Hum Genet* 64:538-546.
37. Zarnegar, B. J., D. E. Webster, V. Lopez-Pajares, B. Vander Stoep Hunt, K. Qu, K. J. Yan, D. R. Berk, G. L. Sen, and P. A. Khavari. Genomic profiling of a human organotypic model of AEC syndrome reveals ZNF750 as an essential downstream target of mutant TP63. *Am J Hum Genet* 91:435-443.
38. Berk, D. R., N. L. Armstrong, M. Shinawi, and A. J. Whelan. ADULT syndrome due to an R243W mutation in TP63. *Int J Dermatol* 51:693-696.
39. Scherer, S. W., P. Poorkaj, H. Massa, S. Soder, T. Allen, M. Nunes, D. Geshuri, E. Wong, E. Belloni, S. Little, and et al. 1994. Physical mapping of the split hand/split foot locus on chromosome 7 and implication in syndromic ectrodactyly. *Hum Mol Genet* 3:1345-1354.
40. Scherer, S. W., P. Poorkaj, T. Allen, J. Kim, D. Geshuri, M. Nunes, S. Soder, K. Stephens, R. A. Pagon, M. A. Patton, and et al. 1994. Fine mapping of the autosomal dominant split hand/split foot locus on chromosome 7, band q21.3-q22.1. *Am J Hum Genet* 55:12-20.
41. Crackower, M. A., S. W. Scherer, J. M. Rommens, C. C. Hui, P. Poorkaj, S. Soder, J. M. Cobben, L. Hudgins, J. P. Evans, and L. C. Tsui. 1996. Characterization of the split hand/split foot malformation locus SHFM1 at 7q21.3-q22.1 and analysis of a candidate gene for its expression during limb development. *Hum Mol Genet* 5:571-579.
42. Clements, S. E., T. Techanukul, S. T. Holden, J. E. Mellerio, H. Dorkins, F. Escande, and J. A. McGrath. Rapp-Hodgkin and Hay-Wells ectodermal dysplasia syndromes represent a variable spectrum of the same genetic disorder. *Br J Dermatol* 163:624-629.
43. McGrath, J. A., P. H. Duijf, V. Doetsch, A. D. Irvine, R. de Waal, K. R. Vanmolkot, V. Wessagowit, A. Kelly, D. J. Atherton, W. A. Griffiths, S. J. Orlow, A. van Haeringen, M. G. Ausems, A. Yang, F. McKeon, M. A. Bamshad, H. G. Brunner, B. C. Hamel, and H. van Bokhoven. 2001. Hay-Wells syndrome is caused by heterozygous missense mutations in the SAM domain of p63. *Hum Mol Genet* 10:221-229.
44. Rinne, T., H. G. Brunner, and H. van Bokhoven. 2007. p63-associated disorders. *Cell Cycle* 6:262-268.

45. Lo Muzio, L., A. Santarelli, R. Caltabiano, C. Rubini, T. Pieramici, L. Trevisiol, F. Carinci, R. Leonardi, A. De Lillo, S. Lanzafame, P. Bufo, and A. Piattelli. 2005. p63 overexpression associates with poor prognosis in head and neck squamous cell carcinoma. *Hum Pathol* 36:187-194.
46. Massion, P. P., P. M. Taflan, S. M. Jamshedur Rahman, P. Yildiz, Y. Shyr, M. E. Edgerton, M. D. Westfall, J. R. Roberts, J. A. Pietenpol, D. P. Carbone, and A. L. Gonzalez. 2003. Significance of p63 amplification and overexpression in lung cancer development and prognosis. *Cancer Res* 63:7113-7121.
47. Crook, T., J. M. Nicholls, L. Brooks, J. O'Nions, and M. J. Allday. 2000. High level expression of deltaN-p63: a mechanism for the inactivation of p53 in undifferentiated nasopharyngeal carcinoma (NPC)? *Oncogene* 19:3439-3444.
48. Dhillon, P. K., M. Barry, M. J. Stampfer, S. Perner, M. Fiorentino, A. Fornari, J. Ma, J. Fleet, T. Kurth, M. A. Rubin, and L. A. Mucci. 2009. Aberrant cytoplasmic expression of p63 and prostate cancer mortality. *Cancer Epidemiol Biomarkers Prev* 18:595-600.
49. Hara, T., H. Kijima, S. Yamamoto, T. Kenmochi, Y. Kise, H. Tanaka, O. Chino, H. Shimada, K. Takazawa, M. Tanaka, S. Inokuchi, and H. Makuuchi. 2004. Ubiquitous p63 expression in human esophageal squamous cell carcinoma. *Int J Mol Med* 14:169-173.
50. Narahashi, T., T. Niki, T. Wang, A. Goto, D. Matsubara, N. Funata, and M. Fukayama. 2006. Cytoplasmic localization of p63 is associated with poor patient survival in lung adenocarcinoma. *Histopathology* 49:349-357.
51. Snizek, J. C., K. E. Matheny, M. D. Westfall, and J. A. Pietenpol. 2004. Dominant negative p63 isoform expression in head and neck squamous cell carcinoma. *Laryngoscope* 114:2063-2072.
52. Karni-Schmidt, O., M. Castillo-Martin, T. H. Shen, N. Gladoun, J. Domingo-Domenech, M. Sanchez-Carbayo, Y. Li, S. Lowe, C. Prives, and C. Cordon-Cardo. Distinct expression profiles of p63 variants during urothelial development and bladder cancer progression. *Am J Pathol* 178:1350-1360.
53. Hanker, L., T. Karn, E. Ruckhaeberle, R. Gaetje, C. Solbach, M. Schmidt, K. Engels, U. Holtrich, M. Kaufmann, and A. Rody. Clinical relevance of the putative stem cell marker p63 in breast cancer. *Breast Cancer Res Treat* 122:765-775.
54. Liao, X. Y., W. C. Xue, D. H. Shen, H. Y. Ngan, M. K. Siu, and A. N. Cheung. 2007. p63 expression in ovarian tumours: a marker for Brenner tumours but not transitional cell carcinomas. *Histopathology* 51:477-483.
55. Hull, D., J. Ma, H. Singh, D. Hossain, J. Qian, and D. G. Bostwick. 2009. Precursor of prostate-specific antigen expression in prostatic intraepithelial neoplasia and adenocarcinoma: a study of 90 cases. *BJU Int* 104:915-918.
56. Urist, M. J., C. J. Di Como, M. L. Lu, E. Charytonowicz, D. Verbel, C. P. Crum, T. A. Ince, F. D. McKeon, and C. Cordon-Cardo. 2002. Loss of p63 expression is associated with tumor progression in bladder cancer. *Am J Pathol* 161:1199-1206.
57. Bishop, J. A., J. Teruya-Feldstein, W. H. Westra, G. Pelosi, W. D. Travis, and N. Rekhtman. p40 (DeltaNp63) is superior to p63 for the diagnosis of pulmonary squamous cell carcinoma. *Mod Pathol* 25:405-415.
58. Comperat, E., P. Camparo, R. Haus, E. Chartier-Kastler, S. Bart, A. Delcourt, A. Houlgatte, R. Francois, F. Capron, and A. Vieillefond. 2006. Immunohistochemical

- expression of p63, p53 and MIB-1 in urinary bladder carcinoma. A tissue microarray study of 158 cases. *Virchows Arch* 448:319-324.
59. Stepan, A., C. Margaritescu, C. Simionescu, and R. Ciurea. 2009. E-cadherin and p63 immunoexpression in dysplastic lesions and urothelial carcinomas of the bladder. *Rom J Morphol Embryol* 50:461-465.
 60. Yamaguchi, H., K. Inokuchi, Y. Sakuma, and K. Dan. 2001. Mutation of the p51/p63 gene is associated with blastic crisis in chronic myelogenous leukemia. *Leukemia* 15:1729-1734.
 61. Yu, Y., M. E. Garber, K. Schluens, M. Pacyna-Gengelbach, and I. Petersen. 2004. [Study on relationship between p63 expression and 3q27-q29 alteration in non-small cell lung cancer]. *Zhongguo Fei Ai Za Zhi* 7:419-422.
 62. Yu, Y. W., M. E. Garber, K. Schluns, M. Pacyna-Gengelbach, and I. Petersen. 2004. [Evaluation of p63 expression in lung cancer by use of complementary DNA and tissue microarray]. *Zhonghua Bing Li Xue Za Zhi* 33:324-327.
 63. Comprehensive genomic characterization of squamous cell lung cancers. *Nature* 489:519-525.
 64. Stransky, N., A. M. Egloff, A. D. Tward, A. D. Kostic, K. Cibulskis, A. Sivachenko, G. V. Kryukov, M. S. Lawrence, C. Sougnez, A. McKenna, E. Shefler, A. H. Ramos, P. Stojanov, S. L. Carter, D. Voet, M. L. Cortes, D. Auclair, M. F. Berger, G. Saksena, C. Guiducci, R. C. Onofrio, M. Parkin, M. Romkes, J. L. Weissfeld, R. R. Seethala, L. Wang, C. Rangel-Escareno, J. C. Fernandez-Lopez, A. Hidalgo-Miranda, J. Melendez-Zajgla, W. Winckler, K. Ardlie, S. B. Gabriel, M. Meyerson, E. S. Lander, G. Getz, T. R. Golub, L. A. Garraway, and J. R. Grandis. The mutational landscape of head and neck squamous cell carcinoma. *Science* 333:1157-1160.
 65. Su, X., D. Chakravarti, M. S. Cho, L. Liu, Y. J. Gi, Y. L. Lin, M. L. Leung, A. El-Naggar, C. J. Creighton, M. B. Suraokar, I. Wistuba, and E. R. Flores. TAp63 suppresses metastasis through coordinate regulation of Dicer and miRNAs. *Nature* 467:986-990.
 66. Mills, A. A., B. Zheng, X. J. Wang, H. Vogel, D. R. Roop, and A. Bradley. 1999. p63 is a p53 homologue required for limb and epidermal morphogenesis. *Nature* 398:708-713.
 67. Senoo, M., F. Pinto, C. P. Crum, and F. McKeon. 2007. p63 Is essential for the proliferative potential of stem cells in stratified epithelia. *Cell* 129:523-536.
 68. Mikkola, M. L., A. Costanzo, I. Thesleff, D. R. Roop, and M. I. Koster. Treasure or artifact: a decade of p63 research speaks for itself. *Cell Death Differ* 17:180-183; author reply 184-186.
 69. Talos, F., S. Wolff, U. Beyer, M. Dobbelstein, and U. M. Moll. Brdm2 - an aberrant hypomorphic p63 allele. *Cell Death Differ* 17:184-186.
 70. Wolff, S., F. Talos, G. Palacios, U. Beyer, M. Dobbelstein, and U. M. Moll. 2009. The alpha/beta carboxy-terminal domains of p63 are required for skin and limb development. New insights from the Brdm2 mouse which is not a complete p63 knockout but expresses p63 gamma-like proteins. *Cell Death Differ* 16:1108-1117.
 71. Suh, E. K., A. Yang, A. Kettenbach, C. Bamberger, A. H. Michaelis, Z. Zhu, J. A. Elvin, R. T. Bronson, C. P. Crum, and F. McKeon. 2006. p63 protects the female germ line during meiotic arrest. *Nature* 444:624-628.

72. Su, X., M. Paris, Y. J. Gi, K. Y. Tsai, M. S. Cho, Y. L. Lin, J. A. Biernaskie, S. Sinha, C. Prives, L. H. Pevny, F. D. Miller, and E. R. Flores. 2009. TAp63 prevents premature aging by promoting adult stem cell maintenance. *Cell Stem Cell* 5:64-75.
73. Di Como, C. J., M. J. Urist, I. Babayan, M. Drobnjak, C. V. Hedvat, J. Teruya-Feldstein, K. Pohar, A. Hoos, and C. Cordon-Cardo. 2002. p63 expression profiles in human normal and tumor tissues. *Clin Cancer Res* 8:494-501.
74. Romano, R. A., K. Smalley, C. Magraw, V. A. Serna, T. Kurita, S. Raghavan, and S. Sinha. DeltaNp63 knockout mice reveal its indispensable role as a master regulator of epithelial development and differentiation. *Development* 139:772-782.
75. Koster, M. I., D. Dai, B. Marinari, Y. Sano, A. Costanzo, M. Karin, and D. R. Roop. 2007. p63 induces key target genes required for epidermal morphogenesis. *Proceedings of the National Academy of Sciences of the United States of America* 104:3255-3260.
76. Fuchs, E., and S. Raghavan. 2002. Getting under the skin of epidermal morphogenesis. *Nat Rev Genet* 3:199-209.
77. Yamaguchi, Y., K. Takahashi, B. Z. Zmudzka, A. Kornhauser, S. A. Miller, T. Tadokoro, W. Berens, J. Z. Beer, and V. J. Hearing. 2006. Human skin responses to UV radiation: pigment in the upper epidermis protects against DNA damage in the lower epidermis and facilitates apoptosis. *FASEB J* 20:1486-1488.
78. Koster, M. I., and D. R. Roop. 2004. Genetic pathways required for epidermal morphogenesis. *Eur J Cell Biol* 83:625-629.
79. Candi, E., A. Rufini, A. Terrinoni, D. Dinsdale, M. Ranalli, A. Paradisi, V. De Laurenzi, L. G. Spagnoli, M. V. Catani, S. Ramadan, R. A. Knight, and G. Melino. 2006. Differential roles of p63 isoforms in epidermal development: selective genetic complementation in p63 null mice. *Cell Death Differ* 13:1037-1047.
80. Weissman, I. 2005. Stem cell research: paths to cancer therapies and regenerative medicine. *JAMA* 294:1359-1366.
81. Nichols, J., B. Zevnik, K. Anastassiadis, H. Niwa, D. Klewe-Nebenius, I. Chambers, H. Scholer, and A. Smith. 1998. Formation of pluripotent stem cells in the mammalian embryo depends on the POU transcription factor Oct4. *Cell* 95:379-391.
82. Mitsui, K., Y. Tokuzawa, H. Itoh, K. Segawa, M. Murakami, K. Takahashi, M. Maruyama, M. Maeda, and S. Yamanaka. 2003. The homeoprotein Nanog is required for maintenance of pluripotency in mouse epiblast and ES cells. *Cell* 113:631-642.
83. Yeom, Y. I., G. Fuhrmann, C. E. Ovitt, A. Brehm, K. Ohbo, M. Gross, K. Hubner, and H. R. Scholer. 1996. Germline regulatory element of Oct-4 specific for the totipotent cycle of embryonal cells. *Development* 122:881-894.
84. Niwa, H. 2001. Molecular mechanism to maintain stem cell renewal of ES cells. *Cell Struct Funct* 26:137-148.
85. Niwa, H. 2000. [Self-renewal and differentiation of ES cells]. *Hum Cell* 13:161-175.
86. Looijenga, L. H., H. Stoop, H. P. de Leeuw, C. A. de Gouveia Brazao, A. J. Gillis, K. E. van Roozendaal, E. J. van Zoelen, R. F. Weber, K. P. Wolffenbuttel, H. van Dekken, F. Honecker, C. Bokemeyer, E. J. Perlman, D. T. Schneider, J. Kononen, G. Sauter, and J. W. Oosterhuis. 2003. POU5F1 (OCT3/4) identifies cells with pluripotent potential in human germ cell tumors. *Cancer Res* 63:2244-2250.

87. Rodda, D. J., J. L. Chew, L. H. Lim, Y. H. Loh, B. Wang, H. H. Ng, and P. Robson. 2005. Transcriptional regulation of nanog by OCT4 and SOX2. *J Biol Chem* 280:24731-24737.
88. Wu, Q., X. Chen, J. Zhang, Y. H. Loh, T. Y. Low, W. Zhang, S. K. Sze, B. Lim, and H. H. Ng. 2006. Sall4 interacts with Nanog and co-occupies Nanog genomic sites in embryonic stem cells. *J Biol Chem* 281:24090-24094.
89. Loh, Y. H., Q. Wu, J. L. Chew, V. B. Vega, W. Zhang, X. Chen, G. Bourque, J. George, B. Leong, J. Liu, K. Y. Wong, K. W. Sung, C. W. Lee, X. D. Zhao, K. P. Chiu, L. Lipovich, V. A. Kuznetsov, P. Robson, L. W. Stanton, C. L. Wei, Y. Ruan, B. Lim, and H. H. Ng. 2006. The Oct4 and Nanog transcription network regulates pluripotency in mouse embryonic stem cells. *Nat Genet* 38:431-440.
90. Briggs, R., and T. J. King. 1952. Transplantation of Living Nuclei From Blastula Cells into Enucleated Frogs' Eggs. *Proc Natl Acad Sci U S A* 38:455-463.
91. Byrne, J. A., D. A. Pedersen, L. L. Clepper, M. Nelson, W. G. Sanger, S. Gokhale, D. P. Wolf, and S. M. Mitalipov. 2007. Producing primate embryonic stem cells by somatic cell nuclear transfer. *Nature* 450:497-502.
92. Takahashi, K., and S. Yamanaka. 2006. Induction of pluripotent stem cells from mouse embryonic and adult fibroblast cultures by defined factors. *Cell* 126:663-676.
93. Nakagawa, M., M. Koyanagi, K. Tanabe, K. Takahashi, T. Ichisaka, T. Aoi, K. Okita, Y. Mochiduki, N. Takizawa, and S. Yamanaka. 2008. Generation of induced pluripotent stem cells without Myc from mouse and human fibroblasts. *Nat Biotechnol* 26:101-106.
94. Yu, J., M. A. Vodyanik, K. Smuga-Otto, J. Antosiewicz-Bourget, J. L. Frane, S. Tian, J. Nie, G. A. Jonsdottir, V. Ruotti, R. Stewart, Slukvin, II, and J. A. Thomson. 2007. Induced pluripotent stem cell lines derived from human somatic cells. *Science* 318:1917-1920.
95. Wang, A., Z. Tang, I. H. Park, Y. Zhu, S. Patel, G. Q. Daley, and S. Li. Induced pluripotent stem cells for neural tissue engineering. *Biomaterials* 32:5023-5032.
96. Chae, J. I., D. W. Kim, N. Lee, Y. J. Jeon, I. Jeon, J. Kwon, J. Kim, Y. Soh, D. S. Lee, K. S. Seo, N. J. Choi, B. C. Park, S. H. Kang, J. Ryu, S. H. Oh, D. A. Shin, D. R. Lee, J. T. Do, I. H. Park, G. Q. Daley, and J. Song. Quantitative proteomic analysis of induced pluripotent stem cells derived from a human Huntington's disease patient. *Biochem J* 446:359-371.
97. Grskovic, M., A. Javaherian, B. Strulovici, and G. Q. Daley. Induced pluripotent stem cells--opportunities for disease modelling and drug discovery. *Nat Rev Drug Discov* 10:915-929.
98. Robinton, D. A., and G. Q. Daley. The promise of induced pluripotent stem cells in research and therapy. *Nature* 481:295-305.
99. Arora, N., and G. Q. Daley. Pluripotent stem cells in research and treatment of hemoglobinopathies. *Cold Spring Harb Perspect Med* 2:a011841.
100. Narsinh, K. H., F. Jia, R. C. Robbins, M. A. Kay, M. T. Longaker, and J. C. Wu. Generation of adult human induced pluripotent stem cells using nonviral minicircle DNA vectors. *Nat Protoc* 6:78-88.

101. Yu, J., K. Hu, K. Smuga-Otto, S. Tian, R. Stewart, Slukvin, II, and J. A. Thomson. 2009. Human induced pluripotent stem cells free of vector and transgene sequences. *Science* 324:797-801.
102. Kim, D., C. H. Kim, J. I. Moon, Y. G. Chung, M. Y. Chang, B. S. Han, S. Ko, E. Yang, K. Y. Cha, R. Lanza, and K. S. Kim. 2009. Generation of human induced pluripotent stem cells by direct delivery of reprogramming proteins. *Cell Stem Cell* 4:472-476.
103. Warren, L., P. D. Manos, T. Ahfeldt, Y. H. Loh, H. Li, F. Lau, W. Ebina, P. K. Mandal, Z. D. Smith, A. Meissner, G. Q. Daley, A. S. Brack, J. J. Collins, C. Cowan, T. M. Schlaeger, and D. J. Rossi. Highly efficient reprogramming to pluripotency and directed differentiation of human cells with synthetic modified mRNA. *Cell Stem Cell* 7:618-630.
104. Shi, Y., C. Despons, J. T. Do, H. S. Hahm, H. R. Scholer, and S. Ding. 2008. Induction of pluripotent stem cells from mouse embryonic fibroblasts by Oct4 and Klf4 with small-molecule compounds. *Cell Stem Cell* 3:568-574.
105. Mali, P., B. K. Chou, J. Yen, Z. Ye, J. Zou, S. Dowey, R. A. Brodsky, J. E. Ohm, W. Yu, S. B. Baylin, K. Yusa, A. Bradley, D. J. Meyers, C. Mukherjee, P. A. Cole, and L. Cheng. Butyrate greatly enhances derivation of human induced pluripotent stem cells by promoting epigenetic remodeling and the expression of pluripotency-associated genes. *Stem Cells* 28:713-720.
106. Silva, J., O. Barrandon, J. Nichols, J. Kawaguchi, T. W. Theunissen, and A. Smith. 2008. Promotion of reprogramming to ground state pluripotency by signal inhibition. *PLoS Biol* 6:e253.
107. Inoue-Yokoo, T., K. Tani, and D. Sugiyama. Mesodermal and Hematopoietic Differentiation from ES and iPS Cells. *Stem Cell Rev*.
108. Song, Z., J. Cai, Y. Liu, D. Zhao, J. Yong, S. Duo, X. Song, Y. Guo, Y. Zhao, H. Qin, X. Yin, C. Wu, J. Che, S. Lu, M. Ding, and H. Deng. 2009. Efficient generation of hepatocyte-like cells from human induced pluripotent stem cells. *Cell Res* 19:1233-1242.
109. Zhang, J., G. F. Wilson, A. G. Soerens, C. H. Koonce, J. Yu, S. P. Palecek, J. A. Thomson, and T. J. Kamp. 2009. Functional cardiomyocytes derived from human induced pluripotent stem cells. *Circ Res* 104:e30-41.
110. Denham, M., and M. Dottori. Neural differentiation of induced pluripotent stem cells. *Methods Mol Biol* 793:99-110.
111. Brunner, M., X. Peng, G. X. Liu, X. Q. Ren, O. Ziv, B. R. Choi, R. Mathur, M. Hajjiri, K. E. Odening, E. Steinberg, E. J. Folco, E. Pringa, J. Centracchio, R. R. Macharzina, T. Donahay, L. Schofield, N. Rana, M. Kirk, G. F. Mitchell, A. Poppas, M. Zehender, and G. Koren. 2008. Mechanisms of cardiac arrhythmias and sudden death in transgenic rabbits with long QT syndrome. *J Clin Invest* 118:2246-2259.
112. Wernig, M., J. P. Zhao, J. Pruszak, E. Hedlund, D. Fu, F. Soldner, V. Broccoli, M. Constantine-Paton, O. Isacson, and R. Jaenisch. 2008. Neurons derived from reprogrammed fibroblasts functionally integrate into the fetal brain and improve symptoms of rats with Parkinson's disease. *Proc Natl Acad Sci U S A* 105:5856-5861.
113. Induced pluripotent stem cells from patients with Huntington's disease show CAG-repeat-expansion-associated phenotypes. *Cell Stem Cell* 11:264-278.

114. Mou, X., Y. Wu, H. Cao, Q. Meng, Q. Wang, C. Sun, S. Hu, Y. Ma, and H. Zhang. Generation of disease-specific induced pluripotent stem cells from patients with different karyotypes of Down syndrome. *Stem Cell Res Ther* 3:14.
115. Raya, A., I. Rodriguez-Piza, G. Guenechea, R. Vassena, S. Navarro, M. J. Barrero, A. Consiglio, M. Castella, P. Rio, E. Sleep, F. Gonzalez, G. Tiscornia, E. Garreta, T. Aasen, A. Veiga, I. M. Verma, J. Surralles, J. Bueren, and J. C. Izpisua Belmonte. 2009. Disease-corrected haematopoietic progenitors from Fanconi anaemia induced pluripotent stem cells. *Nature* 460:53-59.
116. Zou, J., P. Mali, X. Huang, S. N. Dowey, and L. Cheng. Site-specific gene correction of a point mutation in human iPS cells derived from an adult patient with sickle cell disease. *Blood* 118:4599-4608.
117. Wang, Y., C. G. Zheng, Y. Jiang, J. Zhang, J. Chen, C. Yao, Q. Zhao, S. Liu, K. Chen, J. Du, Z. Yang, and S. Gao. Genetic correction of beta-thalassemia patient-specific iPS cells and its use in improving hemoglobin production in irradiated SCID mice. *Cell Res* 22:637-648.
118. Kudva, Y. C., S. Ohmine, L. V. Greder, J. R. Dutton, A. Armstrong, J. G. De Lamo, Y. K. Khan, T. Thatava, M. Hasegawa, N. Fusaki, J. M. Slack, and Y. Ikeda. Transgene-free disease-specific induced pluripotent stem cells from patients with type 1 and type 2 diabetes. *Stem Cells Transl Med* 1:451-461.
119. Pessach, I. M., J. Ordovas-Montanes, S. Y. Zhang, J. L. Casanova, S. Giliani, A. R. Gennery, W. Al-Herz, P. D. Manos, T. M. Schlaeger, I. H. Park, F. Rucci, S. Agarwal, G. Mostoslavsky, G. Q. Daley, and L. D. Notarangelo. Induced pluripotent stem cells: a novel frontier in the study of human primary immunodeficiencies. *J Allergy Clin Immunol* 127:1400-1407 e1404.
120. Somers, A., J. C. Jean, C. A. Sommer, A. Omari, C. C. Ford, J. A. Mills, L. Ying, A. G. Sommer, J. M. Jean, B. W. Smith, R. Lafyatis, M. F. Demierre, D. J. Weiss, D. L. French, P. Gadue, G. J. Murphy, G. Mostoslavsky, and D. N. Kotton. Generation of transgene-free lung disease-specific human induced pluripotent stem cells using a single excisable lentiviral stem cell cassette. *Stem Cells* 28:1728-1740.
121. Banito, A., S. T. Rashid, J. C. Acosta, S. Li, C. F. Pereira, I. Geti, S. Pinho, J. C. Silva, V. Azuara, M. Walsh, L. Vallier, and J. Gil. 2009. Senescence impairs successful reprogramming to pluripotent stem cells. *Genes Dev* 23:2134-2139.
122. Mikkelsen, T. S., J. Hanna, X. Zhang, M. Ku, M. Wernig, P. Schorderet, B. E. Bernstein, R. Jaenisch, E. S. Lander, and A. Meissner. 2008. Dissecting direct reprogramming through integrative genomic analysis. *Nature* 454:49-55.
123. Sridharan, R., and K. Plath. 2008. Illuminating the black box of reprogramming. *Cell Stem Cell* 2:295-297.
124. Sridharan, R., J. Tchieu, M. J. Mason, R. Yachechko, E. Kuoy, S. Horvath, Q. Zhou, and K. Plath. 2009. Role of the murine reprogramming factors in the induction of pluripotency. *Cell* 136:364-377.
125. Zhao, W., Q. Li, S. Ayers, Y. Gu, Z. Shi, Q. Zhu, Y. Chen, H. Y. Wang, and R. F. Wang. Jmjd3 inhibits reprogramming by upregulating expression of INK4a/Arf and targeting PHF20 for ubiquitination. *Cell* 152:1037-1050.
126. Yang, J., G. Q. Liu, and T. P. Hong. 2009. [Therapeutic cloning and somatic cell reprogramming: every road leads to Rome]. *Sheng Li Ke Xue Jin Zhan* 40:101-105.

127. Kawamura, T., J. Suzuki, Y. V. Wang, S. Menendez, L. B. Morera, A. Raya, G. M. Wahl, and J. C. Izpisua Belmonte. 2009. Linking the p53 tumour suppressor pathway to somatic cell reprogramming. *Nature* 460:1140-1144.
128. Li, S. C., Y. Jin, W. G. Loudon, Y. Song, Z. Ma, L. P. Weiner, and J. F. Zhong. Increase developmental plasticity of human keratinocytes with gene suppression. *Proc Natl Acad Sci U S A* 108:12793-12798.
129. Flores, E. R., K. Y. Tsai, D. Crowley, S. Sengupta, A. Yang, F. McKeon, and T. Jacks. 2002. p63 and p73 are required for p53-dependent apoptosis in response to DNA damage. *Nature* 416:560-564.
130. Flores, E. R., S. Sengupta, J. B. Miller, J. J. Newman, R. Bronson, D. Crowley, A. Yang, F. McKeon, and T. Jacks. 2005. Tumor predisposition in mice mutant for p63 and p73: evidence for broader tumor suppressor functions for the p53 family. *Cancer Cell* 7:363-373.
131. Guo, X., W. M. Keyes, C. Papazoglu, J. Zuber, W. Li, S. W. Lowe, H. Vogel, and A. A. Mills. 2009. TAp63 induces senescence and suppresses tumorigenesis in vivo. *Nat Cell Biol* 11:1451-1457.
132. Yang, A., M. Kaghad, Y. Wang, E. Gillett, M. D. Fleming, V. Dotsch, N. C. Andrews, D. Caput, and F. McKeon. 1998. p63, a p53 homolog at 3q27-29, encodes multiple products with transactivating, death-inducing, and dominant-negative activities. *Mol Cell* 2:305-316.
133. Adorno, M., M. Cordenonsi, M. Montagner, S. Dupont, C. Wong, B. Hann, A. Solari, S. Bobisse, M. B. Rondina, V. Guzzardo, A. R. Parenti, A. Rosato, S. Bicciato, A. Balmain, and S. Piccolo. 2009. A Mutant-p53/Smad complex opposes p63 to empower TGFbeta-induced metastasis. *Cell* 137:87-98.
134. Lin, Y. L., S. Sengupta, K. Gurdziel, G. W. Bell, T. Jacks, and E. R. Flores. 2009. p63 and p73 transcriptionally regulate genes involved in DNA repair. *PLoS Genet* 5:e1000680.
135. Lee, R. C., R. L. Feinbaum, and V. Ambros. 1993. The *C. elegans* heterochronic gene *lin-4* encodes small RNAs with antisense complementarity to *lin-14*. *Cell* 75:843-854.
136. Ventura, A., and T. Jacks. 2009. MicroRNAs and cancer: short RNAs go a long way. *Cell* 136:586-591.
137. Lee, Y., M. Kim, J. Han, K. H. Yeom, S. Lee, S. H. Baek, and V. N. Kim. 2004. MicroRNA genes are transcribed by RNA polymerase II. *EMBO J* 23:4051-4060.
138. Borchert, G. M., W. Lanier, and B. L. Davidson. 2006. RNA polymerase III transcribes human microRNAs. *Nat Struct Mol Biol* 13:1097-1101.
139. Wang, X., J. Zhang, F. Li, J. Gu, T. He, X. Zhang, and Y. Li. 2005. MicroRNA identification based on sequence and structure alignment. *Bioinformatics* 21:3610-3614.
140. Winter, J., S. Jung, S. Keller, R. I. Gregory, and S. Diederichs. 2009. Many roads to maturity: microRNA biogenesis pathways and their regulation. *Nat Cell Biol* 11:228-234.
141. Lee, Y., C. Ahn, J. Han, H. Choi, J. Kim, J. Yim, J. Lee, P. Provost, O. Radmark, S. Kim, and V. N. Kim. 2003. The nuclear RNase III Drosha initiates microRNA processing. *Nature* 425:415-419.

142. Gregory, R. I., K. P. Yan, G. Amuthan, T. Chendrimada, B. Doratotaj, N. Cooch, and R. Shiekhattar. 2004. The Microprocessor complex mediates the genesis of microRNAs. *Nature* 432:235-240.
143. Denli, A. M., B. B. Tops, R. H. Plasterk, R. F. Ketting, and G. J. Hannon. 2004. Processing of primary microRNAs by the Microprocessor complex. *Nature* 432:231-235.
144. Bohnsack, M. T., K. Czaplinski, and D. Gorlich. 2004. Exportin 5 is a RanGTP-dependent dsRNA-binding protein that mediates nuclear export of pre-miRNAs. *RNA* 10:185-191.
145. Gregory, R. I., T. P. Chendrimada, N. Cooch, and R. Shiekhattar. 2005. Human RISC couples microRNA biogenesis and posttranscriptional gene silencing. *Cell* 123:631-640.
146. Lee, Y., K. Jeon, J. T. Lee, S. Kim, and V. N. Kim. 2002. MicroRNA maturation: stepwise processing and subcellular localization. *EMBO J* 21:4663-4670.
147. Lytle, J. R., T. A. Yario, and J. A. Steitz. 2007. Target mRNAs are repressed as efficiently by microRNA-binding sites in the 5' UTR as in the 3' UTR. *Proc Natl Acad Sci U S A* 104:9667-9672.
148. Grimson, A., K. K. Farh, W. K. Johnston, P. Garrett-Engele, L. P. Lim, and D. P. Bartel. 2007. MicroRNA targeting specificity in mammals: determinants beyond seed pairing. *Mol Cell* 27:91-105.
149. Lai, E. C. 2002. Micro RNAs are complementary to 3' UTR sequence motifs that mediate negative post-transcriptional regulation. *Nat Genet* 30:363-364.
150. Tay, Y., J. Zhang, A. M. Thomson, B. Lim, and I. Rigoutsos. 2008. MicroRNAs to Nanog, Oct4 and Sox2 coding regions modulate embryonic stem cell differentiation. *Nature* 455:1124-1128.
151. Tay, Y. M., W. L. Tam, Y. S. Ang, P. M. Gaughwin, H. Yang, W. Wang, R. Liu, J. George, H. H. Ng, R. J. Perera, T. Lufkin, I. Rigoutsos, A. M. Thomson, and B. Lim. 2008. MicroRNA-134 modulates the differentiation of mouse embryonic stem cells, where it causes post-transcriptional attenuation of Nanog and LRH1. *Stem Cells* 26:17-29.
152. He, L., X. He, L. P. Lim, E. de Stanchina, Z. Xuan, Y. Liang, W. Xue, L. Zender, J. Magnus, D. Ridzon, A. L. Jackson, P. S. Linsley, C. Chen, S. W. Lowe, M. A. Cleary, and G. J. Hannon. 2007. A microRNA component of the p53 tumour suppressor network. *Nature* 447:1130-1134.
153. Corney, D. C., A. Flesken-Nikitin, A. K. Godwin, W. Wang, and A. Y. Nikitin. 2007. MicroRNA-34b and MicroRNA-34c are targets of p53 and cooperate in control of cell proliferation and adhesion-independent growth. *Cancer Res* 67:8433-8438.
154. Suzuki, H. I., K. Yamagata, K. Sugimoto, T. Iwamoto, S. Kato, and K. Miyazono. 2009. Modulation of microRNA processing by p53. *Nature* 460:529-533.
155. Wang, W., B. Cheng, L. Miao, Y. Mei, and M. Wu. Mutant p53-R273H gains new function in sustained activation of EGFR signaling via suppressing miR-27a expression. *Cell Death Dis* 4:e574.
156. Yamakuchi, M., C. D. Lotterman, C. Bao, R. H. Hruban, B. Karim, J. T. Mendell, D. Huso, and C. J. Lowenstein. P53-induced microRNA-107 inhibits HIF-1 and tumor angiogenesis. *Proc Natl Acad Sci U S A* 107:6334-6339.

157. Wang, Y., R. Medvid, C. Melton, R. Jaenisch, and R. Blelloch. 2007. DGCR8 is essential for microRNA biogenesis and silencing of embryonic stem cell self-renewal. *Nat Genet* 39:380-385.
158. Bernstein, E., S. Y. Kim, M. A. Carmell, E. P. Murchison, H. Alcorn, M. Z. Li, A. A. Mills, S. J. Elledge, K. V. Anderson, and G. J. Hannon. 2003. Dicer is essential for mouse development. *Nat Genet* 35:215-217.
159. Yi, R., H. A. Pasolli, M. Landthaler, M. Hafner, T. Ojo, R. Sheridan, C. Sander, D. O'Carroll, M. Stoffel, T. Tuschl, and E. Fuchs. 2009. DGCR8-dependent microRNA biogenesis is essential for skin development. *Proceedings of the National Academy of Sciences of the United States of America* 106:498-502.
160. Anokye-Danso, F., C. M. Trivedi, D. Juhr, M. Gupta, Z. Cui, Y. Tian, Y. Zhang, W. Yang, P. J. Gruber, J. A. Epstein, and E. E. Morrisey. Highly efficient miRNA-mediated reprogramming of mouse and human somatic cells to pluripotency. *Cell Stem Cell* 8:376-388.
161. Wang, Y., S. Baskerville, A. Shenoy, J. E. Babiarz, L. Baehner, and R. Blelloch. 2008. Embryonic stem cell-specific microRNAs regulate the G1-S transition and promote rapid proliferation. *Nat Genet* 40:1478-1483.
162. Miyoshi, N., H. Ishii, H. Nagano, N. Haraguchi, D. L. Dewi, Y. Kano, S. Nishikawa, M. Tanemura, K. Mimori, F. Tanaka, T. Saito, J. Nishimura, I. Takemasa, T. Mizushima, M. Ikeda, H. Yamamoto, M. Sekimoto, Y. Doki, and M. Mori. Reprogramming of mouse and human cells to pluripotency using mature microRNAs. *Cell Stem Cell* 8:633-638.
163. Calin, G. A., C. D. Dumitru, M. Shimizu, R. Bichi, S. Zupo, E. Noch, H. Aldler, S. Rattan, M. Keating, K. Rai, L. Rassenti, T. Kipps, M. Negrini, F. Bullrich, and C. M. Croce. 2002. Frequent deletions and down-regulation of micro- RNA genes miR15 and miR16 at 13q14 in chronic lymphocytic leukemia. *Proc Natl Acad Sci U S A* 99:15524-15529.
164. Tarasov, V., P. Jung, B. Verdoodt, D. Lodygin, A. Epanchintsev, A. Menssen, G. Meister, and H. Hermeking. 2007. Differential regulation of microRNAs by p53 revealed by massively parallel sequencing: miR-34a is a p53 target that induces apoptosis and G1-arrest. *Cell Cycle* 6:1586-1593.
165. Chang, T. C., E. A. Wentzel, O. A. Kent, K. Ramachandran, M. Mullendore, K. H. Lee, G. Feldmann, M. Yamakuchi, M. Ferlito, C. J. Lowenstein, D. E. Arking, M. A. Beer, A. Maitra, and J. T. Mendell. 2007. Transactivation of miR-34a by p53 broadly influences gene expression and promotes apoptosis. *Mol Cell* 26:745-752.
166. Chen, X., H. Hu, X. Guan, G. Xiong, Y. Wang, K. Wang, J. Li, X. Xu, K. Yang, and Y. Bai. CpG island methylation status of miRNAs in esophageal squamous cell carcinoma. *Int J Cancer* 130:1607-1613.
167. Zhu, N., D. Zhang, H. Xie, Z. Zhou, H. Chen, T. Hu, Y. Bai, Y. Shen, W. Yuan, Q. Jing, and Y. Qin. Endothelial-specific intron-derived miR-126 is down-regulated in human breast cancer and targets both VEGFA and PIK3R2. *Mol Cell Biochem* 351:157-164.
168. Tavazoie, S. F., C. Alarcon, T. Oskarsson, D. Padua, Q. Wang, P. D. Bos, W. L. Gerald, and J. Massague. 2008. Endogenous human microRNAs that suppress breast cancer metastasis. *Nature* 451:147-152.

169. Gregory, P. A., A. G. Bert, E. L. Paterson, S. C. Barry, A. Tsykin, G. Farshid, M. A. Vadas, Y. Khew-Goodall, and G. J. Goodall. 2008. The miR-200 family and miR-205 regulate epithelial to mesenchymal transition by targeting ZEB1 and SIP1. *Nat Cell Biol* 10:593-601.
170. Wang, G., X. Guo, W. Hong, Q. Liu, T. Wei, C. Lu, L. Gao, D. Ye, Y. Zhou, J. Chen, J. Wang, M. Wu, H. Liu, and J. Kang. Critical regulation of miR-200/ZEB2 pathway in Oct4/Sox2-induced mesenchymal-to-epithelial transition and induced pluripotent stem cell generation. *Proc Natl Acad Sci U S A* 110:2858-2863.
171. Papagiannakopoulos, T., A. Shapiro, and K. S. Kosik. 2008. MicroRNA-21 targets a network of key tumor-suppressive pathways in glioblastoma cells. *Cancer Res* 68:8164-8172.
172. Gao, J., and Q. G. Liu. The role of miR-26 in tumors and normal tissues (Review). *Oncol Lett* 2:1019-1023.
173. Ma, L., J. Teruya-Feldstein, and R. A. Weinberg. 2007. Tumour invasion and metastasis initiated by microRNA-10b in breast cancer. *Nature* 449:682-688.
174. Chen, D., Y. Sun, Y. Wei, P. Zhang, A. H. Rezaeian, J. Teruya-Feldstein, S. Gupta, H. Liang, H. K. Lin, M. C. Hung, and L. Ma. LIFR is a breast cancer metastasis suppressor upstream of the Hippo-YAP pathway and a prognostic marker. *Nat Med* 18:1511-1517.
175. Liu, P., N. A. Jenkins, and N. G. Copeland. 2003. A highly efficient recombineering-based method for generating conditional knockout mutations. *Genome Res* 13:476-484.
176. Farley, F. W., P. Soriano, L. S. Steffen, and S. M. Dymecki. 2000. Widespread recombinase expression using FLP_{eR} (flipper) mice. *Genesis* 28:106-110.
177. Lewandoski, M., K. M. Wassarman, and G. R. Martin. 1997. Zp3-cre, a transgenic mouse line for the activation or inactivation of loxP-flanked target genes specifically in the female germ line. *Curr Biol* 7:148-151.
178. Barrandon, Y., and H. Green. 1987. Three clonal types of keratinocyte with different capacities for multiplication. *Proceedings of the National Academy of Sciences of the United States of America* 84:2302-2306.
179. Su, X., M. S. Cho, Y. J. Gi, B. A. Ayanga, C. J. Sherr, and E. R. Flores. 2009. Rescue of key features of the p63-null epithelial phenotype by inactivation of Ink4a and Arf. *EMBO J* 28:1904-1915.
180. Kumar, M. S., R. E. Pester, C. Y. Chen, K. Lane, C. Chin, J. Lu, D. G. Kirsch, T. R. Golub, and T. Jacks. 2009. Dicer1 functions as a haploinsufficient tumor suppressor. *Genes Dev* 23:2700-2704.
181. Kumar, M. S., J. Lu, K. L. Mercer, T. R. Golub, and T. Jacks. 2007. Impaired microRNA processing enhances cellular transformation and tumorigenesis. *Nat Genet* 39:673-677.
182. Huang da, W., B. T. Sherman, and R. A. Lempicki. 2009. Systematic and integrative analysis of large gene lists using DAVID bioinformatics resources. *Nature protocols* 4:44-57.
183. Creighton, C. J., A. L. Benham, H. Zhu, M. F. Khan, J. G. Reid, A. K. Nagaraja, M. D. Fountain, O. Dziadek, D. Han, L. Ma, J. Kim, S. M. Hawkins, M. L. Anderson, M. M. Matzuk, and P. H. Gunaratne. 2010. Discovery of novel

- microRNAs in female reproductive tract using next generation sequencing. *PLoS One* 5:e9637.
184. Creighton, C. J., J. G. Reid, and P. H. Gunaratne. 2009. Expression profiling of microRNAs by deep sequencing. *Brief Bioinform* 10:490-497.
 185. Coarfa, C., F. Yu, C. A. Miller, Z. Chen, R. A. Harris, and A. Milosavljevic. 2010. Pash 3.0: A versatile software package for read mapping and integrative analysis of genomic and epigenomic variation using massively parallel DNA sequencing. *BMC Bioinformatics* 11:572.
 186. Griffiths-Jones, S. 2004. The microRNA Registry. *Nucleic Acids Res* 32:D109-111.
 187. Griffiths-Jones, S., R. J. Grocock, S. van Dongen, A. Bateman, and A. J. Enright. 2006. miRBase: microRNA sequences, targets and gene nomenclature. *Nucleic Acids Res* 34:D140-144.
 188. Griffiths-Jones, S., H. K. Saini, S. van Dongen, and A. J. Enright. 2008. miRBase: tools for microRNA genomics. *Nucleic Acids Res* 36:D154-158.
 189. Kozomara, A., and S. Griffiths-Jones. 2010. miRBase: integrating microRNA annotation and deep-sequencing data. *Nucleic Acids Res* 39:D152-157.
 190. Trapnell, C., B. A. Williams, G. Pertea, A. Mortazavi, G. Kwan, M. J. van Baren, S. L. Salzberg, B. J. Wold, and L. Pachter. 2010. Transcript assembly and quantification by RNA-Seq reveals unannotated transcripts and isoform switching during cell differentiation. *Nature biotechnology* 28:511-515.
 191. Subramanian, A., P. Tamayo, V. K. Mootha, S. Mukherjee, B. L. Ebert, M. A. Gillette, A. Paulovich, S. L. Pomeroy, T. R. Golub, E. S. Lander, and J. P. Mesirov. 2005. Gene set enrichment analysis: a knowledge-based approach for interpreting genome-wide expression profiles. *Proceedings of the National Academy of Sciences of the United States of America* 102:15545-15550.
 192. Landthaler, M., A. Yalcin, and T. Tuschl. 2004. The human DiGeorge syndrome critical region gene 8 and Its D. melanogaster homolog are required for miRNA biogenesis. *Curr Biol* 14:2162-2167.
 193. Su, X., D. Chakravarti, M. S. Cho, L. Liu, Y. J. Gi, Y. L. Lin, M. L. Leung, A. El-Naggar, C. J. Creighton, M. B. Suraokar, I. Wistuba, and E. R. Flores. 2010. TAp63 suppresses metastasis through coordinate regulation of Dicer and miRNAs. *Nature* 467:986-990.
 194. Deng, J. M., K. Satoh, H. Wang, H. Chang, Z. Zhang, M. D. Stewart, A. J. Cooney, and R. R. Behringer. 2011. Generation of viable male and female mice from two fathers. *Biology of reproduction* 84:613-618.
 195. Flores, E. R., B. L. Allen-Hoffmann, D. Lee, C. A. Sattler, and P. F. Lambert. 1999. Establishment of the human papillomavirus type 16 (HPV-16) life cycle in an immortalized human foreskin keratinocyte cell line. *Virology* 262:344-354.
 196. Ma, L. Role of miR-10b in breast cancer metastasis. *Breast Cancer Res* 12:210.
 197. Ma, L., F. Reinhardt, E. Pan, J. Soutschek, B. Bhat, E. G. Marcusson, J. Teruya-Feldstein, G. W. Bell, and R. A. Weinberg. Therapeutic silencing of miR-10b inhibits metastasis in a mouse mammary tumor model. *Nat Biotechnol* 28:341-347.
 198. Bandi, N., and E. Vassella. miR-34a and miR-15a/16 are co-regulated in non-small cell lung cancer and control cell cycle progression in a synergistic and Rb-dependent manner. *Mol Cancer* 10:55.

199. Kashat, M., L. Azzouz, S. H. Sarkar, D. Kong, Y. Li, and F. H. Sarkar. Inactivation of AR and Notch-1 signaling by miR-34a attenuates prostate cancer aggressiveness. *Am J Transl Res* 4:432-442.
200. Liu, C., K. Kelnar, B. Liu, X. Chen, T. Calhoun-Davis, H. Li, L. Patrawala, H. Yan, C. Jeter, S. Honorio, J. F. Wiggins, A. G. Bader, R. Fagin, D. Brown, and D. G. Tang. The microRNA miR-34a inhibits prostate cancer stem cells and metastasis by directly repressing CD44. *Nat Med* 17:211-215.
201. Fujita, Y., K. Kojima, N. Hamada, R. Ohhashi, Y. Akao, Y. Nozawa, T. Deguchi, and M. Ito. 2008. Effects of miR-34a on cell growth and chemoresistance in prostate cancer PC3 cells. *Biochem Biophys Res Commun* 377:114-119.
202. Zhang, Y., P. Yang, T. Sun, D. Li, X. Xu, Y. Rui, C. Li, M. Chong, T. Ibrahim, L. Mercatali, D. Amadori, X. Lu, D. Xie, Q. J. Li, and X. F. Wang. miR-126 and miR-126(*) repress recruitment of mesenchymal stem cells and inflammatory monocytes to inhibit breast cancer metastasis. *Nat Cell Biol* 15:284-294.
203. Liu, Y. N., J. J. Yin, W. Abou-Kheir, P. G. Hynes, O. M. Casey, L. Fang, M. Yi, R. M. Stephens, V. Seng, H. Sheppard-Tillman, P. Martin, and K. Kelly. MiR-1 and miR-200 inhibit EMT via Slug-dependent and tumorigenesis via Slug-independent mechanisms. *Oncogene* 32:296-306.
204. Gibbons, D. L., W. Lin, C. J. Creighton, Z. H. Rizvi, P. A. Gregory, G. J. Goodall, N. Thilaganathan, L. Du, Y. Zhang, A. Pertsemlidis, and J. M. Kurie. 2009. Contextual extracellular cues promote tumor cell EMT and metastasis by regulating miR-200 family expression. *Genes Dev* 23:2140-2151.
205. Vogt, M., J. Munding, M. Gruner, S. T. Liffers, B. Verdoodt, J. Hauk, L. Steinstraesser, A. Tannapfel, and H. Hermeking. Frequent concomitant inactivation of miR-34a and miR-34b/c by CpG methylation in colorectal, pancreatic, mammary, ovarian, urothelial, and renal cell carcinomas and soft tissue sarcomas. *Virchows Arch* 458:313-322.
206. Javeri, A., M. Ghaffarpour, M. F. Taha, and M. Houshmand. Downregulation of miR-34a in breast tumors is not associated with either p53 mutations or promoter hypermethylation while it correlates with metastasis. *Med Oncol* 30:413.
207. Tellez, C. S., D. E. Juri, K. Do, A. M. Bernauer, C. L. Thomas, L. A. Damiani, M. Tessema, S. Leng, and S. A. Belinsky. EMT and stem cell-like properties associated with miR-205 and miR-200 epigenetic silencing are early manifestations during carcinogen-induced transformation of human lung epithelial cells. *Cancer Res* 71:3087-3097.
208. Bates, G. J., S. M. Nicol, B. J. Wilson, A. M. Jacobs, J. C. Bourdon, J. Wardrop, D. J. Gregory, D. P. Lane, N. D. Perkins, and F. V. Fuller-Pace. 2005. The DEAD box protein p68: a novel transcriptional coactivator of the p53 tumour suppressor. *EMBO J* 24:543-553.
209. Han, J., Y. Lee, K. H. Yeom, Y. K. Kim, H. Jin, and V. N. Kim. 2004. The Drosha-DGCR8 complex in primary microRNA processing. *Genes Dev* 18:3016-3027.
210. Fukuda, T., K. Yamagata, S. Fujiyama, T. Matsumoto, I. Koshida, K. Yoshimura, M. Mihara, M. Naitou, H. Endoh, T. Nakamura, C. Akimoto, Y. Yamamoto, T. Katagiri, C. Foulds, S. Takezawa, H. Kitagawa, K. Takeyama, B. W. O'Malley, and S. Kato.

2007. DEAD-box RNA helicase subunits of the Drosha complex are required for processing of rRNA and a subset of microRNAs. *Nat Cell Biol* 9:604-611.
211. Tucci, P., M. Agostini, F. Grespi, E. K. Markert, A. Terrinoni, K. H. Vousden, P. A. Muller, V. Dotsch, S. Kehrlöesser, B. S. Sayan, G. Giaccone, S. W. Lowe, N. Takahashi, P. Vandenabeele, R. A. Knight, A. J. Levine, and G. Melino. Loss of p63 and its microRNA-205 target results in enhanced cell migration and metastasis in prostate cancer. *Proc Natl Acad Sci U S A* 109:15312-15317.
212. Ha, L., R. M. Ponnamperna, S. Jay, M. S. Ricci, and W. C. Weinberg. Dysregulated DeltaNp63alpha inhibits expression of Ink4a/arf, blocks senescence, and promotes malignant conversion of keratinocytes. *PLoS One* 6:e21877.
213. Muller, P. A., and K. H. Vousden. p53 mutations in cancer. *Nat Cell Biol* 15:2-8.
214. Maruya, S., J. P. Issa, R. S. Weber, D. I. Rosenthal, J. C. Haviland, R. Lotan, and A. K. El-Naggar. 2004. Differential methylation status of tumor-associated genes in head and neck squamous carcinoma: incidence and potential implications. *Clin Cancer Res* 10:3825-3830.
215. Jackson, E. L., N. Willis, K. Mercer, R. T. Bronson, D. Crowley, R. Montoya, T. Jacks, and D. A. Tuveson. 2001. Analysis of lung tumor initiation and progression using conditional expression of oncogenic K-ras. *Genes Dev* 15:3243-3248.
216. Landthaler, M., D. Gaidatzis, A. Rothbauer, P. Y. Chen, S. J. Soll, L. Dinic, T. Ojo, M. Hafner, M. Zavolan, and T. Tuschl. 2008. Molecular characterization of human Argonaute-containing ribonucleoprotein complexes and their bound target mRNAs. *RNA* 14:2580-2596.
217. Baffa, R., M. Fassan, S. Volinia, B. O'Hara, C. G. Liu, J. P. Palazzo, M. Gardiman, M. Rugge, L. G. Gomella, C. M. Croce, and A. Rosenberg. 2009. MicroRNA expression profiling of human metastatic cancers identifies cancer gene targets. *J Pathol* 219:214-221.
218. Hua, S., X. Xiaotao, G. Renhua, Y. Yongmei, L. Lianke, G. Wen, and S. Yongqian. Reduced miR-31 and let-7 maintain the balance between differentiation and quiescence in lung cancer stem-like side population cells. *Biomed Pharmacother* 66:89-97.
219. Li, X., J. Zhang, L. Gao, S. McClellan, M. A. Finan, T. W. Butler, L. B. Owen, G. A. Piazza, and Y. Xi. MiR-181 mediates cell differentiation by interrupting the Lin28 and let-7 feedback circuit. *Cell Death Differ* 19:378-386.
220. Ding, X. C., F. J. Slack, and H. Grosshans. 2008. The let-7 microRNA interfaces extensively with the translation machinery to regulate cell differentiation. *Cell Cycle* 7:3083-3090.
221. Shell, S., S. M. Park, A. R. Radjabi, R. Schickel, E. O. Kistner, D. A. Jewell, C. Feig, E. Lengyel, and M. E. Peter. 2007. Let-7 expression defines two differentiation stages of cancer. *Proc Natl Acad Sci U S A* 104:11400-11405.
222. de Pontual, L., E. Yao, P. Callier, L. Faivre, V. Drouin, S. Cariou, A. Van Haeringen, D. Genevieve, A. Goldenberg, M. Oufadem, S. Manouvrier, A. Munnich, J. A. Vidigal, M. Vekemans, S. Lyonnet, A. Henrion-Caude, A. Ventura, and J. Amiel. Germline deletion of the miR-17 approximately 92 cluster causes skeletal and growth defects in humans. *Nat Genet* 43:1026-1030.
223. Jouneau, A., C. Ciaudo, O. Sismeiro, V. Brochard, L. Jouneau, S. Vandormael-Pournin, J. Y. Coppee, Q. Zhou, E. Heard, C. Antoniewski, and M. Cohen-Tannoudji.

- Naive and primed murine pluripotent stem cells have distinct miRNA expression profiles. *RNA* 18:253-264.
224. Lakshmipathy, U., J. Davila, and R. P. Hart. miRNA in pluripotent stem cells. *Regen Med* 5:545-555.
 225. Wang, Y., J. W. Huang, M. Li, W. K. Cavenee, P. S. Mitchell, X. Zhou, M. Tewari, F. B. Furnari, and T. Taniguchi. MicroRNA-138 modulates DNA damage response by repressing histone H2AX expression. *Mol Cancer Res* 9:1100-1111.
 226. Ebi, H., T. Sato, N. Sugito, Y. Hosono, Y. Yatabe, Y. Matsuyama, T. Yamaguchi, H. Osada, M. Suzuki, and T. Takahashi. 2009. Counterbalance between RB inactivation and miR-17-92 overexpression in reactive oxygen species and DNA damage induction in lung cancers. *Oncogene* 28:3371-3379.
 227. Xiong, Y., J. H. Fang, J. P. Yun, J. Yang, Y. Zhang, W. H. Jia, and S. M. Zhuang. Effects of microRNA-29 on apoptosis, tumorigenicity, and prognosis of hepatocellular carcinoma. *Hepatology* 51:836-845.
 228. Cimmino, A., G. A. Calin, M. Fabbri, M. V. Iorio, M. Ferracin, M. Shimizu, S. E. Wojcik, R. I. Aqeilan, S. Zupo, M. Dono, L. Rassenti, H. Alder, S. Volinia, C. G. Liu, T. J. Kipps, M. Negrini, and C. M. Croce. 2005. miR-15 and miR-16 induce apoptosis by targeting BCL2. *Proc Natl Acad Sci U S A* 102:13944-13949.
 229. Christoffersen, N. R., R. Shalgi, L. B. Frankel, E. Leucci, M. Lees, M. Klausen, Y. Pilpel, F. C. Nielsen, M. Oren, and A. H. Lund. p53-independent upregulation of miR-34a during oncogene-induced senescence represses MYC. *Cell Death Differ* 17:236-245.
 230. Tang, R., L. Li, D. Zhu, D. Hou, T. Cao, H. Gu, J. Zhang, J. Chen, C. Y. Zhang, and K. Zen. Mouse miRNA-709 directly regulates miRNA-15a/16-1 biogenesis at the posttranscriptional level in the nucleus: evidence for a microRNA hierarchy system. *Cell Res* 22:504-515.
 231. Williams, A. E., M. M. Perry, S. A. Moschos, H. M. Larner-Svensson, and M. A. Lindsay. 2008. Role of miRNA-146a in the regulation of the innate immune response and cancer. *Biochem Soc Trans* 36:1211-1215.
 232. Polikepahad, S., J. M. Knight, A. O. Naghavi, T. Oplt, C. J. Creighton, C. Shaw, A. L. Benham, J. Kim, B. Soibam, R. A. Harris, C. Coarfa, A. Zariff, A. Milosavljevic, L. M. Batts, F. Kheradmand, P. H. Gunaratne, and D. B. Corry. Proinflammatory role for let-7 microRNAs in experimental asthma. *J Biol Chem* 285:30139-30149.
 233. Babiarz, J. E., J. G. Ruby, Y. Wang, D. P. Bartel, and R. Blelloch. 2008. Mouse ES cells express endogenous shRNAs, siRNAs, and other Microprocessor-independent, Dicer-dependent small RNAs. *Genes Dev* 22:2773-2785.
 234. Nakagawa, A., Y. Shi, E. Kage-Nakadai, S. Mitani, and D. Xue. Caspase-dependent conversion of Dicer ribonuclease into a death-promoting deoxyribonuclease. *Science* 328:327-334.
 235. Rivetti di Val Cervo, P., A. M. Lena, M. Nicoloso, S. Rossi, M. Mancini, H. Zhou, G. Saintigny, E. Dellambra, T. Odorisio, C. Mahe, G. A. Calin, E. Candi, and G. Melino. p63-microRNA feedback in keratinocyte senescence. *Proc Natl Acad Sci U S A* 109:1133-1138.

236. Lena, A. M., R. Shalom-Feuerstein, P. Rivetti di Val Cervo, D. Aberdam, R. A. Knight, G. Melino, and E. Candi. 2008. miR-203 represses 'stemness' by repressing DeltaNp63. *Cell Death Differ* 15:1187-1195.
237. Hong, H., K. Takahashi, T. Ichisaka, T. Aoi, O. Kanagawa, M. Nakagawa, K. Okita, and S. Yamanaka. 2009. Suppression of induced pluripotent stem cell generation by the p53-p21 pathway. *Nature* 460:1132-1135.
238. Li, H., M. Collado, A. Villasante, K. Strati, S. Ortega, M. Canamero, M. A. Blasco, and M. Serrano. 2009. The Ink4/Arf locus is a barrier for iPS cell reprogramming. *Nature* 460:1136-1139.
239. Marion, R. M., K. Strati, H. Li, M. Murga, R. Blanco, S. Ortega, O. Fernandez-Capetillo, M. Serrano, and M. A. Blasco. 2009. A p53-mediated DNA damage response limits reprogramming to ensure iPS cell genomic integrity. *Nature* 460:1149-1153.
240. Utikal, J., J. M. Polo, M. Stadtfeld, N. Maherali, W. Kulalert, R. M. Walsh, A. Khalil, J. G. Rheinwald, and K. Hochedlinger. 2009. Immortalization eliminates a roadblock during cellular reprogramming into iPS cells. *Nature* 460:1145-1148.
241. Koster, M. I., S. Kim, A. A. Mills, F. J. DeMayo, and D. R. Roop. 2004. p63 is the molecular switch for initiation of an epithelial stratification program. *Genes Dev* 18:126-131.
242. Carroll, D. K., J. S. Brugge, and L. D. Attardi. 2007. p63, cell adhesion and survival. *Cell Cycle* 6:255-261.
243. Flores, E. R. 2007. The roles of p63 in cancer. *Cell Cycle* 6:300-304.
244. Ihrie, R. A., M. R. Marques, B. T. Nguyen, J. S. Horner, C. Papazoglu, R. T. Bronson, A. A. Mills, and L. D. Attardi. 2005. Perp is a p63-regulated gene essential for epithelial integrity. *Cell* 120:843-856.
245. Yang, A., Z. Zhu, P. Kapranov, F. McKeon, G. M. Church, T. R. Gingeras, and K. Struhl. 2006. Relationships between p63 binding, DNA sequence, transcription activity, and biological function in human cells. *Mol Cell* 24:593-602.
246. Cho, M. S., I. L. Chan, and E. R. Flores. 2010. DeltaNp63 transcriptionally regulates brachyury, a gene with diverse roles in limb development, tumorigenesis and metastasis. *Cell Cycle* 9.
247. Romano, R. A., K. Smalley, C. Magraw, V. A. Serna, T. Kurita, S. Raghavan, and S. Sinha. 2012. DeltaNp63 knockout mice reveal its indispensable role as a master regulator of epithelial development and differentiation. *Development* 139:772-782.
248. Yi, R., D. O'Carroll, H. A. Pasolli, Z. Zhang, F. S. Dietrich, A. Tarakhovsky, and E. Fuchs. 2006. Morphogenesis in skin is governed by discrete sets of differentially expressed microRNAs. *Nat Genet* 38:356-362.
249. Anokye-Danso, F., C. M. Trivedi, D. Juhr, M. Gupta, Z. Cui, Y. Tian, Y. Zhang, W. Yang, P. J. Gruber, J. A. Epstein, and E. E. Morrisey. 2011. Highly efficient miRNA-mediated reprogramming of mouse and human somatic cells to pluripotency. *Cell Stem Cell* 8:376-388.
250. Judson, R. L., J. E. Babiarz, M. Venere, and R. Blelloch. 2009. Embryonic stem cell-specific microRNAs promote induced pluripotency. *Nature biotechnology* 27:459-461.

251. Xu, N., T. Papagiannakopoulos, G. Pan, J. A. Thomson, and K. S. Kosik. 2009. MicroRNA-145 regulates OCT4, SOX2, and KLF4 and represses pluripotency in human embryonic stem cells. *Cell* 137:647-658.
252. Houbaviy, H. B., M. F. Murray, and P. A. Sharp. 2003. Embryonic stem cell-specific MicroRNAs. *Dev Cell* 5:351-358.
253. Li, Z., C. S. Yang, K. Nakashima, and T. M. Rana. 2010. Small RNA-mediated regulation of iPS cell generation. *EMBO J* 30:823-834.
254. Lin, C. H., A. L. Jackson, J. Guo, P. S. Linsley, and R. N. Eisenman. 2009. Myc-regulated microRNAs attenuate embryonic stem cell differentiation. *EMBO J* 28:3157-3170.
255. Peter, M. E. 2009. An interview with Dr. Marcus E. Peter on his highly cited paper published in *Cell Cycle*. *Cell Cycle* 8:2325.
256. Krizhanovsky, V., and S. W. Lowe. 2009. Stem cells: The promises and perils of p53. *Nature* 460:1085-1086.
257. Chong, M. M., G. Zhang, S. Cheloufi, T. A. Neubert, G. J. Hannon, and D. R. Littman. 2010. Canonical and alternate functions of the microRNA biogenesis machinery. *Genes Dev* 24:1951-1960.
258. Gai, H., E. L. Leung, P. D. Costantino, J. R. Aguila, D. M. Nguyen, L. M. Fink, D. C. Ward, and Y. Ma. 2009. Generation and characterization of functional cardiomyocytes using induced pluripotent stem cells derived from human fibroblasts. *Cell Biol Int* 33:1184-1193.
259. Bilousova, G., J. Chen, and D. R. Roop. Differentiation of mouse induced pluripotent stem cells into a multipotent keratinocyte lineage. *J Invest Dermatol* 131:857-864.
260. Zhang, D., W. Jiang, M. Liu, X. Sui, X. Yin, S. Chen, Y. Shi, and H. Deng. 2009. Highly efficient differentiation of human ES cells and iPS cells into mature pancreatic insulin-producing cells. *Cell Res* 19:429-438.
261. Taura, D., M. Noguchi, M. Sone, K. Hosoda, E. Mori, Y. Okada, K. Takahashi, K. Homma, N. Oyamada, M. Inuzuka, T. Sonoyama, K. Ebihara, N. Tamura, H. Itoh, H. Suemori, N. Nakatsuji, H. Okano, S. Yamanaka, and K. Nakao. 2009. Adipogenic differentiation of human induced pluripotent stem cells: comparison with that of human embryonic stem cells. *FEBS Lett* 583:1029-1033.
262. Hanna, J., M. Wernig, S. Markoulaki, C. W. Sun, A. Meissner, J. P. Cassady, C. Beard, T. Brambrink, L. C. Wu, T. M. Townes, and R. Jaenisch. 2007. Treatment of sickle cell anemia mouse model with iPS cells generated from autologous skin. *Science* 318:1920-1923.
263. Ochiya, T., Y. Yamamoto, and A. Banas. Commitment of stem cells into functional hepatocytes. *Differentiation* 79:65-73.
264. Levine, A. J. 1989. The p53 tumor suppressor gene and gene product. *Princess Takamatsu Symp* 20:221-230.
265. Hollstein, M., B. Shomer, M. Greenblatt, T. Soussi, E. Hovig, R. Montesano, and C. C. Harris. 1996. Somatic point mutations in the p53 gene of human tumors and cell lines: updated compilation. *Nucleic Acids Res* 24:141-146.
266. Singhi, A. D., A. Cimino-Mathews, R. B. Jenkins, F. Lan, S. R. Fink, H. Nassar, R. Vang, J. H. Fetting, J. Hicks, S. Sukumar, A. M. De Marzo, and P. Argani. MYC gene

- amplification is often acquired in lethal distant breast cancer metastases of unamplified primary tumors. *Mod Pathol* 25:378-387.
267. Badiali, M., A. Pession, G. Basso, L. Andreini, L. Rigobello, E. Galassi, and F. Giangaspero. 1991. N-myc and c-myc oncogenes amplification in medulloblastomas. Evidence of particularly aggressive behavior of a tumor with c-myc amplification. *Tumori* 77:118-121.
 268. Brennan, J., T. O'Connor, R. W. Makuch, A. M. Simmons, E. Russell, R. I. Linnoila, R. M. Phelps, A. F. Gazdar, D. C. Ihde, and B. E. Johnson. 1991. myc family DNA amplification in 107 tumors and tumor cell lines from patients with small cell lung cancer treated with different combination chemotherapy regimens. *Cancer Res* 51:1708-1712.
 269. Melo, S. A., S. Roperio, C. Moutinho, L. A. Aaltonen, H. Yamamoto, G. A. Calin, S. Rossi, A. F. Fernandez, F. Carneiro, C. Oliveira, B. Ferreira, C. G. Liu, A. Villanueva, G. Capella, S. Schwartz, Jr., R. Shiekhata, and M. Esteller. 2009. A TARBP2 mutation in human cancer impairs microRNA processing and DICER1 function. *Nat Genet* 41:365-370.
 270. Li, C., Y. Feng, G. Coukos, and L. Zhang. 2009. Therapeutic microRNA strategies in human cancer. *AAPS J* 11:747-757.
 271. Merritt, W. M., Y. G. Lin, L. Y. Han, A. A. Kamat, W. A. Spannuth, R. Schmandt, D. Urbauer, L. A. Pennacchio, J. F. Cheng, A. M. Nick, M. T. Deavers, A. Mourad-Zeidan, H. Wang, P. Mueller, M. E. Lenburg, J. W. Gray, S. Mok, M. J. Birrer, G. Lopez-Berestein, R. L. Coleman, M. Bar-Eli, and A. K. Sood. 2008. Dicer, Drosha, and outcomes in patients with ovarian cancer. *N Engl J Med* 359:2641-2650.
 272. Taulli, R., F. Bersani, V. Foglizzo, A. Linari, E. Vigna, M. Ladanyi, T. Tuschl, and C. Ponzetto. 2009. The muscle-specific microRNA miR-206 blocks human rhabdomyosarcoma growth in xenotransplanted mice by promoting myogenic differentiation. *J Clin Invest* 119:2366-2378.
 273. Ward, A., A. Balwierz, J. D. Zhang, M. Kublbeck, Y. Pawitan, T. Hielscher, S. Wiemann, and O. Sahin. Re-expression of microRNA-375 reverses both tamoxifen resistance and accompanying EMT-like properties in breast cancer. *Oncogene* 32:1173-1182.
 274. Grammatikakis, I., M. Gorospe, and K. Abdelmohsen. Modulation of Cancer Traits by Tumor Suppressor microRNAs. *Int J Mol Sci* 14:1822-1842.
 275. Kota, J., R. R. Chivukula, K. A. O'Donnell, E. A. Wentzel, C. L. Montgomery, H. W. Hwang, T. C. Chang, P. Vivekanandan, M. Torbenson, K. R. Clark, J. R. Mendell, and J. T. Mendell. 2009. Therapeutic microRNA delivery suppresses tumorigenesis in a murine liver cancer model. *Cell* 137:1005-1017.
 276. Lindow, M., and S. Kauppinen. Discovering the first microRNA-targeted drug. *J Cell Biol* 199:407-412.
 277. Burk, U., J. Schubert, U. Wellner, O. Schmalhofer, E. Vincan, S. Spaderna, and T. Brabletz. 2008. A reciprocal repression between ZEB1 and members of the miR-200 family promotes EMT and invasion in cancer cells. *EMBO Rep* 9:582-589.
 278. Hinkal, G. W., G. Grelier, A. Puisieux, and C. Moyret-Lalle. Complexity in the regulation of Dicer expression: Dicer variant proteins are differentially expressed in

- epithelial and mesenchymal breast cancer cells and decreased during EMT. *Br J Cancer* 104:387-388.
279. Lin, Y., Z. Cheng, Z. Yang, J. Zheng, and T. Lin. DNp73 improves generation efficiency of human induced pluripotent stem cells. *BMC Cell Biol* 13:9.
280. Marcel, V., I. Petit, F. Murray-Zmijewski, T. Goullet de Rugy, K. Fernandes, V. Meuray, A. Diot, D. P. Lane, D. Aberdam, and J. C. Bourdon. Diverse p63 and p73 isoforms regulate Delta133p53 expression through modulation of the internal TP53 promoter activity. *Cell Death Differ* 19:816-826.

Vita

Deepavali Chakravarti was born in Kolkata, West Bengal (India) on August 8, 1981, the Daughter of Ratnabali and Dipak Chakrabarti. After finishing her high school from Ballygunge Shiksha Sadan, she went to Bangalore for her college education. She joined PES(People's Education Society) and earned her Bachelor's degree in science with a major in Microbiology in 2003, and Master's degree in science with a major in Biotechnology in 2005. She then moved to the United States to pursue a second Master's in science majoring in Molecular Biology. She earned this degree in 2006, December from University of Houston-Clear Lake. She applied to graduate schools in the following year for the Fall semester and was accepted at the University of Texas Health Science Center at Houston, Graduate School of Biomedical Sciences. In the meantime she worked for nine months in a company called Beckman Coulter in Houston, as an Assay Development Scientist. She joined graduate school in August of 2007. This was followed by a break in her education in 2008 when she went back to India (Hyderabad) and took up a job in Novartis as a Clinical Safety Scientist till the end of 2008. In 2009 she came back to Houston and joined back the University of Texas Health Science Center at Houston, Graduate School of Biomedical Sciences.

Permanent Address:

7900 Cambridge Street, Apt.#6-1D, Houston, Texas,77054